Experimental-numerical material characterization of adobe masonry

Tests and simulations on various types of earthen bricks and mortar in statics and dynamics

li Piani, Tiziano

DOI
10.4233/uuid:f2470c09-e8f0-4c1e-b4e4-effc17ecd373

Publication date
2019

Document Version
Final published version

Citation (APA)
li Piani, T. (2019). *Experimental-numerical material characterization of adobe masonry: Tests and simulations on various types of earthen bricks and mortar in statics and dynamics*. [Dissertation (TU Delft), Delft University of Technology]. https://doi.org/10.4233/uuid:f2470c09-e8f0-4c1e-b4e4-effc17ecd373

Experimental-Numerical Material Characterization of Adobe Masonry

Tests and Simulations on various types of earthen bricks and mortar in statics and dynamics

EXPERIMENTAL-NUMERICAL MATERIAL CHARACTERIZATION OF ADOBE MASONRY

TESTS AND SIMULATIONS ON VARIOUS TYPES OF EARTHEN BRICKS AND MORTAR IN STATICS AND DYNAMICS

Proefschrift

ter verkrijging van de graad van doctor
aan de Technische Universiteit Delft,
op gezag van de Rector Magnificus prof. dr. ir. T.H.J.J. van. der. Hagen,
voorzitter van het College voor Promoties,
in het openbaar te verdedigen op 04 September 2019 om 10:00 uur

door

Tiziano LI PIANI

Master of Science in Civil Engineering
University of Pavia, Italy
geboren te Oristano, Italy.

Dit proefschrift is goedgekeurd door de

Promotor: Prof. dr. ir. L. J. Sluys
Copromotor: Dr. ir. J. Weerheijm

Samenstelling promotiecommissie:

Rector Magnificus,	Voorzitter
Prof. dr. ir. L. J. Sluys	Delft University of Technology
Dr. ir. J. Weerheijm	Delft University of Technology & TNO
Onafhankelijke leden:	
Prof. dr. G. Magenes	University of Pavia
Prof. dr. M. di Prisco	Polytechnic University of Milan
Prof. dr. Ing. N. Gebbeken	Bundeswehr University Munich
Prof. dr. ir. S. Wijte	Eindhoven University of Technology
Prof. dr. ir. J. Rots	Delft University of Technology
And:	
Prof. dr. ir. E. Schlangen	Delft University of Technology

ISBN 978-94-6323-789-5

An electronic version of this dissertation is available at
http://repository.tudelft.nl/.

CONTENTS

SUMMARY

Research in this thesis is aimed at comprehensively characterizing the mechanical performance of adobe components. Adobe is a traditional masonry made of sundried bricks and mortar. Bricks are made of soil mixed with fibers and joined together by mud mortar. Adobe is largely spread in areas of the world prone to seismic risk or involved in military conflicts. Its low environmental impact attracts scientific attention also for sustainable applications in current building industry. Unfortunately, the material and structural properties of adobe are still hardly assessed, as a result of centuries of progressive abandonment of this building technology in western countries after introduction of modern building materials in the market. In this doctoral research, a combined experimental and numerical approach was followed. It has been aimed at fulfilling experimental data and knowledge gaps in the study of the main properties of this material. Experimental tests have been performed on bricks and mortar characterized by different mineralogical compositions, fiber percentages and moisture content. Mechanical tests consisted of bending and compression tests. Tests in compression have been performed at different rates of deformation from statics to high velocity impact. Data derived from tests have constituted a solid dataset aimed at interpreting and modelling the mechanical performance of adobe. Experimental trends resulted in physical theories concerning the main features of the quasi brittle response of adobe. In particular, the role of fibers and water content in the mixture on the mechanical response of adobe bricks and mortar has been addressed in this study in the static and dynamic regimes of the spectrum of strain rate induced loadings. The main mechanical parameters in compression and tension for adobe have been statistically determined from the static and dynamic tests. Mechanical properties and physical theories have been framed in several models that interpret the response of adobe for different applications. Constitutive models have been derived to address the uniaxial response in compression at different strain rates of adobes of different mineralogical composition and water contents. A finite element damage model has been developed to simulate the main failure modes specifically observed in earthen bricks at different loading conditions and rates, including high velocity impacts. The numerical study has been devoted at ensuring objectivity of analysis to the results of simulations performed using different mesh refinements of the geometrical model of the tested brick. Furthermore, engineering ballistic models that address the response of adobe walls to small caliber penetrations have been developed in this doctoral research. This thesis contains the description of the performed experiments, the analysis of data, the theoretical interpretations and the models developed for the material characterization of adobe masonry.

SAMENVATTING

Dit proefschrift betreft een onderzoek dat gericht is op het karakteriseren van de mechanische prestaties van adobe-componenten. Adobe is een traditioneel metselwerk gemaakt van zongedroogde stenen en mortel. De stenen zijn gemaakt van grond, vermengd met vezels. Adobe wordt wereldwijd, op grote schaal toegepast in gebieden die vatbaar zijn voor seismische risico's en daar waar langdurige militaire conflicten zijn. Toepassing van adobe als bouwmateriaal trekt tegenwoordig wetenschappelijke aandacht, vanwege de mogelijkheden voor duurzame toepassingen in de westerse bouwsector. Helaas worden de materiële en structurele eigenschappen van adobe nog nauwelijks benut omdat deze bouwtechnologie in de westerse landen volledig in onbruik is geraakt na de introductie van moderne bouwmaterialen. In dit onderzoek is een gecombineerde experimentele en numerieke benadering gevolgd. Het is gericht op het verkrijgen van experimentele gegevens en het opvullen van kennislacunes voor de belangrijkste mechanische eigenschappen van dit materiaal. Experimenten zijn uitgevoerd op stenen en mortels van adobe materiaal met verschillende mineralogische samenstellingen, vezelpercentages en vochtgehalte. De mechanische beproevingen bestonden uit buig- en compressietesten. De drukproeven zijn uitgevoerd met verschillende vervormingssnelheden zoals die op kunnen treden bij belastingen variërend van statisch tot hoge snelheidsimpact. De verkregen gegevens van alle testen vormen een solide dataset voor het interpreteren en modelleren van de mechanische prestaties van adobe. Experimentele trends resulteerden in fysische theorieën voor het beschrijven van de belangrijkste kenmerken van het quasi-brosse vervormingsgedrag van adobe. In het bijzonder is de rol van vezels en het vochtgehalte in het mengsel op de mechanische respons van adobe-stenen en mortel onderzocht in de statische en dynamische regimes. De belangrijkste mechanische parameters voor de respons van adobe onder druk en trekbelasting zijn statistisch bepaald uit de statische en dynamische testen. Mechanische eigenschappen en fysische theorieën zijn vertaald in de diverse modellen die de respons van adobe voor verschillende condities beschrijven. Constitutieve modellen zijn afgeleid om de uniaxiale respons in compressie te beschrijven voor verschillende reksnelheden van adobe materiaal met verschillende mineralogische samenstelling en watergehaltes. Een "finite element damage model" is ontwikkeld om de belangrijkste bezwijkvormen te simuleren die optreden en waargenomen zijn in adobe stenen onder de verschillende belastingcondities en snelheden. Speciale aandacht is gegeven aan het modelleren van de hoge snelheidseffecten. De numerieke studie was gericht op het waarborgen van de objectiviteit van de analyse en de numerieke resultaten. De objectiviteit is aangetoond door middel van verschillende verfijningen van het geometrische model van het geteste materiaal. Aanvullend zijn semi-empirische ballistische modellen ontwikkeld die de respons van adobemuren op klein kaliber inslag adequaat beschrijven. Dit proefschrift bevat de beschrijving van de uitgevoerde experimenten, de analyse van gegevens, de theoretische interpretaties en de modellen ontwikkeld voor de materiaalkarakterisering van adobe.

1

INTRODUCTION

"... But bespectacled man
on the contrary invents devices outside of his body
and if health and nobility existed in the inventor,
they are almost always lacking in the user..."

from *Zeno's Conscience*, by Ettore Schmitz, 1923

1

1.1. SOCIETAL BACKGROUND

Society has been recently exposed to an increased number of threats and hazards which more and more result from mankind activities on Earth. Not only natural hazards, such as tsunami and floods, but also terrorism and armed conflicts threaten built heritage of the contemporary city (Figure 1.1a). Safety and protection of buildings and infrastructures have raised among the top priorities of governments around the world, including in Europe. Recent increase of asymmetric conflicts in urban environments urges the development of new counter strategies for the material and structural design of buildings for civilian use [1]. In fact, the terrorist attack targeting a single building inserted in a highly urbanised environment, also forms a direct risk for the life and property of people outside the building, starting from the street paths the terrorist walks on to prepare and perform the attack. This "*space of influence*"[1] is limitedly determined by the type of weapon used to conduct the attack. It is rather a property of the building that results from its social function in the city and from the spatial relationships established with the other buildings and streets of the urban fabric (Figure 1.2a) [2]. In this contexts, strategies of target strengthening (e.g. applying "standoff" distances) applied for strategic buildings or in warfare can not be simply transferred to highly urbanized areas [3]. They are neither economically nor socially acceptable with respect to principles of freedom and democracy that contemporary urban planning in Europe should be spatial reflection of (Figure 1.2b-c). Thus, built infrastructure nowadays must become resilient by a design process in which a wider range of loading conditions and loading rates is covered, from statics to impact and explosions (Figure 1.1b)[4]. As a result, after decades of relative silence, the study of the dynamic behaviour of materials to impulsive loadings has lately gained renewed importance.

The study of the dynamic properties of modern building materials used for civilian constructions such as steel and concrete has been consolidated over the last fifty years. For example, research on concrete has been recently focused on the improvement of its behaviour under impact. Among the most recent proposals, cement matrices have been reinforced using fibers to increase properties regarding strength and toughness. Mixing cement matrices with fibers is not a new practice but this actually started with the use of adobe. Adobe is a masonry made of sundried earthen bricks and mud mortar. Raw soil in the field can be randomly mixed using fibers locally available in the field since ancient Egypt and even earlier, making adobe one of the very first building materials in history. As a result of a long tradition, many earthen buildings of architectural value have piled up over millennia. Due to spread availability and cheapness of raw materials, still nowadays more than one third of the world population lives in earthen dwellings, most of which are unfortunately built within an informal settlement in many contexts of scarcity of the world [5] (Figure 1.3a-b). This represents a further element of threat for adobe because, much earlier than modern structures, adobe buildings have been largely exposed to earthquakes or historically involved into wars, terrorisms and military operations, also in areas where European armies are still currently involved (Figure 1.3c). Unfortunately, despite an atavistic exposition to the dynamic threat, a rigorous assess-

[1] This definition was presented at the Italian Parliament describing several attacks recently happened in Europe, including the case of the attack to Parliament in London on 22^{nd} March 2017, which produced casualties in the route (bridge) taken by the terrorist car to reach the final point of impact.

(a)

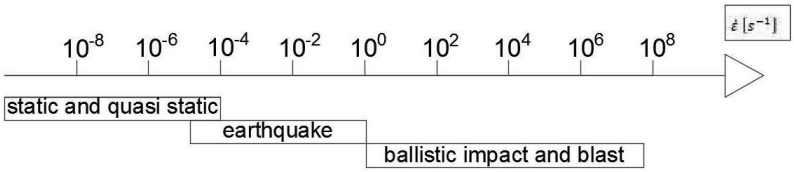

(b)

Figure 1.1: a: Earthquake in Messina, Italy (1908, left) and attacks to twin towers, New York, US, (2001, right) [Source:Google] and b: magnitude of strain rates for different loadings [Source: author, (2018)].

ment of the material and structural performance of adobe is still lacking. This not only holds for high strain rate loadings, but also for statics and for the general treatment of the basic mechanical properties. This situation is the result of centuries of progressive abandoning of this building technology in western countries after industrial revolutions. Considered as a soft and hardly durable material to withstand the requirements of an ambitious society, the use of adobe in Europe has been progressively discouraged after 19^{th} century and surpassed by modern building materials of secure reliance with well defined and controlled quality such as concrete and steel or common bricks.

However, only in very recent times and due to a specific global conjuncture inherent to construction industry, a renewed demand for old building materials and vernacular building technologies also for new applications has increased. The goal number 11 of the UN urban agenda released in 2016 is concerned with making cities inclusive, safe, resilient and also sustainable. The introduction of the concept of sustainability in the building construction industry is urgent in light of its current impact on the increasing threats linked to natural material scarcity and global pollution [6]. Construction industry is responsible for 30% - 50% of the anthropogenic emissions of CO_2. A relevant portion in a range of 10-25% of this contribution regards only the manufacturing stage of materials, which is mostly dominated by cement and concrete productions. Production processes consume more than 50% of all raw materials, 40% of total energy use and 30% of water use. Among modern building materials, only concrete accounts for more than 1% of the total energy use and cement is responsible for more than 80% of diossine emissions inherent to concrete production. Also the use of steel, which does not cause a relevant impact in CO_2 emissions compared with modern geomaterials, is responsible for the production of fine dust waste when used as reinforcement material. Thus,

1

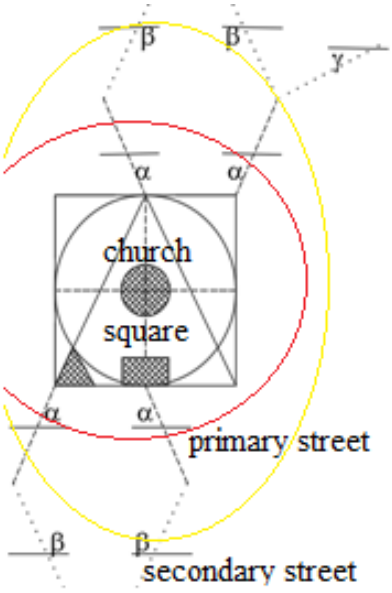

(a)

(b)

(c)

Figure 1.2: *a: Schematic in [1] for the "space of influence" for Churches of different shapes and differently inserted in urban squares and connected by primary streets (from where people are already in danger in case of terrorist attacks in churches) and secondary streets (with lower threat intensity level) [Source: author, (2017)]. b. A fortrness in the past (Castle of Muiderslot in Amsterdam) c. and (perhaps) in the future (recent design for the new American embassy in London) [Source: google]*

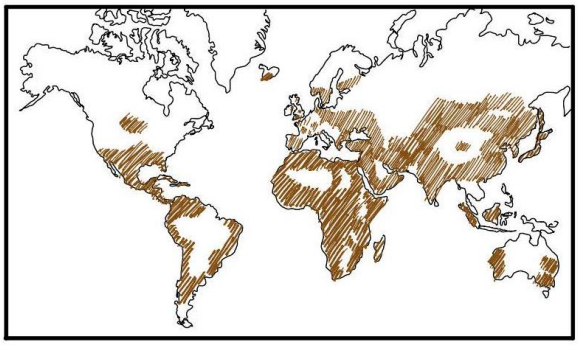

(a)

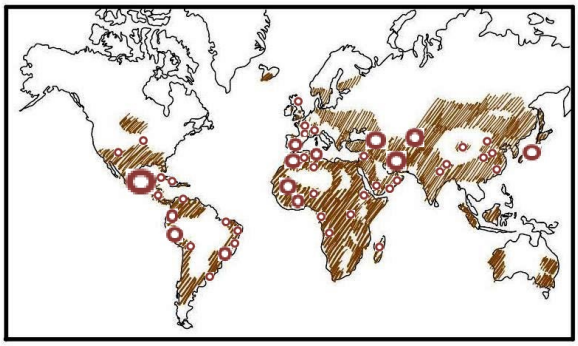

(b)

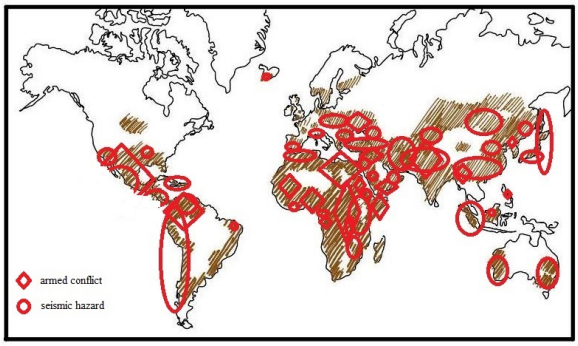

(c)

Figure 1.3: *Earthen structures in the world (a) with focus on cultural heritage sites according to UNESCO (b) and areas of the world with medium and high seismic hazard or armed conflicts (c)*

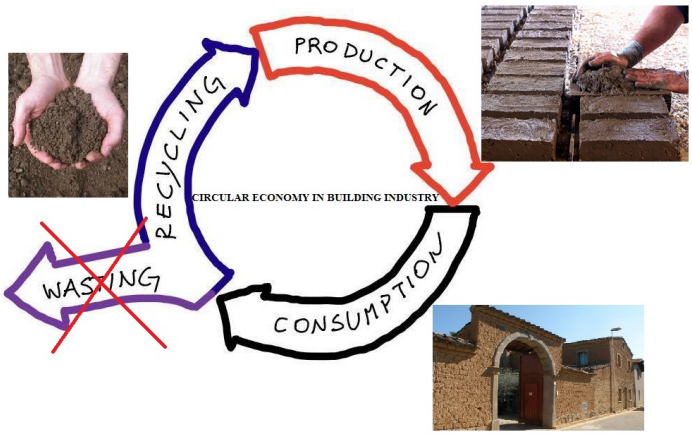

Figure 1.4: *Circular economy vs linear economy in building industry: the case of Adobe, [Source: graphic by Author, photos from google on "ladiri" (adobe bricks) in Sardinia, Italy]*

sustainable alternatives to current building practices have become a priority in building industry and studies aimed at reducing the environmental impact of building materials while respecting performance requirements, have been recently started around the world.

Most of the scientific attention is nowadays devoted to reducing environmental impact by adequate material selection and production phases of construction. For example, biological fibers have been recently tested as sustainable alternatives to steel in reinforced concrete. Natural binders have been partially replacing Portland cement. Especially in the sector of masonry constructions, alternatives to baking processes such as air drying procedures have been studied, which can reduce up to 80% of the greenhouse gas emissions for modern baked clay bricks. These efforts are meant to convert the current building industry according to the principles of the circular economy (Figure 1.4). However, most of the aforementioned practices, despite being applied to new materials, are far from being new. They take their roots in the human history and its resourcefulness of ensuring shelters that maximize the use of available resources [5]. In particular, they belong to the tradition of Adobe. For instance, the possibility to avoid baking processes comes directly from the tradition of raw earthen bricks. In adobe masonry, soil mixtures are cast in moulds. Depending on the local traditions, bricks undergo a preliminary curing period which is followed by a few weeks of hardening in the sun. For these reasons, fibers were originally inserted in the soil mixtures in order to limit shrinkage cracks during drying. Fiber inclusion as well as the air drying processes contribute to the eco-sustainability of adobe as a building material. Adobe is an interesting “circular” building material. It produces almost zero dioxin emissions and it is fully disposable and fully recyclable. Unfortunately, the effects of fiber inclusion and air drying as well as other sustainable practices tied to the tradition of adobe on the mechanical performance have not been addressed yet. Their assessment not only can contribute to the protection of the built heritage of the past but also foster safe applications of sustainable

building traditions in the future.
In the framework of uncertainty that still characterizes knowledge on adobe around the world, different interests converge toward the assessment of the behaviour of this traditional building technology. Starting from the analysis of the physical mechanical properties of its constitutive elements, namely the bricks and mortar of adobe. This is the focus of this doctoral dissertation.

1.2. THE DOCTORAL PROJECT ON ADOBE

1.2.1. RESEARCH MISSION

This project has been aimed at characterizing the physical-mechanical performance of adobe bricks and mortar. This implies the definition of a material class for adobe and the assessment of its constitutive relationships for a wide range of loading rates and conditions. The main mechanical properties in strength and deformation are meant to be quantified in the static and dynamic regimes, including under impact conditions. Strain rate dependency quantified in dynamic increase factors (DIF) for all the main properties are supposed to be addressed for adobe. The role of the mineralogical composition, fibers inclusion and water content in the mixture is supposed to be qualitatively interpreted and quantitatively assessed with respect to the main physical mechanical properties of the resulting bricks and mortar. Material characterization must also result in the development of numerical models capable of consistently simulating the mechanical performance of traditional masonry bricks and mortar for different loading conditions in statics and dynamics, including against projectile penetrations.

1.2.2. RESEARCH METHOD

In late 2015, only limited experimental data on bricks of adobe were available in literature. No tests on adobe mortar were performed yet. No numerical models for the material simulation of adobe were developed nor in statics neither in the dynamic regime. Overall, the goals of this research are inserted in this framework of uncertainty.
In light of this state of the art, a combined experimental-numerical approach was adopted. The experimental phase followed a literature review of the current scientific production on adobe, constantly updated during the research. The characterization started with the production of new experimental data. Campaigns of physical-mechanical characterization were designed, planned and executed (Figure 1.5). Three campaigns performed over the last four years are mentioned:
The "*Adobe-Stat*" campaign has been aimed at characterizing the static performance in compression and tension of bricks and mortar of different mineralogical composition. It was conducted at the Military Engineering Laboratory in Breda from July to October 2016. Earthen samples of bricks and mortar of different mineralogical composition, straw percentages and water content were tested in uniaxial compression and in flexure.
The "*Soil-Adobe*" campaign has been aimed at determining particle size distributions and organic content ratios of the soil mixtures used to produce bricks and mortar in the "Adobe-Stat" campaign. It was conducted at the laboratory of geomechanics of the Civil Engineering faculty of the Delft University of Technology from November 2016 to January 2017. The different soil mixtures tested were subjected to sieving and sedimen-

(a)

(b)

(c)

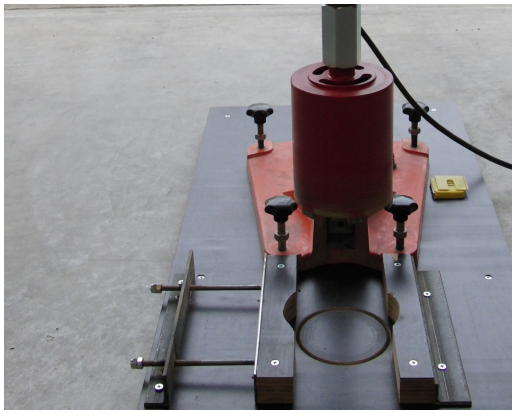

(d)

Figure 1.5: *The tools of the engineer: saw(a), sander (b), clamper (c) and driller (d) used for tests preparation*

tation tests via hydrometer.

The "*Dif-Adobe*" campaign has been aimed at characterizing the material performance of adobe in uniaxial compression at progressively increasing deformation rates. The role of fiber and water in the mixture on the dynamic performance of the material has been addressed. The campaign was conducted at the Joint Research Centre (JRC) of the European Commission in Ispra, Italy, from May 2018 to August 2018. The preparation phase was jointly executed at the Military Laboratories of the Netherlands in Breda and JRC in Italy from March 2018 to June 2018. The campaign resulted from the winning of the announcement "*2017-1-RD-ELSA-HopLab*" called by European Commission, on behalf of a consortium composed by Delft University of Technology, Dutch Academy of Defence, TNO and Dutch Ministry of Defence created in 2017. Samples of adobe bricks with different percentages of fibers and water content were subjected to high velocity deformation tests in compression from $\dot{\epsilon}$=3 10^{-5} s^{-1} to 120 s^{-1}. High strain rates tests were conducted using the modified Split Hopkinson Bar facility at the HopLab of European Commission.

Each experimental campaign resulted in quantitative data as well as photos and videos. Large amount of data have been collected, produced and analysed. For their relevance and amount, they were sometimes organized into databases. Two database are worth to be mentioned because they are meant to be permanently maintained tools for data analysis.

In the "*Adobe Masonry Dataset*" results of 142 tests cases of uniaxial compression tests on adobe bricks available in literature are collected and organized. It has been aimed for the statistical analysis of the main mechanical parameters of adobe in compression, including their dependencies on geometrical and physical factors. Data have been organized similarly to the structure of the database developed at the European Centre for Research in Earthquake Engineering (EUCENTRE) in 2015 extensively described in [2] of the list of publications.

In the "*Adobe Masonry Ballistic Database*" the results of a ballistic campaign conducted in the field of 't Harde in the Netherlands by TNO between 2012 and 2013 are collected, organized and elaborated. The dataset was used to statistically analyse the main ballistic parameters of walls made of different types of bricks tested in the "*Adobe-Stat*" campaign and shot by different types of small caliber bullets at different humidity and temperature conditions.

Physical interpretation of the main trends experimentally observed resulted into the development of numerical models for the simulation of the material performance of adobe. For instance, a predictive law for the compressive strength of bricks and mortar of given fiber and water contents has been formulated in statics. Constitutive models in uniaxial compression have been developed for different strain rates also in the dynamic regimes. The development of a finite element model for the simulation of the main failure patterns observed on bricks and mortar of adobe at various loading conditions and rates was aimed in the doctorate. Numerical analyses started in early 2016 and the model was developed consistently with the analysis and findings experimentally observed along time. Numerical research has been performed at the "*Computational Mechanics*" group of the Applied Mechanics section of the 3MD Department at the Civil Engineering Faculty of the Technical University of Delft. The fem code was developed in C++ using the Jem Jive libraries. Simulations have been performed in the

Figure 1.6: *hpc27.tudelft cluster at Delft University, [Source: photo courtesy of P. Keekstra]*

cluster of TU Delft hpc27.tudelft (Figure 1.6). As a result of the numerical implementation "*The Adobe Delta Damage Model*" has been developed to objectively simulate the static and dynamic performance of quasi brittle materials used in masonry. It is a constitutive framework that adopts a continuum damage mechanics. It adapts a local damage model originally developed for concrete in order to address the main failure modes experimentally observed in all campaigns on adobe previously referred in the statics and dynamic regimes. Numerical objectivity with respect to the spatial discretizations of the physical domain is provided by generalizing the class of bounded damage algorithms of regularization originally developed for composite materials. The original delta formulation was enriched by material and loading rate dependencies that enhance consistency with the physics of adobe also in dynamics. Implicit solvers have been used to integrate the equations of equilibrium.

Finally, it is worth to mention that also a ballistic phenomenological model has been developed as a result of the physical interpretation of the resisting mechanisms inherent to small calibers penetration in adobe walls. It is meant to provide quick and reason-

able estimates of fundamental ballistic parameters needed during military operations in the field involving targets of adobe masonry. "*The Adobe Ballistic Model*" is a phenomenological engineering model aimed at determining the main ballistic parameters against small-caliber impactors into Adobe walls. The model takes its roots from a semi-empirical model developed for concrete targets and was adapted to include principles of soil mechanics against deep penetration tests. Given a conical radius head, diameter and density of the impactor and density and friction angle of the targeted brick, it determines the maximum penetration depth of the projectile inside or its residual velocity at the exit boundary of the target of given density.

1.2.3. RESEARCH OUTLINE

The body of the dissertation consists of seven chapters. In the following, the main topics treated in each chapter are highlighted.

Chapter 2 presents the results of the "*Adobe-Stat*" campaign. A set of technical guidelines is proposed to experimentally characterize bricks and mortar of adobe. A law dependent on the water content in the mixture is defined for the assessment of the compressive strength of sundried masonry components, in which also the influence of soil mineralogical elements and fiber volumes are statistically quantified and physically interpreted.

Chapter 3 presents the "*Adobe Delta Damage Model*". Mesh objectivity of the model is demonstrated in statics and the model is applied to simulate the failure of one type of brick and mortar tested in the "*Adobe-Stat*" campaign.

Chapter 4 presents the results of the "*DIF Adobe*" campaign. Failure modes and curves of response are interpreted and parameters quantified for each strain rate in statics and dynamic regimes. A constitutive model proposed for the static assessment of adobe is updated with strain rate dependent functions that address the curves of response of Adobe in dynamics. A physical theory of the role of fiber inclusion and water content in the soil mixtures of adobe is developed and explained.

Chapter 5 presents an enriched version of the model developed in Chapter 3. Mesh objectivity of the model is demonstrated in dynamics. Parameters mathematically needed to regularize the model are made dependent on rate and material properties which enhance consistency with fracture theory and the physics depicted by dynamic tests on adobe and interpreted in the paper.

Chapter 6 presents the "*Adobe ballistic model*" developed for adobe masonry according to the hypothesized main physical resisting mechanisms inherent to penetration. The model is validated and calibrated using data of the "*Adobe Masonry Ballistic Database*".

Chapter 7 faces the future perspectives and tackles the open areas of research toward the material characterization of adobe according to a critical analysis of the current standards and building codes for adobe in the world.

Resuming conclusions are provided in the last chapter of the dissertation.

1

REFERENCES

[1] T. Li Piani, Operative guidelines for protection of places of worship: A new approach toward security design of sensitive buildings, Institute for Advanced Strategic and Political Studies, p.70., 2017.

[2] T. Li Piani, Structural design and the social function of space as vulnerability factor and solution to urban terrorism (italian), Security Terrorism Society, 2(8), p.10, 2018.

[3] T. Li Piani, Local trends and global dynamics of religious terrorism in the African continent, NATO Defense College Foundation Paper, p.10, 2019.

[4] T. Li Piani, After Sri Lanka: Anatomy of attacks in churches (italian), ISPI (Italian Institute for International Political Studies), analysis, p.10, 2019.

[5] A.R.C. Cavalcanti and T. Li Piani, Housing by people and their work: Design principles for residents of favelas in economies of commerce and service, The Plan Journal, Vol 20, 4(1), 2019.

[6] UN 1987, Report of the world commission on environment and development: our common future, 1987

2

THE EXPERIMENTAL CHARACTERIZATION OF ADOBE IN STATICS

"You know that the beginning
is the most important part of any work,
especially in the case
of a young and tender thing (...)"

Plato, The Republica

Adobe is an ancient building technology, made of sun dried bricks joint together by mud mortar. This paper deals with the physical and mechanical characterization of three different typologies of Adobe bricks and one typology of mud mortar produced in Europe, which were used to build Adobe walls within a recent ballistic test campaign. They differed in terms of internal soil element proportions and amount of organic content. Physical tests consisted of granulometry, moisture content and density tests. The mechanical characterization consisted of uniaxial compressive tests and three point bending tests. Tests were performed according to modern material standards. The main mechanical properties both in tension and compression were determined at different curing conditions. The outcome provided in this study offers a general overview on the assessment of the mechanical performance of Adobe, in relation to the properties and interactions of its soil constituents. In fact, the comparison between components with the same soil mineralogical family and production process made it possible to assess both at a qualitative and quantitative level the effect of the physical properties of the mixture (such as fibers and clay percentages or moisture content), on the mechanical parameters of the resulting bricks and mortar. This

This chapter is based on "The Mechanical Performance of Traditional Adobe Masonry Components: An experimental-analytical characterization of soil bricks and mud mortar" in *Journal of Green Building*, 2018

paper proposes new predictive formulations of the most relevant material parameters in strength and deformation, such as compressive strength, deformation at peak stress and ultimate displacement for both Adobe bricks and mortar. They quantify the influence that water content, clay percentage and fiber reinforcement produce on the mechanical performance of the tested Adobe components. This was made possible by means of multivariate statistical analyses on the mechanical parameters derived from all the tested samples.

2.1. INTRODUCTION

Traditional Adobe, literally "sun-dried brick" according to the Arabic *Al Tob* [1], defines one of the most ancient forms of masonry on earth, constituted by unpressed sun dried bricks joint together by mud mortar. Despite a millenary history [2] characterized by buildings of architectural value [3], its spread in European countries in modern age is limited as a consequence of the introduction of modern building materials during industrial revolutions [4]. As a result, the assessment of the physical-mechanical properties of this traditional masonry was not a priority of the scientific community until modern age. Only recently Adobe has started gaining significant attention [4, 5]. Two main world socio-economic trends are at the basis of the renewed interest towards this masonry typology. On one hand, governments of developing and third world countries in the recent past have hardly met their housing targets, leading people to build houses by themselves within an informal settlement [6]. As a result, more than one third of the world population still lives in earthen dwellings which are often spread in areas of the world characterized by seismic risk or involved into military operations, with dramatic loss of human lives and cultural heritage [7]. In fact, Adobe dwellings erected by local farmers in the field, without proper knowledge of structural systems and awareness of the suitability of the applied soil for building purposes, result into an intrinic vulnerability to dynamic loadings [8–10]. On the other hand, developed countries, within the goal of energy efficiency and pollution reduction, are promoting Adobe because of its favourable acoustic and thermal properties and the related minimum environmental impact [11, 12].

Despite that knowledge on Adobe is still scarce at both a material and structural level[13]. The number of characterization campaigns on Adobe bricks is still limited and in the case of mortar even rare[14]. The current stage of production on its material properties and their influencing factors is discussed in the following chapter. From its analysis, it is inferred that different or also opposite trends can be found in literature in terms of the influence of the adopted soil mixture on the resulting mechanical performance. This happens because mechanical values are compared using bricks made with various soil mineralogy, different reinforcement materials and methods of construction. Brick composition varies significantly according to building traditions and the local availability of materials, which affects the resulting performance of the material [15]. As a result, there is often no homogeneity in the prescriptions and formulations contained in the few building codes currently available for Adobe. European standards for production, testing and design of Adobe even do not exist yet. In this study, the comparison of the effects of soil mixture on the static performance of both bricks and mortar have been investigated at both a qualitative and quantitative level. The paper presents the results of a physical-mechanical characterization campaign performed in 2016 by the authors on three dif-

ferent types of bricks and mortar made of the same mineralogical family and the same building process. The bricks were subjected to two different drying conditions (namely air drying and fire burnt) consistent with the traditions of different geographic regions of interest[16]. No study on the influence of moisture content on the performance of Adobe components was found in literature so far. Therefore, the analysis and data elaboration resulted from an extended dataset. The statistical analysis revealed relationships between the mechanical performance of the components and their mineralogical composition with drying process. A novel assessment of the compressive strength parameter of Adobe was carried out, which could be defined adapting a law originally developed for predicting the strength of unbaked modern clay bricks according to its internal moisture content. It consists of an exponential function of moisture content multiplied with a fully dried compressive strength value, which is dependent on the percentage of clay and fiber reinforcement. The reinforcement was confirmed to largely determine the deformation capacity of Adobe. The found relations in strenght and deformation, calibrated according to data on tested bricks, could fit significantly well also the performance of mortar. This findings link the material class of mortar and bricks in case of Adobe masonry. Overall, this study aims at sharing an experimental dataset already used in other research on the dynamic properties of Adobe masonry [17, 18]. But in general, it provides a clear indication of the mechanical material performance assessment of adobe according to its physical properties. That was made possible by conducting tests according to standards developed for modern materials and adapting them to adobe. After the introductory section, this paper presents the characterization campaigns, detailing both the standards and setup adopted and the related results. Next, the mechanical performance is investigated in the fourth Section according to the physical characterization.

2.2. LITERATURE REVIEW ON THE ADOBE BRICKS AND MORTAR PERFORMANCE

Sun-dried Adobe bricks contain mixtures of clay, silt, sand water and possibly straw [19]. Mortar is usually made of the same or similar mixture as the bricks, although it is often free of straw [20]. Only one recent work was found in which a characterization campaign on the response of Adobe mortar was performed [14].

According to published works, typical ranges of element proportions in soils suitable for brick production are: 12-25% clay, 55-75% sand, 10-30% silt ([2] - [13]).

Clay and silt, cohesive elements in nature, form a matrix in which the sand particles are enclosed, acting as a binder for the cohesionless granular fraction of the soil [2]. Thus, clay is supposed to provide strength to the dried material, although it is also the main cause for shrinkage cracks which occur during the drying process of the bricks due to its affinity towards water [2, 32]. Therefore, it is often recommended to set an upper bound to its volume in the mixture, usually around 20% [22, 33]. Actually, spectroscopy investigations have revealed that not only its relative content in the mixture, but also the clay mineralogical family plays a significant role regarding the performance of the product [34]. A correct balance between expandable clay minerals (i.e. smectite), that provide strength but are responsible for undesirable cracks, and non-expandable clay minerals (i.e. kaolinite), responsible for less shrinkage problems and cohesion, is often

required [2, 19, 25].

Adobe bricks can contain only soil elements, or also include fibers [19]. Actually, the addition of straw into the soil mixture is common practice according to many building traditions [35, 36]. This insertion can significantly influence the resulting properties of Adobe components. First of all, fibre is often associated to a reduction of shrinkage rates in the drying material, limiting the formation of cracks as a consequence of a more efficient drainage system [22, 37]. Straw also lightens the weight of the resulting brick and it boosts the thermal properties of the material [38]. On the other hand, an excessive amount of fiber can result in a too fast drying process and thus in an intrinsic brittleness of the product [24]. Also with reference to the fiber content percentage, upper bounds are suggested in literature [5, 36, 39]. In fact, besides the influence of fibres on the drying process, its contribution to strength and deformation performance of the dried brick is more controversial. This happens because a common approach in literature is to quantitatively compare results obtained from different types of bricks from different regions, resulting in a lack of definite assessment (Figure 2.1). In general, a fibre-free earthen brick under compression is generally characterized by quasi-brittle failure similar to unconfined concrete, while a straw reinforced brick shows more often the development of an increased number of microcracks accompanied by more ductile behaviour [13, 22, 24]. From the physical point of view, this can be due to the redistribution of forces within the soil matrix due to the fibres that can held together parts of the soil matrix at large deformations [13]. On the other hand, the presence of straw is often associated to a decrease in strength and elasticity with respect to unreinforced bricks [24]. The observed trend may be a consequence of adherence problems between the fibres and the soil matrix, that is likely to be influenced also by the type and geometry of the adopted fibre reinforcement [40]-[43]. Actually, these weakening effects on bricks are not always noticeable and they seem to be even inverted in case of highly sandy mixtures [22]. Similar controversies exist regarding fibre reinforcement and the performance under tensile loading of reinforced Adobe [20, 24]. Recent elaborations on a heterogeneous dataset relate strength with dry density of bricks [20]. It is known that the amount of water required for mixing the soil elements depends on their relative percentage and inherent mutual interactions, especially in case of a fibre reinforced mixture [2]. Usually, as the fibres or the clay content increases, the water fraction needs to be increased as well [24]. On the other hand, an excessive increase of water with respect to the strictly necessary amount in order to obtain an acceptable workability of the mixture can compromise the unit weight and the strength of the specimen [24, 35]. In fact, a high moisture content is a prominent risk for the strength and the durability of Adobe structures during their entire life cycle [19]. The preservation of the mechanical performance of Adobe seems to be mainly governed by the capability of keeping the structures dry [2]. This can be assured in the field by adding external plaster layers to the brickworks [19].

Finally, it is worth stressing that the absence of production chains and quality control which is common practice for Adobe buildings erected by local farmers in the field, make the mechanical properties of the resulting products extremely difficult to be assessed, independently from the contribution of the applied mixture. Despite the method of production and erection are unavoidable discriminant features within the material mechanical performance assessment [15, 37], their influence will not be taken into con-

sideration within the present work.

2.3. THE CHARACTERIZATION CAMPAIGN

A characterization campaign was performed on the components already used to assemble Adobe walls in a previous research [44]. To this end, three pallets of bricks with different mixture proportions but from the same mineralogical family were ordered from the same supplier, together with two bags of mortar (Figure 2.2).
The characterization campaign consisted of physical and mechanical tests. Static tests were performed at the military engineering laboratory of the Netherlands (NLDA) in Breda, while the physical characterization was performed at the laboratory of geoscience and engineering of Delft University, in the Netherlands.
The physical characterization consisted of density, moisture content and granulometric tests, while mechanical tests consisted of uniaxial compressive tests and three point bending tests. All tests were conducted adopting European standards developed for modern building materials adapted to the nature of the material if necessary. In fact, a European normative framework is still lacking for Adobe. A preliminary study of the few existing technical codes for Adobe in the world was conducted [45] - [48] and set up emplaced in previous research were acknowledged [4]. As a result, the application of each adopted standard possibly resulted in modifications in the setup. The adopted standards and the complete list of precautions are resumed in Table 2.1 in order to provide a characterization reference on Adobe.
In particular, all the samples were rectified preliminary to mechanical tests due to the significant geometrical irregularities of many bricks (Figure 2.2b). Mortar was hardened for twenty one days and all tests were performed after 28 days of air curing at controlled laboratory condition. Tests in compression were performed on both air dried and oven dried samples in order to address also the behaviour of burnt Adobe bricks [16].
In the following paragraphs, bricks are identified as: Type A, Type B, Type C according to the different soil mixture and mortar is denoted with Type M. The initial geometrical properties are determined according to UNI EN 772-16 [49] and given in Table 2.2. Each tested sample in the following paragraphs is indicated by a set of letters representing the type of bricks and the type of test (C for compressive and T for tensile), followed by numbers representing the specific sample extracted. For compressive tests, a further number distinguishes between air dried (1) or oven dried (2) samples.
In the following sections, the physical and mechanical characterization of Adobe are described.

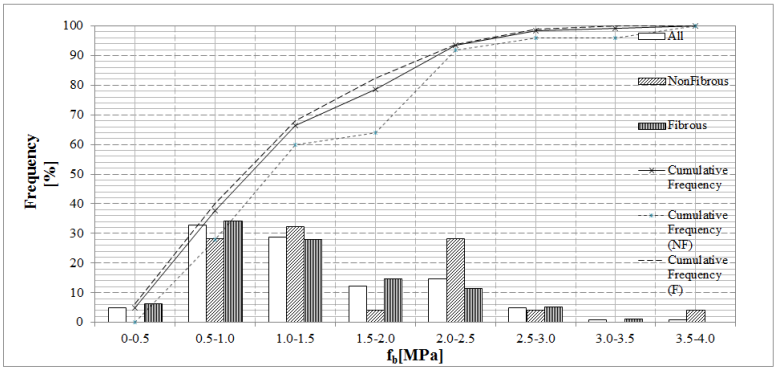

(a)

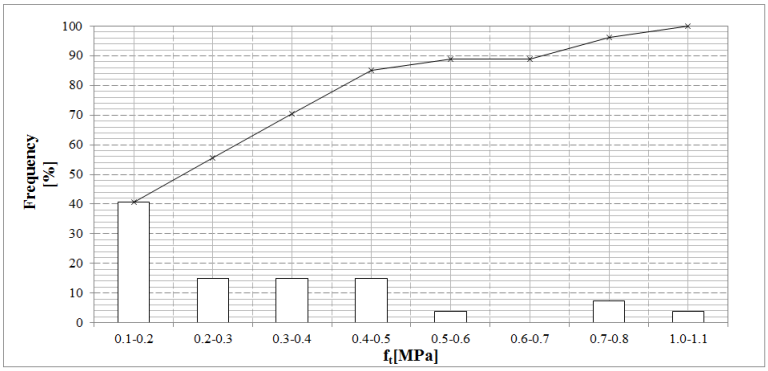

(b)

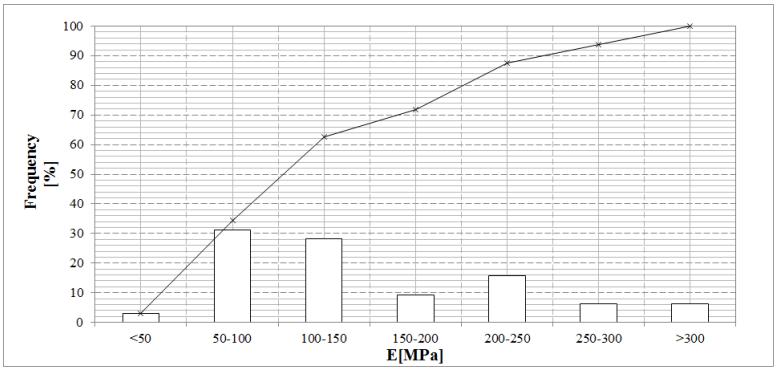

(c)

Figure 2.1: *Relative and cumulative frequency for compressive strength (a), tensile strength (b) and elastic modulus (c) of Adobe bricks according to statistical analysis using data from available experimental tests [17-27]*

(a)

(b)

(c)

Figure 2.2: *Bricks from "Type B" pallet (a) with one significantly damaged sample (b) and mortar cast in laboratory (c)*

Table 2.1: List of test, test standards and initial test setup per type ($_{ad}$= air dried;$_{od}$= oven dried)

Test	no.Tests	Standard	Precautions
Granulometry	3	BS 1377-2	Preliminary sieving
			H_2O_2 treatment
Moisture content	6	NT Build 333	Temperature at 85°C
Density	6	NT Build 333	Temperature at 85°C
Uniaxial compression	>7 (od)	UNI EN 772-1	Rectification
	>7 (ad)		Def.rate 2 mm/min
Three point bending	4 (ad)	UNI EN 12390-5	Rectification
			Def.rate 1 mm/min
			Wooden strip

Table 2.2: Mean values and standard deviations (in brackets) of the initial samples' geometry

	Length(L)	Width(W)	Height(H)
Type	*mm*	*mm*	*mm*
A	24.57 (0.26)	11.60 (0.21)	6.69 (0.06)
B	25.44 (0.17)	12.03 (0.18)	6.82 (0.20)
C	23.10 (0.20)	11.80 (0.21)	10.91 (0.30)
M	22.30 (0.00)	9.21 (0.00)	5.20 (0.10)

(a) (b)

Figure 2.3: *Soil sample (a) and fibres after sieving (b)*

2.3.1. PHYSICAL CHARACTERIZATION

GRANULOMETRIC TEST

Standard, Set up and Testing Procedures Three samples per type, extracted from randomly chosen bricks were pulverized and subjected to granulometric tests (Figure 2.3). Tests were performed according to standard BS 1377-2 [50]. However, the direct insertion of hydrogen peroxide in the solution before the hydrometer tests, as the procedure prescribes for a soil with organic content, was not a plausible option for Adobe. In fact, it appeared that a significant amount of fibres in the Adobe bricks causes unstable chemical exotermal reactions characterized by solution leakage. Thus, it was decided to apply a preliminary mechanical separation of the largest part of the organic content by means of 2mm sieving (Figure 2.3b). The subsequent chemical treatment was repeated three times in two days until no further reaction was noticed. The total loss in weight was registered.

Observations and Results For each test, the percentages of sand, silt and clay of the soil mixture were derived from the MIT classification system [51]. Also the relative amount of fibre by weight was calculated. The tests revealed the presence of a large variety of reinforcement materials in the same mixture, from straw to chopped wood. Therefore in the following the term fibre refers to whatever organic content present in the mixture.
The results are reported in Table 2.3 expressed as ranges of values for each type [13]. Furthermore, a graphical comparison of typical granulometric curves for each type of sample is reported (Figure 2.4).
Brick mixtures are characterized by high fibre content. In particular, Type B and Type C display similar reinforcement percentages but they significantly differ in soil composition. The soil of Type A and B is defined as a clayey sandy silt according to the MIT system, while Type C is a clay and silt with some sand. The amount of clay is similar for Type A and B but it is less than half its percentage presence in Type C. All brick mixtures show similar values in terms of silt percentage which is generally the dominant component of the mixture. Mortar samples contain a low percentage of fibre reinforcement with respect to bricks, and a mixture composition which is characterized by a high level of silt and a modest percentage of clay (sandy silt with some clay).

Table 2.3: Percentages of soil elements and fibre content by weight

	Clay	**Silt**	**Sand**	**Fibre**
Type	%	%	%	%*b.w.*
A	24-25	47-48	27-28	17-18
B	18-19	43-46	30-33	32-37
C	46-50	40-43	7-10	32-33
M	11-12	66-68	21-22	3-5

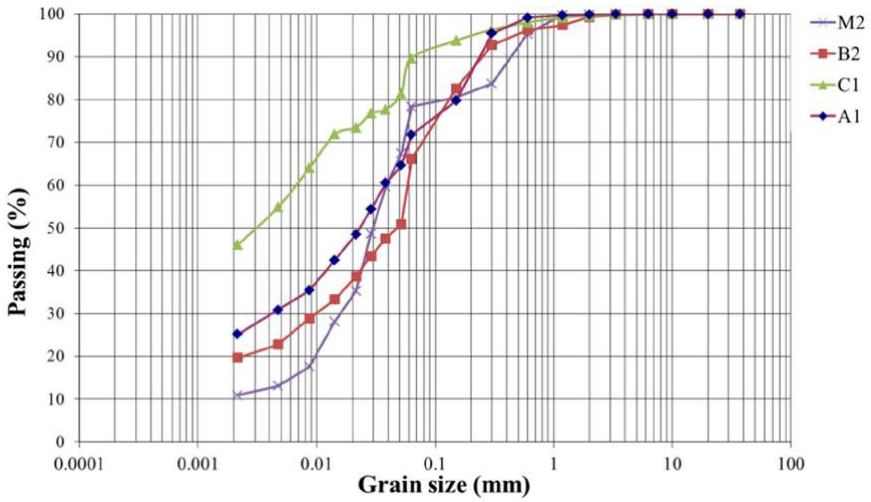

Figure 2.4: Examples of comparison in granulometric distributions for different types of Adobe mixtures

DRY DENSITY AND MOISTURE CONTENT TESTS

Standard, Set up and Testing Procedures Moisture content at laboratory conditions and density were determined according to NT Build 333 [52]. Six samples of each type were analysed.
It is worth mentioning that because of the unbaked nature of the bricks and mortar, the temperature of the oven was set at 85 degrees Celsius instead of the prescribed value of 105 degrees Celsius.

Observations and Results The density and moisture content results obtained from the tests are summarized in Table 2.4 in terms of mean values and related standard deviations.
Type B and C bricks have similar values of dry density, although the latter are characterized by higher uncertainty. Type A has higher values while mortar samples are more dense than the tested types of bricks.
At 28 days of air drying, Type M is also characterized by the lowest moisture content values, while for Type C the mean moisture content is almost twice the values associated to all other bricks. At the same conditions, the highest moisture content per dry mass is associated to the mixture with the highest clay content percentage (Type C). This was already observed in previous research on clay samples [53]. Type A and B bricks and the mortar may be classified as “dried” according to NZS standard [54], that assumes a range of 3-5% in terms of moisture content level for sun dried samples after 28 days of air curing.

Table 2.4: Mean values and corresponding standard deviations (in brackets) of dry density and moisture content at laboratory conditions for each type

	Density	Moisture Content
Type	kg/m^3	%
A	1233.9 (24.12)	3.25 (0.10)
B	799.3 (29.6)	3.89 (0.17)
C	821.5 (45.33)	6.36 (0.34)
M	1414.0 (25.1)	1.39 (0.04)

2.3.2. MECHANICAL CHARACTERIZATION

UNIAXIAL COMPRESSION TESTS

Standard, Set up and Testing Procedures Uniaxial compression tests were performed according to UNI EN 772-1 and the Australian code [48, 55]. Sample dimensions were decided after review of compression test standards for masonry materials in the literature, since the plate dimensions were not compatible with the initial geometry of the entire bricks. Samples with a height of 90 mm and slenderness ratio equal to two were tested. Prismatic samples were sawn from the corners of rectified entire bricks and surfaces in direct contact with the steel plates of a Universal machine were further rectified to ensure plane parallelism (Figure 2.5a). In order to analyse the mechanical response of adobe according to the drying process, half of the samples were oven dried at 85 Celsius degrees. Samples which were heavily damaged after the cutting process were not tested. Displacement controlled tests were performed using an Universal testing machine (Figure 2.5b). Deformation was recorded from the relative displacement of the steel plate, which was prescribed to descend at a speed rate of 2 mm/min. In the following paragraphs test results are reported for the different sample types and drying conditions in terms of cracking pattern and resulting force-displacement plots. Since the mechanical characterization is the ultimate goal of this paper, an entire section is devoted to this end while the raw data and visual observations are reported in the next paragraphs.
In the following paragraphs test results are reported for the different sample types and drying conditions in terms of cracking pattern and resulting force displacement plots. Since the mechanical characterization is the ultimate goal of this paper, an entire chapter is devoted to this end while the raw data and visual observations are reported in the next paragraphs.

Observations and Results For each test, the failure patterns were observed and the corresponding force (F) - displacement (d) diagram was recorded. They are reported in Figure 2.6 for each material type and drying condition.
Most of the tests revealed four different regions in the force-displacement curve, independently from type and drying condition (Figure 2.7). After an initial nonlinear phase, due to plate-top surface setting (not shown in Figure 2.7(a)), a linear elastic branch (I) is followed by a non linear hardening phase (II) until the attainment of the peak load, which

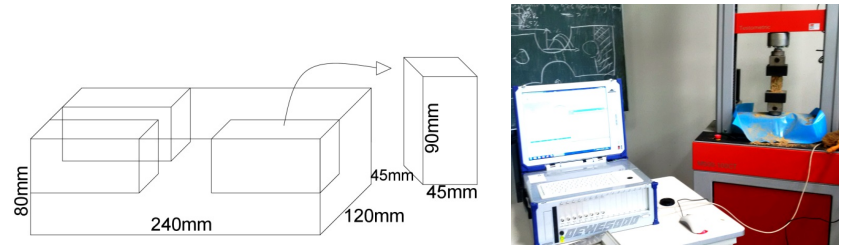

(a) (b)

Figure 2.5: *Mean geometrical dimensions of tested samples (a), and Universal testing machine (b)*

is followed by softening behaviour and collapse (III). Exceptions to the depicted F-d are ascribable to (few) samples with pronounced irregularities such as visible reinforcement concentration (Type B) or clay agglomeration (Type C) as showed in Figure 2.7(b-c).
Also a dominant cracking pattern was observed. In fact the failure mechanism of the majority of air and oven dried samples was characterized by diagonal cracking (Figure 2.8(a)). A first crack appeared nearby the opposite edges of both the frontal or lateral surfaces after the attainment of the peak load and cracks progressively spread in at least three surfaces of the sample. Almost all Type A specimens were characterized by this failure pattern. A similar mechanism was recognized in the majority of tests of Type M, which were also often characterized by exfoliation of the external layers of mortar (Figure 2.8(d)). Furthermore, in a not negligible number of samples from Type B (and sometimes in Type C), a main crack starting from the edges of opposite faces propagated all along the total height of the sample causing collapse by spalling (Figure 2.8(b-c)).

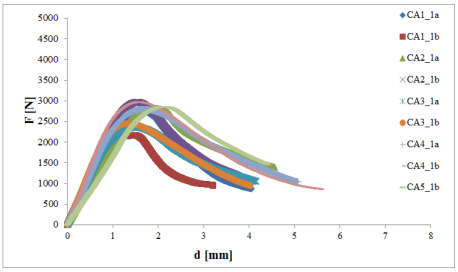

(a)

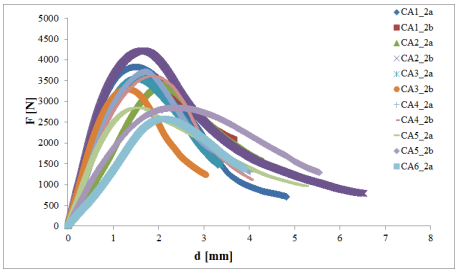

(b)

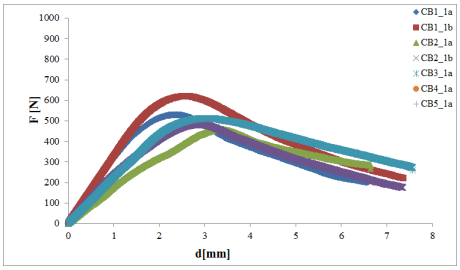

(c)

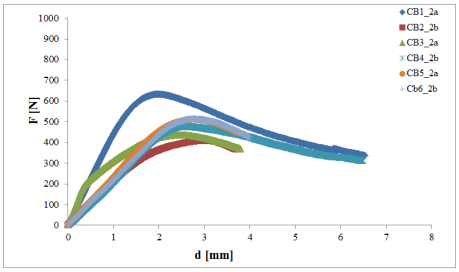

(d)

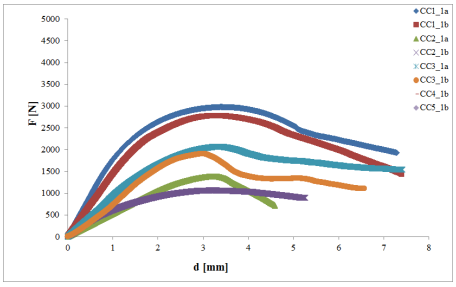

(e)

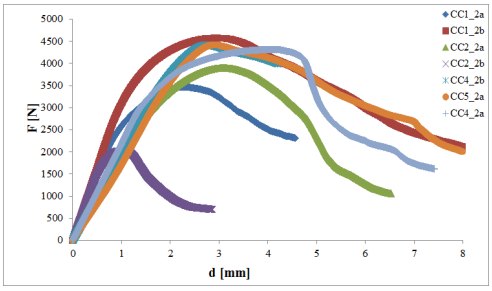

(f)

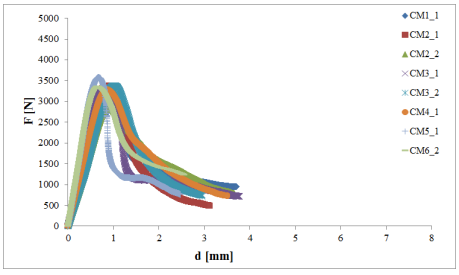

(g)

Figure 2.6: *Force (F)- displacement (d) curves for air-dried (left) and oven-dried (right) samples of Type A (a-b) B (c-d) C (e-f) and M (g)*

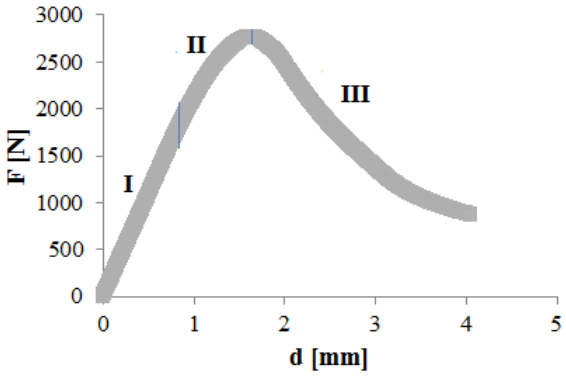

(a)

(b)

(c)

Figure 2.7: *Typical F-d regions in compression(a), Type B sample (CB21a) with visible piece of wood (b) and Type C sample (CC22b) with large voids*

The main mechanical parameters characterizing the material in compression were derived from each force displacement curve, for both air dried (Table 2.5) and oven dried (Table 2.6) samples. The compressive strength f_b is calculated normalizing the peak load of each curve with respect to the geometrical dimensions of the sample. Furthermore, also the unconfined compressive strength f_{bu} is calculated according to the Australian standard HB195[48]. The Young modulus E was calculated both as the secant modulus between strains at 5% and 33% of the peak strength E_{5-33} [56, 57] and as chord modulus at 60% of the peak strength E_{60} [57]. In deformation, the strain at peak strength ε_{f_b} and a ductility parameter d, defined as ratio between displacements at 80% of the strength in the post peak regime and peak load, were derived. These values are reported in the following Tables.

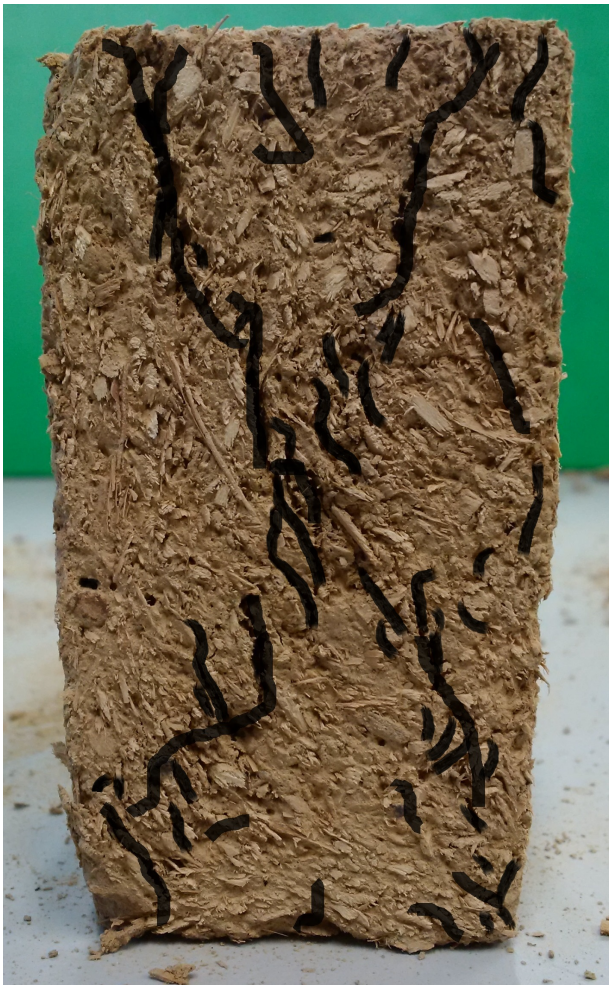

(a)

(b)

(c)

(d)

Figure 2.8: *Typical cracked surface in compression (a) and example of different failure mode for Type B (b), C(c), M(d) samples*

Table 2.5: Summary of results for air-dried Adobe bricks and mortar's mechanical properties

	f_b	f_{bu}	E_{5-33}	E_{60}	ε_{f_b}	d_u
Type	MPa	MPa	MPa	MPa	%	-
A	1.33 (0.13)	1.06 (0.13)	101.5 (16.1)	104.0(16.8)	1.9 (0.3)	1.4 (0.2)
B	0.24 (0.03)	0.19 (0.02)	11.5 (2.3)	11.2(2.5)	3.1 (0.3)	1.5 (0.1)
C	1.14 (0.40)	0.91 (0.33)	50.0 (23.0)	50.5(23.8)	3.4 (0.4)	1.5 (0.2)
M	1.61 (0.11)	1.29 (0.09)	205.8 (56.0)	204.9(52.6)	0.9 (0.2)	1.4 (0.1)
All	0.9	0.7	54.3	55.2	2.8	1.5

Table 2.6: Summary of results for oven-dried Adobe bricks and mortar's mechanical properties

	f_b	f_{bu}	E_{5-33}	E_{60}	ε_{f_b}	d_u
Type	MPa	MPa	MPa	MPa	%	-
A	1.71 (0.20)	1.38 (0.16)	141.0 (35.0)	140.3(34.9)	1.9 (0.3)	1.5 (0.1)
B	0.25 (0.04)	0.20 (0.03)	14.0 (6.4)	13.8(4.4)	2.9 (0.3)	1.6 (0.2)
C	1.91 (0.44)	1.53 (0.35)	109.6 (29.3)	108.5(26.9)	3.0 (0.9)	1.5 (0.4)
All	1.3	1.0	88.2	87.6	2.6	1.5

(a)

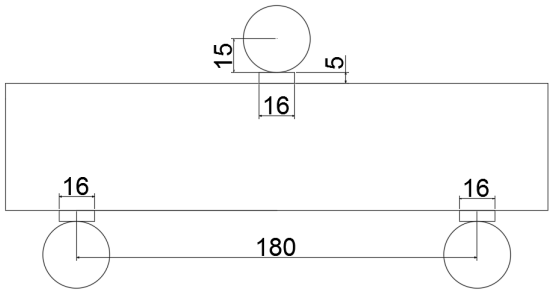

(b)

Figure 2.9: *Three point bending test setup with indication of geometrical dimensions in mm (b)*

THREE POINT BENDING TEST

Standard and testing procedures Three point bending tests were performed according to UNI EN 12390-5 [58] on entire air-dried bricks. The horizontal surfaces were rectified in order to ensure plane parallel surfaces.
Two further corrections were applied in the test setup. The bottom and upper 3 cm diameter steel rolls were interposed by 5mm thick ply wooden strips approximately 16 mm long, equal to the maximum thickness of the samples (Figure 2.9). The strips were added in order to avoid possible indendation on Adobe due to the large difference in stiffness between the steel rolls and Adobe. At the end of the tests, the wooden strips were slightly concave, but no sample showed indentation. The span (s) in each test follows the prescriptions of the adopted standard. Furthermore, a low displacement rate of 1mm/min was applied in order to avoid dynamic effects during the test.

Observations and Results For each test, the failure mechanisms were observed and the corresponding force (F) - displacement (d) diagram was recorded. They are shown in Figure 2.10 according to each type. In all tests, the plot revealed two distinct regions. An elastic phase until peak load, characterized by a dominant linear branch with possible slight pre peak damage (Type B), and a post peak softening response of exponential shape. In samples M, the attainment of the peak load corresponds to a sudden stop of machine records, which refers to possible snap back behaviour, followed by a residual strength tail (Figure 2.10(d)).
Failure was characterized by the formation and propagation of a single crack. It appeared at the bottom side of the front and rear faces, corresponding to the loading upper roll (Figure 2.11) and it very quickly propagated through the thickness.
As exceptions to this trend, in two tests of type C, two different cracks were formed at the bottom of the front and rear faces of the bricks, not aligned with the vertical of the upper roll, without coalescence in the middle of the bottom face (sample 2 and 3 in Figure 2.11(c)).

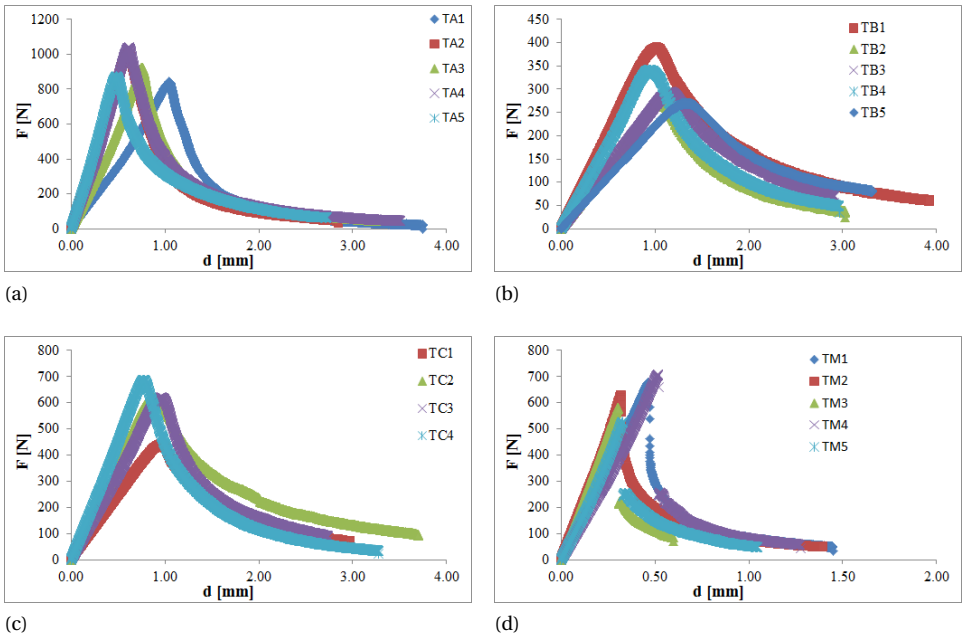

(a) (b)

(c) (d)

Figure 2.10: *Force - Displacement curves for air dried Type A(a), B(b), C(c) and M(d)*

The main mechanical parameters characterizing the material in tension were derived from each force displacement curve. The tensile strength (f_t) and the flexural modulus (E_t) were calculated according to elastic material hypothesis, which is considered an acceptable approximation. The parameters are calculated according to the following equations:

$$\begin{cases} f_t = \dfrac{3F_{max}s}{2th^2} \\ E_t = \dfrac{3F_{max}s^3}{4th^3d_{F_{max}}} \end{cases} \tag{2.1}$$

where the peak load (F_{max}) and the displacement at peak load ($d_{F_{max}}$) with the geometrical dimensions in thickness (t) and height (h) were input. The mean values are reported in Table 2.7 together with the resulting mean mechanical parameters calculated.

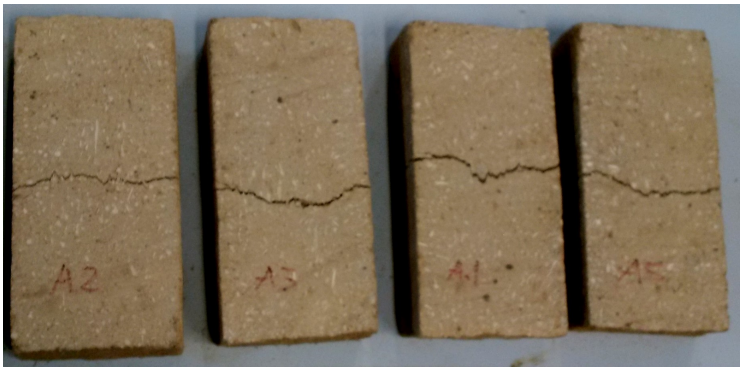

(a)

(b)

(c)

(d)

Figure 2.11: *Failure mode in bending tests for air dried Type A(a), B(b), C(c) and M(d): view of the bottom face*

Table 2.7: Derivation of mechanical parameters in tension for air-dried Types

	l	t	h	F_{max}	$d_{F_{max}}$	f_t	E_t
Type	*mm*	*mm*	*mm*	*N*	*mm*	*MPa*	*MPa*
A	244	115	57	958 (64)	0.60 (0.10)	0.69 (0.05)	108.2(16.0)
B	256	122	55	314 (46)	1.10 (0.13)	0.23 (0.03)	20.9 (4.3)
C	230	110	51	592 (91)	0.90 (0.10)	0.59 (0.12)	72.9 (17.7)
M	233	91	52	624 (65)	0.40 (0.10)	0.70 (0.10)	192.2 (23.4)

2.4. STATISTICAL ANALYSIS ON RESULTS

The previous chapter resumed the results of the mechanical characterization campaign on Adobe samples made with different soil element composition at different drying conditions. The information contained has been already used for research on the mechanical performance of Adobe [17, 59]. This chapter is meant to deepen the analysis in order to quantify the influence of the physical properties of the mixture on the mechanical performance in compression of the resulting Adobe components. Moreover, as for masonry materials, the relationships between strength and Young's modulus in compression and the corresponding parameters in tension were also investigated. Statistical analyses were used to this end. The results are presented in the following subdivided for compression and tension.

2.4.1. PARAMETERS IN COMPRESSION

Considering all tests, the compressive strength ranges between 0.21 MPa (CB22b) and 2.26 MPa (CC12b). The mean mechanical parameters corresponding to each type and drying conditions reported in Table 2.5-6 are shown in graphical form in Figure 2.13. Considering air dried samples, strength significantly differs for the four types of constituent proportions. Mortar has the highest values in terms of compressive strength and stiffness while samples belonging to Type B show the lowest performance. In particular, the mean compressive strength for Type B is not within the range indicated in the Australian earth building book for Adobe elements (1-5 MPa) [48] and it does not meet the lower threshold for unconfined strength requirement as it is prescribed by the New Zealand standard for Adobe bricks (the least unconfined strength value out of five tests above 0.9 MPa) [45, 60]. Comparing the strength values from Table 2.5-6, the effect of curing conditions is also immediately recognizible. For all types, the mean compressive strength of oven dried bricks is higher than the corresponding air dried ones, but the proportion of increment varies among mixtures (Figure 2.13). Possible systematic relations between the aforementioned physical factors and the resulting compressive strength value for Adobe components were statistically investigated. To this end, it was decided to test a law recently proposed to address the influence of moisture content on the strength of modern unfired clay bricks [61, 62]. The compressive strength at a given moisture content is given by eq 2.2:

$$f_{ba} = Aw^{-B} \tag{2.2}$$

where f_{ba} is the air-dried strength, w is the moisture content, B is an unit-less positive constant and A is a stress dependent term depending on the type of soil particle in the mixture and increasing with clay amount [61]. In the present analysis, it was decided to link the stress unit term A to the compressive strength f_{bo}, which is investigated according to the granulometry proportions of each type. Considering the mean values in terms of relative moisture content and strength for each type of brick, multivariate statistical analysis resulted in best fit formulations for the oven dried strength f_{bo} and for the material coefficient b, both as functions of mixture elements percentages according to eq.2.3:

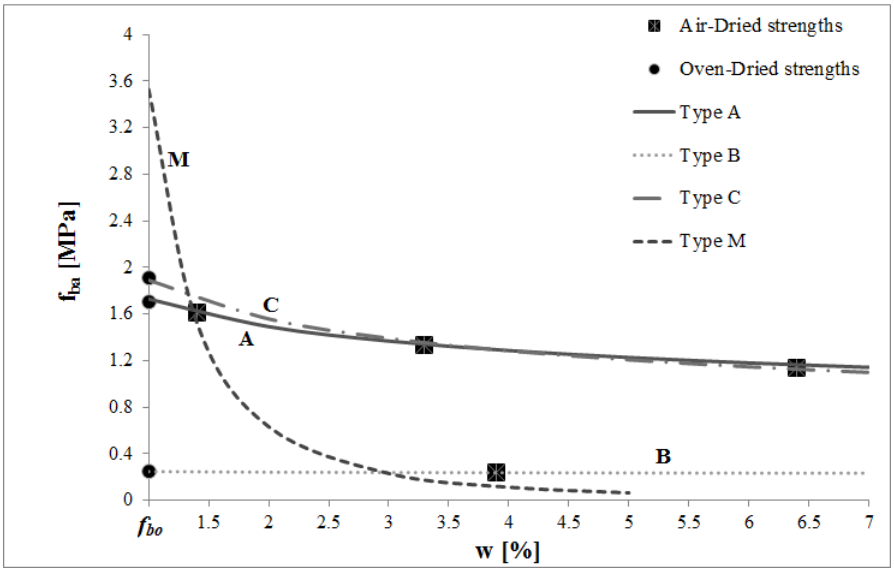

Figure 2.12: Predicted compressive strength laws for each type as a function of water content using eq.2.2 calibrated in eq. 2.3 and comparison with experimental values for each type and drying conditions.

$$\begin{cases} A(\equiv f_{bo}) = 1.8\left(\dfrac{clay(\%)}{1+fiber(\%)}\right) - 0.7 \\ \\ b = 0.8\%e^{2.5\left(\dfrac{clay(\%)}{1+fiber(\%)}\right)} \end{cases} \tag{2.3}$$

According to eq.2.3, the stress term f_{bo} increases with the amount of clay as shown in [61]. However, in case of adobe, it appears to also be dependent on the fiber percentage, which weakens the overall strength.

The theoretical trends of Adobe compressive strength as a function of moisture content according to eq.2.2-3 are plotted for each type of brick in Figure 2.12, together with the mean experimental values of the air-dried and oven-dried compressive strengths values (Table 2.5-6). The theoretical air dried and oven dried compressive strength values were calculated using eq.2.3. The results are reported in Table 2.8. Considering all types of bricks, the relative errors with respect to experimental values are always below 1%.

Furthermore, as a final validation a blind prediction was performed. The formulation in eq.2.2 calibrated with respect to bricks in eq.2.3 was used to predict the compressive strength at laboratory condition of Adobe mortar. The theoretical trend is also plotted in Figure 2.12 togheter with the ones associated to Adobe bricks. The resulting compressive strength value of 1.53 MPa at 1.4% moisture content reported in Table 2.8 is close to the average experimental one and it lies within the standard deviation associated to Type M (Figure 2.13).

Considering all tests, elastic stiffness ranged between 7.7 MPa (CB21a) and 289 MPa

Table 2.8: Predicted and experimental mean compressive strengths both for air dried and oven dried Adobe

	$f_{b_{a_{calc}}}$	$f_{b_{a_{exp}}}$	$f_{b_{o_{calc}}}$	$f_{b_{o_{exp}}}$
Code	MPa	MPa	MPa	MPa
A	1.34	1.33	1.73	1.71
B	0.24	0.24	0.25	0.25
C	1.14	1.14	1.89	1.91
M	1.53	1.61		

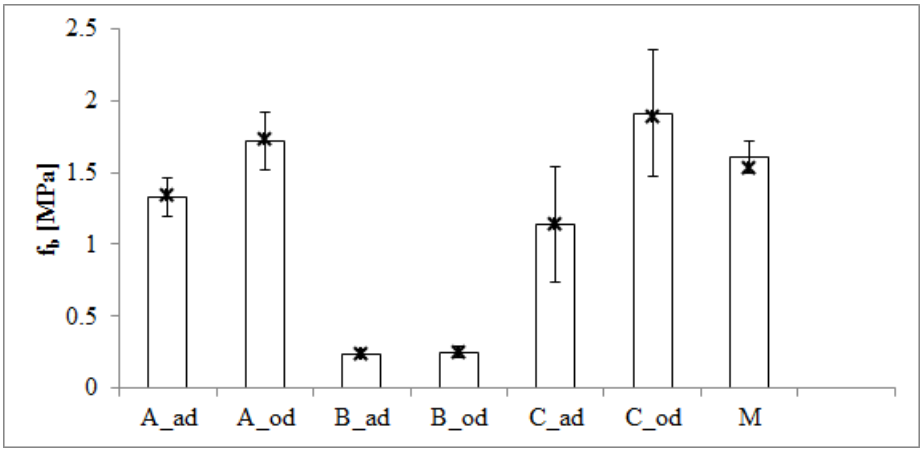

Figure 2.13: Experimental mean values and standard deviations of sun dried ($_{ad}$) and oven dried ($_{od}$) bricks and mortar and predicted values of strength (x cross) according to eq.2.1-3

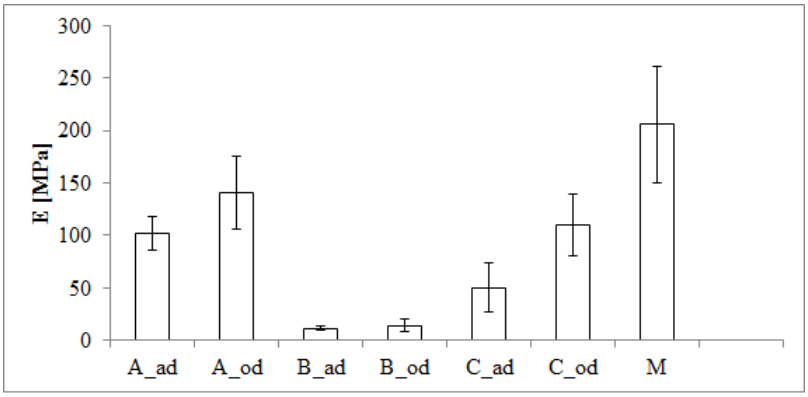

Figure 2.14: Experimental elastic stiffness mean values and standard deviations of sun dried ($_a$) and oven dried ($_o$) bricks and mortar according to the different type of soil

(CM51) (Table 2.5-6). Values show little discrepancy considering the two different formulations proposed to calculate the elastic stiffness (E_{60} and E_{5-33} in Table 2.5-6). Therefore, in the following only the latter column is analyzed and it is simply referred to as E (Figure 2.14). The same influence in terms of drying conditions and mixture proportions on strength is observed in terms of stiffness (Figure 2.14). The Young's modulus was investigated according to the following relationship for unreinforced masonry [63]:

$$E = k f_b \tag{2.4}$$

where k is a coefficient that can significantly vary in literature [64]. Within the performed tests on Adobe, a different slope is revealed considering mortar or bricks. Considering all bricks, both air-dried and oven-dried tests, an average slope of k=66.2 is found with a discrete correlation factor and a minor difference between the oven-dried and the air-dried bricks (Figure 2.15a). On the other hand, including also the mortar in the analysis, the best fit of the slope increases to k=79.4, with a correlation factor r^2 = 0.55 (Figure 2.15b). In both cases, the slope is significantly lower than the ratio between strength and elasticity modulus prescribed by codes for Adobe for walls (k=300) [60].

Considering all tests, the deformation at peak stress ranged between 0.7% (CM62) and 4.5% (CC42) mm/mm (Table 2.5-6). An analysis of strain capacity revealed no significant differences between air-dried and oven-dried samples, especially considering the high scatter that characterizes Type C (Figure 2.16a). Instead, the mean strain at peak stress was significantly different among types, with the highest performance associated to both Type B and Type C and with the lowest for mortar. The dependency of this mechanical parameter with respect to the soil mixture composition was statistically investigated. This leads to a best fit formulation of ϵ_{f_b} dependent only on fiber content. Calibrated with respect to oven dried values, it resulted in the relation given in eq.2.5:

$$\epsilon_{fb} = 7\% fiber(\%) + 0.7 \tag{2.5}$$

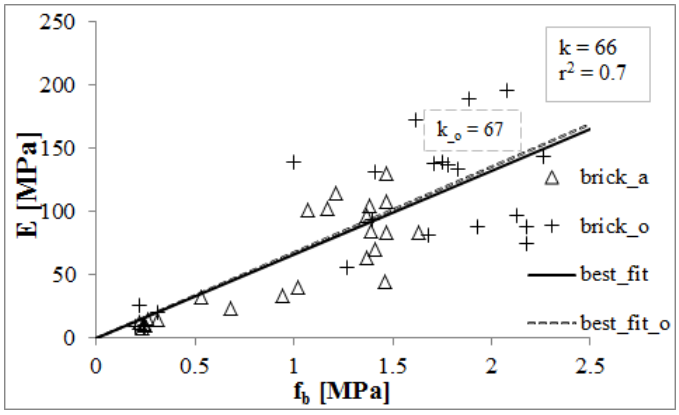

(a)

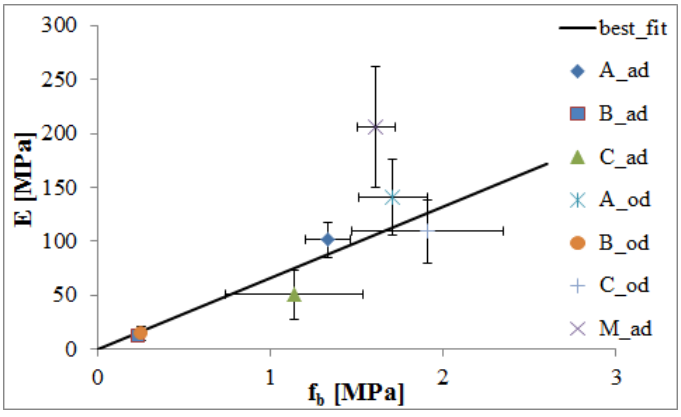

(b)

Figure 2.15: *Elasticity-Strength values considering only bricks (a) and mean E-fb values with standard deviations associated to each Type, including mortar (b)*

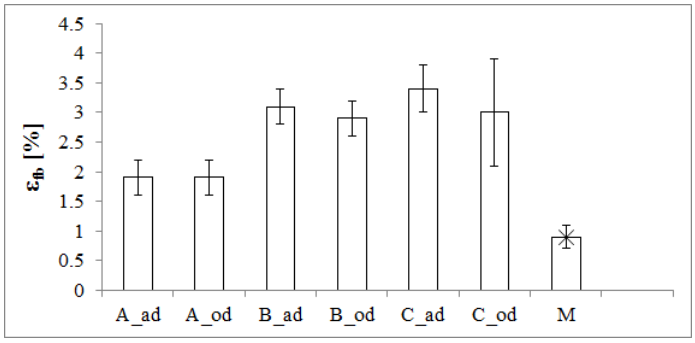

(a)

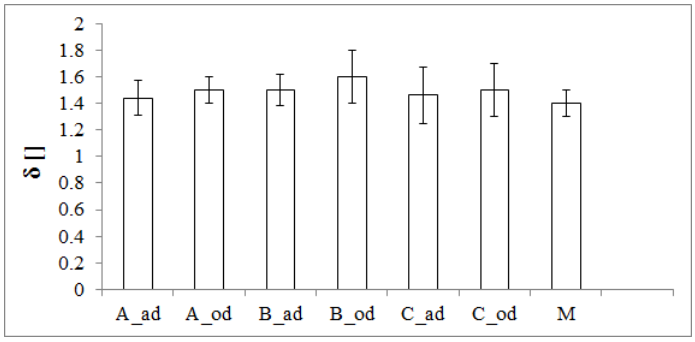

(b)

Figure 2.16: *Mean values and standard deviations of strain at peak stress and predicted deformation at peak stress for mortar according to eq.2.5 (a) and ductility (b) for each type and drying condition*

Table 2.9: Predicted strain at peak strength and relative errors with respect to experimental mean values for each Type

Code	$\varepsilon_{fb_{cal}}$ %	$\varepsilon_{fb_{exp}}$ %
A	1.9	1.9
B	2.9	3.1
C	3.0	3.0
M	0.9	0.9

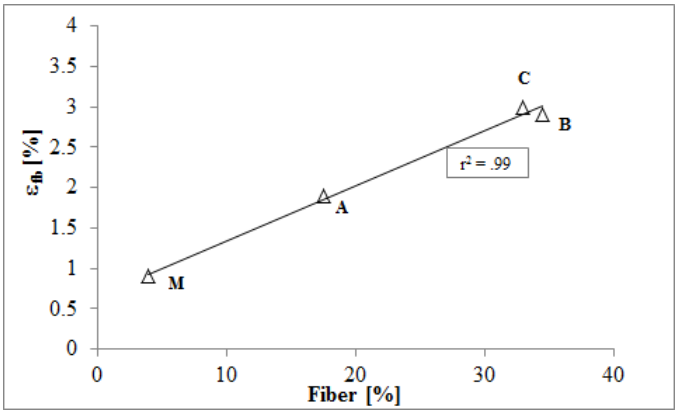

Figure 2.17: *Deformation at peak stress as function of fiber reinforcement percentage for bricks and mortar: experimental values and analytical formulation*

The formulation provides a good correlation with respect to bricks performance (Figure 2.17). Also in this case, a blind prediction was performed using eq.2.5 for mortar and an appreciable match was obtained (Table 2.8, Figure 2.16a).

Ductility was almost a constant parameter among all tests, independent of drying condition and mineralogical composition, ranging between 1.4 and 1.6 (Figure 2.16b).

2.4.2. PARAMETERS IN TENSION

Only air-dried samples were subjected to three point bending tests. Considering all tests, the flexural strength ranged between 0.2 (TB2) and 0.8 (TM4) MPa. The mean values for each material components in Figure 2.18a. All mean values are in the typical range for bending strength required for Adobe (0.1-0.5 MPa) in the Australian standard [48]. Only Type B did not meet the requirement for Adobe bricks provided by the New Zealand Code in tension (minimum value of strength from individual flexural tests above 0.25 MPa) [60].
The flexural stiffness ranged between 14.7 (TB5) and 226 (TM2) MPa (Figure 2.18b). Also in tension, a relationship between strength and elasticity was investigated in the form of eq.2.4. A slope of k=138 was found considering all bricks while the introduction of mortar in the analysis increases the slope to k = 191 with a decay of accuracy (Figure 2.19).
As in compression, strength and stiffness varied significantly with soil mixture proportions (Table 2.9). Plotting for each type the mean strength in tension vs the corresponding unconfined strength in compression, the best fit slope considering all the tests was approximately to 0.6. This value slightly increased to 0.64 if mortar was excluded from the analysis, with an increase in accuracy (Figure 2.20a). In both cases, the found slope was higher than the typical range indicated for Adobe in the New Zealand Standard, where flexural strength lies between 10% and 20% of the compressive strength [60]. Finally, proceeding with a similar approach as for elastic moduli, a clear correlation was found within the tested samples, with an almost unitary slope (k=0.98) (Figure 2.20b)

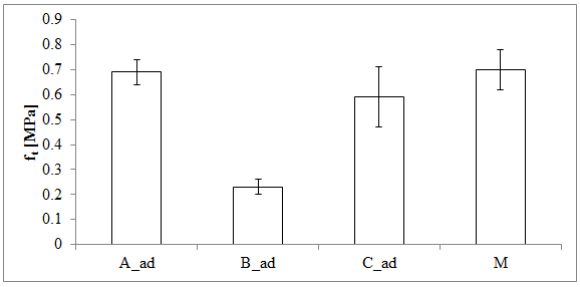

(a)

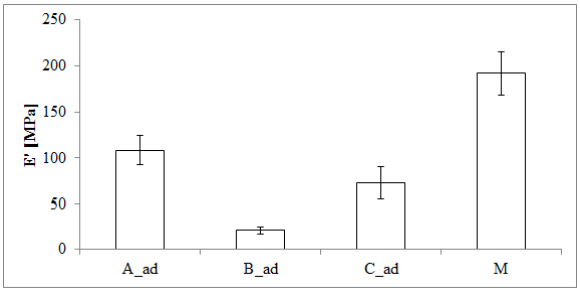

(b)

Figure 2.18: *Mean values and related standard deviation of flexural strength (a) and stiffness (b) for all the Types and drying conditions*

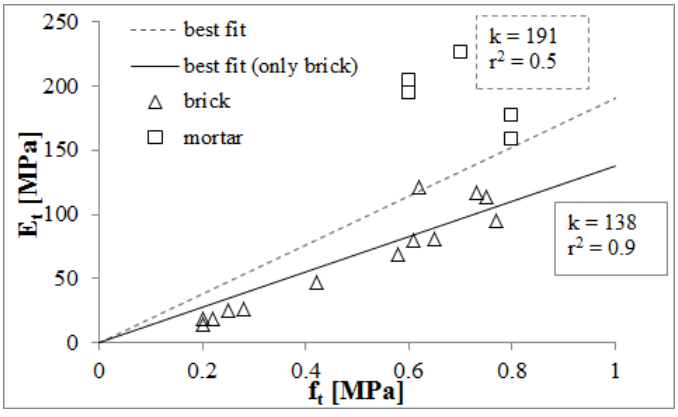

Figure 2.19: Flexural stiffness-strength values considering all tests or only bricks

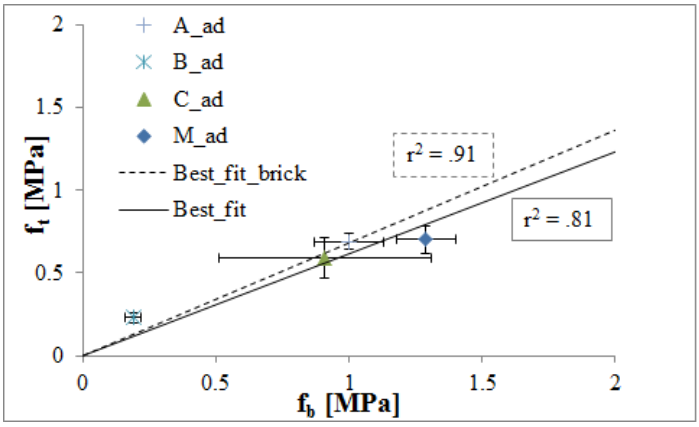

(a)

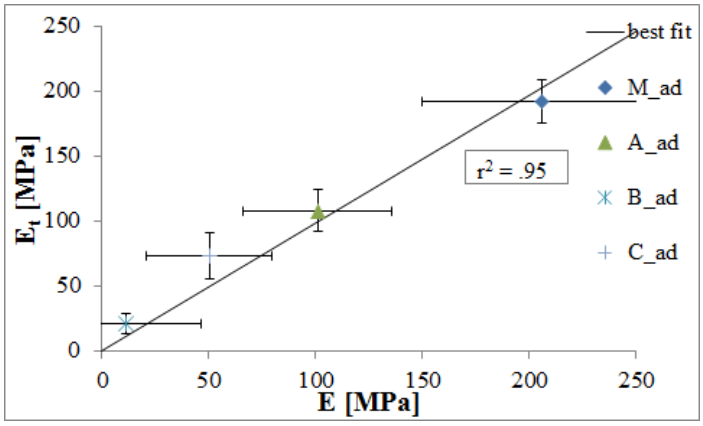

(b)

Figure 2.20: *Mean flexural-compressive strength considering only air-dried bricks or also mortar (a) and mean flexural-compressive stiffness considering all air dried types (b)*

2.5. CONCLUSIONS AND FINAL RECOMMENDATION

An experimental characterization campaign was conducted on three types of bricks and one mortar with different mixture components proportions from the same mineralogical family, produced in Europe with the same production process. The resulting mechanical properties were statistically investigated in order to determine possible relations with respect to the physical properties of the mixture. The research revealed the important influence that its physical state has on the mechanical performance of the resulting adobe component, leading to the definition of predictive formulations in strength and deformation. The compressive strength of adobe components at a given moisture content was predicted adapting a law used for unbaked clay bricks. According to the formulation, the air-dried compressive strength is inversely related to the water content of the mixture and directly proportional to the fully dried compressive strength value. Furthermore, the compressive strength of adobe improved increasing the ratio between clay and fiber reinforcement percentages. Although the inclusion of fiber within the soil mixture resulted in a reduction of the strength of adobe, it enhanced the deformability of the material. A predictive formulation for the compressive strain at peak stress was found dependent only on fiber percentages in the mixture and independent of its water content. It is worth noting that the found laws are strictly valid for the tested types of adobe and their general applicability should be confirmed experimentally through further investigations accounting for different types of mineralogical families, reinforcement typologies, and soil and fiber elements' proportions.

However, the formulations for strength and strain in compression proposed in this study, calibrated according to results on bricks, were determined to be valid also for assessing the mechanical performance of one type of mortar tested, which shared similar failure modes and force-displacement slopes. These trends reveal that in the case of adobe, the feature of structural heterogeneity typical of modern masonry is no longer valid. Both bricks and mortar of this traditional masonry belong to the same material class, and they share the same general properties. These are only determined by the mineralogical composition and granulometry proportions of the adopted mixture.

Among the tested samples, Type A assured the best compromise in terms of strength and ductility performance. This resulted from a better proportion between clay and fiber percentage. In general, the research demonstrates that an optimal combination of soil element proportions and fiber reinforcement capable of providing both adequate levels of strength and deformation capacity can exist and be determined. This does not necessarily comply with the recommendations in terms of soil mixture proportions contained in standards developed in different countries, which are based on the results of specific types of soil and production methods.

In Europe, designing codes are urgently needed for the rehabilitation of existing structures of adobe (present in many countries including Germany, Italy, France and Portugal) but also for the design of new buildings according to the growing principles of "sustainable architecture." The normative effort should start from the study and evaluation of standards for the execution and interpretation of granulometry tests on adobe soil with respect to the resulting mechanical parameters. This issue is still not sufficiently addressed within the existing legislative tools, and it is often neglected in scientific re-

search.

REFERENCES

[1] A. Costa, J. M. Guedes, H. Varum, Structural Rehabilitation of Old Buildings, Buildings Pathology and Rehabilitation (2014) 350arXiv:arXiv:1011.1669v3, doi:10.1007/978-3-642-39686-1.

[2] P. W. Brown, J. R. Clifton, The properties of Adobe, International Institute for Conservation of Historic and Artistic Works, Taylor & Francis, Ltd. 23 (1978) 139–146.

[3] Alberti, De Re Aedificatoria, 1443.

[4] D. Silveira, Al., Mechanical properties of adobe bricks in ancient constructions, Construction and Building Materials 28 (1) (2012) 36–44. doi:10.1016/j.conbuildmat.2011.08.046.
URL http://dx.doi.org/10.1016/j.conbuildmat.2011.08.046

[5] H. Danso, D. Martinson, M. Ali, J. Williams, Physical, Mechanical, Durability Properties of soil building blocks reinforced with natural fibres, Construction and Building Materials 101 (1) (2015) 797–809.

[6] A. Agarwal, Mud as a Traditional Building Material, The Changing Rural Habitat; edited by Brian Brace Taylor. Singapore: Concept Media/Aga Khan Award for Architecture 1 (1975) 137–146.

[7] L. E. Yamin, C. A. Phillips, J. C. Reyes, D. M. Ruiz, Seismic Behavior and Rehabilitation Alternatives for Adobe and Rammed Earth Buildings, 13 th World Conference on Earthquake Engineering (2942) (2004) 10.

[8] D. Silveira, H. Varum, A. Costa, Influence of the testing procedures in the mechanical characterization of adobe bricks, Construction and Building Materials 40 (March) (2013) 719–728. doi:10.1016/j.conbuildmat.2012.11.058.

[9] A. Anand, Non-Engineered Construction in Developing Countries – an, in: 12 Wcee Conference, Vol. 91, 2000, pp. 1–22.

[10] A. Arya, T. Boen, Y. Ishiyama, Guidelines for earthquake resistant non-engineered construction, no. iv, UNESCO, 1986.

[11] G. Minke, Building with earth: Design and Technology of a sustainable architecture, BirkhauserarXiv:arXiv:1011.1669v3, doi:10.1017/CBO9781107415324.004.

[12] F. Champiré, A. Fabbri, J. C. Morel, H. Wong, F. McGregor, Impact of relative humidity on the mechanical behavior of compacted earth as a building material, Construction and Building Materials 110 (2016) 70–78. doi:10.1016/j.conbuildmat.2016.01.027.

[13] R. Illampas, I. Ioannou, D. C. Charmpis, Adobe bricks under compression : Experimental investigation and derivation of stress – strain equation, Construction and Building Materials 53 (2014) 83–90. doi:10.1016/j.conbuildmat.2013.11.103.
URL http://dx.doi.org/10.1016/j.conbuildmat.2013.11.103

[14] R. Aguilar, M. Montesinos, S. Uceda, Mechanical characterization of the structural components of Pre-Columbian earthen monuments: Analysis of bricks and mortar from Huaca de la Luna in Peru, Case Studies in Construction Materials 6 (2017) 16–28. doi:10.1016/j.cscm.2016.11.003.
URL http://dx.doi.org/10.1016/j.cscm.2016.11.003

[15] E. W. Smith, Adobe bricks in New Mexico, Circular 188, New Mexico Bureau of Mines and Mineral Resources (1982).

[16] M. Larcher, M. Peroni, G. Solomos, N. Gebbeken, P. Bieber, J. Wandelt, N. T. Tran, Dynamic Increase Factor of Masonry Materials: Experimental Investigations ISIEMS 2013, Postdam, September (2013).

[17] T. Li Piani, L. Koene, J. Weerheijm, L. Sluys, The Ballistic Resistance of Adobe Masonry: An analytical model for penetration in soil bricks and mortar 17th ISIEMS, Bad Neuenahr, Germany, (2017).

[18] A. Heine, M. Wickert, Scale-independent description of the rigid-body penetration of spherical projectiles into semi-infinite adobe targets, International Journal of Impact Engineering 75 (2015) 27–29. doi:10.1016/j.ijimpeng.2014.07.009.
URL http://dx.doi.org/10.1016/j.ijimpeng.2014.07.009

[19] G. Austin, Adobe as a building material, New Mexico Bureau of Mines and Mineral Resources, Socorro (1984) 69–71.

[20] A. Caporale, F. Parisi, D. Asprone, R. Luciano, A. Prota, Comparative micromechanical assessment of adobe and clay brick masonry assemblages based on experimental data sets, Composite Structures 120 (2015) 208–220. doi:10.1016/j.compstruct.2014.09.046.
URL http://dx.doi.org/10.1016/j.compstruct.2014.09.046

[21] J. W. Garrison, E. F. Ruffner, Adobe, practical & technical aspects of adobe conservation, The Journal of Arizona History 25 (1983) 448–450.

[22] E. Quagliarini, S. Lenci, The influence of natural stabilizers and natural fibres on the mechanical properties of ancient Roman adobe bricks, Journal of Cultural Heritage 11 (3) (2010) 309–314. doi:10.1016/j.culher.2009.11.012.

[23] E. Adorni, E. Coïsson, D. Ferretti, In situ characterization of archaeological adobe bricks, Construction & Building Materials 40 (2013) 1–9. doi:10.1016/j.conbuildmat.2012.11.004.
URL http://dx.doi.org/10.1016/j.conbuildmat.2012.11.004

[24] S. Yetgin, O. Cavdar, A. Cavdar, The effects of the fiber contents on the mechanic properties of the adobes, Construction and Building Materials 22 (222-227). doi:10.1016/j.conbuildmat.2006.08.022.

[25] E. Baglioni, F. Fratini, L. Rovero, the Materials Utilised in the Earthen Buildings Sited in the Drâa Valley (Morocco): Mineralogical and Mechanical Characteristics, IX Seminario Iberoamericano de Construcción con Tierra (9º SIACOT), (May 2016).

[26] D. Liberatore, G. Spera, M. Mucciarelli, M. R. Gallipoli, D. Santarsiero, C. Tancredi, Typological and Experimental Investigation on the Adobe Buildings of Aliano (Basilicata , Italy), Structural Analysis of Historical Constructions Constructions (January) (2006) 851–858.

[27] C. Galán-marín, C. Rivera-gómez, J. Petric, Clay-based composite stabilized with natural polymer and fibre, Construction and Building Materials 24 (8) (2010) 1462–1468. doi:10.1016/j.conbuildmat.2010.01.008.
URL http://dx.doi.org/10.1016/j.conbuildmat.2010.01.008

[28] F. Wu, G. Li, Strength and stress – strain characteristics of traditional adobe block and masonry, Materials and Structures 46 (2013) 1449–1457. doi:10.1617/s11527-012-9987-y.

[29] D. Silveira, H. Varum, A. Costa, Influence of the testing procedures in the mechanical characterization of adobe bricks, Construction and Building Materials 40 (March) (2013) 719–728. doi:10.1016/j.conbuildmat.2012.11.058.

[30] F. Fratini, E. Pecchioni, L. Rovero, U. Tonietti, The earth in the architecture of the historical centre of Lamezia Terme (Italy): Characterization for restoration, Applied Clay Science 53 (3) (2011) 509–516. doi:10.1016/j.clay.2010.11.007.

[31] F. Parisi, D. Asprone, L. Fenu, A. Prota, Experimental characterization of Italian composite adobe bricks reinforced with straw fibers, Composite Structures 122 (July) (2015) 300–307. doi:10.1016/j.compstruct.2014.11.060.

[32] F. Fratini, E. Pecchioni, L. Rovero, U. Tonietti, The earth in the architecture of the historical centre of Lamezia Terme (Italy): Characterization for restoration, Applied Clay Science 53 (3) (2011) 509–516. doi:10.1016/j.clay.2010.11.007.

[33] C. H. Kouakou, J. C. Morel, Strength and elasto-plastic properties of non-industrial building materials manufactured with clay as a natural binder, Applied Clay Science 44 (1-2) (2009) 27–34. doi:10.1016/j.clay.2008.12.019.
URL http://dx.doi.org/10.1016/j.clay.2008.12.019

[34] Y. Millogo, M. Hajjaji, R. Ouedraogo, Microstructure and physical properties of lime-clayey adobe bricks, Construction and Building Materials. 22.

[35] A. A. Hammond, Prolonging the life of earth buildings in the tropics, Building Research and Practice 1 (3) (1973) 154–163. doi:10.1080/09613217308550234.

[36] H. Binici, Investigation of fibre reinforced mud brick as a building material, Construction and Building Materials 19 (2005) 313–318. doi:10.1016/j.conbuildmat.2004.07.013.

[37] J. Vargas, J. Bariola, M. Blondet, P. K. Mehta, Seismic strength of adobe masonry, Materials and Structures 19 (4) (1986) 253–258. doi:10.1007/BF02472107.

[38] H. Binici, O. Aksogan, M. N. Bodur, E. Akca, S. Kapur, Thermal isolation and mechanical properties of fibre reinforced mud bricks as wall materials, Construction and Building Materials 21 (4) (2007) 901–906. doi:10.1016/j.conbuildmat.2005.11.004.

[39] M. Bouhicha, F. Aouissi, S. Kenai, Performance of composite soil reinforced with barley straw, Cement & Concrete Composites 27 (2005) 617–621. doi:10.1016/j.cemconcomp.2004.09.013.

[40] H. Danso, B. Martinson, M. Ali, J. Williams, Effect of fibre aspect ratio on mechanical properties of soil building blocks, Construction & Building Materials 83 (2015) 314–319.

[41] M. M. S. Islam, K. Iwashita, Seismic Response of Fiber-Reinforced and Stabilized Adobe Structures, Proceedings of the Getty Seismic Adobe Project 2006 Colloquium 11 (3) (2006) 13.

[42] Y. Millogo, J. C. Morel, J. E. Aubert, K. Ghavami, Experimental analysis of Pressed Adobe Blocks reinforced with Hibiscus cannabinus fibers, Construction and Building Materials 52 (January) (2014) 71–78. doi:10.1016/j.conbuildmat.2013.10.094.

[43] A. Vatani Oskouei, M. Afzali, M. Madadipour, Experimental investigation on mud bricks reinforced with natural additives under compressive and tensile tests, Construction and Building Materials 142 (2017) 137–147. doi:10.1016/j.conbuildmat.2017.03.065.
URL http://dx.doi.org/10.1016/j.conbuildmat.2017.03.065

[44] Resultaten miniMOUT: effect van veroudering op ballistische weerstand van adobe muren met twee steensterkten, TNO Report, Tech. rep., TNO (2013).

[45] California Code of Regulations for Adobe in New Constructions (2011).

[46] New Mexico Earthen Building Materials Code - Title 14, Chapter 7 (Part 4),2004.

[47] NZS 4298 (1998): Materials and workmanship for earth buildings [Building Code Compliance Document E2 (AS2)] (1998).

[48] HB 195 - 2002 The Australian earth building handbook-Standards Australia International, NSW 2001 (2001).

[49] UNI EN 772-16: Metodi di prova per elementi di muratura. Parte 16: Determinazione delle dimensioni (2005).

[50] BS 1377-2:1990 Methods of test for soils for civil engineering purposes. Classification tests.

[51] D. Shah, A. Shroff, Soil Mechanics and Geotechnical Engineering, CRC Press, 2003.

[52] NT Build 333: Bricks and masonry blocks: Moisture content (1988).

[53] S. K. Vanapalli, D. G. Fredlund, D. E. Pufahl, The influence of soil structure and stress history on the soil-water characteristic of a compacted till, Geotechnique 49 (2) (1999) 143–159.

[54] NZS 4298, NZS 4298 (1998): Materials and workmanship for earth buildings, New Zealand Technical Committe 4298 (1998) 91.

[55] UNI EN 772-1:2015 “Metodi di prova per elementi per muratura - Parte 1: Determinazione della resistenza a compressione”.

[56] R. Drysdale, A. Hamid, L. Baker, Masonry Structures: behaviour and design, The Masonry Society, Boulder, Colorado, United States, Boulder, Colorado, 1999.

[57] EN 1052-1:2002 Methods of test for masonry - Part 1: determination of compressive strength. Brussels: European Committee for Standardization (CEN), 2002.

[58] NEN-EN 12390-5 Testing hardened concrete Part 5:Flexural Strength of test specimens (2009).

[59] T. Li Piani., J. Weerheijm., L. Koene, L.J. Sluys, The Adobe delta damage model, Computational Modelling of Concrete Structures (EURO-C 2018), CRC Press, 2018.

[60] New Zeland Standards, NZS 4297 (1998): Engineering design of earth buildings NZS 4297 (1998) 63.

[61] A. Heath, P. Walker, C. Fourie, M. Lawrence, Compressive strength of extruded unfired clay masonry units, Proceedings of the Institute of Civil Engineers Construction Materials 162 3 162 (3) (2009) 105–112. doi:10.1680/coma.2009.162.3.105. URL http://dx.doi.org/10.1680/coma.2009.162.3.105

[62] E. J. d. P. Hansen, K. Kielsgaard Hansen, Unfired clay bricks - moisture properties and compressive strength, in: A. Gustavsen, J. V. Thue (Eds.), Proceedings of the 6th Symposium on Building Physics in the Nordic Countries, Vol. 2, Norwegian University of Science and Technology, 2002, pp. 453–460.

[63] European Committee for Standardization (CEN), "Eurocode 6:Design of masonry structures-Part1-1: General rules for unreinforced and reinforced masonry structures", 2005.

[64] R. Lumantarna, D. T. Biggs, J. M. Ingham, D. M. Asce, J. M. Ingham, M. Asce, Uniaxial Compressive Strength and Stiffness of Field-Extracted and Laboratory-Constructed Masonry Prisms, Journal of Materials in Civil Engineering 26 (4) (2014) 567–575. doi:10.1061/(ASCE)MT.1943-5533.0000731.

3

THE NUMERICAL SIMULATION OF ADOBE IN STATICS

"Be rejoicing in hope,
patient in tribulation,
persistent in prayer."

Romans 12:12

A local damage model is proposed for the numerical assessment of the static performance of Adobe masonry components. The model was applied to simulate the experimental behaviour of sundried soil bricks and mud mortar tested in uniaxial compression and bending. Numerical simulations of the model are made mesh objective by means of a rate dependent regularization algorithm in statics. This is achieved using a generalization of the damage delay concept based on a decomposition of the Dirichlet boundary condition. It allows non-dimensionality of model parameters mathematically needed to prevent loss of ellipticity of the equilibrium equations of the model. The entire regularization algorithm is integrated within an implicit Newton-Raphson solver.

This chapter is based on "The Adobe delta damage model: A locally regularized rate-dependent model for the static assessment of soil masonry bricks and mortar" in *Engineering Fracture Mechanics*, 2018.

3.1. INTRODUCTION

The complexity of natural and man-made hazard scenarios in current society from which buildings in urban environments must be protected, requires the development of efficient interpretative tools [1, 2]. This task is translated in the field of computational mechanics into the need for effective material and structural models which demonstrate numerical robustness, computational efficiency and physical consistency. Industry and research face a serious challenge when continuum damage mechanics is adopted to simulate the response of quasi brittle materials, such as concrete, commonly used for civil constructions. In fact, quasi brittle materials are typically characterized by softening behaviour, that is the slope of the post peak stress region is negative [3, 4]. This happens because the material is progressively degraded by the stemming and coalescence of internal microcracks bridging into macro-cracks [5, 6]. Interpreting failure as a progressive degradation of the elastic stiffness of the material, continuum damage mechanics constitutes a numerical approach conceptually close to the phenomenology of quasi brittle materials [4, 7]. However, this class of models suffers from a serious numerical pathology named mesh dependence [8]. That is, numerical simulations of softening materials result into localization of damage within the smallest area allowed by the spatial discretization of the material domain [9]. This happens because the boundary value problem becomes ill posed, due to loss of ellipticity of the governing equations of equilibium [3, 10]. As a consequence, results of numerical simulations using local damage models depend on the adopted discretization, both in terms of extension of failure regions and force displacement diagrams, depicting a progressively more brittle response upon mesh refinement.

Mesh sensitivity is a well known issue and several numerical treatments, defined as regularization methods, have been developed over the years [5]. All methods imply the introduction of localization limitizers (or length scale) in the local model, meant to prevent hyperbolicity of the equilibrium equations to occur and differently introduced according to the adopted strategy of regularization [11]. Unfortunately in most cases, these algorithms solve mesh dependence at the expense of the aforementioned requirements needed for an effective numerical model. The use of a nonlocal model is the most popular regularization method nowadays [3, 12]. The general principle is that the stress at a given integration point is not uniquely determined by the history of the strain at this point, but also by the mutual interactions with nearby ones [13, 14]. Despite being usually effective in obtaining mesh objective simulations, nonlocal models often imply non standard code developments, difficult parameter identification procedures and inadequacies close to free boundaries, besides extra computational costs inherent to nonlocal models [15, 16]. As an alternative, gradient models may also be employed to solve mesh dependence. They prescribe enrichment of the equilibrium equations with extra gradients of the state variables to solve ill posedess of the boundary value problem. Similar to the use of non local models, numerical simulations using gradient models are often prone to a broadening of the damage field, which does not resemble the response of many brittle materials, unless the internal length scale is made dependent on the local strain or stress [17], that in turn often results in additional computational costs [7]. On the other hand, rate dependent models have been proposed to solve mesh dependence keeping the strain at each material point independent of the nearby ones [3]. In gen-

eral, this is done by implementing viscosity (rate dependent) functions directly in the governing equilibrium equations. Theoretically, the use of rate is still the most computationally efficient and physically consistent strategy to solve mesh dependency in the case of quasi brittle building materials sensitive to rate, such as concrete [5]. Unfortunately, only a limited number of these models proved to provide full regularization to damage models [5]. Using rate to restore ellipticity of the governing equations is a challenge especially in case of quasi-static simulations. This also counts for well known local regularization models [8]. A local damage model based on the last μ model for concrete structures [18] was recently developed by Pereira et al. [2] to simulate concrete. Among the conclusions, it was stated that rate functions within the equilibrium equations only have a weak regularization role and instead a nonlocal algorithm was supplemented [18].

In the current study, a numerical algorithm based on rate dependency is presented, which is integrated within the constitutive laws of the local model of [2], with the coupled aim of mesh regularization in statics and material property [19]. This is obtained by generalizing the concept of damage delay introduced by Allix et al., in which a certain delay after damage initiation is defined while keeping its rate bounded [20, 21]. The generalization is based on a decomposition of the Dirichlet boundary conditions, which allows the parameters of the rate functions mathematically needed to regularize the model to be non-dimensional, and not necessarily time-dependent [22]. Thus, they can be calibrated from experimental tests performed in statics.

Many commercial software packages available nowadays use explicit solution schemes to approximate the solution of the partial differential equations of equilibrium at each step of a numerical simulation. They are easy to implement and computationally efficient but they need restricted time steps. On the contrary, besides harder implementation costs, only implicit solvers enforce equilibrium at each iteration, assuring robust and accurate evaluations of the state of the system. Thus, integration of equations of equilibrium of the regularized model has been implemented within a Newton-Raphson solver, which provides robusteness to the resulting new algorithm. The model was called "Adobe delta damage model" because it has been applied for the static assessment of the mechanical performance of Adobe components.

Adobe is a traditional masonry whose bricks made of sundried mixtures of soil with reinforcing natural fibre are joined together using mud mortar [23]. As a consequence of a lack of knowledge on the physical-mechanical performance of Adobe, no adequate numerical models have been developed for Adobe and only a few attempts to numerically simulate the constitutive response of bricks and mortar of Adobe were found in literature [24]. This situation occurs because this building technology was progressively abandoned starting from industrial revolutions in favour of modern materials introduced in the construction market [25]. Nevertheless, in recent times Adobe has gained scientific interest, as a result of a specific socio-economic conjuncture [26]. Earthen buildings, which provide shelter to more than one third of the world population constituting 10% of the built heritage [27], are spread in areas of the world prone to natural hazards or involved into military operation, with the related treats for human beings and their property. Moreover, attractive thermal and acoustic material properties make Adobe still a suitable building technology for Western countries involved within enviromental impact reduction tasks inherent building industry production processes [28]. Several ex-

perimental campaigns were performed by the authors on Adobe over the last five years, ranging from granulometry tests on soil mixtures to impact tests on walls [26, 29, 30]. The research led to the conclusions that Adobe can be regarded as a quasi brittle geomaterial of the same class as concrete, with a pronounced influence of soil granulometry on the overall mechanical performance [31, 32]. The new numerical model herein presented was adopted to simulate the static response of Adobe bricks and mortar subjected to uniaxial compression and three point bending tests in [26].

The Adobe delta damage model is presented in the following. Mesh objectivity of the model is demonstrated in the third section. Next, the model is applied to simulate the response of Adobe bricks and mortar in static tests performed by the authors in [26].

3.2. THE ADOBE DELTA DAMAGE MODEL

The “Adobe delta damage model" is presented in this chapter. Implementation of the model starts from the classical formulation for isotropic damage in eq.3.1 [33]:

$$\sigma = (1-D)\tilde{\sigma} \quad \text{with} \quad \tilde{\sigma} = E : \varepsilon \,, \tag{3.1}$$

where $\tilde{\sigma}$ is the effective stress vector, ε is the strain vector, E the elastic stiffness tensor and D is the damage scalar, a parameter which ranges between 0 (integer material) and 1 (fully damaged material). Damage starts when the loading function f in eq.3.2 becomes negative:

$$f = k_0 - \varepsilon_{eq} \,, \tag{3.2}$$

where ε_{eq} and k_0 are the equivalent strain and the damage initiation strain, respectively. A modified Drucker-Prager damage loading surface is adopted in the model like in [2, 18]. Two equivalent strain functions for compression crushing (ε_{eq_c}) and tensile cracking (ε_{eq_t}) are expressed as a combination of the first (I_ε) and second deviatoric (J_{ε_d}) invariants of strain [34]. In eq.3.(3-4), they are presented within the octraedical space, as a combination of its normal (ε_{oct}) and tangential (γ_{oct}) components as in soil mechanics [35]:

$$\begin{cases} \varepsilon_{eq_t} = c_1\varepsilon_{oct} + c_2\gamma_{oct} \\ \varepsilon_{eq_c} = c_3\varepsilon_{oct} + c_4\gamma_{oct} \end{cases} \tag{3.3}$$

in which:

$$\begin{cases} \varepsilon_{oct} = \dfrac{1}{3} I_\varepsilon = \dfrac{\varepsilon_1 + \varepsilon_2 + \varepsilon_3}{3} \\ \gamma^2_{oct} = -\dfrac{8}{3} J_{\varepsilon_d} = \dfrac{4}{9}[(\varepsilon_1 - \varepsilon_2)^2 + (\varepsilon_2 - \varepsilon_3)^2 + (\varepsilon_3 - \varepsilon_1)^2] \end{cases} \tag{3.4}$$

where subscripts $_{1,2,3}$ denote principal values of the strain tensor. Parameters $c_1 - c_4$ are defined as [18]:

$$\begin{cases} c_1 = \frac{1}{(1-2\nu)} \\ c_2 = \frac{1}{2\sqrt{2}(1+\nu)} \\ c_3 = \frac{3}{5(1-2\nu)} \\ c_4 = \frac{3\sqrt{3}}{5\sqrt{2}(1+\nu)} \end{cases} \tag{3.5}$$

where ν is the Poisson's ratio.
Evolution of damage is directly related to the growth of two monotonic internal variables which account for the historical maximum equivalent strains reached during loading history. They are implemented separately for compression (k_c) and tension (k_t) according to [36]:

$$\begin{cases} k_c(i) = \max[\, \varepsilon_{eq_c}(1-r^\alpha), k_{0c}(\tau)] \quad \text{for all} \quad i \geq \tau \\ k_t(i) = \max[\, \varepsilon_{eq_t} r^\alpha, k_{0t}(\tau)] \quad \text{for all} \quad i \geq \tau \end{cases} \tag{3.6}$$

Where r is derived from the triaxiality factor proposed by Lee and Fenves [37] for multiaxial loading states, α is a constant set to 0.1 as in [2] and the mechanical parameters k_{0t} and k_{0c} are the damage initiation strains in tension and compression [34].
The value of damage in eq.3.7 combines two damage evolution laws in compression (D_c) and tension (D_t) as in [2], in which the respective equivalent strains enter:

$$D = 1 - (1 - D_c^{RD})(1 - D_t^{RD}) \tag{3.7}$$

where RD stands for rate dependent (regularized).
Both evolution laws in compression and tension start from rate independent softening functions generalized as combinations of exponential and linear softening showed in eq.3.8 [2]:

$$(D)_{c,t}^{RI} = 1 - \frac{1}{e^{A_{c,t}(k_{c,t} - k_{0_{c,t}})}} - \frac{k_{0_{c,t}}}{B_{c,t} k_{c,t}} \tag{3.8}$$

Where A and B are material parameters and RI stands for rate independent.
To address mesh dependence without introducing non locality in the model as in [36], the concept of bounded damage rate is adapted [22]. This consists of introducing a certain delay after local damage initiation while keeping the rate of damage bounded [15, 38]. Originally developed for composite laminates, the concept is considered to be suitable to address failure of quasi brittle materials used for masonry. In the model for adobe, the local damage evolution laws in compression and tension are then made directly dependent on the loading history based on a decomposition of the Dirichlet boundary condition. Given an arbitrary displacement law evaluated in N points by the Newton-Raphson solver, at each progressive step i of the analysis after damage initiation, both the loading evolution laws in compression and tension enter rate dependent functions (RD) according to eq. 3.9, in order to account for a "*delta*"(δ) increment based on the prescribed loading history:

$$D_{c,t_i}^{RD} = \delta D_{c,t_i} + D_{c,t_{i-1}}^{RD} \tag{3.9}$$

Table 3.1: Ranges of tested values using the “Adobe delta Damage Model” for mesh sensitivity analysis

Parameter	**Value**	**Parameter**	**Value**
E, E_t	10-250 MPa	$A_{c,t}, B_{c,t}$	25-1000
k_{0c}, k_{0t}	0.3-1.5%	$\Delta_{c,t}$	3-500
ν	0.0-0.15	$\frac{k_{0d}}{k_0}$	10-30%

where the delta functions δD at each step are calculated using a function of exponential shape as in [20] modified according to eq.3.10:

$$\delta D_{c,t_i} = \frac{\Delta_{c,t}}{N}(1 - e^{-(D^{RI}_{c,t_i} - D^{RD}_{c,t_{i-1}})}) \tag{3.10}$$

in which the Adobe delta damage model, Δ represents a further non-dimensional material parameter and N is needed to make the results independent of discretization of the applied law. The regularizing properties of the model come from the exponential damage-delay functions and will be demonstrated in Sec. 3.3
The set of governing equations are integrated within an implicit Newton-Raphson solver. The code has been developed in C++ environment using the opensource libraries of JemJive [39].

3.3. MESH SENSITIVITY ANALYSIS

This chapter demonstrates the mesh objectivity of the “Adobe delta damage model" in statics. Four different tests commonly used in literature to diagnose the mesh sensitivity are adopted [3, 40]. The analysed tests are an uniaxially loaded tapered bar, a shear layer test, a shear band test and a cantiveler beam test in bending. They are used to verify the local damage distribution and the global reaction force plots for different levels of mesh refinement. The first two are classical tests from literature which analyse the unidirectional performance of the model. The latter two reproduce physical problems characterized by complex stress states.
Mesh dependence was analysed for wide ranges of variations of elastic (E, ν) and inelastic (Δ, A, B) parameters of the model in compression ($_c$) and tension ($_t$), consistently with ranges of mechanical values found in literature for Adobe [19] (Table 3.1). In the following paragraphs, examples of results obtained from specific combinations are shown for each test.
Four node plane stress elements are used in the model. A value of N=2000 and a precision of $10e^{-5}$ is prescribed to the implicit solver.

3.3.1. UNIAXIALLY LOADED TAPERED BAR TEST

A classical test from theory widely used to diagnose mesh dependence is the tapered cantilever bar uniaxially loaded [3]. The response of a tapered bar to uniaxial compression is analysed. A displacement is applied at the free edge of a 100mm long bar fixed at the bottom (Figure 3.1). In order to trigger localization, a 3% tapering is applied along

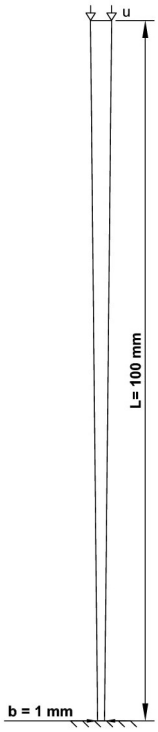

Figure 3.1: Setup for mesh sensitivity study for the uniaxially loaded tapered bar test: geometry and boundary conditions

the height of the bar starting from 1mm thickness. The mesh of the bar is progressively refined starting from 10 up to 160 elements. The results of this analysis for progressive mesh refinement are shown in the following in terms of global reaction-displacement plots (Figure 3.2) and local damage profiles along the bar (Figure 3.3). They correspond to the following set of values inserted as mechanical parameters of the model: A_c=60, B_c=0, Δ_c = 5, ν =0.0, E=150 MPa, k_{0_c}=1.0%.
Force displacement plots nearly overlap, with maximum relative errors lower than 1% (Figure 3.4(a)), while the damage profile is consistent for all meshes during the entire simulation (Figure 3.4(b)).

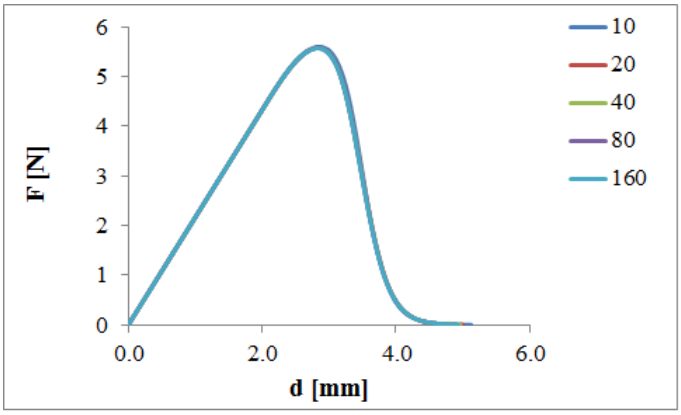

Figure 3.2: Force-displacement diagrams for progressive mesh refinement for the uniaxially loaded tapered bar test

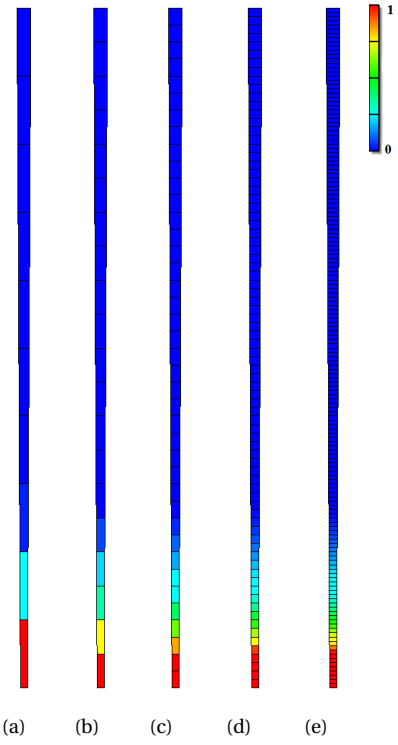

Figure 3.3: Damage profile for progressive mesh refinement for the uniaxially loaded tapered bar test at d=4.0mm

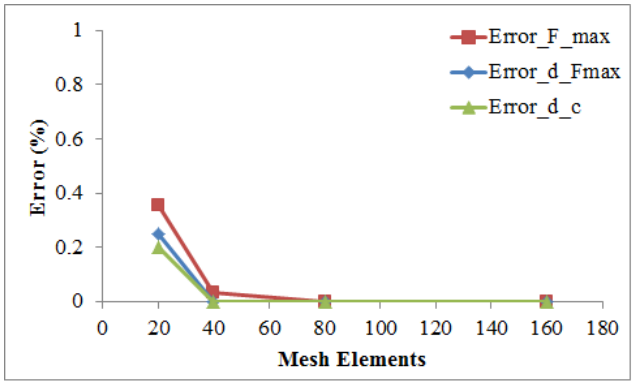

(a)

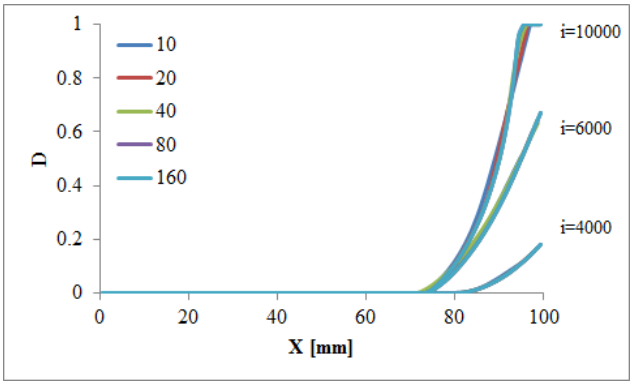

(b)

Figure 3.4: Relative errors in terms of maximum reaction force (F_{max}), displacement at peak load ($d_{F_{max}}$) and strain at 20% decay of reaction (d_c) for different mesh elements (a) and damage profile along the bar at different stage of simulations (i) (b)

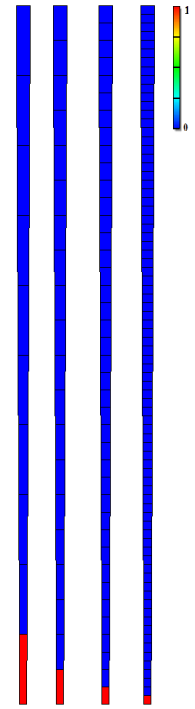

(a)

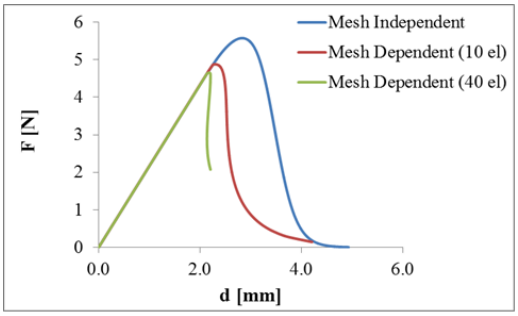

(b)

Figure 3.5: Damage profile for progressive mesh refinement for the uniaxially loaded tapered bar test using the rate independent local model (a) and comparisons of force-displacements graphs for progressive mesh refinement with respect to mesh independent solution (b)

Analysis of results yields the conclusion that the model is capable of producing mesh independent simulations and good results are obtained already with the coarsest mesh. For explanatory purposes, the performance of the Adobe delta damage model is compared with respect to the corresponding rate independent version. Results confirm the numerical pathology of the local model. The damage distribution and force displacement plots depict a not-consistent progressively more brittle behaviour upon mesh refinement (Figure 3.5).

3.3.2. SHEAR LAYER TEST

Another test performed to verify mesh dependence is the shear layer transversally loaded (Figure 3.6) [10, 41]. The response of the model in pure shear is analysed. A thick column fixed at its bottom and constrained vertically along the height is subjected to a shear load at the free edge at the top. The set up is given in Figure 3.6. In order to trigger localization, a mechanical imperfection is inserted along the first 10mm of the beam in terms of a 15% decrease of the damage initiation strain. The mesh of the shear column is progressively refined starting from 10 elements up to 160.

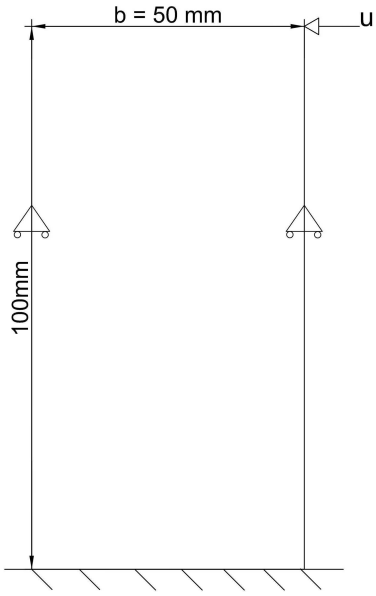

Figure 3.6: Setup for mesh sensitivity study for the shear layer test: geometry and boundary conditions

The results for progressive mesh refinement are shown in Figure 3.7(a) in terms of overall reaction-displacement plots and in Figure 3.7(b) in terms of failure damage profile along the bar. They correspond to the following set of mechanical parameters of the model: A_c=100, B_c=0, A_t=0, B_t=100, Δ_c = 6, Δ_t = 6, ν =0.0, E=200 MPa, k_{0_c}=0.6%, k_{0_t}=0.6%. Force displacement plots nearly overlap and the damage profiles match for the different meshes.
The analysis is mesh independent and good results are obtained already for the coarsest mesh.

3.3.3. SHEAR BAND TEST

Specimens under compression are usually characterized by the formation of shear bands. The mesh objective determination of shear bands is of primary interest [42]. A constrained cube of 50x50mm is compressed at the top in Figure 3.8. A shear band is triggered by a mechanical imperfection introduced by a 30% reduction of the damage initiation strain, in the left bottom corner in the grey region in Figure 3.8. The first mesh is chosen to have one element included in the weakest region and progressive mesh refinement is adopted.
The results of the mesh refinement analysis are shown in the following in terms of reaction-displacement plots (Figure 3.9(a)) and failure damage distribution within the specimen (Figure 3.9(b)). They correspond to the following set of values inserted as mechanical parameters of the model: A_c=250, B_c=0, A_t=0, B_t=100, Δ_c = 9, Δ_t = 9, ν =0.1, E=200 MPa, k_{0_c}=0.7%, k_{0_t}=0.2%.
Also in a shear band test, the model is capable of performing simulations in a mesh ob-

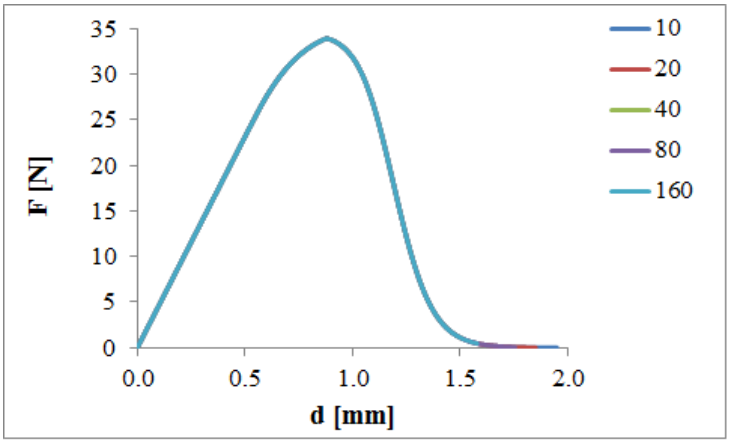

(a)

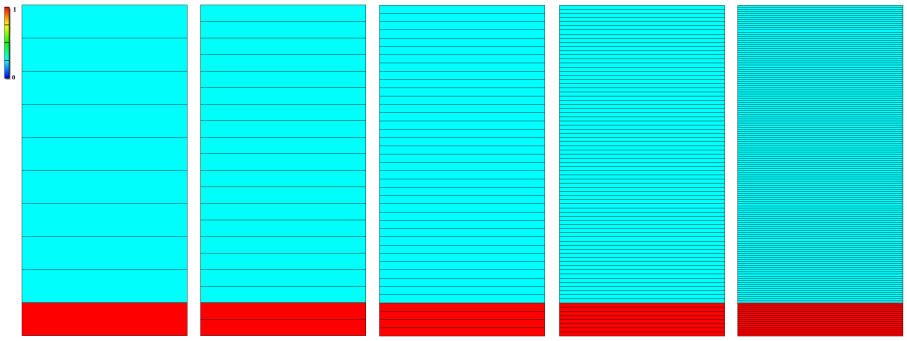

(b)

Figure 3.7: Force displacement (a) and damage profile at d = 1.5 mm (b) for progressive mesh refinement for the shear layer test

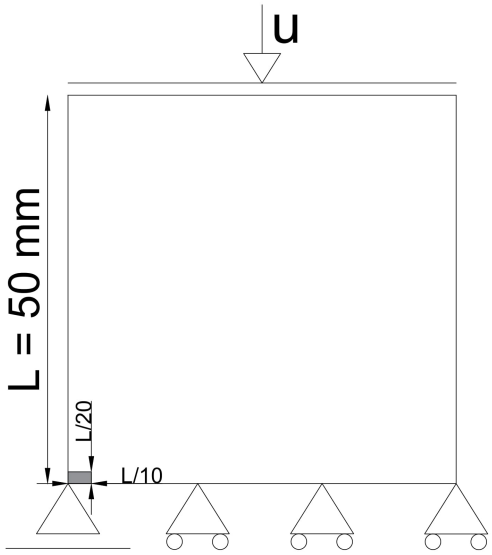

Figure 3.8: Setup for mesh sensitivity study for the shear band test: geometry and boundary conditions

jective manner.

3.3.4. CANTILEVER BEAM IN BENDING

The last test verifies the numerical response of the model in bending. A slender cantilever beam (L/b=4) is subjected to a distributed transversal load at the free edge (Figure 3.10). Due to the stress distribution, neither a geometrical nor a mechanical imperfection is used to trigger localization.
Results using the same mesh refinements as in the shear band test are demonstrated in terms of reaction-displacement plots (Figure 3.11(a)) and failure damage distribution within the specimen (Figure 3.11(b)). They correspond to the following set of values inserted as mechanical parameters of the model: A_c=500, B_c=5, A_t=500, B_t=0, Δ_c = 6, Δ_t = 6, ν =0.1, E=350 MPa, k_{0_c}=0.4%, k_{0_t}=0.2%.
Mesh objectivity is again confirmed.

3.3.5. PARAMETER SENSITIVITY ANALYSIS

This paragraph briefly presents a parameter sensitivity analysis of the model. The uniaxially loaded tapered bar presented in Sect. 3.3.1 is used for variation of the parameter A for the same mesh of 20 elements (Figure 3.12 (a-b)). The original parameter A=60 is doubled and halved. Similary, results of an analysis using half and double values of the original Δ=5 are presented in (Figure 3.12 (c-d)). From both analyses, it is evident that by increasing the values of the numerical parameters, brittleness is enhanced demonstrated by a steeper softening post-peak branch and more localized damage. This effect is more pronounced for a variation of A than for Δ (Figure 3.12 (e-f)).
All analyses confirmed to be mesh independent already for the coarsest discretization

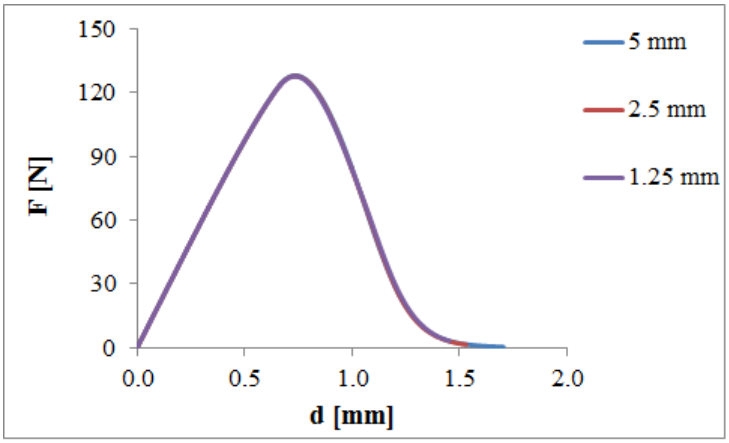

(a)

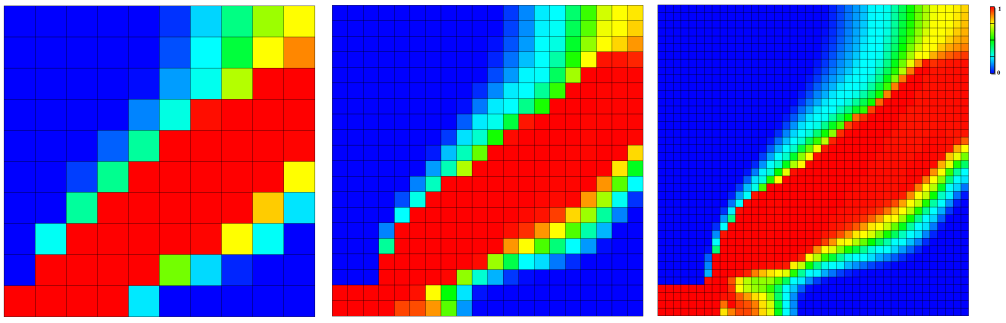

(b)

Figure 3.9: Force displacement (a) and damage profile at d = 1.3 mm (b) for progressive mesh refinement in the shear band test

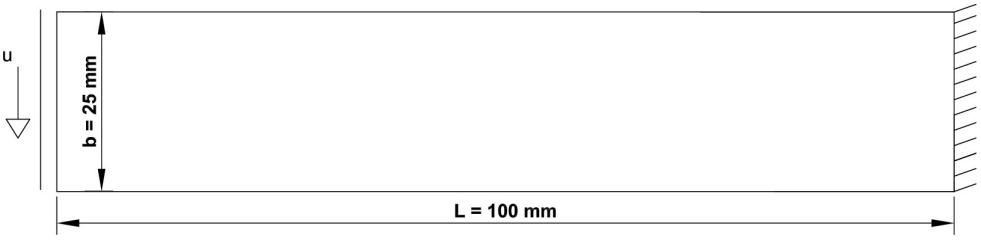

Figure 3.10: Setup for mesh sensitivity study for the cantilever bending test: geometry and boundary conditions

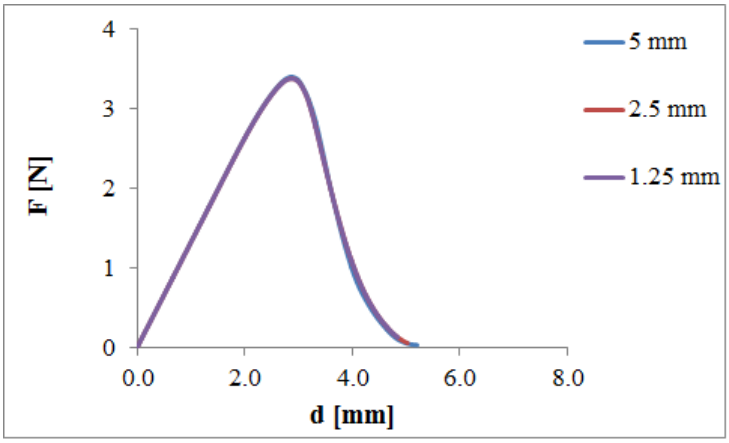

(a)

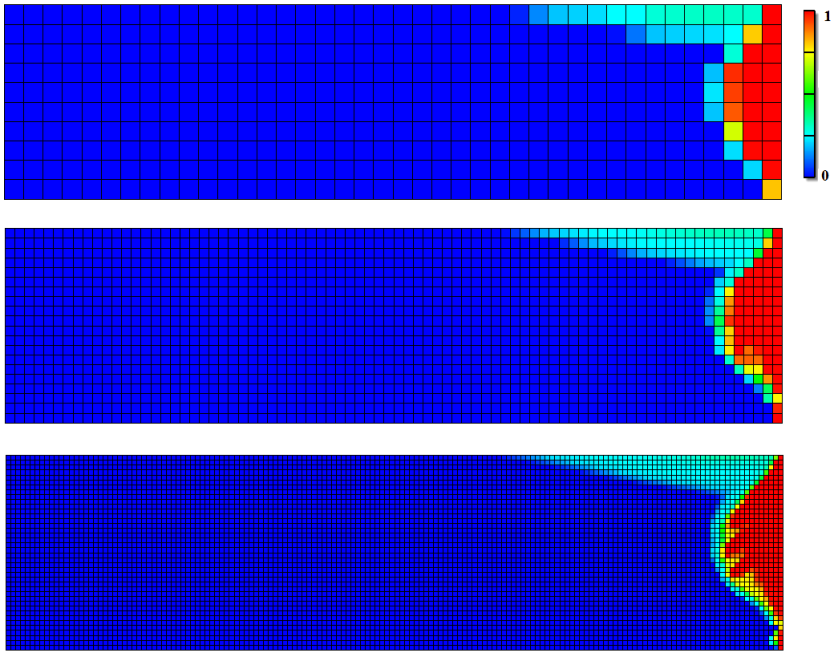

(b)

Figure 3.11: Force displacement (a) and damage profile at d = 4.3 mm (b) for progressive mesh refinement in the cantilever bending test

(Figure 3.13 (a-b)). The only noticible difference is related to the initial jump in maximum force and displacement at peak load errors with respect to the first level of mesh refinement, which is more pronounced for higher values of Δ or lower values of A; nevertheless all errors are significantly lower than 1%.

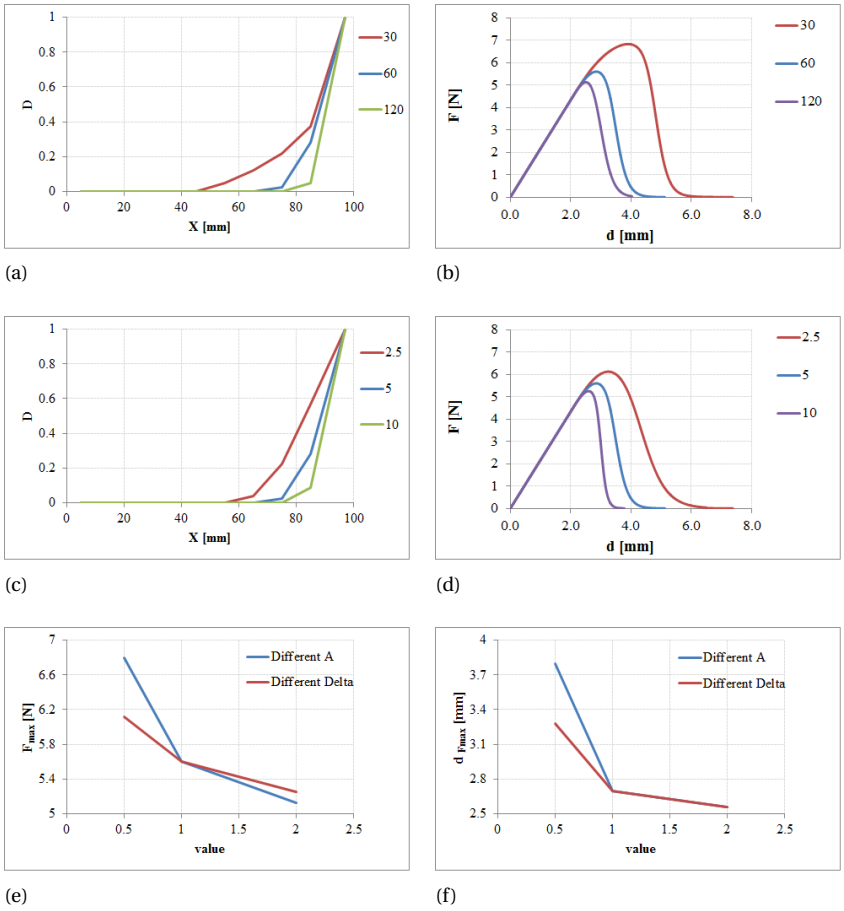

Figure 3.12: Damage profile in the bar (a,c) and force displacement plots (b,d) varying values of A (a-b) or Δ (c-d) and comparison of the variation of response in terms of maximum force (e) and displacement at peak force (f)

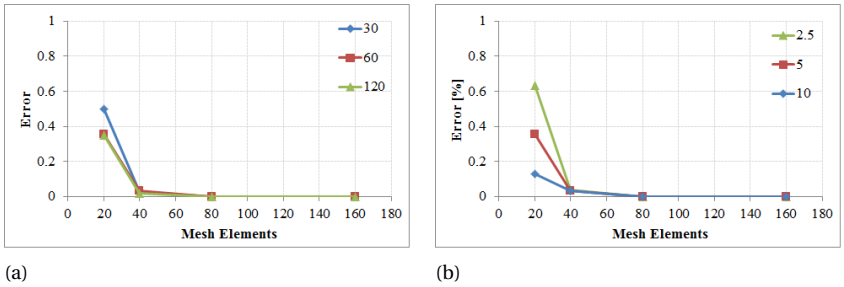

Figure 3.13: Error comparison for progressive mesh refinements using half and double A (a) or Δ (b)

3.4. A NUMERICAL APPLICATION OF THE MODEL ON ADOBE

3.4.1. THE EXPERIMENTAL REFERENCE

Once mesh objectivity of the model has been proven, numerical simulations are performed in order to verify the suitability of the framework for the assessment of the mechanical response of Adobe components in statics. A physical-mechanical characterization campaign performed by the authors on unfired soil bricks (which are fiber reinforced) and mortar (fiber free) is chosen as experimental reference [26]. It consisted of compressive and bending tests on four types of bricks and one mortar characterized by different percentages of fiber reinforcements. Displacement controlled tests at very low rate (1 mm/min) were performed on prisms with a slenderness equal to two in unixial compression or on entire bricks in bending. Interpretation of results led to the conclusion that Adobe components belong to the material class of concrete [31].

The typical force-displacement diagram in compression shows three distinct phases (Figure 3.14(a)). The initial behaviour is linear-elastic and the brick is supposed to be intact. At a stress level between 60% (typically for adobe bricks) and 75% (mainly for mortar samples) of the compressive strength, pre-peak non linearity is observed. This is the likely consequence of the coalescence and development of micro cracking processes occurring inside the sample. After peak load, diagonal and vertical macro-cracks are visible at opposite edges; correspondingly softening behaviour is observed in the force displacement curve, while cracks spread over the whole sample with a conical pattern (Figure 3.14(b)). When the soil matrix is mixed with fiber, the behaviour of Adobe becomes more ductile. Pre-peak non linearity starts at lower strain levels, while values for strain at peak load increase, as well as the slope of the post-peak slope of softening [26].

A more brittle behaviour characterizes the mechanical response of Adobe in bending. The typical force-displacement diagram is linear until 95% (bricks) or 98% (mortar) of the peak load is reached (Figure 3.14(c)). A single crack is then immediately visible at the lateral surfaces of the mid span and a corresponding softening branch in the force diagrams with typical exponential shape is obtained (Figure 3.14(d)). The crack propagates quickly along the height, and at 50% of the peak load, it reaches a relative length (with respect to the height of the sample) of approximately 45% (bricks) and 54% (mortar). Also in bending, strain at peak stress and slope of the softening curve are dominated by the fiber amount in the mixture.

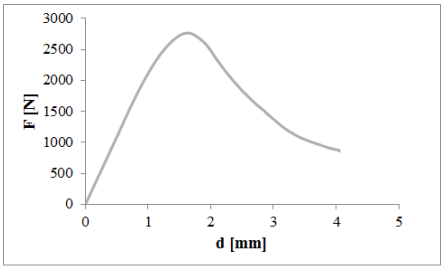

(a)

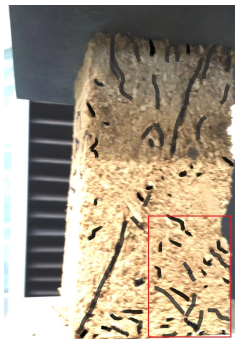

(b)

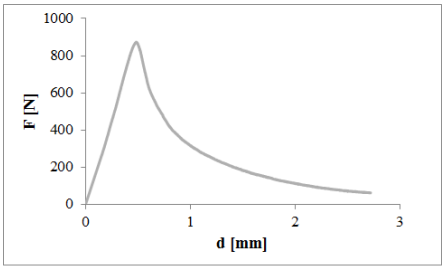

(c)

(d)

Figure 3.14: *Typical regions of the F-d diagrams and related cracking patterns in compression (a-b) and bending(c-d)*

3.4.2. THE NUMERICAL HYPOTHESES OF THE MODEL

Numerical simulations were performed for all types of adobe experimentally tested in [26]. In the following, numerical simulations using the new model are shown for one type of brick (reinforced using 17% by weight of straw in the mixture and named “Brick" in the following) and one type of mortar with only little traces of organic content (named “Mortar" in the following).
Assumptions for the material parameters of the model and simulation goals are made:

- For the Young's modulus, the mean values of elastic stiffness experimentally derived in [26] for Brick (E = 100 MPa) and Mortar (E= 200 MPa) are used. A 0.1 value for the Poisson's ratio is assumed, which is equal to the value used in the only known research devoted to the determination of this material parameter for Adobe [25];

- Consistently with the hypotheses of a new phenomenological model recently developed by the authors to address the ballistic resistance of Adobe [32], the Drucker Prager surface of eq.3.2 in Sec.3.2 used in [19] is updated to include an inscribed Drucker Prager smoothed version of Mohr Coloumb failure in compression (Figure 3.15(a)) [43]. In the octraedical space used in Sec.3.2, this implies the modification of the set of parameters c_1-c_4 of the equivalent strain formulations as follows:

$$\begin{cases} c_1 = \frac{1}{(1-2\nu)} \\ c_2 = \frac{1}{2\sqrt{2}(1+\nu)} \\ c_3 = \frac{tg(\phi)}{(1-2\nu)} \\ c_4 = \frac{\sqrt{3}}{2(1+\nu)} \end{cases} \tag{3.11}$$

  in which the internal friction angle ϕ=10^o is chosen corresponding to organic soil [44].

- For the damage initiation strains in compression, the mean values of initial deviation from linearity in the averaged stress strain diagrams experimentally derived in [26] are used for Brick (k_{0_c} = 1.3%) and Mortar (k_{0_c} = 0.7%). Elastic stiffness and initial damage strain in tension are determined in agreement with the sigma-epsilon method of the RILEM standard for fibre reinforced concrete [45]. Symmetry in elastic slope in tension and compression is thus hypothisezed and as damage initiation strain in tension, the mean value of strain corresponding to the formation of the first crack in bending tests experimentally derived in [26] is used for Brick (k_{0_t} = 0.7%) and Mortar (k_{0_t} = 0.3%).

- The damage evolution laws in eq. 3.7 are simplified. Different functions are used for compression and tension (Figure 3.15(b)). A steeper linear softening is adopted for tension while a smoother exponential shape is chosen for compression consistently with experimental trends of Par. 3.4.1. The resulting damage evolution laws are:

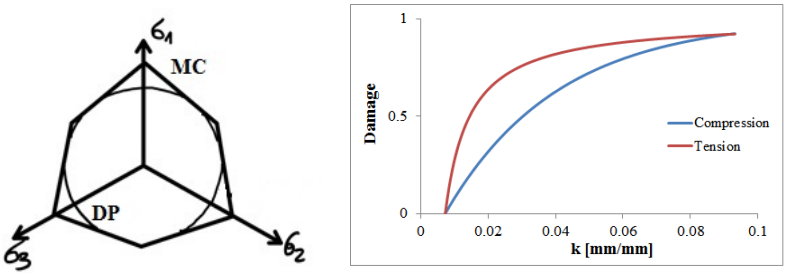

(a) (b)

Figure 3.15: Smoothed Drucker-Prager damage surface (DP) of the Mohr-Coulomb (MC) failure used in compression (a) and damage profiles in tension (T=1) and compression (C=30) (b)

$$\begin{cases} D_c = 1 - \dfrac{1}{e^{C(k_c - k_{0c})}} \\ \\ D_t = 1 - \dfrac{k_{0t}}{T k_t} \end{cases} \tag{3.12}$$

- Mean approximate dimensions are used for Brick and Mortar (Figure 3.16(a)) taken from [26]. In bending, the imposed interspan and the size of the distribuited constraining rolls are kept equal to experiments (Figure 3.16(b)). In order to trigger localization, in compression a mechanical defect, with damage initiation strain equal to 0.1%, is imposed at the corners of the specimen. Because of symmetry, only half of the brick is meshed. In bending a geometrical imperfection is used and a quadrilateral 1mm mesh with four integration points is applied. Displacement controlled analyses with small incremental steps ($5*10^{-4}$) are imposed at the upper side of the sample in compression and at the mid span in bending. A precision of $1*10^{-5}$ is prescribed to the solver.

- Calibration of parameters C, T, Δ in compression is performed in order to interpolate as closely as possible the mean displacements at peak stress and the 90% pre and post peak (named ultimate displacement in [26]) strength decay experimentally derived in [26] for Brick and Mortar. Calibration of damage function parameters in tension is performed in order to match as closely as possible the mean slope of the post peak exponential softening curve experimentally derived in [26] for Brick and Mortar. All material parameters used in compression are taken the same for bending tests. For sake of simplicity, the value of Δ is initially assumed constant for Brick and Mortar in tension and compression.

3.4.3. THE NUMERICAL RESULTS AND COMPARISONS WITH EXPERIMENTS

The best fit simulations in compression and bending are shown for Brick and Mortar in Figure 3.17. They are presented together with the targeted mean experimental plots

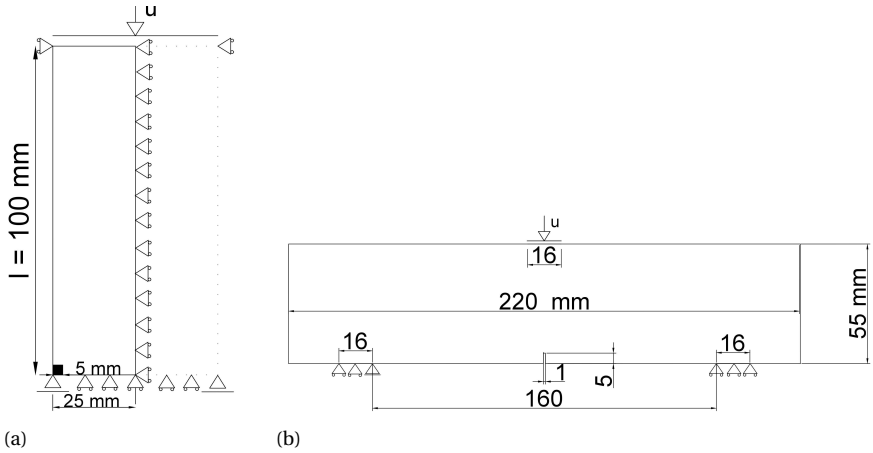

Figure 3.16: Numerical setup in compression (a), and three point bending test (b), including geometry and boundary conditions

associated to each type. Both curves are inserted within the minimum and maximum envelopes of experimental data related to compressive and bending tests on bricks and mortar. The corresponding failure patterns are compared in Figure 3.18.

In compression, the numerical results match the experimental data well at least until ultimate displacements for both Brick and Mortar in Figure 3.17(a-b). As a result of the simple formulation of eq.3.12, the numerical reaction plots do not capture the experimental trends of the post-peak experimental regions for large displacements (which could be experimentally recorded only for a limited number of specimens). Differences may be due to a more distributed failure pattern in the tests due to material heterogeneity which can not be addressed using deterministic models. Advanced softening laws with more ductility in the final failure stage may also provide a better match between test and simulation. Nevertheless, the numerical curves lie within the experimental envelopes associated to bricks and mortar at least up to 50% of the post peak stress.

The numerical failure resembles the principal experimental cracking patterns depicted for Adobe in Par. 3.4.1, despite the simplifications as two-dimensional modelling, isotropy and setup of the model to simulate developments of cracks usually starting from fiber-induced areas of de-adherence, clay concentrations or defects [26](Figure 3.18(a)).

Also for three point bending tests it was possible to accomplish the goal and the numerical f-d plots match most of the elastic and post peak softening experimental curves for both Brick and Mortar (Figure 3.17(c-d)). Also here a slight deviation between experiment and simulation is observed in the later stage of loading. However, also in bending the numerical plots remain within the experimental envelope for values higher than 50% of the post peak stress. Moreover, using the material parameters derived in compression and the flexural strain as given in RILEM for concrete, the resulting values of tensile strength derived from eq.3.13 well approximate the strength values experimentally derived in [26] for both components (Figure 3.19(b)).

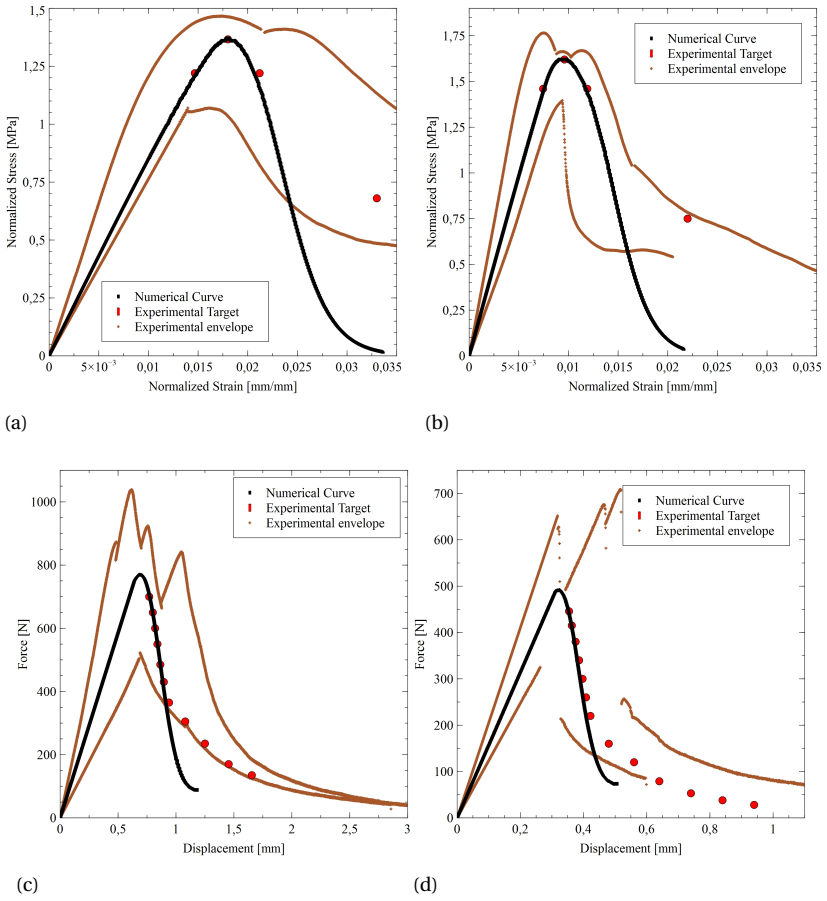

Figure 3.17: Experimental-Numerical force-displacement comparisons in compressions (a-b) and flexure (c-d) for Brick (left) and Mortar (right)

$$f_t = \frac{3F_{max}s}{2th^2} \tag{3.13}$$

where the peak load (F_{max}) and the displacement at peak load ($d_{F_{max}}$) with the geometrical dimensions in thickness (t), height (h) and span (s) are input from numerical results.

Almost full resemblance is extended to the depiction of the failure mode, where a single crack starts after damage initiation and it propagates quickly along the heigth (Figure 3.18(b)). Match with experiments is quantitatively extended to the evaluation of the cracking rate, meant as the ratio between length and height with respect to the same decay of strength after peak load (Figure 3.19(a)).

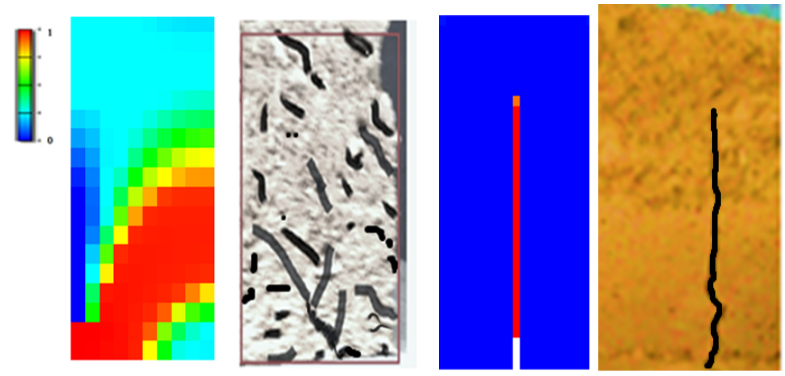

(a) (b)

Figure 3.18: *Experimental-Numerical comparison in terms of failure pattern in compression of Brick with quarter of CA11a (brick) at about 2mm (a) and in bending at mid span of Mortar with M3 (mortar) at a decay of about 20% of the strength (b)*

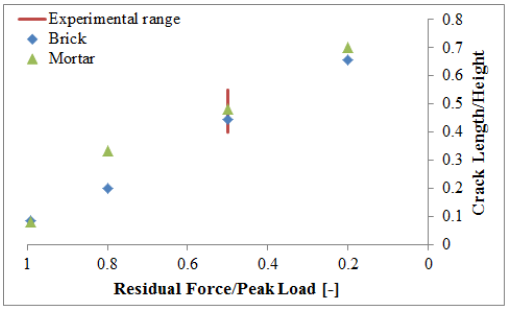

(a)

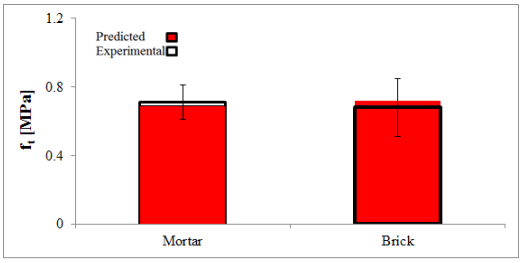

(b)

Figure 3.19: *Experimental-Numerical comparison in terms of crack propagation in bending (a) and in terms of tensile strength evaluation (b) for Brick and Mortar*

Table 3.2: Best fit material parameters in compression and tension for Brick and Mortar

Type	C	Δ_c	T	Δ_t
Brick	140	5.0	1000	160
Mortar	180	5.0	1000	440

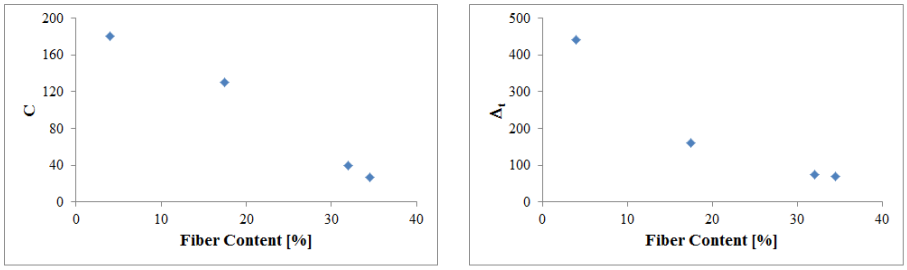

(a) (b)

Figure 3.20: Relationships between *calibrated* material parameters of the numerical model and experimental fibre content for four different types of bricks and mortar (including Brick and Mortar) tested in [26]

3.4.4. A PHYSICAL INTERPRETATION OF NUMERICAL CALIBRATION

The material parameters used for calibration are listed in Table 3.2. In compression it was possible to keep Δ_c constant for Brick and Mortar, while the brittle curves in bending required the use of a very high value for T for Adobe components, leaving Δ_t as calibrating parameter. Calibration of numerical parameters is qualitatively consistent with observed experimental trends [26]. Given a fixed value for Δ_c, the difference in value of the material parameter C, higher for Mortar than Brick, is consistent with the experimental evidence that mixtures with higher fiber content show higher ductility in compression. They are shown in Figure 3.20 (a), where the material parameter C for Brick and Mortar is given as function of the corresponding reinforcement ratio. The calibration of parameter C for all types of bricks tested was performed in [19]. A similar trend is shown for parameter Δ_t in tension (Figure 3.20 b).

3.5. CONCLUSIONS

A rate-dependent damage model has been developed to numerically assess the material performance of Adobe masonry components in statics. It originates from a local model recently developed for concrete with limiting regularization properties. In this study, the numerical model has been made fully mesh objective in statics, integrating rate dependent damage functions within an implicit solution scheme. The resulting rate dependent model assures mesh independence within a robust algorithm prone to preserve coherence with the physics of quasi brittle materials. A decomposition of the Dirichlet boundary condition allows all the numerical parameters of the damage evolution laws to be non dimensional. Thus, they could be calibrated with respect to the static experimental results in compression and bending of one type of brick and mortar experimentally tested by the authors. Despite simplicity, the current version of the model could cover the main features of the experimental response of components in compression and tension. Therefore it constitutes a valid framework to numerically assess the mechanical performance of Adobe components and the modified Drucker Prager failure surface is confirmed to well addresses the material response in compression.

REFERENCES

[1] T. Li Piani, Operative Guidelines for Protection of Places of Worship: A new approach toward security design of sensitive buildings, Institute for Advanced Strategic and Political Studies, ISBN:97888940373-2-6, Milan, 2017.

[2] L. F. Pereira, J. Weerheijm, L. J. Sluys, A new effective rate dependent damage model for dynamic tensile failure of concrete, Engineering Fracture Mechanics 176 (2017) 281–299. doi:10.1016/j.engfracmech.2017.03.048.
URL http://linkinghub.elsevier.com/retrieve/pii/S001379441630474X

[3] L. J. Sluys, R. de Borst, Wave propagation and localization in a rate-dependent cracked medium-model formulation and one-dimensional examples, International Journal of Solids and Structures 29 (23) (1992) 2945–2958. doi:10.1016/0020-7683(92)90151-I.

[4] P. Grassl, M. Jirásek, On mesh bias of local damage models for concrete, Proc., 5th Int. Conf. on Fracture Mech. of Concrete Structures (FraMCoS-5) (5) (2004) 255–262.

[5] L. J. Sluys, R. De Borst, Mesh-sensitivity analysis of an impact test on a double-notched specimen, Rock Mechanics, 1991.

[6] L. J. Sluys, R. De Borst, Rate dependent modelling of concrete fracture, Heron 36(2), 3-16. (1991).

[7] M. Jirasek, Z. Bazant, Model for Localization of Softening and Size Effect, in: Inelastic Analysis of Structures, 2002, Ch. 26.

[8] A. Needleman, Material rate dependence and mesh sensitivity in localization problems, Computer Methods in Applied Mechanics and Engineering 67 (1) (1988) 69–85. doi:10.1016/0045-7825(88)90069-2.

[9] F. van der Meer, L. J. Sluys, Continuum Models for the Analysis of Progressive Failure in Composite Laminates, Journal of Composite Materials 43 (20) (2009) 2131–2156. doi:10.1177/0021998309343054.
URL http://jcm.sagepub.com/cgi/doi/10.1177/0021998309343054

[10] F. Meftah, J. M. Reynouard, O. Merabet, Localisation and mesh sensitivity in gradient dependent softening plasticity, Fracture Mechanics of Concrete Structures, Proceedings FRAMCOS-2, edited by Folker H. Wittmann, Aedificatio Publishers, D-79104 Freiburg (1995) 1069–1078.

[11] M. Jirasek, Regularized continuum damage formulations acting as localization limiters, in: Computational Modelling of Concrete and Concrete Structures: EURO-C 2018, CRC Press, Bad Hofgastein (Austria), 2018, pp. 25–43.

[12] O. Allix, P. Feissel, Composite Damage Model For Dynamic Fracture Prediction : Identification Issues, ICF 11-11th International Conference on Fracture 2005.

[13] G. Pijaudier-Cabot, Z. Bazant, Nonlocal damage theory, Engineering Mechanics 113 (10) (1988) 1512–1533.

[14] Z. P. Bažant, Fracture mechanics of concrete structures, ACI Committee 446 on Fractures Mechanics 140 (1992) (1992) 1–140.
URL http://www.civil.northwestern.edu/people/bazant/PDFs/Papers/S25.pdf

[15] O. Allix, The bounded rate concept: A framework to deal with objective failure predictions in dynamic within a local constitutive model, International Journal of Damage Mechanics 22 (6) (2012) 808–828. doi:10.1177/1056789512468355.
URL http://ijd.sagepub.com/cgi/doi/10.1177/1056789512468355

[16] C. Giry, F. Dufour, J. Mazars, Stress-based nonlocal damage model, International Journal of Solids and Structures 48 (25-26) (2011) 3431–3443. doi:10.1016/j.ijsolstr.2011.08.012.

[17] R. de Borst, C. V. Verhoosel, Gradient damage vs phase-field approaches for fracture: Similarities and differences, Computer Methods in Applied Mechanics and Engineering 312 (2016) 78–94. doi:10.1016/j.cma.2016.05.015.

[18] J. Mazars, F. Hamon, S. Grange, A new 3D damage model for concrete under monotonic, cyclic and dynamic loadings, Materials and Structures (2015) 3779–3793doi:10.1617/s11527-014-0439-8.
URL http://link.springer.com/10.1617/s11527-014-0439-8

[19] T. Li Piani, J. Weerheijm, L. Koene, L. J. Sluys, The Adobe Delta Damage Model, in: Computational Modelling of Concrete Structures (EURO-C 2018), CRC Press, Bad Hofgastein (Austria), 2018, pp. 921–932.

[20] P. Ladevèze, O. Allix, J. F. Deü, D. Lévêque, A mesomodel for localisation and damage computation in laminates, Computer Methods in Applied Mechanics and Engineering 183 (1-2) (2000) 105–122. doi:10.1016/S0045-7825(99)00214-5.

[21] O. Allix, J.-F. Deu, Delayed-Damage Modelling for Fracture Prediction of Laminated Composites under Dynamic Loading, Engineering Transactions 45 (1).
URL http://et.ippt.gov.pl/index.php/et/article/view/680

[22] A. Suffis, T. A. A. Lubrecht, A. Combescure, Damage model with delay effect analytical and numerical studies of the evolution of the characteristic damage length, International Journal of Solids and Structures 40 (13-14) (2003) 3463–3476. doi:10.1016/S0020-7683(03)00153-7.

[23] R. Coffman, N. Agnew, G. Austin, E. Doehne, Adobe mineralogy: characterization of adobes from around the world, 6th International Conference on the Conservation of Earthen Architecture, Las Cruces, New Mexico, U.S.A., October 14-19, 1990 1 (May) (1990) 424–429. doi:0892361816.

[24] R. Illampas, D. C. Charmpis, I. Ioannou, Finite Element Simulation of the Structural Response of Adobe Masonry Buildings Subjected To Lateral (October) (2014) 14–17.

[25] D. Silveira, Al., Mechanical properties of adobe bricks in ancient constructions, Construction and Building Materials 28 (1) (2012) 36–44. doi:10.1016/j.conbuildmat.2011.08.046.
URL http://dx.doi.org/10.1016/j.conbuildmat.2011.08.046

[26] T. Li Piani, D. Krabbenborg, J. Weerheijm, L. Koene, L. J. Sluys, The Mechanical Performance of Traditional Adobe Masonry Components: An experimental-analytical characterization of soil bricks and mud mortar, Journal of green building 13 (3) (2018) 17–44.

[27] World Heritage Earthen Architecture Programme (WHEAP), United Nation: Inventory of earthen architecture (2012).

[28] G. Minke, Building with earth: Design and Technology of a sustainable architecture, BirkhauserarXiv:arXiv:1011.1669v3, doi:10.1017/CBO9781107415324.004.

[29] T. Li Piani, J. Weerheijm, L. Koene, L. J. Sluys, The Ballistic Resistance of Adobe Masonry : An analytical model for impacts on mud bricks and mortar, in: The 17th International Symposium on the Interaction of the Effects of Munitions with Structures (17th ISIEMS), no. October, Bad Neuenahr, Germany, 2017.

[30] Resultaten miniMOUT: effect van veroudering op ballistische weerstand van adobe muren met twee steensterkten, TNO Report, Tech. rep., TNO (2013).

[31] T. Li Piani, J. Weerheijm, L. Koene, L. J. Sluys, Modelling the Mechanical Response of Adobe Components under Uniaxial Loading, Key Engineering Materials 774 (2018) 650–657.

[32] T. Li Piani, J. Weerheijm, L. J. Sluys, Ballistic model for the prediction of penetration depth and residual velocity in Adobe: A new interpretation of the ballistic resistance of earthen masonry, Defence Technology 14 (5) (2018) 4–8. doi:10.1016/j.dt.2018.07.017.
URL https://doi.org/10.1016/j.dt.2018.07.017

[33] J. Lemaitre, J. Chaboce, Mechanics of Solid materials, 1990.

[34] L. Pereira, J. Weerheijm, L. J. Sluys, Simulation of dynamic behaviour of quasi brittle materials with new rate dependent damage model, in: 9th International Conference on Fracture Mechanics of Concrete and Concrete Structures (FraMCos-9), 2015, p. 14. doi:10.21012/FC9.036.

[35] R. Lancellotta, Geotechnical engineering, 2nd Edition, CRC Press, 2008.

[36] L. F. Pereira, J. Weerheijm, L. J. Sluys, A new rate-dependent stress-based nonlocal damage model to simulate dynamic tensile failure of quasi-brittle materials, International Journal of Impact Engineering 94 (2016) 83–95. doi:10.1016/j.ijimpeng.2016.04.002.
URL http://dx.doi.org/10.1016/j.ijimpeng.2016.04.002

[37] J. Lee, G. L. Fenves, Plastic-Damage Model for Cyclic Loading of Concrete Structures, Journal of Engineering Mechanics 124 (8) (1998) 892–900. doi:10.1061/(ASCE)0733-9399(1998)124:8(892).
URL http://dx.doi.org/10.1061/(ASCE)0733-9399(1998)124:8(892){%}5Cnhttp://ascelibrary.org/doi/pdf/10.1061/(ASCE)0733-9399(1998)124:8(892)

[38] P. Ladevèze, A damage computational approach for composites: Basic aspects and micromechanical relations, Computational Mechanics 17 (1995) 4–15. doi:10.1007/BF00356486.

[39] V. P. Nguyen, Multiscale failure modelling of quasi-brittle materials. Manual to the implemented jem/jive code, Ph.D. thesis, Delft University of Technology (2011).
URL https://repository.tudelft.nl/islandora/object/uuid{%}3A1af168bf-7975-4044-8eb4-dd42216f7aaf

[40] G. Pijaudier Cabot, Z. P. Bažant, M. Tabbara, Comparison of various models for strain softening, Engineering Computations 5 (2) (1988) 141–150. doi:10.1108/eb023732.
URL http://www.emeraldinsight.com/doi/10.1108/eb023732

[41] E. C. Simons, J. Weerheijm, L. J. Sluys, A viscosity regularized plasticity model for ceramics, European Journal of Mechanics 72 (July 2017) (2018) 310–328. doi:10.1016/j.euromechsol.2018.05.009.
URL https://doi.org/10.1016/j.euromechsol.2018.05.009

[42] A. Simone, H. Askes, L. J. Sluys, Incorrect initiation and propagation of failure in non-local and gradient-enhanced media, International Journal of Solids and Structures 41 (2) (2004) 351–363. doi:10.1016/j.ijsolstr.2003.09.020.

[43] H. Jiang, Y. Xie, A note on the Mohr-Coulomb and Drucker-Prager strength criteria, Mechanics Research Communications 38 (4) (2011) 309–314. doi:10.1016/j.mechrescom.2011.04.001.

[44] Swiss Standard SN 670 010b, Characteristic Coefficients of soils, Association of Swiss Road and Traffic Engineers.

[45] RILEM TC 162-TDF: Test and design methods for steel fibre reinforced concrete. Sigma-epsilon design method. Final Recommendation.

4

The Experimental Characterization of Adobe in Dynamics

"(..)The most reliable and useful courage
is the one that arises from the fair estimation
of the encountered peril(...)

Starbuck in *Moby Dick*, by H. Melville

This paper presents the results of an experimental research aimed at assessing the material performance of adobe bricks in compression for a wide range of induced strain rates, from statics to high velocity impact. Adobe is a traditional masonry whose bricks are made of sundried soil mixtures possibly reinforced with natural fibers and joined together using mud mortar. The inclusion of fiber and the presence of water in the mixtures have a dominant effect on the mechanical performance of adobe. Their influence on the dynamic behaviour of this material is quantified and interpreted in this study at high strain rates also with data produced through Hopkinson bar testing. Appropriate dynamic increase factors and constitutive equations for adobe in dynamics are also investigated. The paper presents the experimental campaign, shows the main results and offers qualitative and quantitative interpretations for the principal damage patterns observed.

This chapter is based on "Dynamic behaviour of Adobe in compression: the role of fibers and water content at various loading rates" *under review*, 2019.

4.1. INTRODUCTION

Contemporary society is confronted with many threats of different nature, from international terrorism to environmental emergency. Safety and protection of critical buildings and infrastructures are among the top priorities of governments around the world including the European Commission and its Joint Research Centre [1]. In Europe terrorist attacks have recently involved targets within the domain of the city, inside or in the proximity of dwellings and infrastructure for civilian use [2]. In this context, strategies of strengthening of the target [3] are neither economically nor socially sustainable. Thus, built infrastructure nowadays must be made resilient through the design process with respect to a wide range of dynamic loadings which not only include natural hazards such as floods and earthquakes, but also impacts and explosions as man-made threats [4]. These dynamic phenomena, with different intensity, are characterized by higher deformation rates imposed to the material with respect to static loadings [5].

Many civilian buildings and constructions are mainly made of brittle materials, such as concrete, ceramics, glass and rocks [6]. The properties of these materials are sensitive to the rate of loading [7]. That means that their physical-mechanical behaviour changes according to the imposed loadings. If assuming static properties within the design process may constitute a known approximation with respect to seismic loadings, using the same approach with regards to strain rates corresponding to impacts and blasts may lead to serious errors in the prediction of structural damage and fragmentation effects [8, 9].

These dynamic loadings require also the adoption of constitutive models capable of addressing the changes in the response of the material to high strain rates [6]. In order to incorporate these effects in analytical and numerical models, it is of paramount importance to experimentally characterize the material performance at all relevant deformation rates [5].

The study of the dynamic properties of cement-based materials has been consolidated over the last fifty years. It is generally accepted that strength of concrete increases with strain rate [10]. However, not all typical features related to the dynamic response of the material have been clarified and interpreted yet [11]. On the other hand, very limited sources of knowledge concern building materials for masonry constructions such as clay or stone, despite being of paramount importance for a reliable design of masonry [9]-[13]. If this is true for modern bricks and mortar, the state of knowledge is even more limited with regards to traditional masonry building materials, such as adobe [14].

Adobe is a traditional masonry whose bricks are made of raw mixtures of clay, sand and silt. Soil is mixed with natural fibers in the field according to local availability of resources and cast in moulds to be sundried according to building traditions. After air curing, bricks are joined together using mud mortar. Adobe is one of the first forms of masonry on earth [15]. More than 1/3 of the world population still lives in earthen dwellings, which constitute 10% of the built heritage [16]. Unfortunately, they are spread in areas of the world prone to earthquakes or involved into military operations, with severe numbers of human losses and built heritage disruption every year [17]. Moreover, despite the presence of many examples of this building technique in Europe, the use of adobe has declined after the industrial revolutions in today's building industry [18].

Two critical factors threaten more than others built heritage of adobe and limit its use in current practice. They are its low strength and durability properties [19]. These effects

are directly linked to the material selection and production processes inherent to adobe masonry. They result from common practices adopted for adobe in the field while their implications on the material properties are not standardized and scarcely addressed in literature [19]. For instance, avoiding industrial baking processes makes the material properties dependent on the water content in the mixture over its life cycle [20]. Furthermore, bricks and mortar are still often produced mixing soil with organic content locally available, regardless of the mineralogical properties of soil elements and the chemical interactions with fibers and water. Instead, a proper characterization of adobe must address the influence of such inclusions on the microstructure of the resulting component of adobe masonry.

Addressing the role that fibers and water contents in the mixture play on the material properties is of paramount importance because these are among the features which configure adobe as a eco-friendly building material [21]. Natural fibers improve the thermal and acoustic properties of adobe [16]. Traditional production and construction processes are characterized by limited costs and minimum carbon footprint with respect to industrial products. For these reasons, natural fibers or binders and traditional drying processes have been recently applied also in modern building materials such as concrete and clay [22] - [24]. Therefore, assessing the influence of fibers and drying processes on the properties of adobe is crucial in a global conjuncture.

This paper presents an experimental and numerical study of the material performance of bricks of traditional adobe at a wide range of strain rates. It addresses the effects on the material behaviour of low (statics), intermediate and high strain rates. High strain rates on the material are simulated using Hopkinson bar tests. The influence of water content and fiber contained in the mixture on the material performance is addressed and interpreted both in statics and dynamics.

In the following paragraphs, the experimental campaign is described and its results are reported. Observed effects of strain rates, fiber and water contents on the mechanical performance of adobe are described and dynamic increase factors are quantified in the third section. Next, these observations are further interpreted.

4.2. THE EXPERIMENTAL CAMPAIGN

A joint experimental campaign including Delft University of Technology (TU Delft), TNO, Dutch Ministry of Defence and the Joint Research Centre of the European Commission, was carried out in 2018.

The investigation was aimed to characterize the physical and mechanical performance of components of adobe masonry loaded in compression at a wide range of strain rates corresponding to induced loadings ranging from statics to the ones corresponding to earthquakes and impacts [25].

The influence of fiber reinforcement and water content in the soil mixture on the material properties for each strain rate was aimed to be quantified and evaluated.

4.2.1. MATERIALS

Two types of adobe bricks were selected for testing. They resulted from the same soil selection but only one of them contained substantial percentages of natural fibres.

(a) (b)

Figure 4.1: Example of tested fiber free (a) and fiber reinforced (b) adobe

Cylindrical samples of about 40mm in diameter with unitary slenderness were drilled from both bricks types and basal surfaces rectified to achieve parallel planes with a tolerance of 0.1mm (Figure 4.1). 40mm is the minimum size required for static testing on masonry components in codes [26] and it was considered as sufficiently large to represent the average heterogeneous structure of adobe in this campaign. Shape and size were chosen also to limit radial confinement due to inertia during the Hopkinson bar tests which is found to be proportional to the cross sectional area, while assuring equilibrium along the height, which is usually assured for low slenderness [9].
Each type of adobe was tested at two different water contents in the mixture. Air dried samples were air cured for 28 days at laboratory conditions while fully dried samples were further baked in the oven.

4.2.2. TEST SETUP AND METHODS

Physical characterization tests were performed at the laboratory of soil mechanics and geo-engineering of the Delft University of Technology. Mechanical tests were performed at the European Laboratory for Structural Assessment (ELSA) of the Joint Research Centre in Ispra, Italy.

PHYSICAL TESTS

Granulometric composition of the tested adobe was determined on three samples per type according to standard BS 1377-2 [27]. Density and moisture content at laboratory conditions were determined on fifteen samples per type according to NT Build 333 [28]. However, the prescribed temperature of 105°C for the oven-drying process was lowered to 85°C, in order to prevent damage in the micro-structure, which is found to happen in cementitious materials for temperatures higher than 100°C [29]. In fact, samples subjected to moisture content and density tests were also used for mechanical tests. The complete drying process was considered to be achieved when in two subsequent measurements, the variation in mass was lower than 1 g. Three days were needed in average to fully dry adobe samples.

STATIC TESTS

Static tests at a strain rate $\dot{\epsilon_1}$ of about 3 10^{-4} s^{-1} (calculated as ratio between deformation rate and specimen height), were performed on five samples per type and drying conditions. Tests were performed using an MTS universal testing machine (810 Material Testing System-50kN). Two special compression platens (of 115mm in diameter) were used to correctly load the specimens in compression. Displacement controlled tests at constant velocity of 0.01mm/s were performed. Displacement and forces were recorded by a FlexTest 40 Digital controller unit. Average stress-strain plots were derived normalizing each curve over the corresponding cross section areas and heights. A camera was installed to acquire high resolution photo sequences at 1 frames/second synchronized with the sensors data recorded by the testing machine at sample rate of 10Hz. Test setup is shown in Figure 4.2(a).

DYNAMIC TESTS

Dynamic tests were performed at two different strain rates, in the range corresponding to impacts and blasts [25]. Five tests per type and drying conditions were performed. Tests at an intermediate strain rate of about 3 s^{-1} ($\dot{\epsilon_2}$) were performed using the same setup and machine of Figure 4.2(a), with two differences. Displacement controlled tests were performed at approximately 100mm/s. Moreover, force and displacement signals have been recorded (at a sample-rate of 20kHz) using a National Instruments acquisition board (NI USB-6366) controlled with the Labview software and photo sequences were recorded at 5000 frames/second with a Photron SA1.1 high speed camera. At both strain rates in dynamics, average stress-strain plots were derived normalizing each curve of response over the corresponding cross section areas and heights.
Strain rates of the order of hundreds s^{-1} can be obtained only using specific setup and machines, namely drop hammer machines or split Hopkinson bars. A modified Hopkinson bar at the Hop-Lab of JRC was used to test adobe at approximate strain rates of 120 s^{-1} ($\dot{\epsilon_3}$). The input and output bars of 40mm diameter are made of aluminium. The

input pulse was generated through the pre-stressing of a portion of the input bar and abruptly releasing it. Test setup is shown in Figure 4.2(b). A scheme of the machine provided with geometrical information is graphically reported in Figure 4.2(c). For a detailed report of the dynamic test machine the reader is referred to [14, 30]. In the tests, the incident bar applied a constant velocity of about 4200 mm/s to the sample. For each test, a thin layer of vaseline was applied at the interfaces between the bar end and the sample surfaces to minimize friction and maximise plane-parallelism. Moreover, samples were pre-stressed up to 5% of the static strength for clamping and horizontal positioning purposes. For each test, specimen loading conditions and corresponding bar ends displacements were calculated by properly processing the strain signals record with a chain of semiconductor strain gages applied on the bars. For this purpose, a sample-rate of 5 MHz was used and the data acquisition system GAGE Module A/D Express CSE8482-H2 with dedicated software was employed. Time-syncronized high-resolution videos were also recorded at 50000 frames/second using the Photron SA1.1 digital camera. Image resolution is adequate to track failure patterns also in case of high velocity impacts.

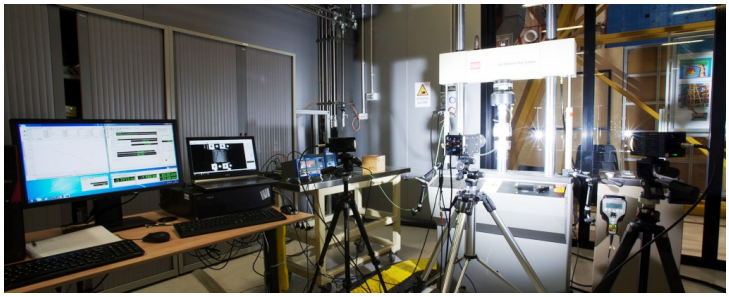

(a)

(b)

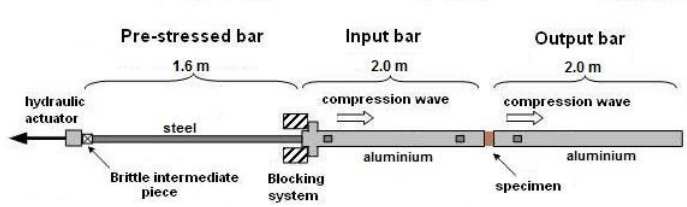

(c)

Figure 4.2: Setup of servo-hydraulic machine tests (a); Detail of Hopkinson bar in front of the specimen (b); Schematic picture of the JRC modified Hopkinson test setup for compression (c)

Table 4.1: Ranges of percentages of soil elements and fiber content by weight for the tested adobe and mean values (and standard deviations) for dry density and water content

	Soil Granulometry				Density	Water content
Type	% Clay	% Silt	% Sand	%bw Fiber	kg/m^3	%
A	24-25	47-48	27-28	<2	1790 (12)	2.3 (0.2)
B	24-25	47-48	27-28	17-18	1180 (20)	2.4 (0.2)

4.2.3. ELABORATION OF RESULTS

PHYSICAL TESTS

The mean curve of the soil granulometry distribution of the tested adobe is shown in Figure 4.3(a). The volume percentages ranges of soil elements are reported in Table 4.1 according to particle sizes (2-0.06mm sand; 0.06-2μm silt; < 2 μm clay). The soil of the tested adobe is defined as a clayey sandy silt. The percentages of organic content are also included in the table. Soil of Type B contains a mixture of wooden and straw fibers of different sizes and shapes (maximum dimension of 20mm (Figure 4.3b)). Traces of organic content were also found in Type A.

The average densities of the two types of adobe differ significantly, whereas their moisture content at laboratory conditions after 28 days of air curing shows similar values (Table 4.1).

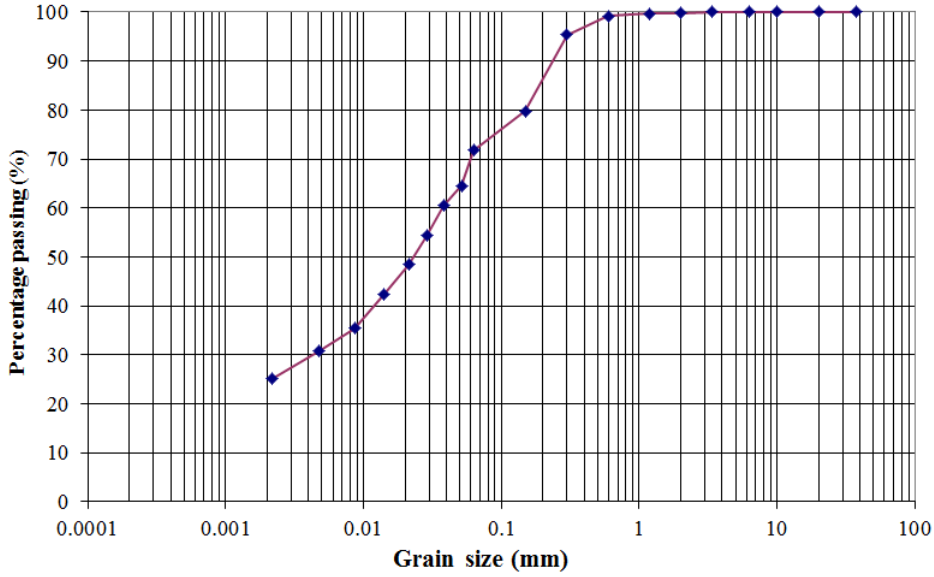

(a)

(b)

Figure 4.3: Typical soil granulometric distribution (a) and microscopic image zoom on fiber reinforcement (b) of the tested adobe

STATIC TESTS

Failure of cylindrical samples in compression is characterized by a mixed vertical-diagonal cracking pattern. Cracks start from random points of the sample spreading irregularly over the surface. The first cracks appear before the attainment of the maximum load. In case of fiber free samples, this occurs at an earlier stage (0.85 of the strain corresponding to peak load in average) with respect to the fiber enriched samples (0.93). Typical crack distributions and their progression are shown through snap shots in Figure 4.4 and Figure 4.5 for both types at different deformation stages (first rows). Samples from Type B are characterized by more diffuse and less visible cracks. These often follow the visible fibre orientation. Moreover, fiber reinforced samples show significantly larger lateral volume expansion, remaining coherent until larger displacements (Figure 4.6(b-c)). These trends do not change if samples are fully dried. However, for both types, in oven dried specimens the first crack in average appears at higher load levels (0.91 of peak for Type A and 0.97 for Type B) and they tend to be slightly less spread (Figure 4.7(a-c)).
Averaged stress strain plots are shown from Figure 4.6a by averaging test quantities over height and cross section areas of the specimen. Despite common practice, it should be noted that this is rigorous only when deformations in the post peak part of the curve are not too localized [31]. Values of key material parameters in compression were derived from each curve. They are the compressive strength f_b, the corresponding critical strain ϵ_{f_b} and the elastic modulus E (meant as chord modulus between 5% and 33% of compressive strength). Moreover, an ultimate deformation value ϵ_u, meant as the strain corresponding to 20% decay of the maximum load was calculated to characterize the early post peak deformation capacity [32]. In static (as well as in dynamic tests), possible outliers were excluded using the Interquartile Range Method and no more than one test was excluded for each type and drying condition. Average values and related standard deviations are listed in Table 4.2. Mean stress strain curves are shown for both adobe types and drying conditions in Figure 4.9. A similar scatter (slightly more pronounced for Type B) characterizes the curves of both types which is typical scatter associated to adobe in literature (Figure 4.10a) [19]. Four different regions are distinguished in all curves of response. A nonlinear initial phase ("1" in Figure 4.9(a-b)) is followed by a dominant linear elastic region (2). A second pre-peak non linearity (3) precedes the attainment of the peak load, which is followed by a softening branch (4). In fiber reinforced samples, larger extensions of the pre-peak non linear phases in the stress-strain are observed with respect to fiber free and the degradation of the softening curve occurs at a significantly lower rate (Figure 4.9b). This corresponds to an enhanced ductility associated to Type B in terms of critical strain (order of 1:3) and ultimate strain (order of 1:4). On the contrary, the mechanical performance of fiber free samples is higher both in terms of compressive strength (order 1:2) and elastic modulus (order of 1:3).
The depicted trends in the shape of stress curves and corresponding relationships among types do not change if samples are oven dried (Figure 4.9(a-b)). For both, fully dried samples show higher strength (order of 1:2) and higher Young's modulus (Figure 4.7(a-c)). However, the influence on parameters regarding deformation is negligible (Table 4.2).

DYNAMIC TESTS

Also in dynamics, failure pattern of adobe samples is characterized by the development of vertical-diagonal systems of cracks (Figure 4.4-Figure 4.5 (second and third rows)).

However, the first cracks have systematically a more straight orientation than in statics. This is particularly the case for fiber free samples, while a more diffuse and random initial crack pattern remains associated to Type B as in statics (Figure 4.6(second and third rows)). For both types and drying conditions, damage initiation processes appear visible in cylinders at later deformation stages of the dynamic curves of response. This is valid also comparing results from the intermediate and the high strain rate tests. On air dried samples, the first crack appears just at peak load for $\dot{\epsilon_2}$ (0.95 of the critical strain for Type A and 0.99 for Type B) and in softening for $\dot{\epsilon_3}$ (1.06 for Type A and 1.12 for Type B). However, more severe damage characterizes the sample response at large deformation levels in softening. Fragmentation and pulverization occur in the softening phase (Figure 4.8). This is particularly the case for Type A.

Considering dynamic tests separately at each strain rate, the regions which compose the stress-deformation curves correspond to those observed in statics (Figure 4.9(c-d)). As in statics, for each rate the tests on fiber reinforced samples show enhanced ductility and smoother curves than the corresponding fibre free tests, which in turn are characterized by higher values of strength and elastic modulus. For both types, oven drying does not change the failure pattern while it improves the strength parameters as observed in the previous paragraph (Figure 4.7(second and third rows)).

Analysing each type and drying condition at all the strain rates tested, it emerges that the values associated to the main key material properties change in dynamics (Table 2). In the following, the effects of strain rate on material properties are quantified in terms of mean dynamic increase factors (DIF), the ratios between the value for the dynamic and the static property [33]. Mean values are shown as a log-scale function of the applied strain rate in Figure 4.11- 4.12 and standard deviations are included in symbol thickness [34]. The validity of the essential assumption in the Hopkinson bar tests of stress equilibrium in the specimen has been checked. Figure 4.10b shows examples of the recorded forces at both sides of the specimen as function of time. For all tests it counts that the ratio of the difference in forces and the average force did not exceed 0.1 for the response regions 2 and 3 (Figure 4.9).

For both types and drying conditions, all tests in dynamics reveal higher values for the compressive strength with respect to the corresponding static ones. This trend is not linear: higher ratios are associated to results of split Hopkinson bar tests (Figure 4.11). The rate of increment is lower for samples reinforced with fibers. This happens for both strain rates with similar proportions. For both types, air dried samples show a strength increase proportionally larger if compared with corresponding air dried samples (Figure 4.11a). The maximum *DIF* is associated to air dried type A samples (1.84 at high rate) and the lowest to oven dried type B samples (1.66).

Similar trends denote the sensitivity to rate on adobe in terms of elastic modulus at high rates (Figure 4.11b). The maximum rate effect is of the same order of magnitude as for compressive strength (1.73). Similarly, the dynamic increase is the largest for the air dried fiber free adobe and the lowest for oven dried fiber reinforced samples (1.40). Negligible sensitivity to the rate is associated to the initial tangent stiffness (Figure 4.7a,d,g).

Higher uncertainty concerns the assessment of the influence of rate on the deformations. In general, the ductility parameters are characterized by a minimal rate effect with respect to the performance in strength and not always consistent trends characterize re-

Table 4.2: Average values (and standard deviations) for the main materials properties in compression at the three different strain rates for the two types and drying conditions. A_{ad}=Type A, air dried; A_{od}=Type A, oven dried; B_{ad}=Type B, air dried; B_{od}=Type B, oven dried

Strain Rate	Type / Parameter	**A_{ad}**	**A_{od}**	**B_{ad}**	**B_{od}**
$\dot{\epsilon_1}$ (s^{-1})	$f_b[MPa]$	2.6(0.2)	3.3(0.1)	1.4(0.2)	1.6(0.1)
	$E[MPa]$	170(34)	267(29)	54(7)	65(11)
	$\epsilon_{f_b}[\%]$	2.4(0.3)	2.2(0.2)	5.7(0.6)	5.6(0.6)
	$\epsilon_u[\%]$	3.7(0.2)	3.5(0.1)	12.1(0.2)	12.9(0.3)
$\dot{\epsilon_2}$ (s^{-1})	$f_b[MPa]$	3.5(0.1)	4.2(0.1)	1.6(0.2)	1.8(0.1)
	$E[MPa]$	208(60)	306(59)	68(11)	71(10)
	$\epsilon_{f_b}[\%]$	2.5(0.4)	2.3(0.3)	5.2(0.3)	5.3(0.4)
	$\epsilon_u[\%]$	3.7(0.2)	3.4(0.2)	13.2(0.3)	13.3(0.1)
$\dot{\epsilon_3}$ (s^{-1})	$f_b[MPa]$	4.8(0.3)	5.6(0.5)	2.3(0.2)	2.6(0.3)
	$E[MPa]$	300(40.1)	401(50)	84(12)	92(10)
	$\epsilon_{f_b}[\%]$	1.8(0.1)	1.6(0.3)	4.5(0.4)	4.5(0.4)
	$\epsilon_u[\%]$	3.7(0.5)	3.5(0.5)	13.6(0.5)	13.1(0.6)

sults for Type A and Type B (Figure 4.12). Critical strain is slightly larger than in statics for fiber-free samples (*DIF* of 1.09) at intermediate strain rate. A slight reduction is shown by fiber reinforced matrix (0.96) for the same loading. For both, the critical strain more clearly decays in Hopkinson bar tests in a similar range for both types included between 0.81 (Type B) and 0.77 (Type A). Variation in the softening parameter is minimal for all dynamic tests (Figure 4.12b). For both parameters of deformation, the rate of enhancement does not change if samples are oven dried (Figure 4.12).

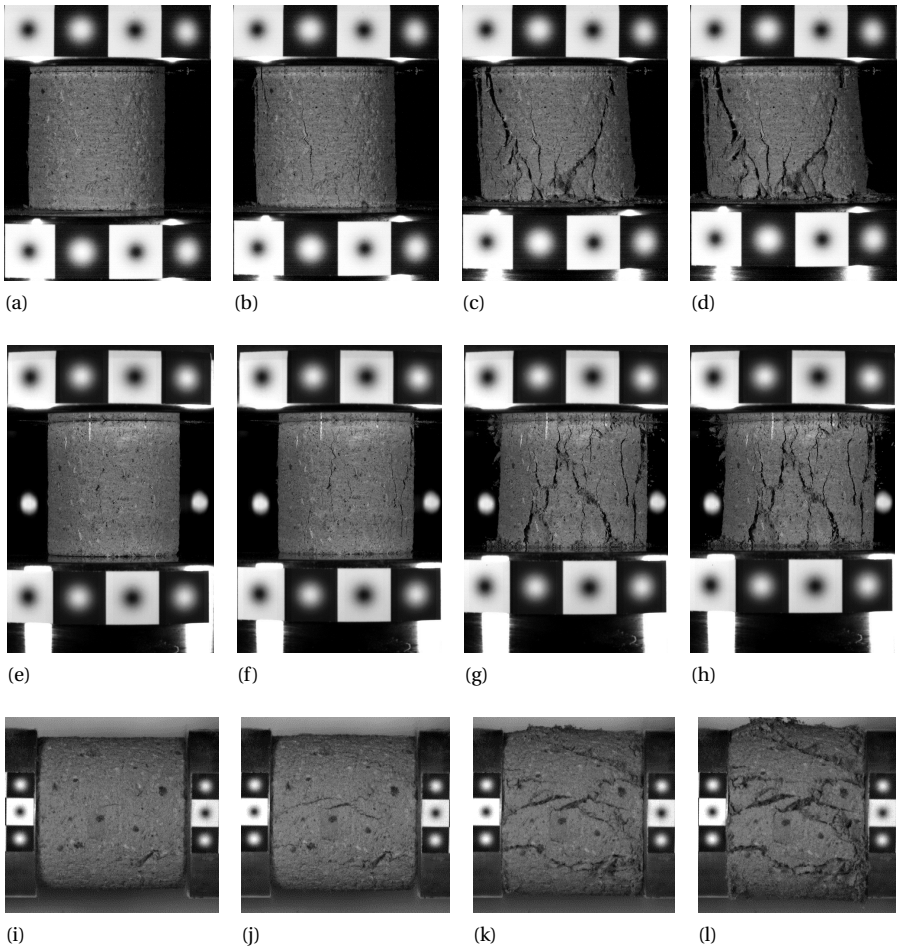

Figure 4.4: Comparison of typical damage progression for air dried Type A, at first crack appearance and 4%, 8%, 10% strain levels for static test (first row), intermediate strain rate test (second row) and split Hopkinson bar test (third row)

.

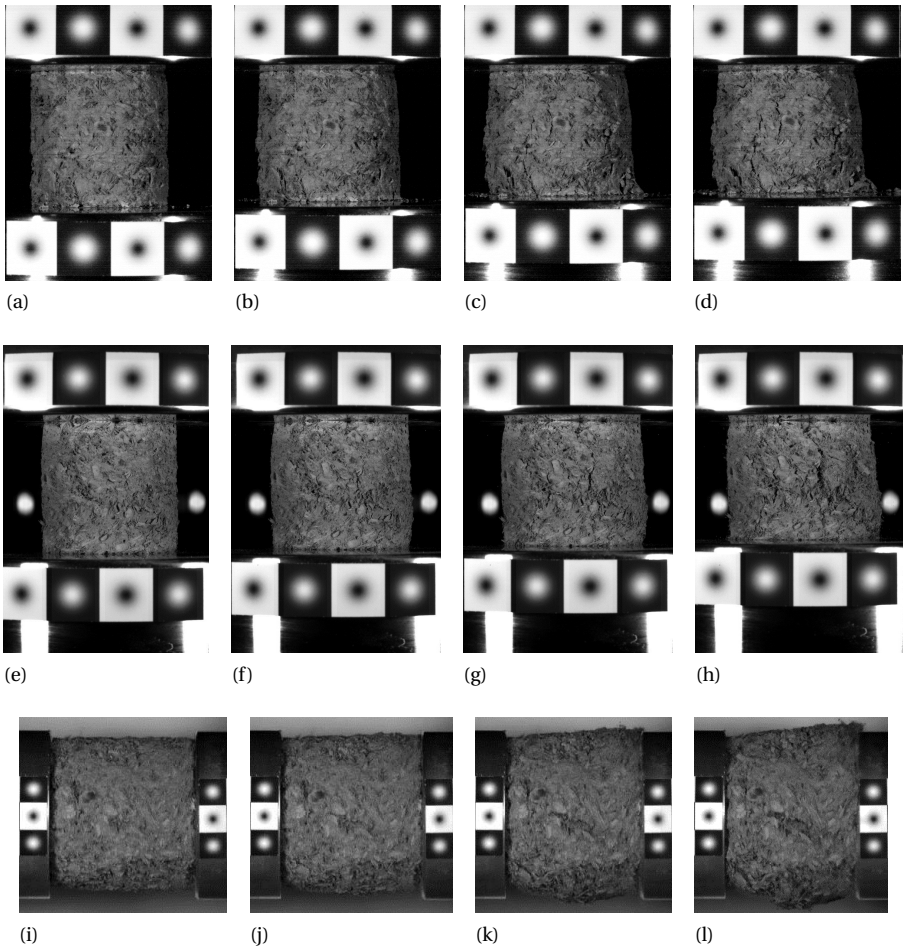

Figure 4.5: Comparison of typical damage progressions for air dried Type B at first crack appearance and 8%, 12%, 15% strain levels for static test (first row), intermediate strain rate test (second row) and Hopkinson bar test (third row)

.

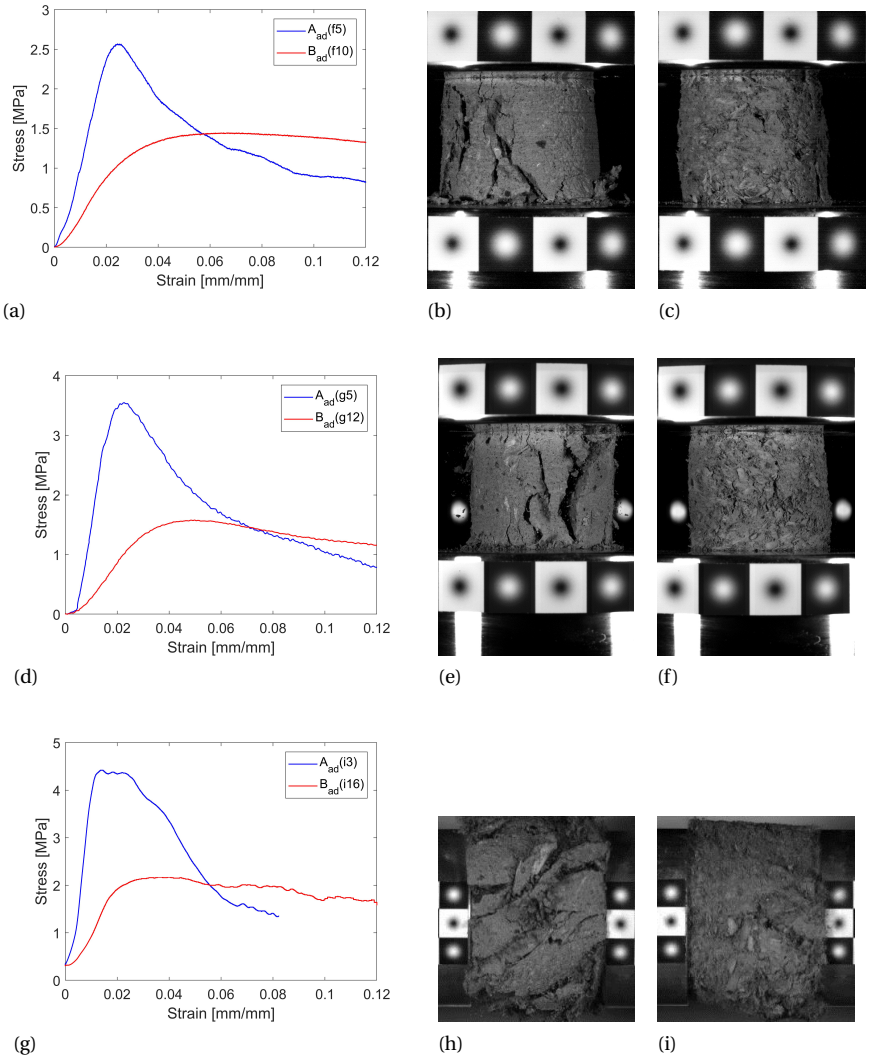

Figure 4.6: Examples of stress strain plots and corresponding cracking patterns at 12% deformation for air dried Type A (left) and Type B (right) for static test (first row), intermediate strain rate test (second row) and Hopkinson bar test (third row)

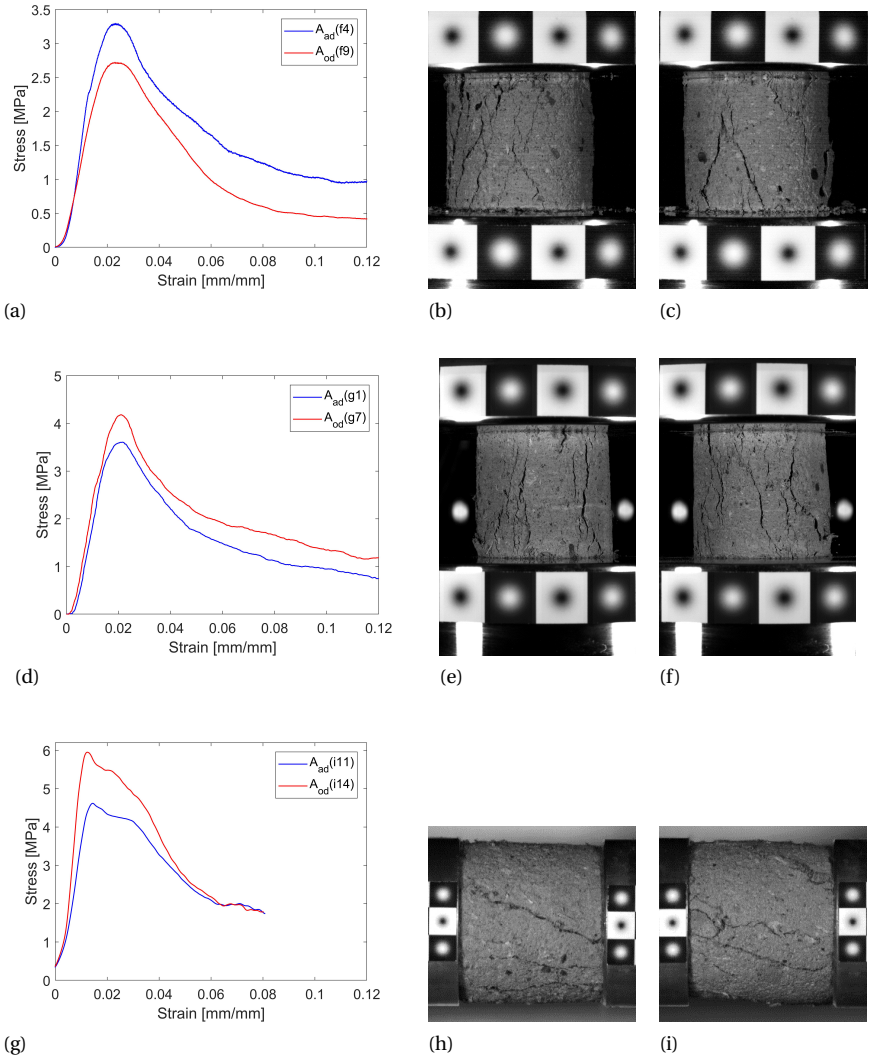

Figure 4.7: Examples of stress strain plots and corresponding cracking patterns at 50% stress decay for air dried (b,e,h) and oven dried (c,f,i) Type A for static test (first row), intermediate strain rate test (second row) and Hopkinson bar test (third row)

Figure 4.8: Typical post-mortem comparison of Type A (right) and Type B(left) for static test (first row), intermediate strain rate test (second row) and split Hopkinson bar test (third row)

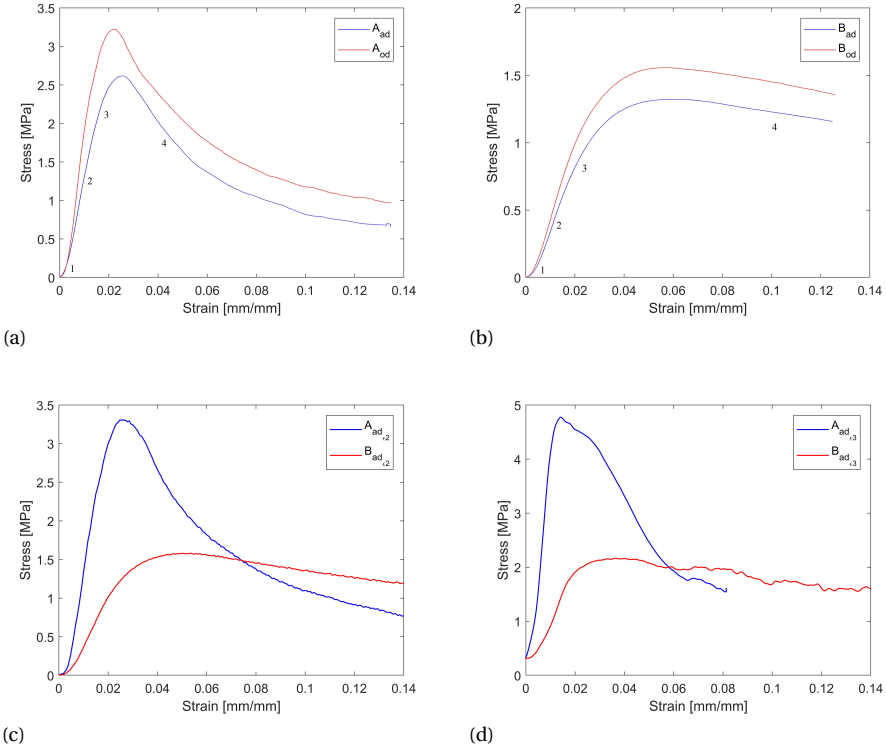

Figure 4.9: Average normalized stress-strain plots for Type A and Type B in statics for both drying conditions (a-b) and in dynamics at intermediate strain rates (c) and Hopkinson bar tests (d) for air dried condition

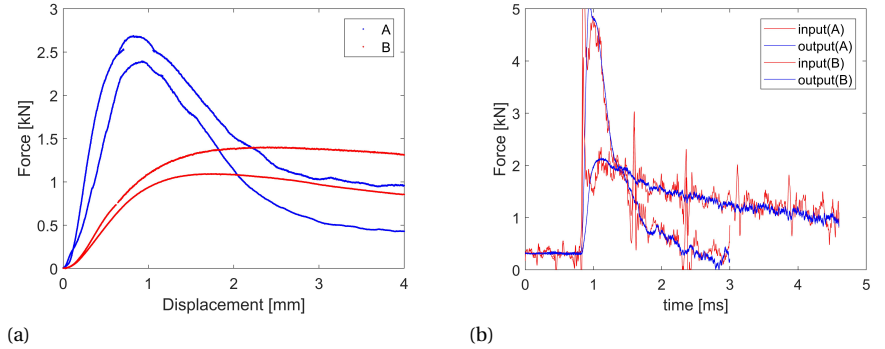

Figure 4.10: Typical envelopes of the response curves (a) and specimen equilibrium check during a Hopkinson bar test (b) for air dried Type A (“A”) and Type B (“B”), (where in (b) input and output correspond respectively to the resultant of the incident and reflected waves and to the transmitted waves at interfaces of the bar with the specimen)

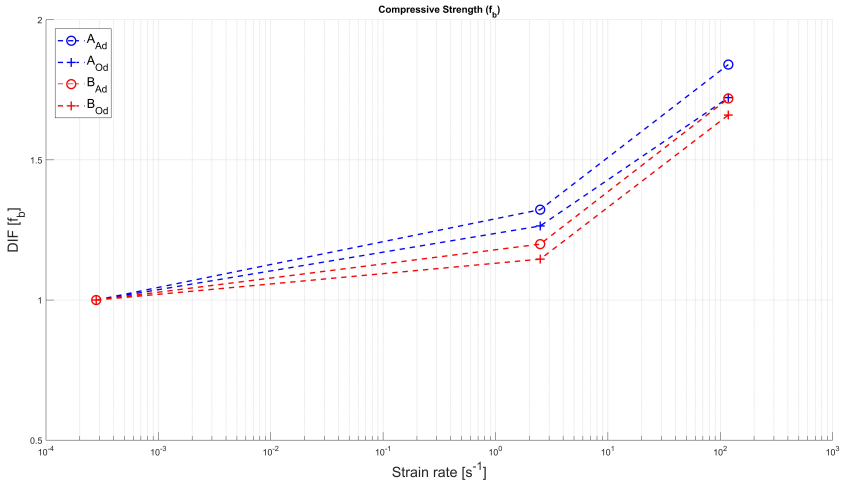

(a)

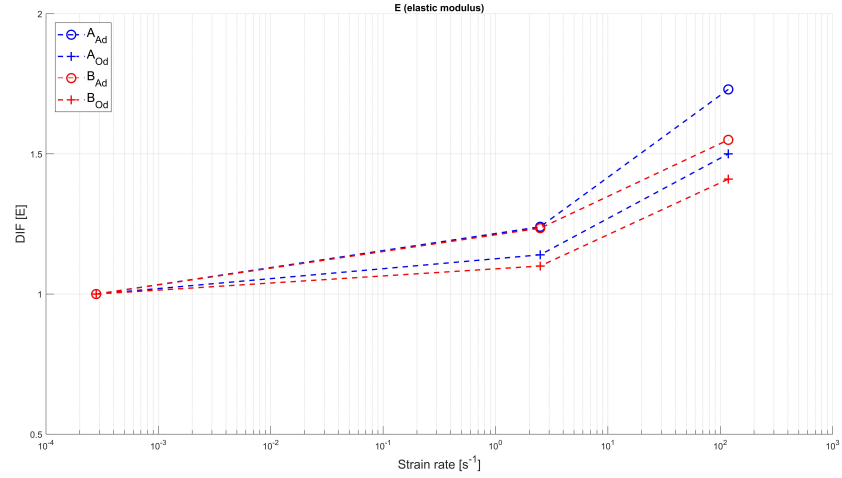

(b)

Figure 4.11: Dynamic increase factor in strength (a) and elastic modulus (b) for both types and drying conditions

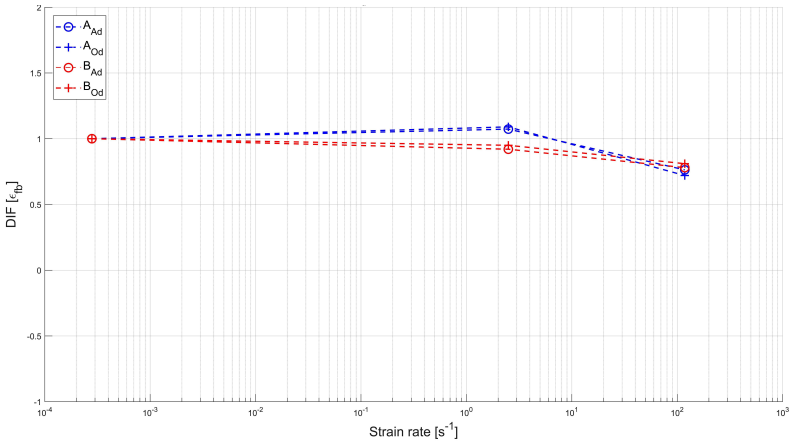

(a)

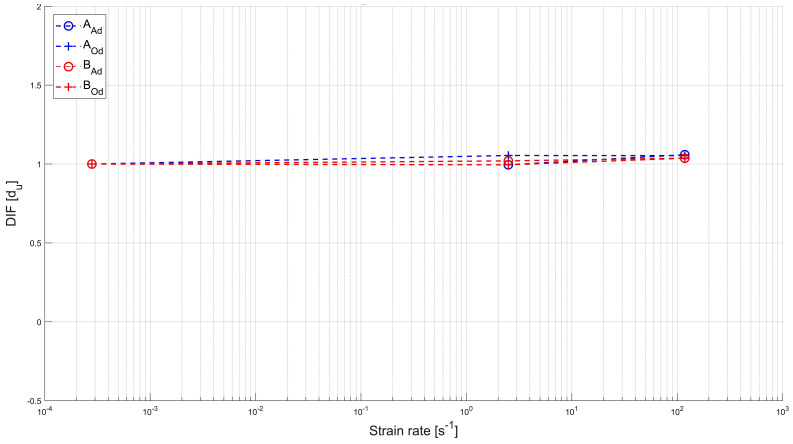

(b)

Figure 4.12: Dynamic increase factor in critical strain (a) and ultimate displacement (b) for both types and drying conditions

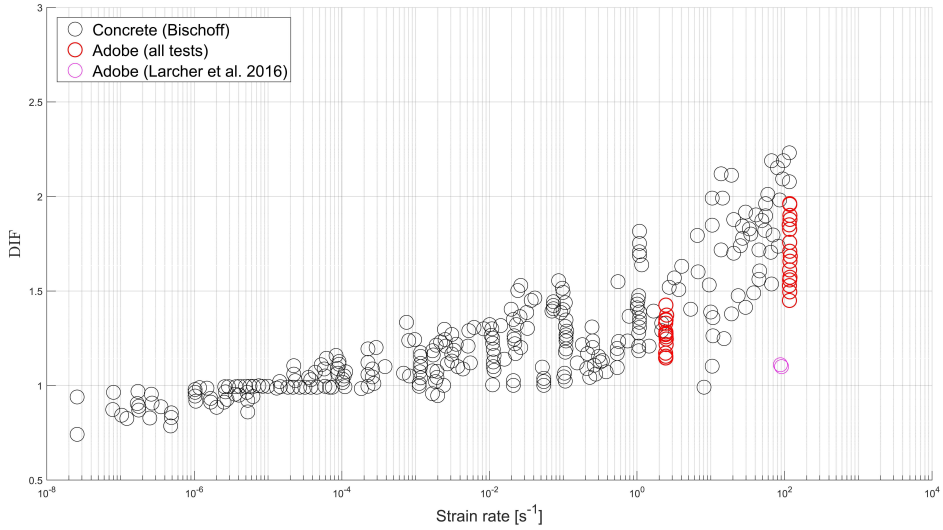

Figure 4.13: Typical dynamic increase factors in compressive strength for concrete and test results for adobe

4.3. ANALYSIS OF RESULTS: A MODEL FOR ADOBE IN STATICS AND DYNAMICS

As for cement-based materials, the mechanical parameters of the tested adobe show sensitivity to the applied rate of loading. In concrete, rate sensitivity in dynamics is usually measured in terms of strength enhancement ratio. Its dynamic increase factor is usually higher in tension than in compression [29]. In compression strength can increase up to three times [9] and guidelines suggest to consider an increment of 85% in the design for impact loadings for ordinary concrete subjected to high strain rates [25]. For the tested adobe material, rate sensitivity in strength is slightly less pronounced than reported for concrete. This is in agreement with the only other source of information available in literature regarding impact tests on adobe at high strain rates (Figure 4.13) [14, 35]. In Figure 4.13 dynamic increase factors for adobe lie on the lower boundary of the cloud of data usually associated to concrete [25]. This is especially valid for strain rate $\dot{\epsilon_3}$ (Hopkinson bar tests).

The enhancement of the strength in compression can be addressed in dynamics using rate dependent functions. Many different formulations have been proposed in literature for a wide range of cementitious materials [9, 33]. They are usually implemented into numerical models to simulate the mechanical response under highly dynamic loadings [12, 36].

In order to address the increase in the compressive strength of quasi brittle materials at high rates, the most commonly adopted formulations are log-log power functions. The most comprehensive and widely accepted reference to design the compressive strength of normal concrete ($f_b \leq 50$ MPa) in dynamics is the CEB-FIB model [37]. It defines DIF as :

$$\begin{cases} D.I.F. = (\frac{\dot{\epsilon}}{\dot{\epsilon_s}})^{(1.026\alpha)} for\, \dot{\epsilon} \leq 30 s^{-1} \\ D.I.F. = \gamma(\frac{\dot{\epsilon}}{\dot{\epsilon_s}})^{(0.33)} for\, \dot{\epsilon} \geq 30 s^{-1} \end{cases} \tag{4.1}$$

where $\dot{\epsilon}$ is the current strain rate in dynamics, $\dot{\epsilon_s}$ is the reference static strain rate (equal to 3 10^{-5}) and:

$$\begin{cases} \alpha = \frac{1}{5+9(\frac{f_b}{f_{bo}})} \\ \gamma = 10^{6.156\alpha-2} \end{cases} \tag{4.2}$$

where f_{bo} is a reference strength of 10 MPa. Figure 4.14 shows the CEB model for a concrete of 30 MPa of strength. It matches relatively well with experimental data on concrete. However, it clearly overestimates rate dependency of adobe, represented by average plots and standard deviations associated to air dried Type A and Type B, as representatives of the two types tested in Sec. 4.2 (Figure 4.13). Other log-log functions proposed in literature for concrete, mortar and clay also overestimate the dynamic performance of adobe [9]- [13], [38]. The overestimation is also enhanced if the values of the reference parameters in eq.4.2 (f_{bo} and $\dot{\epsilon_s}$) are adapted on tests on adobe. This is shown in Figure 4.14, where the f_{bo} of the CEB formula is equal to 1.35 MPa, taken as the average of the compressive strength of 110 static tests collected from literature for traditional adobe in [19]. Other versions of the CEB formula are recently found in literature to address high performing steel fiber concrete (SFRC). Few tests found to address dynamic strength of concrete mixed with steel fiber proportions lower than 5% b.w. reveal lower sensitivity to rate with respect to plain concrete [39–41]. In [40], the CEB model was modified prolonging the yielding strain rate ($\dot{\epsilon_s}$=53 s^{-1}) and decreasing the dynamic increase factor beyond with approximately a factor 0.7. In Figure 4.14 the resulting function for a high performing concrete of strength of 80 MPa is shown. The plot is closer to the experimental rate of enhancement showed by fiber reinforced adobe. Underestimation of experimental data of adobe is also encountered considering other bi-linear functions for concrete tested on different dataset. This is the case of the function proposed by Tedesco and Ross and described in eq. 4.3 [10].

$$\begin{cases} D.I.F. = 0.00965\dot{\epsilon} + 1.058 for\, \dot{\epsilon} \leq 63.1 s^{-1} \\ D.I.F. = 0.758\dot{\epsilon} - 0.289 for\, \dot{\epsilon} > 63.1 s^{-1} \end{cases} \tag{4.3}$$

Aside from piecewise functions in standards, linearly increasing equations with power or logarithmic shapes are used in literature to define rate dependent models for quasi brittle materials (eq.4.4-5):

$$D.I.F. = (\frac{\dot{\epsilon}}{\dot{\epsilon_s}})^{\alpha} \tag{4.4}$$

$$D.I.F. = A_o + A_1 log(\frac{\dot{\epsilon}}{\dot{\epsilon_s}}) + A_2 log^2(\frac{\dot{\epsilon}}{\dot{\epsilon_s}}) + (...) A_n log^n(\frac{\dot{\epsilon}}{\dot{\epsilon_s}}) \tag{4.5}$$

where n defines the degree of the function and A_0-A_n and α are non dimensional parameters to be determined according to interpolation of extensive experimental dataset. Most formulations belong to the second class [42] (eq.4.5) while the model proposed by

Table 4.3: Best fit parameters (rounded to the first significant digit) for logarithmic and power functions and square roots errors

	Logarithmic					Power	
Type	A_o	A_1	A_2	A_3	err	β	err
A_{ad}	0.7	0.03	0.03	≃0.0	0.01	27	0.2
A_{od}	0.7	0.03	0.03	≃0.0	0.02	31	0.1
B_{ad}	0.5	0.02	0.03	≃0.0	0.02	34	0.1
B_{od}	0.5	0.02	0.03	≃0.0	0.02	36	0.2

Mihashi and Wittman in [43] belongs to the first approach based on a stochastic theory of fracture in conjunction with thermodynamics (where α is equal to $\frac{1}{1+\beta}$ with β a material parameter to be interpolated) [44].

Equations 4.4-5 can be used to interpolate the average strengths of adobe types at different strain rates. Interpolation was based on least square method on mean compressive strength for both types and water contents. Examples of interpolating functions (for Type A_{ad}) are shown in Figure 4.14 for each equation. Best fit parameters and mean errors are reported for both types of functions and tested adobe in Table 4.3. The power function does not address satisfactorily experimental data on adobe. It tends to overestimate the dynamic strength at intermediate strain and to under-value the maximum dynamic strength above $\dot{\epsilon}$=100 s^{-1}. Best fit values are however slightly higher than the ones proposed originally [43] (β=14 for flexural strength).

An overall better approximation is obtained using third order logarithmic functions. Best fit values are lower than the usual ones proposed for concrete materials and are contained in a narrow range for the two types at different drying conditions (Table 4.3) [5].

An integrative approach consists in using these rate dependent formulations to extend the validity of constitutive models developed in statics to the dynamic regime. In fact, for masonry materials the whole softening curve of response, besides the quantification of the value of strength, is important in case of nonlinear dynamic analyses [45]. This is the approach used for instance by Priestley et al. in [46], where analytical $\sigma-\epsilon$ curves developed for the constitutive assessment of concrete masonry in statics ($\dot{\epsilon}$=3 10^{-6} s^{-1}) were adapted via a multiplying factor of 1.25 for both deformation and strength parameters of the model to simulate the mechanical response at $\dot{\epsilon}$=0.01 s^{-1}. A similar approach is attempted in this section. A constitutive model from literature is proposed for the static assessment of the tested adobe components [47]-[49]. In fact, statistical analyses confirm that models originally developed for concrete can be used to interpolate the curve of response of adobe [50, 51]. In this case, the stress-strain equation in compression proposed by Popovics for normal concretes of given aggregates compositions [52] is used to address both the tested types and drying conditions of adobe in Sec. 4.2. The model is reported in eq.4.6 as:

$$\sigma = (E_o)\left(\frac{n}{n-1+(\frac{\epsilon E_o}{f_b})^n}\right)\epsilon \tag{4.6}$$

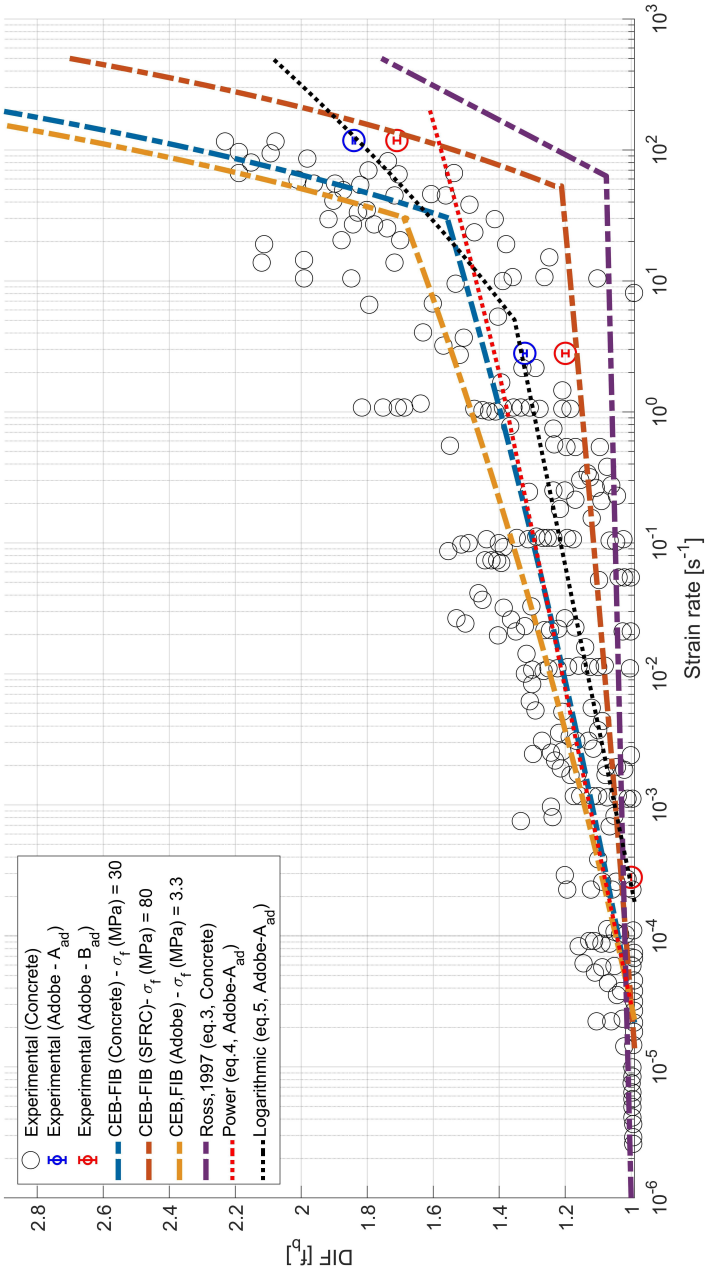

Figure 4.14: DIF functions for the compressive strength of adobe ($TypeA_{ad}$) at different strain rates

where E_o is the ratio between the compressive strength and the corresponding strain while n is the only material parameter of the model, which in the original work of [53] varies between 2-4 for mortars and 1.5-5 for concrete according to porosity and internal matrix composition.
For each test in statics n was calibrated to match the curve of response at least until ultimate strain. The model fits well all experimental results of unfired bricks, independently from water and fiber inclusions in the mixture (Figure 4.15a,b), with limited standard deviations for n associated to each type and drying conditions. Mean best fit values for n are found to be almost double for fiber free air dried samples (3.1 ±0.2) compared to fibre reinforced ones (1.7 ±0.1). Values slightly differed if samples were oven dried both for Type A (3.0 ±0.2) and Type B (1.7 ±0.1). As in [52], statistical inference suggests that n is a property of the soil mixture quantitatively linked to the 18% of fibers added in the soil mixture. A value of 3 and 1.7 respectively for Type A and Type B is thus kept as a material constant for the constitutive assessment of adobe in dynamics. Similarly to [46] approach, eq. 4.6 is thus modified in dynamics to:

$$\sigma = (kE_o)\left(\frac{n}{n-1+\left(\frac{\epsilon kE_o}{DIF f_b}\right)^n}\right)\epsilon \tag{4.7}$$

where DIF corresponds to the best fit functions calibrated for each type and drying conditions in eq.4.5 and k is a function on the dynamic strength enhancement statistically derived by interpolating all dynamic functions for each type, drying conditions and applied rate. As a result of multivariate analyses, a formulation for k is derived:

$$\frac{k}{DIF} \approx 1 + (3e^{-3}n - 3e^{-3})(1 + 0.03w)\dot{\epsilon} \tag{4.8}$$

where statistical inferences confirms higher sensitivity for higher water content (w) and minor organic content (n). Figure 4.15(c-f) show the analytical-experimental comparisons between the constitutive model calibrated in statics integrated with rate dependent functions and the mean experimental curves for each type, drying conditions and strain rates. Considering the wide range of strain rates targeted and the natural scatter inherent tests on not engineered materials, the model well addresses the experimental data on adobe also in dynamics. This is particularly the case for Type B.

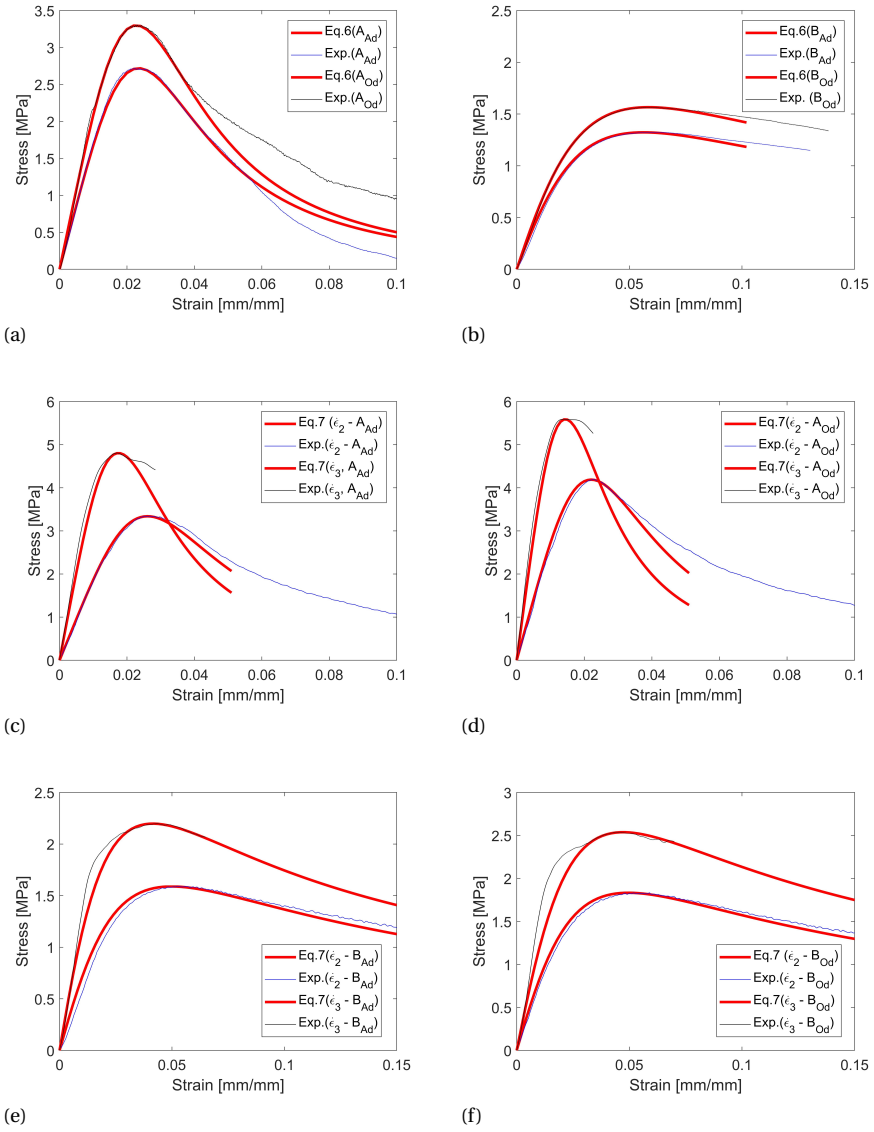

Figure 4.15: Experimental-analytical comparison in statics for air dried and oven dried Type A (a) and Type B (b) and experimental-analytical comparisons in dynamics at both strain rates ($\dot{\epsilon_2}$ and $\dot{\epsilon_3}$) for air dried and oven dried Type A (c-d) and Type B (e-f)

4.4. INTERPRETATION OF THE ROLE OF FIBERS AND WATER IN STATICS AND DYNAMICS

The experimental study has revealed that the mechanical performance of adobe is sensitive to the applied strain rate and its material resistance is enhanced when solicited by dynamic loadings. Analysis of data proves that macro-models developed for cementitious materials are suitable to simulate the mechanical response of adobe components [50] and the associated DIF parameters are within the same experimental ranges usually associated to modern geomaterials as concrete and mortar [5, 54].

This section focuses on the meso-scale interpretation of the role of fibers and water content in adobe mixtures according to the observed patterns in Sec. 4.2-3. As cement and concrete, adobe is a quasi-brittle geomaterial which can be considered as macroscopically homogeneous at a certain length scale. However, the physical interpretation of the mechanisms which are activated inside the material of adobe when solicited by dynamic loadings can not be done without a detailed analysis of its meso-structure. Each component in adobe, including water and air pores, plays a role and interacts with the others in the mixture according to mineralogical properties and production processes determining the overall system strength. Its rigorous assessment is possible only using advanced experimental techniques [29]. These have been largely used to investigate the behaviour of modern building materials but they have been only rarely applied on adobe [55]. Furthermore, production processes in adobe are not standardized and quantity, materials and proportions of mixture components are often decided in the field according to local availability and different vernacular building traditions.

However, water and fiber content were the isolated variables of this experimental study and analysed for a wide range of loading conditions from statics to high velocity impacts. Thus, the resulting information constitutes a solid qualitative as well as quantitative dataset which allows to propose interpretations on the effect of fibers and water content in the meso-structure on the macro-properties of adobe at different rates. For both factors, interpretation starts from the analysis of the dynamic behaviour exhibited by adobe and they are verified with respect to the trends observed in statics. The resulting theory for adobe resorts to principles of fracture mechanics and of geotechnics and soil investigations, which are actually commonly adopted also to interpret the micro-behaviour in modern geo-based building materials.

4.4.1. WATER IN ADOBE MIXTURES: THE ROLE OF CHEMICAL BONDS

The higher sensitivity in strength to high strain rates exhibited by samples containing interstitial water is explained at a meso scale by "*Stefan adhesion*" [56]. According to this principle of viscosity, a layer of water between two parallel plates separated by a certain distance exerts a normal force which is proportional to the velocity with which the plates are approximated or separated [57]. This inter-capillary phenomenon is supposed to happen between the surfaces of soil particles of adobe solicited by high velocities of deformation (Figure 4.16) [58].

The Stefan effect has been used to interpret the dependence of moisture content on dynamic performance in tension which has been observed also for concrete [7, 59]. Tests in [60] on concrete samples revealed that rate sensitivity in tensile strength can almost dou-

Table 4.4: Comparison of compressive strength of different masonry materials (HC: hollowed clay; CS: calcium silicate; LAC: lightweight concrete; AAC: autoclaved aerated concrete; AD: oven dried fiber free adobe) using the database for masonry in [64]

Parameter	HC	CS	LAC	AAC	AD
Strength [MPa]	16.9	26.1	14	3.8	3.3

ble when saturated with respect to normal cured concrete. The lower sensitivity shown by the tested adobe is explained by the low water content in samples air cured under sun for 28 days and by the possible effect of high water reactivity inherent in clay toward water [61].

Inter-particle chemical bonds explain also the higher static performance associated to fully dried adobe tested in the study. Interstitial water weakens the bonds between binder particles in the mixture. Its evaporation allows the formation of stronger chemical binding which ensure a denser inter-particle arrangement [62]. This is consistent with the Lambe's model for compacted soils: on a dry state, the distance between two clay platelets is small enough for the Van der Waal forces to dominate, inducing clay flocculation and making up the structure [61, 63].

Also for concrete materials, higher strength is observed in literature for baked cement pastes with respect to normal cured concrete [29, 40]. Fiber free baked adobe reveals values for static strength which are comparable with some building materials commonly used for masonry constructions. Table 4.4 compares the mean strength of baked adobe with respect to values associated to other modern building materials used for masonry [64]. Comparison reveals that oven dried strength of fibre free adobe is close to lightweight aerated concrete.

The drying process does not significantly influence the deformation capacity of adobe in statics and dynamics [19]. This is related to the cracking process of the material, which is associated to the role of fibers in the matrix discussed in the following paragraph. Areas of the matrix inherent fibers are considered as fully dried after 28 days of curing. This is consistent with the observation of similar water content for the two types in Par. 2.1 despite different fiber amount: fibres and surrounding areas are fully dried while water is retained in clay and at interstitial level of the matrix.

4.4.2. FIBERS IN ADOBE MIXTURES: THE ROLE OF HETEROGENEITY

The lower sensitivity of strength to high strain rates exhibited for adobe samples containing fibers is interpreted by linking principles of fracture mechanics to hypotheses on the specific heterogeneity level of fiber enriched mixtures of adobe. Actually, as showed in Sec. 4.3, also the few multi-strain rate experimental tests available in literature on fiber reinforced concrete reveal a lower DIF compared to plain concrete. This was also explained for concrete as a result of a higher homogeneity and lower porosity levels provided by steel fibers at a meso-scale [39, 40]. This is consistent with the positive effects of fibers on the toughness and strength of the material in statics [65]. In fact, fibers in concrete have been lately added in the mixtures to enhance the mechanical performance

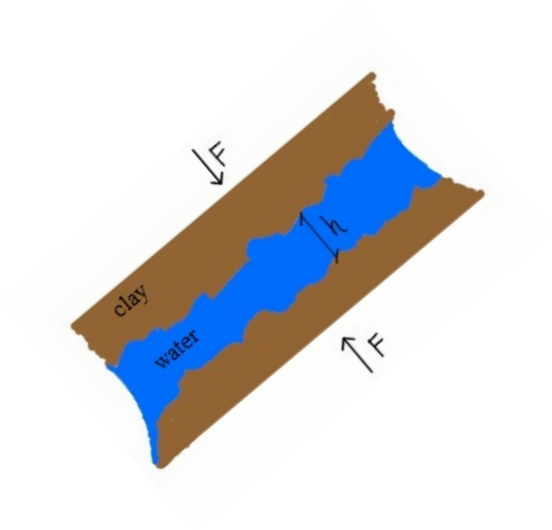

Figure 4.16: Schematic picture of Stefan effect between two clay floccules (Source: authors)

of the material through the employment of the specific mechanical properties of both elements and including their proper interaction. Instead adding fibers represents an ancient practice for adobe, originally meant to reduce shrinkage cracks inherent to air drying processes of bricks mixtures during production processes. Their role on the mechanical performance is scarcely addressed in literature.

Interpretation provided in this study on the role of fibers on the mechanical performance of adobe both in dynamics and statics requires to mention a few fracture mechanics principles.

For a generic quasi brittle material tested in dynamics, the enhancement of strength performance can be explained considering a change of fracture planes at a meso-scale with respect to statics [7]. In statics, given a limited set of flaws inside the material, the most critically sized and oriented ones undergo crack initiation and propagation. As these microcracks approach the vicinity of other propagating ones, they may interact and coalesce into a macro crack which leads to loss of structural integrity and failure at a macro-scale [66, 67]. In fact, if propagating flaws encounter stiffer areas, they have the time to deviate around them bridging into macro-cracks and the fracture and stress path with minimum energy demand is defined. Instead in dynamics, loadings characterized by short time duration and high supply rates induce a forced crack development inside the material also through its stiffer areas, while stress intensity is reduced by the coalescence of other similar micro-cracks nearby the loaded areas [68]. As a result, more diffuse patterns of short and straight cracks initiated at multiple weak spots are often observed in quasi brittle materials such as concrete, corresponding to higher values for compressive strength and strain at peak [7, 25]. Also in adobe a strength enhancement is displayed at high strain rates, which is lower than the typical ranges associated to concrete. Cracking patterns in dynamics of the tested adobe clearly show parallel crack orientations to the

loading direction only at the first stages of deformation in dynamics. This is especially the case for fiber enriched mixtures, which experience the lowest rate of increment in the performance and whose failure pattern in dynamics tends to follow the static ones with negligible influence of rate on deformation capacity. The theory of fracture mechanics links with the experimental evidence for adobe given that the rate of enhancement of the dynamic material properties depends on the spatial distributions of the micro-flaws inside the material, that is by the level of uniformity of a mixture. If the number of micro-flaws increases, the probability of interaction increases also in case of dynamic loadings [69]. It means that if density of initial flaws distribution is sufficiently high, the effect of loading rates on the crack bridging processes is limited and a stress path with energy demand close to statics can be developed also in the dynamic regime (Figure 4.17). This can explain the lower DIF of adobe with respect to concrete and the lower DIF of fiber enriched mixtures with respect to fiber free ones. In fact, for industrialized cementitious materials, selection and production processes are highly standardized in order to ensure prescribed levels of uniformity to the mixture and resulting material performance. For adobe appropriate material standards and related quality controls do not exist yet. Moreover, traditional adobe is not pressed during curing, potentially increasing the number of voids in the mixture. Therefore, the level of heterogeneity of traditional adobe is higher than the one associated to modern building materials. This is especially the case for mixtures containing organic content. This is consistent with the interpretation that fibers constitute weak interfaces of the soil matrix of adobe in statics [51]. Their inclusions in soil mixtures potentially determine extensive areas of de-adherence between the adopted soil matrix and natural organic materials, which enhance porosity in the mixture and exasperates the material heterogeneity [31]. Void distribution and porosity is in fact found to weaken the strength also in mortar used in modern masonry [70].

The interpretation of the role of fibers in adobe in dynamics is consistent with the experimental trends observed in statics. In fact, low levels of strength and stiffness associated to the tested adobe including fibers are commonly observed also in literature [19, 71]. Only in rare cases, fibers are found to enhance macro properties in strength [72]. The success of fiber inclusion on the strength is indeed determined by the bonding between the different micro-elements which determines the meso structure of the mixture; that is by soil mineralogical family, elements proportions and organic materials, contents, sizes and shapes [51]. To a minor extent, this also counts for modern building materials. In steel reinforced concrete for instance, the level of bonding in the matrix is found to be dependent on the percentage of steel reinforcement [73].

The major contribution associated to the presence of fibres in the mixture on the mechanical performance of adobe is related to the material ductility. This is a common trend observed for the material of adobe in literature and this is considered the “reinforcing” effect on adobe [71] [74]. Its role is visible from early stages of deformation up to the softening phase of the material response and it is due to the stress-transfer occurring at meso-scale in the mixture. Presence of fibers determines higher heterogeneity to the mixture and larger number and areas of flaws, that causes a more pronounced non linear slope also in the pre-peak curve of response. However, the bridging effect of the fibers allow stresses to be transferred through cracks, limiting their entity and holding

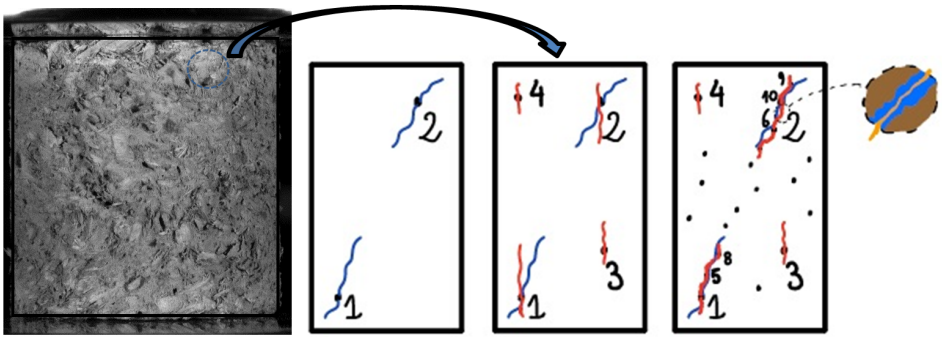

Figure 4.17: Schematic meso-scale representation of micro-flaws numbered in descending order of entity and crack paths, in blue lines for statics (left) and in red in dynamics for low (center) and high (right) number and density of flow distribution, with zoom on possible clay floccules separated by fibers

together the vital cores of the soil particles which are separated by fibers in the post peak region [75]. A similar role is attributed to fiber inclusion in concrete (SFRC), with fibres disperse in the matrix capable of holding together the matrix while reducing the overall lateral expansion of specimens [40, 41].

Fibers are also confirmed to boost the physical properties of the mixture, decreasing the weight of the brick [76].

4.5. CONCLUSIONS

An experimental campaign was performed on specimens of adobe, a masonry made of unsaturated soil bricks and mud mortar. Two types of bricks were tested. They had the same mineralogical composition but they differed in the presence of organic content. For both, half of the samples were fully dried in the oven. Samples were subjected to compressive loadings at three different strain rates corresponding to static, intermediate and high rate loading conditions. A substantial, high-quality set of experimental data has been produced. Data have been elaborated and some constitutive models originally developed for modern geomaterials have been reviewed and proposed for modelling the adobe strain rate sensitivity of strength in this study. In fact tests revealed that the material properties in strength are enhanced by the rate of loadings while a minor influence was encountered in the deformation performance. Strength increases more in fully dried adobe and in mixtures not containing fibers. This is interpreted as that water induces a viscous inter-capillary phenomenon which strengthens inter-particles bonds in the matrix proportionally to the rate of loading. Adding fibers in the mixture enhances the heterogeneity of material for adobe and fibers weaken inter-particle bonds in the matrix causing the presence of weak regions at a meso-scale.

It has also been shown that the macro-properties of adobe, including dynamic increase factors and softening curves, can be addressed using numerical models developed for concrete-based materials. However, many of these numerical models used in engineering are mainly based on assumptions of material homogeneity. This is an accepted approximation for modern building materials which are heterogeneous at a meso-scale but whose mixture selection and production processes are standardized to ensure prescribed levels of homogeneity at a given length scale. As explained above, this assumption can not be a-priori transferred to the traditional adobe produced in the field. Adobe is still a site dependent material and the selection of the mineralogical and geometrical properties of the elements involved in the mixture is not standardized according to optimization requirements but rather chosen for opportunity reasons. In absence of manufacturing regulations and production chain control, high fiber fractions can cause serious material inhomogeneity and void increase in certain soil mixtures of adobe. Proper material selection and production procedures with resulting optimum product quality is essential to ensure a safe use to a sustainable material in current society.

REFERENCES

[1] https://ec.europa.eu/jrc/en/research/commission-priorities (2018).

[2] T. Li Piani, Operative Guidelines for Protection of Places of Worship: A new approach toward security design of sensitive buildings, Institute for Advanced Strategic and Political Studies, ISBN:97888940373-2-6, Milan, 2017.

[3] J. Coaffee, P. O'Hare, M. Hawkesworth, The Visibility of (In)security: The Aesthetics of Planning Urban Defences Against Terrorism, Security Dialogue 40 (4-5) (2009) 489–511. doi:10.1177/0967010609343299.
URL http://sdi.sagepub.com/cgi/doi/10.1177/0967010609343299

[4] T. Li Piani, Structural Design and Social Function of Space as vulnerability factor

and solution to the progression of terrorist treat in urban enviornment (italian), Society, Terrorism, Security (Sicurezza, terrorismo, societa) 8 (2) (2018) 7–17.

[5] D. Grote, S. Park, M. Zhou, Dynamic behavior of concrete at high strain rates and pressures: I. experimental characterization, International Journal of Impact Engineering 25 (9) (2001) 869–886. doi:10.1016/S0734-743X(01)00020-3.

[6] P. Forquin, Brittle materials at high-loading rates: an open area of research, Philosophical Transactions of the Royal Society A: Mathematical, Physical and Engineering Sciences 375 (2085) (2017) 20160436. doi:10.1098/rsta.2016.0436.
URL http://rsta.royalsocietypublishing.org/lookup/doi/10.1098/rsta.2016.0436

[7] R. Pedersen, Computational Modelling of dynamic failure of cementitious materials, Ph.D. thesis, TU Delft University (2010).

[8] J. Baylot, B. Bullock, T. Slawson, S. Woodson, Blast Response of lightly attached concrete masonry units walls, Journal of Structural Engineering 131 (8) (2005) 1186–1193.

[9] H. Hao, B. Tarasov, Experimental Study of Dynamic Material Properties of Clay Brick and Mortar at Different Strain Rates 8 (2) (2008) 117.
URL http://search.informit.com.au/documentSummary;dn=137784543477420;res=IELENG

[10] Q. M. Li, Y. B. Lu, H. Meng, Further investigation on the dynamic compressive strength enhancement of concrete-like materials based on split Hopkinson pressure bar tests. Part II: Numerical simulations, International Journal of Impact Engineering 36 (12) (2009) 1335–1345. doi:10.1016/j.ijimpeng.2009.04.010.
URL http://dx.doi.org/10.1016/j.ijimpeng.2009.04.010

[11] P. Bischoff, S. Perry, Impact behavior of plain concrete loaded in uniaxial compression, Journal of engineering mechanics 121 (June) (1995) 685–693. doi:10.1061/(ASCE)0733-9399(1995)121:6(685).
URL http://ascelibrary.org/doi/abs/10.1061/(ASCE)0733-9399(1995)121:6(685)

[12] X. Wei, H. Hao, Numerical derivation of homogenized dynamic masonry material properties with strain rate effects, International Journal of Impact Engineering 36 (3) (2009) 522–536. doi:10.1016/j.ijimpeng.2008.02.005.
URL http://dx.doi.org/10.1016/j.ijimpeng.2008.02.005

[13] J. M. Pereira, A. Dias, P. B. Lourenço, Dynamic properties of clay brick at different strain rates, Proc. of the 12th Canadian Masonry Symposium 1300 (1990).

[14] M. Larcher, M. Peroni, G. Solomos, N. Gebbeken, P. Bieber, J. Wandelt, N. T. Tran, Dynamic Increase Factor of Masonry Materials: Experimental Investigations, in: ISIEMS, International Symposium for the Interaction of Munitions with Structures, no. September, 2013, p. 10.

[15] D. Silveira, Al., Mechanical properties of adobe bricks in ancient constructions, Construction and Building Materials 28 (1) (2012) 36–44. doi:10.1016/j.conbuildmat.2011.08.046.
URL http://dx.doi.org/10.1016/j.conbuildmat.2011.08.046

[16] P. W. Brown, J. R. Clifton, The properties of Adobe, International Institute for Conservation of Historic and Artistic Works, Taylor & Francis, Ltd. 23 (1978) 139–146.

[17] Adobe masonry in current society: material performance under extreme events (https://www.youtube.com/watch?v=2mxwoS9vFlw) (2018).

[18] D. Silveira, H. Varum, A. Costa, Influence of the testing procedures in the mechanical characterization of adobe bricks, Construction and Building Materials 40 (March) (2013) 719–728. doi:10.1016/j.conbuildmat.2012.11.058.

[19] T. Li Piani, D. Krabbenborg, J. Weerheijm, L. Koene, L. J. Sluys, The Mechanical Performance of Traditional Adobe Masonry Components: An experimental-analytical characterization of soil bricks and mud mortar, Journal of green building 13 (3) (2018) 17–44.

[20] A. A. Hammond, Prolonging the life of earth buildings in the tropics, Building Research and Practice 1 (3) (1973) 154–163. doi:10.1080/09613217308550234.

[21] F. Pacheco-Torgal, S. Jalali, Earth construction: Lessons from the past for future eco-efficient construction, Construction and Building Materials 29 (2012) 512–519. doi:10.1016/j.conbuildmat.2011.10.054.
URL http://dx.doi.org/10.1016/j.conbuildmat.2011.10.054

[22] E. J. d. P. Hansen, K. Kielsgaard Hansen, Unfired clay bricks - moisture properties and compressive strength, in: A. Gustavsen, J. V. Thue (Eds.), Proceedings of the 6th Symposium on Building Physics in the Nordic Countries, Vol. 2, Norwegian University of Science and Technology, 2002, pp. 453–460.

[23] R. Yu, P. Spiesz, H. J. Brouwers, Static properties and impact resistance of a green Ultra-High Performance Hybrid Fibre Reinforced Concrete (UHPHFRC): Experiments and modeling, Construction and Building Materials 68 (2014) 158–171. doi:10.1016/j.conbuildmat.2014.06.033.

[24] S. R. Ferreira, M. Pepe, E. Martinelli, F. de Andrade Silva, R. D. Toledo Filho, Influence of natural fibers characteristics on the interface mechanics with cement based matrices, Composites Part B Engineering 140 (September 2017) (2018) 183–196. doi:10.1016/j.compositesb.2017.12.016.
URL https://doi.org/10.1016/j.compositesb.2017.12.016

[25] P. H. Bischoff, S. H. Perry, Compressive behaviour of concrete at high strain rates, Materials and Structures 24 (6) (1991) 425–450. doi:10.1007/BF02472016.

[26] EN 772-1:2000 "Methods of test of masonry units: Determination of compressive strength".

[27] BS 1377-2:1990 Methods of test for soils for civil engineering purposes. Classification tests.

[28] NT Build 333: Bricks and masonry blocks: Moisture content (1988).

[29] I. Vegt, Concrete in dynamic tension: The fracture process, Ph.D. thesis, TU Delft (2016). doi:10.4233/uuid.

[30] M. Peroni, G. Solomos, N. Babcsan, Development of a Hopkinson bar apparatus for testing soft materials: Application to a closed-cell aluminum foam, Materials 9 (1). doi:10.3390/ma9010027.

[31] R. Illampas, D. C. Charmpis, I. Ioannou, Dynamic Finite Element Analysis of Earth Masonry Structures Based on Experimental Material Data, Conference on Computational Methods in Structural Dynamics and Earthquake Engineering (May) (2011) 26–28.

[32] E. Cosenza, G. Maddaloni, G. Magliulo, M. Pecce, R. Ramasco, Seismic design of concrete structures (italian), Iuss Press, Pavia, 2007.

[33] S. Mishra, H. Meena, V. Parashar, A. Khetwal, T. Chakraborty, V. Matsagar, P. Chandel, M. Singh, High Strain Rate Response of Rocks Under Dynamic Loading Using Split Hopkinson Pressure Bar, Geotechnical and Geological Engineering 36 (1) (2017) 531–549. doi:10.1007/s10706-017-0345-2.
URL http://link.springer.com/10.1007/s10706-017-0345-2

[34] T. Li Piani, J. Weerheijm, M. Peroni, D. Krabbenborg, L. Koene, L. J. Sluys, Dynamic Characterization of Adobe in compression: The effect of fibres with soil binsders, in: FraMCoS-X : Fracture Mechanics of Concrete and Concrete Structures, Bayonne (France), 2019.

[35] N. Gebbeken, T. Linse, T. Araújo, Masonry Under Dynamic Actions: Experimental Investigations, Material Modeling and Numerical Simulations, Advances in Protective Structures Research (October 2015) (2012) 131–161. doi:doi:10.1201/b12768-6.
URL http://dx.doi.org/10.1201/b12768-6

[36] Z. liang Wang, Y. chi Li, R. F. Shen, J. G. Wang, Numerical study on craters and penetration of concrete slab by ogive-nose steel projectile, Computers and Geotechnics 34 (1) (2007) 1–9. doi:10.1016/j.compgeo.2006.09.001.

[37] CEB (Comite Euro-International du Beton) : CEB-FIP Model Code 1990.

[38] X. Q. Zhou, H. Hao, Modelling of compressive behaviour of concrete-like materials at high strain rate, International Journal of Solids and Structures 45 (17) (2008) 4648–4661. doi:10.1016/j.ijsolstr.2008.04.002.

[39] L. Yang, X. Lin, R. J. Gravina, Evaluation of dynamic increase factor models for steel fibre reinforced concrete, Construction and Building Materials 190 (2018) 632–644. doi:https://doi.org/10.1016/j.conbuildmat.2018.09.085.

URL http://www.sciencedirect.com/science/article/pii/S0950061818322633

[40] S. Wang, M.-H. Zhang, S. T. Quek, Effect of high strain rate loading on compressive behaviour of fibre-reinforced high-strength concrete, Magazine of Concrete Research 63 (11) (2011) 813–827. doi:10.1680/macr.2011.63.11.813.
URL http://dx.doi.org/10.1680/macr.2011.63.11.813

[41] Z. Wu, C. Shi, W. He, D. Wang, Static and dynamic compressive properties of ultra-high performance concrete (UHPC) with hybrid steel fiber reinforcements, Cement and Concrete Composites 79 (2017) 148–157. doi:10.1016/j.cemconcomp.2017.02.010.
URL http://dx.doi.org/10.1016/j.cemconcomp.2017.02.010

[42] X. Chen, S. Wu, J. Zhou, Experimental and modeling study of dynamic mechanical properties of cement paste, mortar and concrete, Construction and Building Materials 47 (2013) 419–430. doi:10.1016/j.conbuildmat.2013.05.063.
URL http://dx.doi.org/10.1016/j.conbuildmat.2013.05.063

[43] H. Mihashi, F. H. Wittmann, Stochastic Approach To Study the Influence of Rate of Loading on Strength of Concrete., Heron 25 (3).

[44] K. S. H. O. K. Jitsu, K. Shirai, C. Ito, Effects of strain rate on concrete strength subjected to impact load-Dynamic compressive strength test by Split Hopkinson Pressure Bar method, Transactions on the Built Environment 32 (1998) 1–3.

[45] H. B. Kaushik, D. C. Rai, S. K. Jain, Stress-Strain Characteristics of Clay Brick Masonry under Uniaxial Compression, Journal of Materials in Civil Engineering 19 (9) (2007) 728–739. doi:10.1061/(ASCE)0899-1561(2007)19:9(728).
URL http://www.iitk.ac.in/nicee/RP/2007{_}Masonry{_}Properties{_}ASCE.pdf

[46] B. Scott, R. Park, M. Priestley, Stress strain behaviour of concrete confined by overlapping hoops at low and high strain rates, ACI Journal 79 (1) (1982) 13–27.

[47] T. Li Piani, J. Weerheijm, L. Koene, L. J. Sluys, Modelling the Mechanical Response of Adobe Components under Uniaxial Loading, Key Engineering Materials 774 (2018) 650–657.

[48] D C Kent and R.Park, Flexural members with confined concrete, Journal of the structural division, ASCE 97 (1990).

[49] R. Illampas, I. Ioannou, D. C. Charmpis, Adobe bricks under compression : Experimental investigation and derivation of stress – strain equation, Construction and Building Materials 53 (2014) 83–90. doi:10.1016/j.conbuildmat.2013.11.103.
URL http://dx.doi.org/10.1016/j.conbuildmat.2013.11.103

[50] T. Li Piani, J. Weerheijm, L. Koene, L. Sluys, The Adobe delta damage model: A locally regularized rate-dependent model for the static assessment of soil masonry bricks and mortar, Engineering Fracture Mechanics 206 (2019) 114–130.

doi:10.1016/j.engfracmech.2018.11.026.
URL https://linkinghub.elsevier.com/retrieve/pii/S0013794418308956

[51] T. Li Piani, J. Weerheijm, L. Koene, L. Sluys, Modelling the Mechanical Response of Adobe Components under Uniaxial Loading, 17th International Conference on Fracture and Damage Mechanics 774 (2018) 650–657. doi:10.4028/www.scientific.net/KEM.774.650.

[52] S. Popovics, A review of stress strain relationships for concrete, American Concrete Institute Journal 67 (3) (1970) 243–248.

[53] Popovics, A numerical approach to the complete stress strain curve of concrete, Cement and Concrete Research 3 (1973) 583–599.

[54] J. W. Tedesco, J. C. Powell, C. A. Ross, M. L. Hughes, A strain-rate-dependent concrete material model for ADINA, Computers and Structures 64 (5-6) (1997) 1053–1067. doi:10.1016/S0045-7949(97)00018-7.

[55] Y. Millogo, M. Hajjaji, R. Ouedraogo, Microstructure and physical properties of lime-clayey adobe bricks, Construction and Building Materials. 22.

[56] J. Stefan, Versuche über die scheinbare adhäsion, Sitzungs- berichte der Kaiserlichen Akademie der Wissenschaften, Mathematisch-Naturwissenschaftliche Classe1 (1874) 713–735.

[57] P. Rossi, A physical phenomenon which can explain the mechanical behaviour of concrete under high strain rates, Materials and Structures 24 (6) (1991) 422–424. doi:10.1007/BF02472015.

[58] S. Zeng, X. Ren, J. Li, Triaxial Behavior of Concrete Subjected to Dynamic Compression, Journal of Structural Engineering 139 (9) (2013) 1582–1592. doi:10.1061/(ASCE)ST.1943-541X.0000686.
URL http://ascelibrary.org/doi/10.1061/{%}28ASCE{%}29ST.1943-541X.0000686

[59] J. Cao, D. D. Chung, Effect of strain rate on cement mortar under compression, studied by electrical resistivity measurement, Cement and Concrete Research 32 (5) (2002) 817–819. doi:10.1016/S0008-8846(01)00753-0.

[60] E. Cadoni, K. Labibes, C. Albertini, M. Berra, M. Giangrasso, Strain-rate effect on the tensile behaviour of concrete at different relative humidity levels, Materials and Structures 34 (February) (2001) 21–26. doi:10.1007/BF02482196.

[61] P. Delage, M. Audiguier, Y.-j. Cui, M. Howat, Microstructure of a compacted silt, Can. Geotech. 33 (1996) 150–158.

[62] J. A. Calabria, W. L. Vasconcelos, A. R. Boccaccini, Microstructure and chemical degradation of adobe and clay bricks, Ceramics International 35 (2) (2009) 665–671. doi:10.1016/j.ceramint.2008.01.026.

[63] T. Lambe, The structure of compacted clay, Journal of the Soil Mechanics and Foundations Division 84 (1958) 1–34.

[64] P. Morandi, L. Albanesi, F. Graziotti, T. Li Piani, A. Penna, G. Magenes, Development of a dataset on the in-plane experimental response of URM piers with bricks and blocks, Construction and Building Materials 190 (2018) 593–611. doi:10.1016/j.conbuildmat.2018.09.070.
URL https://doi.org/10.1016/j.conbuildmat.2018.09.070

[65] H. Singh, Steel Fiber Reinforced Concrete Behavior, Modelling and Design - Chapter 2:Material Models, Vol. 25, 2017. doi:10.1617/s11527-010-9596-6.
URL http://www.jsce.or.jp/committee/concrete/e/newsletter/newsletter05/JSCE-VIFCEAJointSeminarPapers.htm{%}0Ahttp://pubsindex.trb.org/view.aspx?id=25485

[66] M. Jirasek, Z. Bazant, Model for Localization of Softening and Size Effect, in: Inelastic Analysis of Structures, 2002, Ch. 26.

[67] P. D. Washabaugh, W. G. Knauss, A reconciliation of dynamic crack velocity and Rayleigh wave speed in isotropic brittle solids, International Journal of Fracture 65 (2) (1994) 97–114. doi:10.1007/BF00032282.

[68] J. K. Zhou, L. M. Ge, Effect of strain rate and water-to-cement ratio on compressive mechanical behavior of cement mortar, Journal of Central South University 22 (3) (2015) 1087–1095. doi:10.1007/s11771-015-2620-9.

[69] K. Ravi-Chandar, An experimental investigation into dynamic fracture: I. Crack initiation and arrest, International Journal of Fracture 3 (4) (1984) 105–262. doi:10.1007/s00018-012-1041-2.

[70] M. O'Farrell, S. Wild, B. B. Sabir, Pore size distribution and compressive strength of waste clay brick mortar, Cement and Concrete Composites 23 (1) (2001) 81–91. doi:10.1016/S0958-9465(00)00070-6.

[71] . Yetgin, O. Çavdar, A. Çavdar, The effects of the fiber contents on the mechanic properties of the adobes, Construction and Building Materials 22 (3) (2008) 222–227. doi:10.1016/j.conbuildmat.2006.08.022.

[72] F. Parisi, D. Asprone, L. Fenu, A. Prota, Experimental characterization of Italian composite adobe bricks reinforced with straw fibers, Composite Structures 122 (2015) 300–307. doi:10.1016/j.compstruct.2014.11.060.
URL http://dx.doi.org/10.1016/j.compstruct.2014.11.060

[73] S. Wang, M. H. Zhang, S. T. Quek, Mechanical behavior of fiber-reinforced high-strength concrete subjected to high strain-rate compressive loading, Construction and Building Materials 31 (2012) 1–11. doi:10.1016/j.conbuildmat.2011.12.083.
URL http://dx.doi.org/10.1016/j.conbuildmat.2011.12.083

[74] G. Araya-Letelier, F. C. Antico, M. Carrasco, P. Rojas, C. M. García-Herrera, Effectiveness of new natural fibers on damage-mechanical performance of mortar, Construction and Building Materials 152 (2017) 672–682. doi:10.1016/j.conbuildmat.2017.07.072.
URL http://dx.doi.org/10.1016/j.conbuildmat.2017.07.072

[75] D. Daviau-Desnoyers, J.-P. Charron, B. Massicotte, P. Rossi, J.-L. Tailhan, Characterization of macrocrack propagation under sustained loading in steel fibre reinforced concrete, Materials and Structures 49 (3) (2016) 969–982. doi:10.1617/s11527-015-0552-3.

[76] M. L. Parra-Saldivar, W. Batty, Thermal behaviour of adobe constructions, Building and Environment 41 (12) (2006) 1892–1904. doi:10.1016/j.buildenv.2005.07.021.

5

THE NUMERICAL SIMULATION OF ADOBE IN DYNAMICS

"To improve is to change,
so to be perfect is to have changed often."

W. Churchill, 1925

A local damage model has been recently developed for the numerical simulation of the static behaviour of adobe bricks. Mesh insensitivity of the local model was obtained by generalizing the damage delay concept based on a Dirichlet boundary condition decomposition integrated in an implicit solver. The regularization properties of the model were proven before only in statics. In this study, mesh independence is demonstrated in dynamics analysing the problem of a cantilever bar uniaxially loaded at high deformation rates. Furthermore, the physical background of the delay formulation is interpreted regarding the main failure processes in compression exhibited by quasi brittle materials used in masonry. Two limitations of the model in correctly simulating the dynamic behaviour of masonry bricks have been observed. Corrections to the original damage delay formulation are proposed in this study. These enhance the capability of the model to address also distributed failure of traditional geo-materials and the inherent rate dependence also at high strain rate regimes. The improvements are demonstrated in this paper by means of numerical simulations of both theoretical tests and practical applications. These consists of experimental tests in compression recently performed by the authors at different strain rates, from statics to high velocity impact tests.

This chapter is based on "Dynamic simulations of traditional masonry materials at different loading rates using an enriched damage delay: theory and practical applications" in *Engineering Fracture Mechanics*, 2019.

5.1. INTRODUCTION

Built heritage of the contemporary city is more and more exposed to dynamic hazards of different nature [1]. Not only natural events such as floods or earthquakes may happen but also man-made threats such as ballistic impacts and blast explosions due to an increase of the terrorist threat in Europe [2]. Because of high amplitudes and strain rates induced locally on the target, these events can produce severe damage in structures made of quasi brittle materials such as concrete [3]. In fact, the response of softening geo-materials is highly sensitive to the applied rate of loading [4]. Therefore, the development of interpretative tools capable of addressing the dynamic behaviour of quasi brittle materials is of paramount importance nowadays [5].

In engineering software, numerical simulations of material failure often use a damage framework [6]. Continuum damage mechanics constitutes a pragmatic approach close to the physics of the material because it interprets failure as a progressive degradation of the elastic capacity of the material [7]. In fact, in quasi brittle materials failure starts when the first micro-cracks coalesce starting from voids or defects inside the material and bridge into a macro-crack which may cause the progressive loss of structural integrity [8].

However, the link between many damage models and the corresponding physical mechanisms aimed to be addressed still represents a controversial issue not fully solved [9]. This is also the case because damage models suffer from a numerical pathology which prevents objective evaluations of failure for different spatial discretizations [10]. In statics, this is because the boundary value problem becomes ill posed when strain softening takes place due to the loss of ellipticity of the governing equations [11]. To solve this issue, so-called regularization algorithms are coupled to local damage models. As a result, extra functions must be implemented, sometimes at the cost of controversial physical interpretations for the inherent numerical parameters. This is the case, e.g. for non local regularization models [9].

Local regularization algorithms may solve mesh dependence using rate dependent damage laws and thus constitute the closest approach to the physics of quasi brittle materials in dynamics [11]. Unfortunately, only a limited number of these models are capable of fully regularizing the model [12]. The regularization properties of a particular local algorithm have been recently demonstrated in statics [13]. It integrates a-dimensional damage delay functions based on decomposition of Dirichlet boundary conditions into the constitutive equations of a local model for concrete and solved using an implicit solver [13]. The regularization algorithm is based on the concept of a bounded rate of damage, which was originally applied for simulating delamination problems in composites materials [14]. However, this can constitute a valid approach also for cement or clay-based quasi brittle materials commonly used in masonry [15].

The model developed in [13] for static loadings is briefly presented in Section 5.2 of this paper. The aim of this study is twofold. The regularization properties of the model are herein analysed for the dynamic problem at high loading rates including inertia effects (Section 5.3). Furthermore, the original delay algorithm is modified. Its formulation is enriched with two new material and external conditions dependencies in Section 5.4. The modifications address the specific limitations observed in numerical simulations of the dynamic response of quasi brittle materials using the original formulation. The op-

portunity of the proposed solutions are interpreted in light of the theory on the dynamic behaviour of quasi brittle materials commonly used in masonry. For both cases, they are numerically demonstrated via simulations of theoretical problems and validated via numerical simulations of two real dynamic compression tests recently performed by the authors on different types of masonry bricks [16]. Many of these tests concerned the material characterization of adobe components, sundried made of silt, sand and clay. The numerical simulations of the model presented in [13] were aimed at addressing the static behaviour of this traditional material. Therefore the model was originally named "adobe delta damage model" [15].

5.2. THE ADOBE DELTA DAMAGE MODEL

The model developed in [13] is briefly presented in this section. This model adapts a damage delay algorithm originally developed for laminated composites [17] in a local damage framework recently modified for the dynamic assessment of concrete [3, 18]. Implementation of the model starts from the classical formulation for isotropic damage in eq. 5.1 [19]:

$$\sigma = (1-D)\tilde{\sigma} \quad \text{with} \quad \tilde{\sigma} = E\varepsilon\,, \tag{5.1}$$

where $\tilde{\sigma}$ is the effective stress vector, ε is the strain vector, E the elastic stiffness matrix and D is the damage scalar, a parameter which ranges between 0 (integer material) and 1 (fully damaged material). Damage starts when the loading function ψ in eq.5.2 becomes positive:

$$\psi = \varepsilon_{eq} - k_0\,, \tag{5.2}$$

where ε_{eq} and k_0 are the equivalent strain and the damage initiation strain, respectively. The thermodynamic variables of the material states are expressed as equivalent strains for compression crushing (ε_{eq_c}) and tensile cracking (ε_{eq_t}) [20]. A modified Drucker-Prager damage surface is represented, which is suitable for a wide range of pressure-dependent building materials [21]. The equivalent strains are expressed as a combination of normal (ε_{oct}) and tangential (γ_{oct}) strain components in the octahedral space:

$$\begin{cases} \varepsilon_{eq_t} = c_1\varepsilon_{oct} + c_2\gamma_{oct} \\ \varepsilon_{eq_c} = c_3\varepsilon_{oct} + c_4\gamma_{oct} \end{cases} \tag{5.3}$$

which are related to the first (I_ε) and second deviatoric (J_{ε_d}) invariants of strain as in eq.5.4:

$$\begin{cases} \varepsilon_{oct} = \dfrac{1}{3}I_\varepsilon = \dfrac{\varepsilon_1+\varepsilon_2+\varepsilon_3}{3} \\ \gamma^2_{oct} = -\dfrac{8}{3}J_{\varepsilon_d} = \dfrac{4}{9}[(\varepsilon_1-\varepsilon_2)^2+(\varepsilon_2-\varepsilon_3)^2+(\varepsilon_3-\varepsilon_1)^2] \end{cases} \tag{5.4}$$

where ν is the Poisson's ratio and subscripts $_{1,2,3}$ denote a principal value.
Parameters $c_1 - c_4$ are taken equal as in [3], but also other options are available according to the material properties [15]:

$$\begin{cases} c_1 = \frac{1}{(1-2\nu)} \\ c_2 = \frac{1}{2(\sqrt{2}(1+\nu))} \\ c_3 = \frac{3}{5(1-2\nu)} \\ c_4 = \frac{3\sqrt{3}}{5(\sqrt{2}(1+\nu))} \end{cases} \tag{5.5}$$

Evolution of damage is directly related to the growth of two monotonic internal variables which account for the maximum equivalent strains reached during loading history in case of non-monotonic loadings. These are implemented separately for compression (k_c) and tension (k_t) according to [12]:

$$\begin{cases} k_c(i) = \max[\, \varepsilon_{eq_c}(1-r^{\alpha}), k_{0c}(\tau)] \quad \text{for all} \quad i \geq \tau \\ k_t(i) = \max[\, \varepsilon_{eq_t} r^{\alpha}, k_{0t}(\tau)] \quad \text{for all} \quad i \geq \tau \end{cases} \tag{5.6}$$

Where r is derived from the triaxiality factor proposed by Lee and Fenves [22] for multi-axial loading states, α is a constant set to 0.1 as in [5] and the mechanical parameters k_{0t} and k_{0c} are the damage initiation strains in tension and compression [23].
Two damage evolutions laws called for compression and tension are dependent on the damage initiation strains determined by the stress state of the integration point. These are rate-independent laws resulting from linear and exponential softening functions [24]:

$$d_{c,t} = 1 - \frac{1}{e^{a_{c,t}(k_{c,t}-k_{0_{c,t}})}} - \frac{k_{0_{c,t}}}{b_{c,t}k_{c,t}} \tag{5.7}$$

Where a and b are non dimensional parameters.
For both compression and tension, eq.5.7 enters a damage delay function. At a certain time τ of the generic loading history evaluated in N points by the Newton-Raphson solver, non dimensional delta functions are introduced according to a principle of decomposition of the Dirichlet boundary condition [13]:

$$\delta D^{\tau}_{c,t} = D^{\tau}_{c,t} - D^{\tau-1}_{c,t} = \frac{\Delta_{c,t}}{N}(1 - e^{-(d^{\tau}_{c,t} - D^{\tau-1}_{c,t})}) \tag{5.8}$$

where Δ is a non dimensional parameter that bounds the maximum damage rate [13]. The final value of damage at each time step results from the combination of the values in compression and tension [5]:

$$D = 1 - (1 - D_c)(1 - D_t) \tag{5.9}$$

In the dynamic problem, a consistent mass matrix has been implemented in the equilibrium equation of the finite element model. Time integration of the field equations has been done using the implicit Newmark unconditionally stable scheme [25]. The set of governing equations is integrated within an implicit Newton-Raphson solver. The code has been developed in a C++ environment [26].

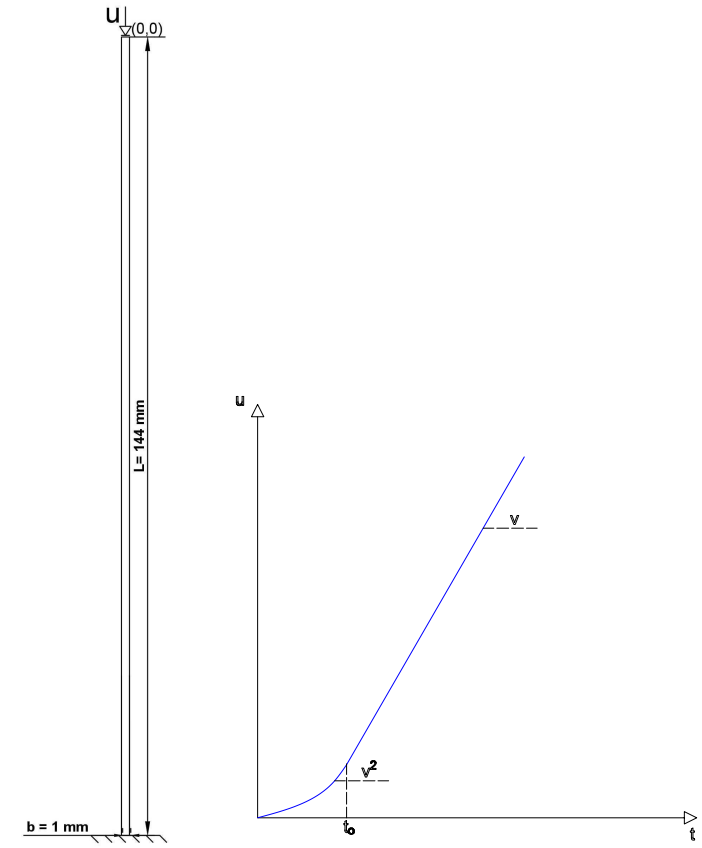

(a) (b)

Figure 5.1: Setup for mesh sensitivity study for the uniaxially loaded bar test: geometry (a) and boundary conditions (b)

5.3. MESH SENSITIVITY STUDY IN DYNAMICS

The capability of the model to perform mesh objective analyses in statics was demonstrated in [13]. This section analyses its regularization properties in dynamics. To this end, a classical test from literature used to diagnose mesh dependence is adopted [27]. This is the cantilever bar uniaxially loaded in compression [11]. A piecewise velocity profile is commonly applied at the free edge of a 100mm long bar fixed at the bottom (Figure 5.1) [28]. The same analysis is performed for different levels of spatial discretizations. The mesh of the bar is progressively refined starting from a coarse mesh of 10 elements up to 160 elements. Results from numerical analyses are used to verify the local damage

distribution and the global reaction force for different levels of mesh refinement.

5.3.1. QUASI STATIC REGIME

Prior to the dynamic analysis, the results of a test using the model are compared with the static counterpart to verify the correctness of software implementation in dynamics. The analysis is carried out at a low deformation rate (v=1mm/min) which implies a negligible contribution of inertia in the dynamic equilibrium equation. The following set of material parameters of the model are used: a=1000, Δ = 10, ν =0.0, E=200 MPa, ρ=1400 $\frac{kg}{m^3}$, k_0=1e^{-3}, while t_0=0 s and N=2000. Values are valid for both tension and compression [15]. Results are evaluated with the static analysis in terms of force displacement and damage evolution profile. Considering natural oscillations inherently present in dynamic simulations, the analyses provide the same results. Furthermore, mesh objectivity is verified in terms of reaction force plots and damage profiles resulting from dynamic equilibrium equations (Figure 5.2). The model provides the same results independently of the adopted spatial discretizations and the damage profiles are consistent along the process of failure (Figure 5.2b).

5

5.3.2. WAVE PROPAGATION PROBLEM

To verify mesh objectivity of the model for a wave propagation problem, sensitivity tests are performed in the case of a significant inertia contribution in the dynamic equilibrium equations. The numerical setup introduced by Sluys in 1992 is adopted [11]. A constant value for the velocity v calculated as $\frac{\kappa f_b}{C\rho}$ (with f_b, C the uniaxial strength and longitudinal wave speed determined by the elastic property of the model respectively and κ a parameter lower than 1) is instantaneously applied (t_o=0 s) to generate a block wave pulse along the bar which guarantees a linear elastic response of the bar until the loading wave reaches the bottom boundary. The doubling of the stress after reflection assures immediate damage at the boundary and localization of intense straining emerges [10]. The same set of values used in par.5.3.1 for the rate independent parameters of the model is applied. In order to force localization for the fast loading scenario, the parameter Δ in the damage delay formulation is magnified with a factor 500. The adopted time step is 2e^{-6}s, calculated approximately as 1% of the ratio between the length of the bar and the speed of sound C, which is about 400m/s for the assumed set of elastic parameters.

Time history of the reaction force at the bottom boundary nearly overlap for all mesh refinements (Figure 5.3). Maximum errors in peak load values and toughness of the stress strain curve are always lower than 2%. Damage profiles are consistent for all meshes during the entire simulation (Figure 5.4).

Results of wave propagation sensitivity test yields the conclusion that the model produces objective simulations in dynamics.

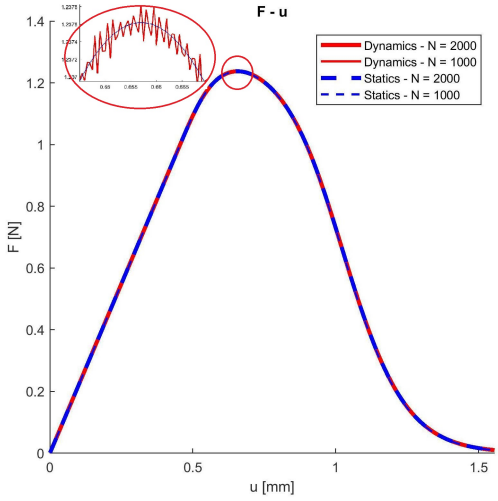

(a)

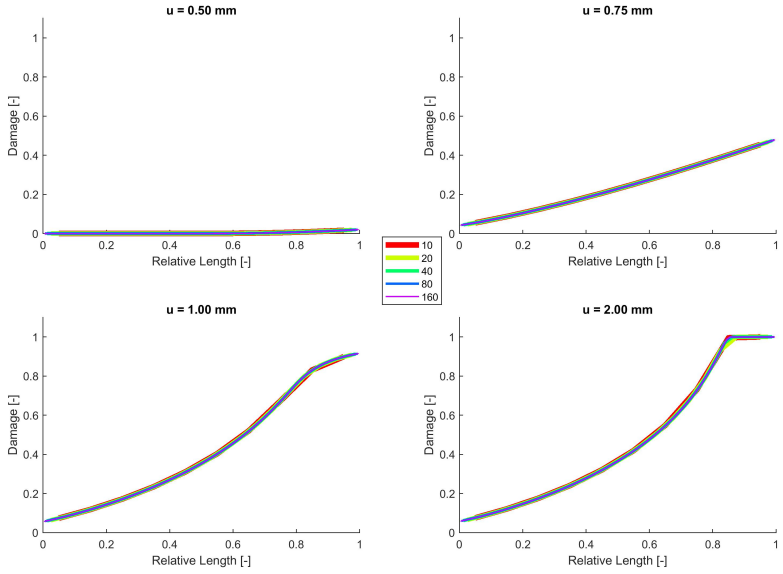

(b)

Figure 5.2: Force displacements plots (a) and damage profile extensions along the bar at different stages of simulation (b) for static and quasi static tests at different time (N:1000-2000) and spatial (mesh elements: 10-160) discretizations (relative length expressed as ratio of x over L)

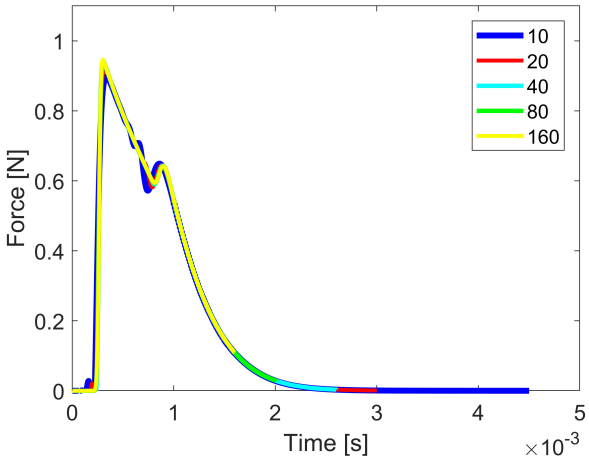

Figure 5.3: Reaction force time plots at bottom boundary for a shock wave propagation test for different meshes

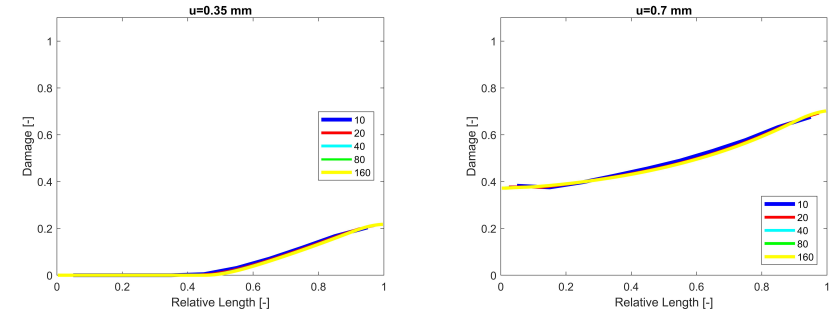

(a)

(b)

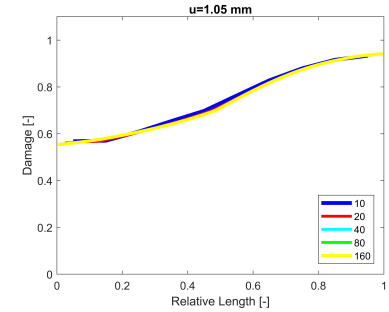

(c)

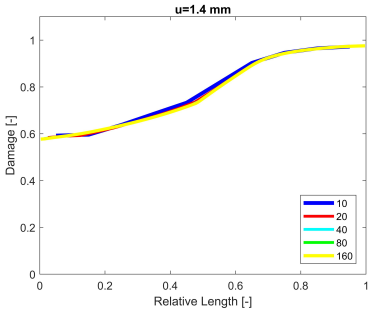

(d)

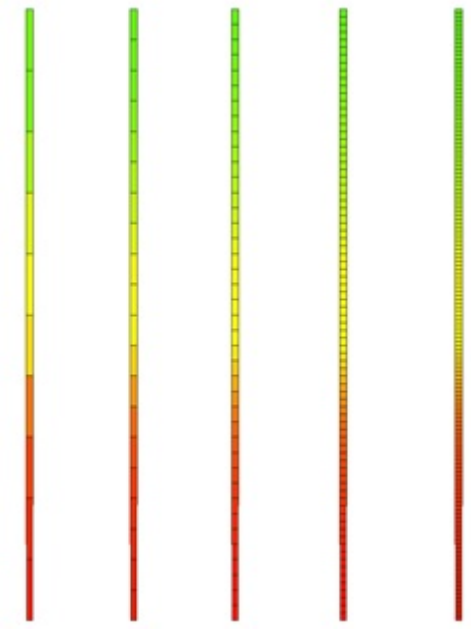

(e)

Figure 5.4: Damage profile evolution in the bar at different stages of simulation (a-d) and extension of damage in the bar at t=1.8e^{-3}s(e) for a shock wave propagation test for different meshes

5.4. A PHYSICAL INTERPRETATION OF THE MODEL FOR SOFTENING MATERIALS

In the previous section the performance of the model in dynamics in terms of mesh independence has been verified. In this section, the original formulation of the delay function is modified according to eq. 5.10:

$$\delta D^{\tau} = \frac{\Delta\mu(\dot{\epsilon_s}^{\tau})}{N} \quad (1 - e^{-\beta(d^{\tau})(d^{\tau} - D^{\tau-1})}) \tag{5.10}$$

where μ is a function of the loading rate and β a function of the local damage d. The new inclusions are meant to improve the performance of the original formulation. An extra dependence in the delay function on the value of the local damage d at a given time τ is aimed at enhancing the flexibility of the model to track different shapes of the softening behaviour for various masonry materials. A function μ is introduced to control the maximum damage rate for high loading rates and it allows to use the same model to simulate the material response tested at different deformation rates. In the following two paragraphs, the two modifications are interpreted in the light of the current knowledge on the mechanical behaviour of quasi brittle materials, using principles of fracture mechanics as well as experimental evidence. Physical consistency and mesh objectivity are firstly numerically tested using the same uniaxial compression test setup shown in Sec. 5.3 (Figure 5.1), with loading profiles at the upper boundary of the quasi static regime (1-5 mm/s). Next, modifications are validated against real dynamic tests recently performed by the authors on various clay based masonry materials [16]. Uniaxial tests consisted of dynamic impacts at velocities ranging from 80 mm/s to 4000 mm/s on cylindrical samples of only clay baked and air dried fibrous adobe materials.

5.4.1. NUCLEATION TIME IN QUASI BRITTLE MATERIALS AND THE NUMERICAL DELAY FOR DUCTILE CURVES OF RESPONSE

A sample of a generic masonry material subjected to an external load in compression does not instantaneously fail due to the formation of the first (micro)-crack. Inside the sample, micro-flaws and defects coalesce and grow until bridging in the macro-crack leads to failure [29]. Thus, a variation in the external load does not result in an immediate damage visible in the sample. There is always a certain *nucleation time* inherent to micro-crack bridging processes.

The delay function of exponential shape in eq. 5.10 numerically includes this physical property: damage variation due to a variation in the external equilibrium equation of forces at the boundary is not instantaneous but delayed [17].

In quasi brittle materials, spatial and temporal progression of micro-cracking processes from first flaws is found to be dependent on the intrinsic properties of the material and on the external load applied [30, 31].

It is experimentally observed that the nucleation time leading to the bridging process for adobe as well as for other masonry materials is significantly influenced by the external rate [32]. In statics, if propagating flaws encounter stiffer areas, they have the time to deviate around these zones, bridging into macro-cracks, and fracture along a crack path with minimum energy demand is followed. Instead in dynamics, loadings characterized

by short time duration and high supply rates induce a forced crack development inside the material also through its stiffer areas, while stress intensity is reduced by the coalescence of other similar micro-cracks nearby the loaded areas [33]. As a result, higher values for compressive strength and strain at peak are observed in the dynamic response of concrete-like materials [34, 35]. In the original delay formulation of eq.5.8, the influence of loading history on the nucleation time numerically results from the delay $1-e^{-(d-D)}$ between d at time τ and D at $\tau-1$. For increasing velocity profiles on the bar of Figure 5.1, strength (Figure 5.5a) and damage profiles (Figure 5.5b) using the original model and set of parameters as in par. 5.3.1. progressively increase.

However in [13] a limitation of the original function was observed in correctly capturing the ductile response of masonry bricks and mortar in softening after strength attainment. This particularly occurs when simulating traditional materials like adobe. These are characterized by a non linear response along the entire deformation process and often denoted by a more ductile softening slope corresponding to a distributed failure due to fiber inclusions. These process could not be fully addressed in [13] using eq.5.8 and the available set of functions and parameters. The experimental-numerical discrepancy was attributed to a more distributed failure pattern in tests caused by the development of extensive micro cracking during advanced stages of deformation. The influence of the micro-flaws developing along the entire deformation process is mathematically translated in the variable β of the new eq. 5.10. An increasing brittleness in the response for higher values of the parameters ahead of the exponent of the delay function was already observed in [9]. However, besides a decay of the strength, the shape of the resulting softening slope remained the same using constant parameters. Instead, the mineralogical properties and inter-particle interactions influence the micro-flaws size and distribution which dictate the speed and progression of the micro-cracks coalescing into the structural macro-crack up to failure [31]. As a result, the softening slope can be significantly different between different materials and change during the deformation process according to the mineralogical properties of the mixture. The effects of these properties on material failure are phenomenologically represented in damage models by the parameters inherent to the local damage evolution laws (eq.5.7). Thus, the dependence of the softening process on the intrinsic mixture properties is represented by a β function in the delay of eq.5.10 that governs the actual history of the local damage d along the whole deformation process. This results into a direct dependence of β on the value of the local damage d at time step τ. The entire non linear phase of the material response changes after introducing β, including the initial damage rate and the softening slope evolution. They vary according to the particular function used for the evolution for β. This is shown in the following, using the test of the compressed bar presented in Sec. 5.3. Four different continuous functions of the local damage d are presented in eq. 5.11 are applied for the same model already calibrated in Par. 5.3.1 (Figure 5.6a).

$$\begin{cases} \beta_1 = e^{5(d-1)} & \\ \beta_2 = d & \beta_5 = 0.2 \ (if \ d \le 0.5) \\ \beta_3 = -d^2 + d & \beta_5 = 1.0 \ if \ (d \ge 0.5) \\ \beta_4 = -3d^2 + 6d & \end{cases} \tag{5.11}$$

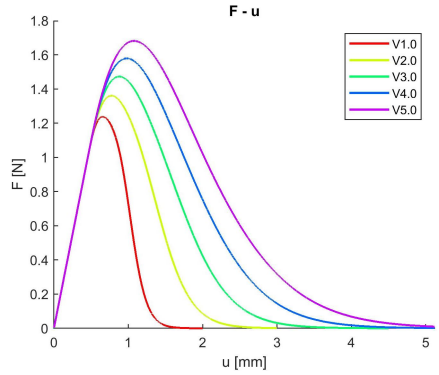

(a)

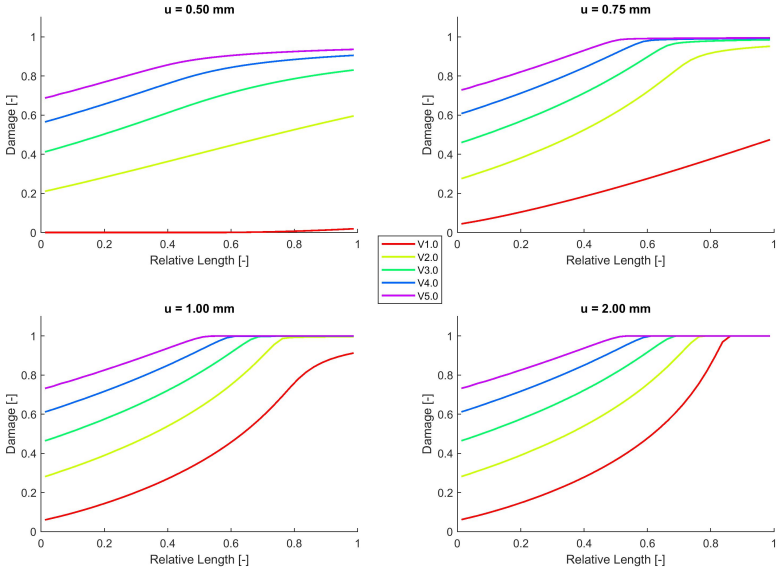

(b)

Figure 5.5: Force displacement plots (a) and damage profile evolutions (b) for dynamic analyses at velocities from 1 mm/s to 5 mm/s using delay formulation of eq. 8 and parameters in par. 5.3.1

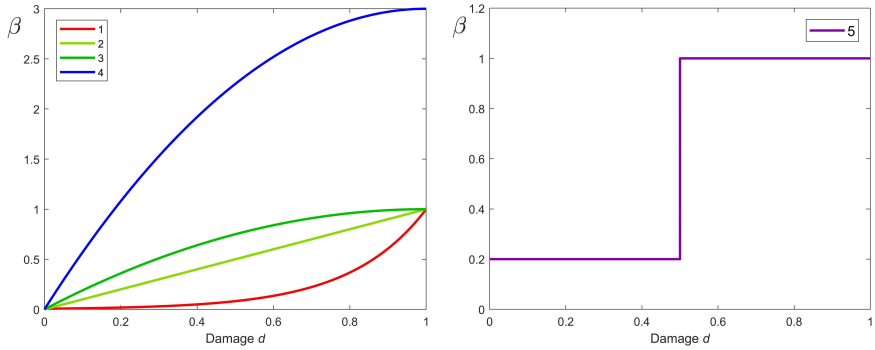

Figure 5.6: Different functions for β: continuous (β_{1-4}) and Heaviside function (β_5)

According to the different functions and inherent slopes at a given damage d, the corresponding four curves are characterized by different damage rates, softening branch slopes (Figure 5.7a) and damage evolution (Figure 5.7b). The flexibility of the new formulation is further emphasized using a discontinuous function of d for β. A Heaviside function which presents a sudden jump in the middle of the damage evolution d is applied in the model (Figure 5.6b). This may correspond to a material response characterized by a quasi brittle meso-structure that is dramatically weakened at a certain deformation level. This can result from a change of rate in the micro-cracks bridging processes inside the material due to the specific properties of the mixture. According to the depicted trend, curve 5 in Figure 5.7 initially shows a significant non linear response and a distributed damage profile, before sudden failure with damage localization and a brittle softening branch after crisis. The choice of the peculiar relationship for β depends on the empirical evidence characterizing the material response in compression that in turn results from its internal processes.
The enrichment in eq. 5.10 does not affect the mesh dependence regularization properties of the algorithm for all the proposed functions (Figure 5.8).

A NUMERICAL APPLICATION OF THE NEW FORMULATION

Correctly capturing the complete failure in compression is fundamental for non linear analyses of masonry materials [36, 37]. The effect of the new formulation is tested in this paragraph on the simulation of the dynamic failure in compression of masonry applications. For this purpose, the dynamic response of adobe is used as an experimental reference. Adobe bricks are commonly constituted by soil mixed with fibers and dried under the sun. As a result, their behaviour in compression is usually characterized by a non-linear response with ductile softening and a distributed failure pattern that progresses during the entire deformation process, with the development of secondary cracks starting after attainment of the main one.
A joint experimental campaign between Delft University of Technology, TNO, Dutch

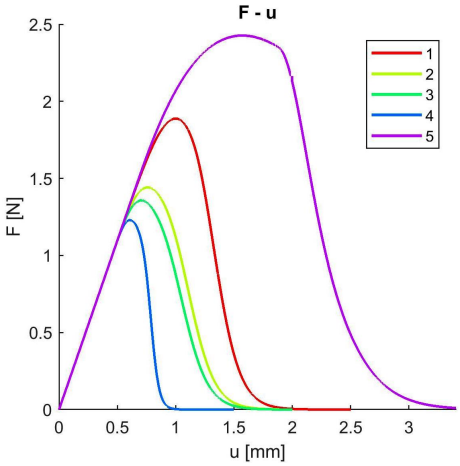

(a)

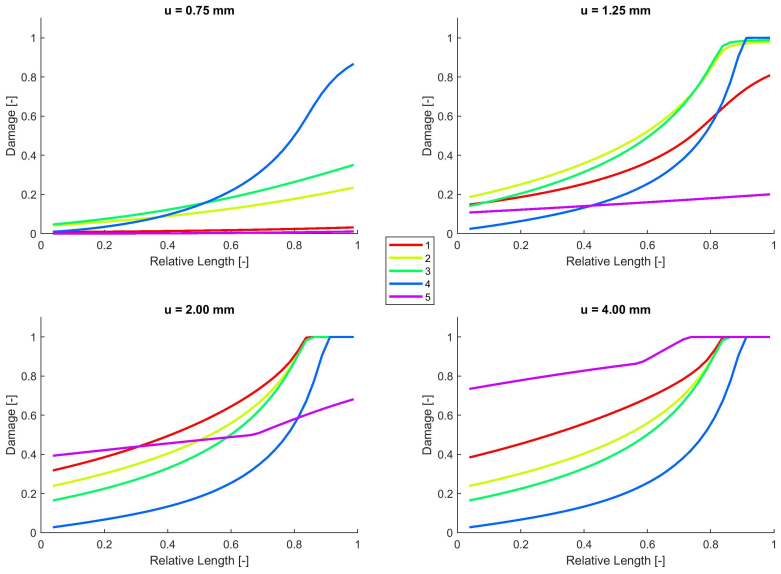

(b)

Figure 5.7: Force displacement plots (a) and damage profile evolution (b) for dynamic analyses at v=1 mm/s using the five functions in eq.5.11

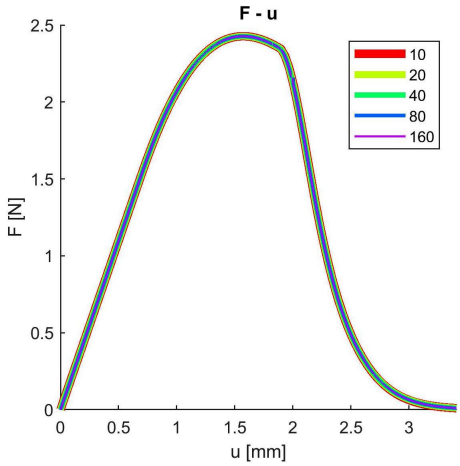

(a)

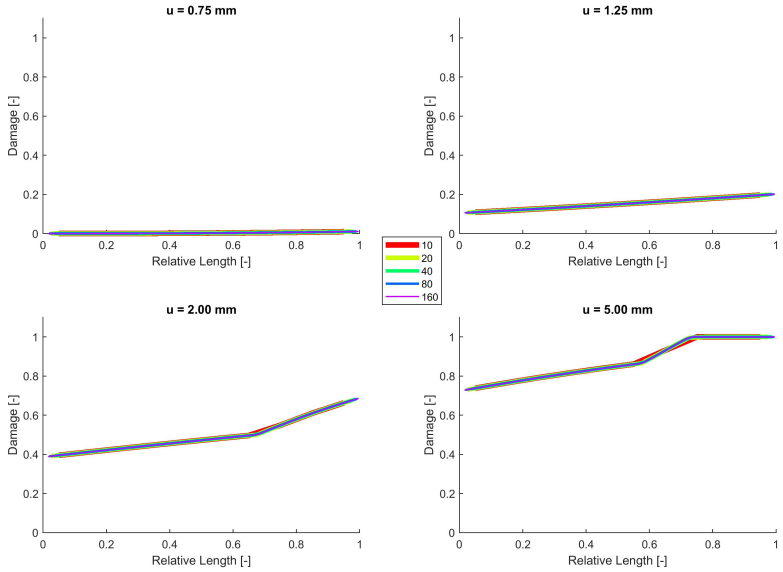

(b)

Figure 5.8: Force displacement plots (a) and damage profile evolution (b) for different meshes using β_5 (for an applied velocity of 1 mm/s)

Ministry of Defence and European Commission performed uniaxial compression tests on adobe samples at high rates of deformations [16]. Cylindrical samples of 40mm in diameter and with unitary slenderness of an adobe brick with 20% b.w.fibers in the soil mixture were subjected to displacement controlled analyses at a constant rate of 90mm/s. The response of the samples was characterized by a more ductile softening slope and a distributed pattern of cracks observed on the entire surface. These usually started before reaching the maximum reaction force. At least two main cracks developing at different moments of the test in softening of whom the first usually starting from one corner of the specimen were observed during testing. A representative test is chosen as the experimental reference.
For numerical simulation purposes, the constant loading profile experimentally applied to the specimen by the displacement driven steel platens is directly extracted from the test and applied at the top of the numerical setup. Boundary conditions are shown in Figure 5.9. Axial symmetry is implemented in the model to simulate the 3D cylindrical shape of the sample and only half of the brick is simulated and meshed with a 0.5mm element size. Geometrical dimensions of the numerical sample are approximately the same as in experiments.
To enhance consistency in the comparison of the effects of the new formulation, the same set of hypotheses used in [13] to simulate the static tests on adobe are adopted. In the following, only the main ones are recalled:

- For the Young's modulus, the mean values of secant elastic stiffness experimentally derived is used (E=40 MPa). Symmetry in the parameter in tension is assumed. A 0.1 value for the Poisson's ratio is assumed [38]. In addition to the static hypotheses, the average value of density found for adobe from tests (1100 kg/m^3) is used;
- The parameters of the modified Drucker Prager surface of eq.5.3 in Par.5.2 are modified to include an inscribed Drucker-Prager smoothed version of Mohr Coloumb failure in compression. The coefficient $c_1 - c_4$ of eq.5.5 now are:

$$\begin{cases} c_1 = \frac{1}{(1-2\nu)} \\ c_2 = \frac{1}{2\sqrt{2}(1+\nu)} \\ c_3 = \frac{tg(\phi)}{(1-2\nu)} \\ c_4 = \frac{\sqrt{3}}{2(1+\nu)} \end{cases} \tag{5.12}$$

  in which the internal friction angle ϕ=15^o is chosen corresponding to organic soil [39].
- For the damage initiation strains in compression, the mean value for the initial deviation from linearity in the stress strain diagrams is used (k_{oc}= 2.5 e^{-2}). Half of this value is taken for the damage initiation strain in tension (k_{ot}= 1.25 e^{-2}).
- A mechanical defect, with damage initiation strain equal to 1 e^{-3}, is imposed at the corner of the specimen.
- The damage evolution laws in eq.5.7 are simplified in compression according to a pure exponential law whereas in tension according to the linear softening characterized by a steeper slope (a=0).

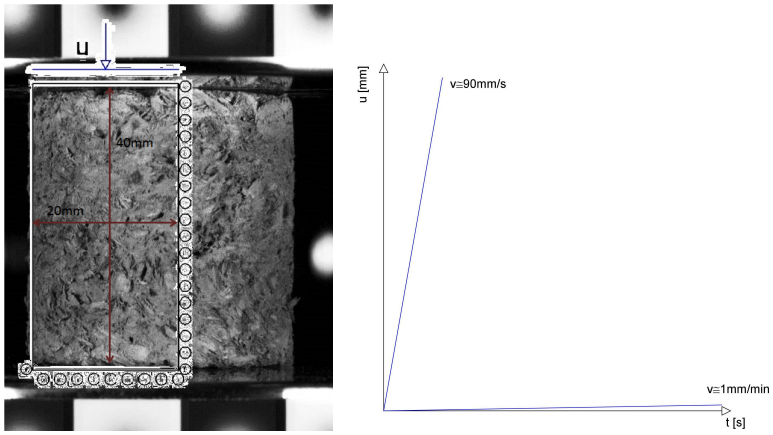

(a) (b)

Figure 5.9: Shape and geometry of experimental and numerical setup (a), with experimentally derived loading history at the top boundary (b)

As in [13], at first only the two parameters in compression (a, Δ) of the original formulation in eq.5.8 (β=1 in eq 5. 10) have been calibrated to match the maximum reaction force and the corresponding displacement experimentally derived in the force displacement curve by dynamic testing (a=200, β=1, Δ=350). The best fitting numerical curve and the corresponding failure mode are compared with the response observed in experiment in Figure 5.10 ("original model"). As in [13], the numerical plot shows a brittle slope in softening against the more ductile experimental response. Furthermore, the corresponding failure mode is only recalled in the simulation, with a too large width of the primary crack starting from the corner and a more localized damage distribution in the numerical sample.
Next, the dependence of β on d as discussed in Par. 5.4.1 is fully integrated in the formulation. In order to further test the flexibility of the model after β inclusion, the same simulation is repeated using the set of parameters previously calibrated (a, Δ) and only combined with the new dependency on β. After testing different functions with shapes as in eq.5.11, a linear function of the type $\beta_2 = (r_1 - r_2)\, d + r_2$ proves to be the best fit, with r constant parameters calibrated as r_1=0.2 and r_2=1. The resulting curve and the corresponding failure mode are compared again with experiments in Figure 5.10 ("enriched model").
Despite restrictions in the initial setup and hypotheses, after inclusion of the new function, the model is capable to correctly capture the ductile softening branch of response experimentally observed. Furthermore, given the limitation of deterministic models to correctly capture cracks that in adobe usually start from clay concentrations or fiber-induced areas of de-adherence, the total extension of the numerical damage is larger than before and more consistent with the area of the tested sample interested by cracks. In addition, a localized primary crack starting from the corner followed by a second numerical crack with branching now numerically resembles the progression experimentally observed (Figure 5.11d).

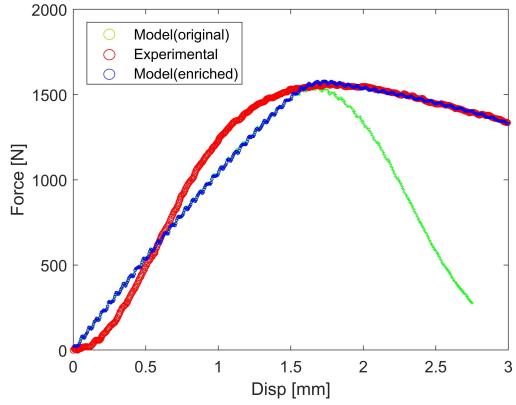

(a)

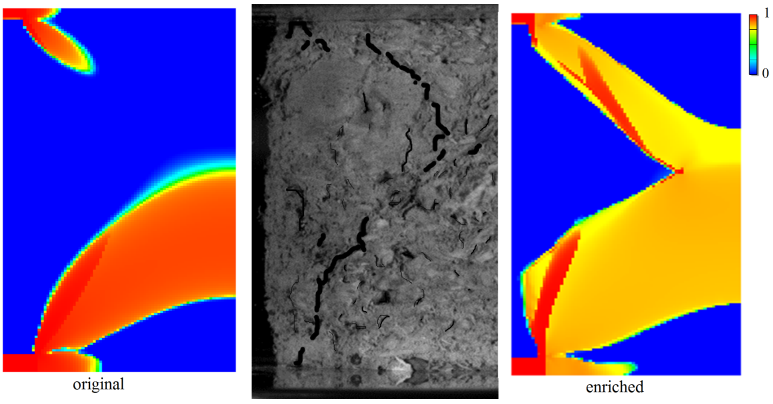

(b)

Figure 5.10: Force displacements and cracking patterns (at about 3 mm of deformation) comparisons with experimental results in compression at velocity of 90mm/s between best fit numerical curve using β=1 (original model) and β as a linear function of damage d (enriched model)

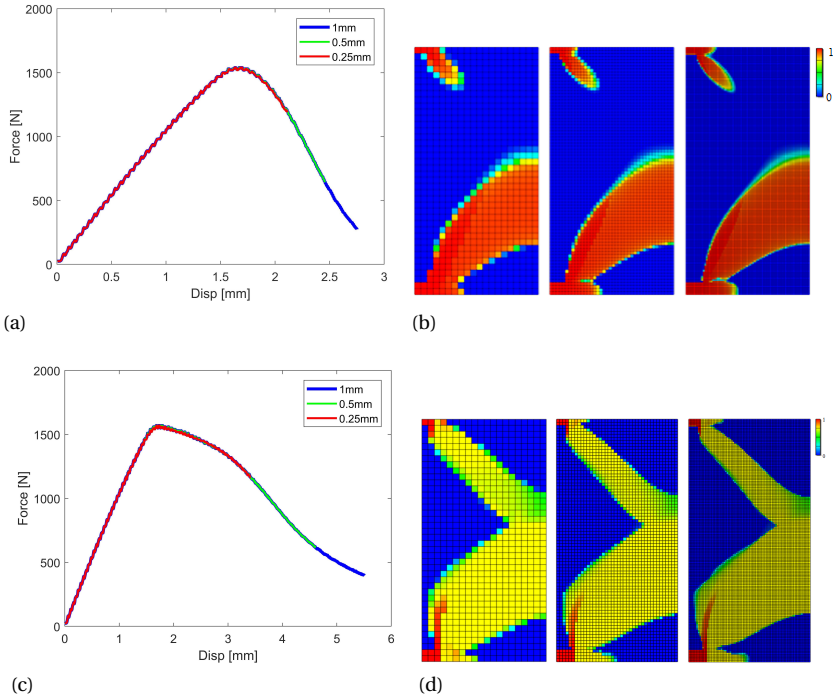

Figure 5.11: F-d curves and failure pattern at step i=550 for different meshes using the original model (a-b) and the enriched formulation (c-d)

As a confirmation of the findings in Par. 5.4.1, the formulation including the new dependency preserves the feature of mesh independence of the original model (Figure 5.11a-b) along deformation history, including the first stages of the non linear softening, where maximum discontinuity in slope arises with respect to the original curve (Figure 5.11c-d).

5.4.2. CRACK PROPAGATION VELOCITY IN QUASI BRITTLE MATERIALS AND THE NUMERICAL DELAY FOR RATE DEPENDENT ANALYSES

The amount of delay in the cracking process is numerically scaled by a factor Δ in the model. For a given loading profile, it mathematically determines the maximum value of damage rate. In the early nineties, bounded models introduced a cap to damage dependent models ($\dot{\tau_c}$ in the original formulation in [40]). This is consistent with assuming a maximum velocity to crack propagation. In quasi brittle materials, many micro-cracks coalesce into a dominant macro-crack propagating through the specimen at a certain speed and orientation according to the mineralogical composition of the material meso-structure [30]. Thus it is common practice in literature to attribute a constant value usually calibrated in single tests of the dynamic regime to the numerical parameters that define the maximum failure rate [24, 41]. However, this property is not solely determined by the mineralogical composition of the material. In quasi-brittle materials, the rate of crack bridging is significantly influenced by temperature, moisture and loading conditions, with the applied loading rate in particular [42]. In this regards, macro-crack growth rate depends on the supply energy rate to fracture zone and increases with increasing loading rate [43, 44]. Thus, a maximum damage rate $\dot{D}$ for a given loading velocity applied exists but this numerical property must vary with the loading rate [40, 45]. This feature is integrated in the delay formulation of eq. 5.10 by introducing a direct dependence between Δ and a function μ of the applied strain rate. In fact, assuming a constant value for the Δ parameter as in eq. 5.8 results in an unrealistic sensitivity of the model when higher loading rates are applied. This is shown analysing the response of the compressed bar in Par. 5.3.1 and loaded at increasing applied velocities, from a quasi static constant rate (v_1=1mm/s in Figure 5.13) to one and two higher orders of magnitude (v_2=10 mm/s, v_3=100mm/s). Using the original formulation of eq. 5.8 (μ_0 in eq. 5.13) on the model calibrated in Par. 5.3.1, numerical simulations show a high sensitivity in the response to higher loading regimes (Figure 5.13a). In particular, a dynamic increase factor in strength of 10 is achieved for a jump of two orders of magnitude in the maximum velocity applied at the boundary of the bar (Table 5.1). Instead, experimental values of the increment of strength in dynamics for the same dynamic ranges are usually lower than 3 for quasi brittle materials [46].

Dependence of Δ on the loading rate is incorporated using a function μ of the slope of the Dirichlet boundary condition applied at each time step. Average strain rates are then determined according to the selected geometry and loading direction. Three different continuous functions as in eq. 5.13 have been tested. Linear, root and parabolic functions have been tested to incorporate different viscous contributions in Δ (Figure 5.12).

$$\begin{cases} \mu_0 = 1 \\ \mu_1 = 10^{-3}\dot{\epsilon}_s + 1 \\ \mu_2 = 3\dot{\epsilon}_s^2 \\ \mu_3 = 10\sqrt{\dot{\epsilon}_s} \end{cases} \tag{5.13}$$

The sensitivity to rate inherent to the original model (μ_0) for all the material properties is significantly limited at high strain rates by the functions μ_{1-3} in eq.5.10. Dynamic increase factor values at both velocities applied are now closer to experimental results for quasi brittle materials dynamically tested [47]. This new dependence in the model in-

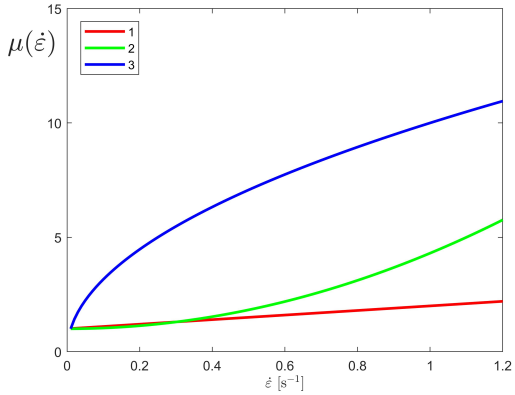

Figure 5.12: Slope of the different rate dependent functions used in eq. 5.13 as μ_{1-3}

Table 5.1: Dynamic increase factors for the compressive strength, displacement at peak and ultimate displacement in softening after 20 % of strength decay for velocity v_2 and v_3 using μ_{0-3} in eq. 5.13

	DIF_{f_b}		$DIF_{d_{f_b}}$		DIF_{d_u}	
v	*2*	*3*	*2*	*3*	*2*	*3*
μ_0	1.76	9.52	2.39	18.83	2.77	32.27
μ_1	1.69	5.10	2.29	9.68	2.59	16.25
μ_2	1.73	2.80	2.30	4.57	2.71	7.74
μ_3	1.20	1.77	1.36	2.25	1.49	4.64

duces a specific material sensitivity to rate in the slope of the force displacement curves of the bar loaded at increasing velocities according to the particular function used for μ (Figure 5.13). Thus, the dynamic increase factors in strength and deformation differently vary in dynamics according to the influence that function μ exerts on damage localization determined by the maximum damage rate at a given strain rate (Table 5.1). Among the tested functions, μ_3 is found to cause the most limited variation on the enhancement of the dynamic material properties (Figure 5.13c-e).
Also in this case, the new dependence does not alter the regularization properties of the model for any of the functions tested in eq. 5.13 and applied velocities (Figure 5.14).

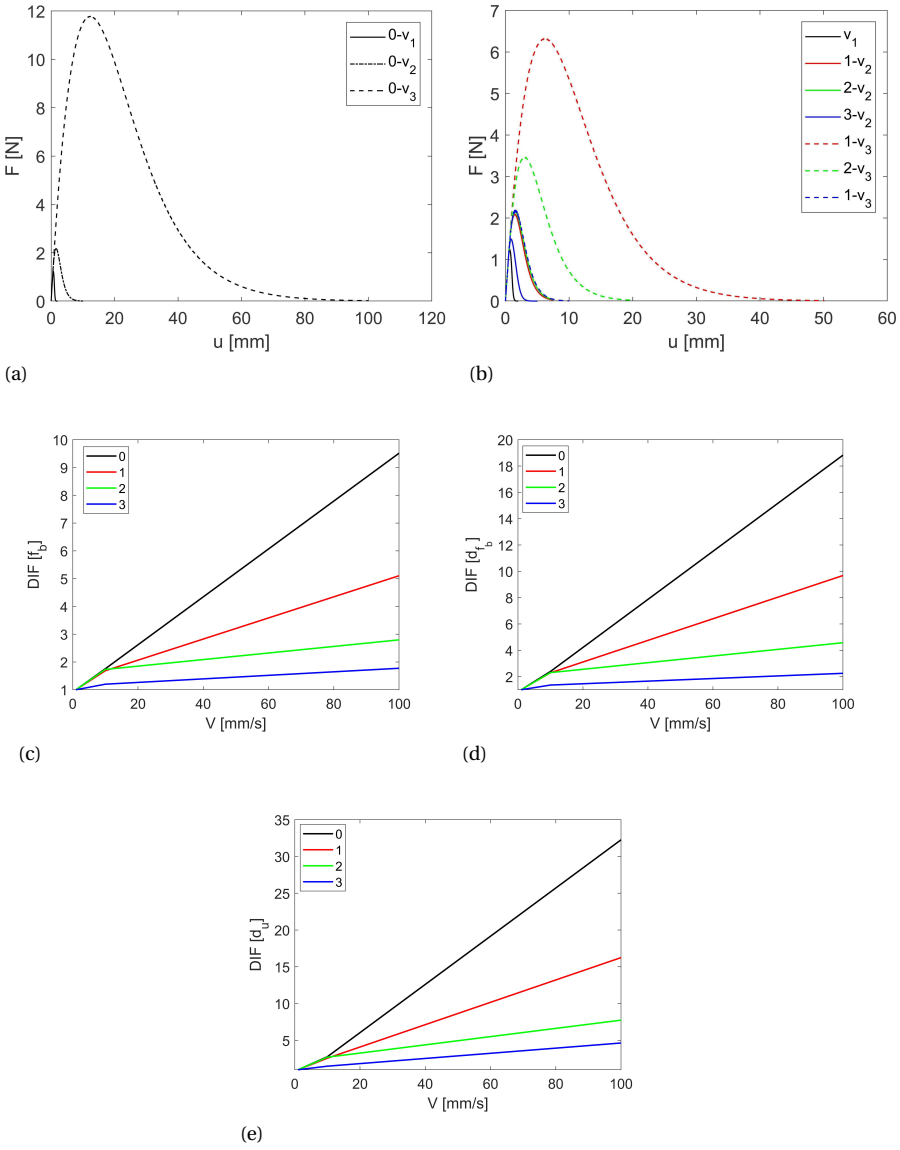

Figure 5.13: Force-displacement plots for v_1=1 mm/s, v_2=10 mm/s and v_3=100mm/s using the original model (a) and the three functions μ_{1-3} (b), with plots of the dynamic increase factor in strength, displacement at peak load and ultimate displacement based on linear interpolation

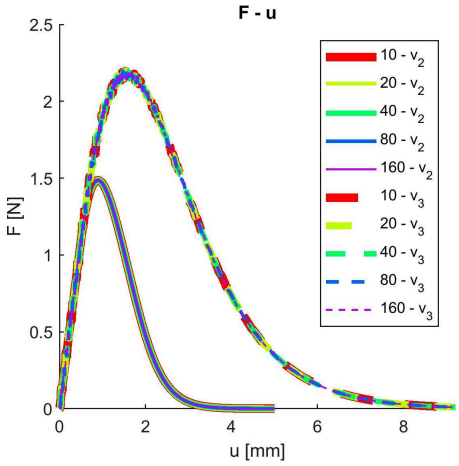

(a)

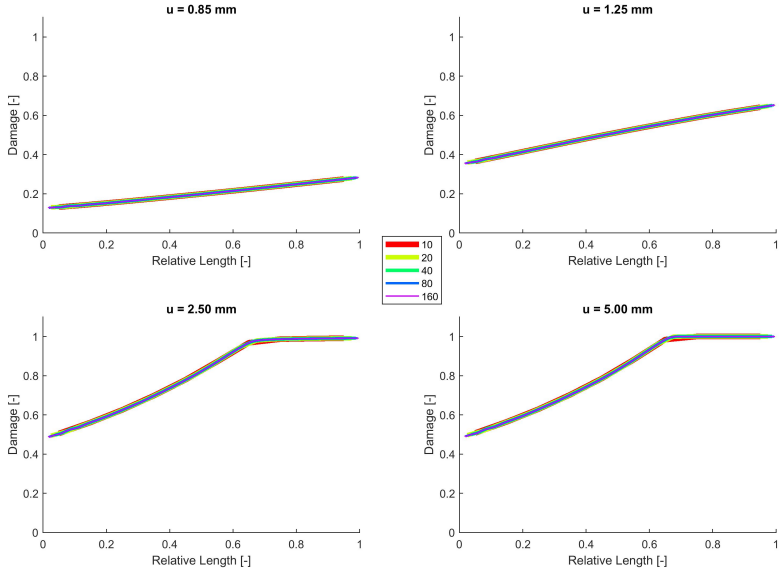

(b)

Figure 5.14: Force displacement plots (a) and damage profile evolution (v_2) (b) for four different mesh refinements (10-160 elements) of the bar using μ_3 dynamically loaded

A NUMERICAL APPLICATION OF THE NEW FORMULATION

Correctly addressing the dynamic rate of increment of the property of strength with respect to its static value (dynamic increase factor) is of paramount importance for engineering design of masonry against highly dynamic loadings [48]. Compression tests on modern geomaterials in literature always indicate a certain increment in the unconfined compressive strength of the material in the dynamic regime, included between 1.5 and 3 times the static strength for high strain rates loadings [35]. Strength increment rates for quasi brittle materials are currently hypothesized mainly using analytical formulations developed empirically from tests on modern cementitious materials with different properties and compositions than traditional bricks [47]. Many concrete modellers use the widely accepted standard reference for concrete by Comite Euro-International du Beton (CEB) [49]. The CEB recommends the strain rate induced strength increment formulation for normal concrete as:

$$\begin{cases} D.I.F. = (\frac{\dot{\epsilon}}{\dot{\epsilon}_s})^{(1.026\alpha)} for\, \dot{\epsilon} \leq 30 s^{-1} \\ D.I.F. = \gamma(\frac{\dot{\epsilon}}{\dot{\epsilon}_s})^{(0.33)} for\, \dot{\epsilon} \geq 30 s^{-1} \end{cases} \tag{5.14}$$

5

where $\dot{\epsilon}$ is the current strain rate in dynamics, $\dot{\epsilon}_s$ is the reference static strain rate (equal to 3 10^{-5}) and:

$$\begin{cases} \alpha = \frac{1}{5+9(\frac{f_b}{f_{bo}})} \\ \gamma = 10^{6.156\alpha - 2} \end{cases} \tag{5.15}$$

where f_{bo} is a reference strength of 10 MPa. Instead, only few numerical applications aimed at assessing the increment rate of this property can be found in literature [50].
The capability of the new delay formulation to limit the rate sensitivity in dynamics of the original model and correctly addressing the rates of increment in strength experimentally associated to masonry materials at higher strain rates is validated in this paragraph. The effect of the new formulation for Δ in eq. 5.10 in the model of Sec.5.2 is tested on the numerical simulation of the dynamic increase factors in strength at different dynamic rates experimentally derived for clay masonry bricks. To this end, the results of an experimental campaign recently performed by the authors is chosen as a reference [16]. This was aimed to analyse the rate of enhancement of the maximum strength exhibited by cylindrical clay samples baked in the oven and subjected to uniaxial compression tests at three sequent orders of strain rates, from statics to high velocity impacts. Strain rates of the order of 120 s^{-1} were achieved using a Hopkinson bar. Thus, cylindrical samples with same geometry as in Sec 5.4.1.2 were uniaxially compressed at constant rates of respectively 1 mm/min, 90 mm/s and 4200 mm/s. As a result of the experimental campaign, a normalized strength of 2.5 MPa was derived in statics averaging the peak reaction to load over the cross section areas. The average dynamic increase factors in strength were consequently calculated after dynamic testing as circa 1.3 times the static value for strain rates of 3 s^{-1} and 1.8 for strain rates of 120 s^{-1}. The experimental dynamic increase factors for the tested bricks lie on the lower region of the cloud of data commonly associated to the dynamic performance of concrete. Therefore, models commonly used to design concrete in dynamics like the CEB model in eq.5.14 only hardly address the dynamic trend associated experimentally to clay bricks (Figure 5.16a).

Next, the numerical model is used to predict the variation in normalized strength experimentally observed for clay at all the different rates. A proper assessment of the true material properties from experimental test data at high rates requires the evaluation of the contribution of radial inertia and platens-specimen friction on the dynamic strength enhancement. However, this paragraph is limited to reveal the functionality of the implemented feature of μ in the delay function against experimental trends recently found. Therefore, the effects of friction or inertia on the experimental results are not quantitatively included in the numerical discussion.

Static tests using the model are performed on the setup of Figure 5.9. Similarly to the set of hypotheses described in Par.5.4.1.2, the elastic properties of the model are taken from the average values experimentally derived in statics for the clay bricks (ρ=1800; ν=0.1; $k_{0_{c,t}}$=0.6 e^{-2} and E= 135 MPa). Similarly, the parameters of the original delay of eq. 5.8 in Sec.5.2 are calibrated to address the force and displacement coordinates corresponding to the maximum reaction force experimentally derived in the test (a=108;b=0;Δ=6.0). As a result, the first point of the DIF plot numerically determined for the static regime in the graph of Figure 5.16b (DIF=1) coincides with the experimental value.

With the set of parameters calibrated in statics, the model is used to perform numerical simulations in the dynamic regime at the two different loading rates. For this purpose, the average displacements histories are directly extracted from the laboratory tests at both rates and applied on the model with same geometry as in test. For the intermediate loading regime corresponding to an applied displacement rate of v = 90mm/s, the same setup shown in Figure 5.9 and used in Par. 5.4.1.2 is herein applied for simulations purposes. In the case of high strain rate tests using the Hopkinson bar, the deformation rates extracted from the reflected and transmitted waves experimentally derived as functions of time are directly applied to the setup of Figure 5.15.

Firstly, dynamic simulations are performed using the original model calibrated in statics with a constant μ_0=1 in eq.5.10. The values of normalized strength in compression are numerically derived from both tests and correspondingly plotted as dynamic increase factors in Figure 5.16 together with the experimental values in [16]. Numerical simulations using the original model clearly show an unrealistic over-estimation of the compressive strength of the brick for the considered range of strain rates in dynamics (Figure 5.16b). Next, the dependence of Δ on the rate $\dot{\epsilon}$ via the function μ in eq. 5.10 is integrated in the model. The same dynamic analyses are thus repeated using different shapes for μ as in Figure 5.12. A linear dependence for μ=2($\dot{\epsilon}$ + 1) proved to be the best fit.

The normalized compressive strengths numerically derived from the reaction plots of both tests are plotted again as dynamic increase factors of the static strength in Figure 5.17 and compared with the experimental values. The model is now capable to correctly quantify the experimental strengths of the tested bricks with a good approximation at all loading rates, including above 100 s^{-1}, where standard are found to overestimate the experimental data [51]. Full consistency with the experimental stress-strain curves goes beyond the specific goal of the current simulations. However, the numerical plots already lie within the experimental envelopes of the material for the two dynamic regimes and the numerical assessment of the average critical time t at which the maximum strength arises is close to the experimental results at both rates (Figure 5.17).

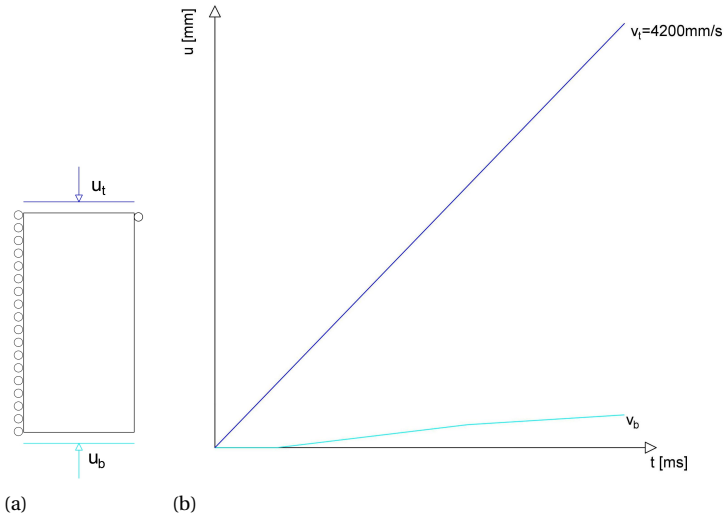

Figure 5.15: Geometry and numerical setup (a) with applied loading history at the boundaries of the sample derived from split hopkinson bar tests (b)

As for Par. 5.4.1.2, the formulation including the new dependence preserves the feature of mesh independence of the original model and refining the mesh the dynamic increase factors do not change at the intermediate (DIF≈1.3) and high (DIF≈1.8) rates (Figure 5.17).

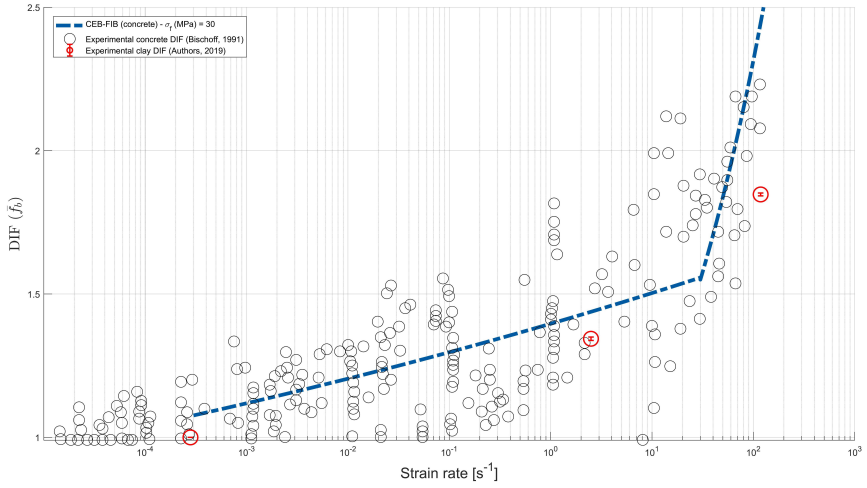

(a)

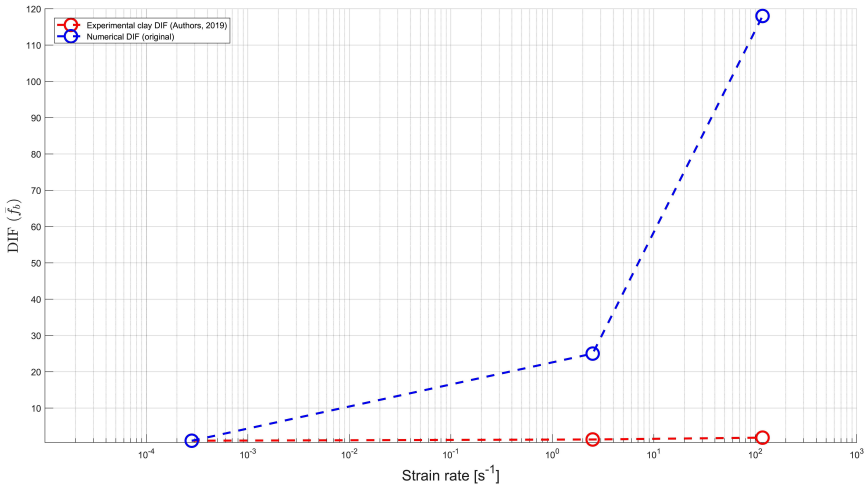

(b)

Figure 5.16: Experimental dynamic increase factors for the clay bricks tested by authors (in red), with respect to experimental data usually associated to concrete at the same strain rates (in black) and CEB-FIB predictive model for high strain rate loadings (in blue) (a); Experimental-numerical comparison of the Dynamic Increase Factor Function using the original numerical model (b)

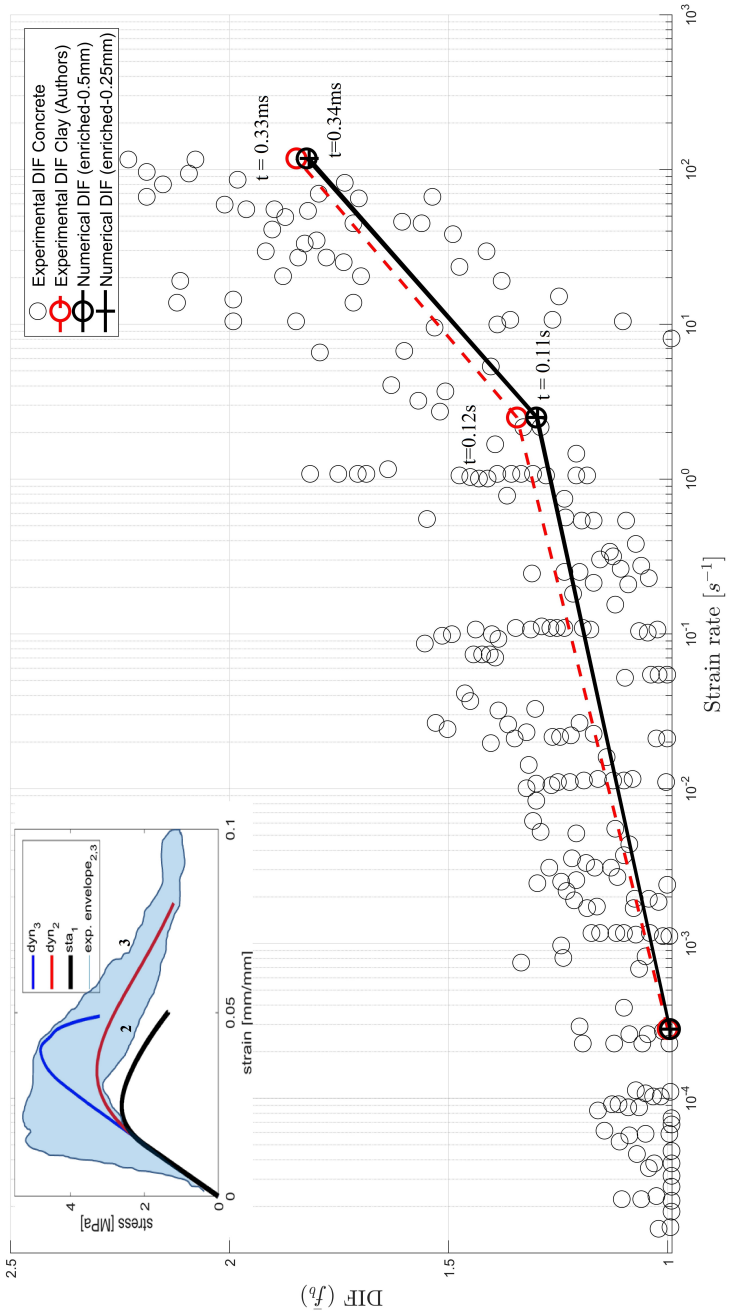

Figure 5.17: Experimental-numerical comparisons of the Dynamic Increase Factor Functions using the enriched numerical model for two different mesh refinements, with examples of numerical stress strain curves within experimental envelopes for the two dynamic rates and numerical-experimental assessment of the critical time t at strength attainment

5.5. CONCLUSIONS

In this study, the proper regularization properties of a local rate dependent damage model have been demonstrated in dynamics. Furthermore, the formulation of the original delay regularization algorithm has been improved in order to address the dynamic behaviour of quasi brittle materials used in masonry.

The original model has a limited capability in addressing failure of ductile materials characterized by mild softening and distributed damage. In this study, the original damage delay model has been enriched by a direct dependence on the actual local state of damage. This physically refers to the influence that the mineralogical properties of the meso structure of a material exerts on the coalescence and propagation of micro-flaws during the entire deformation process. As a result, the model has gained flexibility in the capability of correctly addressing the dynamic response in compression of various materials, also when characterized by ductile failure.

Furthermore, the response of the original model in compression showed an extreme sensitivity to the applied loading rate when the maximum damage rate of delay is a constant and calibrated with respect to only one loading condition. As a result, the dynamic increase factors for the main mechanical parameters were not consistent with experimental data for most building materials in dynamic compression tests. In this study, the original damage delay formulation has been enriched by a direct dependence on the actual applied loading rate. This physically refers to the viscous influence that deformation rate exerts on the damage progress and maximum crack velocity in the material. As a result, the model is capable of describing the rate dependence exhibited in masonry materials in dynamics, including the assessment of dynamic increase factor functions in strength characterized by limited variations for high strain rates.

REFERENCES

[1] T. Li Piani, Operative Guidelines for Protection of Places of Worship: A new approach toward security design of sensitive buildings, Institute for Advanced Strategic and Political Studies, ISBN:97888940373-2-6, Milan, 2017.

[2] L. Pereira, New computational approach towards the simulation of concrete structures under impulsive loading, Ph.D. thesis, Delft University of Technology (TU Delft) (2018).

[3] J. Mazars, F. Hamon, S. Grange, A new 3D damage model for concrete under monotonic, cyclic and dynamic loadings, Materials and Structures (2015) 3779–3793doi:10.1617/s11527-014-0439-8.
URL http://link.springer.com/10.1617/s11527-014-0439-8

[4] P. Forquin, Brittle materials at high-loading rates: An open area of research, Philosophical Transactions of the Royal Society A: Mathematical, Physical and Engineering Sciences 375 (2085) (2017). doi:10.1098/rsta.2016.0436.

[5] L. F. Pereira, J. Weerheijm, L. J. Sluys, A new effective rate dependent damage model for dynamic tensile failure of concrete, Engineering Fracture Mechanics 176 (2017)

281–299. doi:10.1016/j.engfracmech.2017.03.048.
URL http://linkinghub.elsevier.com/retrieve/pii/S001379441630474X

[6] M. Jirasek, Z. Bazant, Model for Localization of Softening and Size Effect, in: Inelastic Analysis of Structures, 2002, Ch. 26.

[7] F. van der Meer, L. J. Sluys, Continuum Models for the Analysis of Progressive Failure in Composite Laminates, Journal of Composite Materials 43 (20) (2009) 2131–2156. doi:10.1177/0021998309343054.
URL http://jcm.sagepub.com/cgi/doi/10.1177/0021998309343054

[8] P. Ladevèze, A damage computational method for composite structures, Computers and Structures 44 (1-2) (1992) 79–87. doi:10.1016/0045-7949(92)90226-P.

[9] O. Allix, P. Feissel, Composite Damage Model For Dynamic Fracture Prediction : Identification Issues, ICF 11-11th International Conference on Fracture 2005 (2005).

[10] L. J. Sluys, R. De Borst, Mesh-sensitivity analysis of an impact test on a double-notched specimen, Rock Mechanics, 1991 (1991).

[11] L. J. Sluys, R. de Borst, Wave propagation and localization in a rate-dependent cracked medium-model formulation and one-dimensional examples, International Journal of Solids and Structures 29 (23) (1992) 2945–2958. doi:10.1016/0020-7683(92)90151-I.

[12] L. F. Pereira, J. Weerheijm, L. J. Sluys, A new rate-dependent stress-based nonlocal damage model to simulate dynamic tensile failure of quasi-brittle materials, International Journal of Impact Engineering 94 (2016) 83–95. doi:10.1016/j.ijimpeng.2016.04.002.
URL http://dx.doi.org/10.1016/j.ijimpeng.2016.04.002

[13] T. Li Piani, J. Weerheijm, L. Koene, L. Sluys, The Adobe delta damage model: A locally regularized rate-dependent model for the static assessment of soil masonry bricks and mortar, Engineering Fracture Mechanics 206 (2019) 114–130. doi:10.1016/j.engfracmech.2018.11.026.
URL https://linkinghub.elsevier.com/retrieve/pii/S0013794418308956

[14] P. Ladeveze, E. LeDantec, Damage modelling of the elementary ply for laminated composites, Composites Science and Technology 43 (3) (1992) 257–267. doi:10.1016/0266-3538(92)90097-M.

[15] T. Li Piani, J. Weerheijm, L. Koene, L. J. Sluys, The Adobe Delta Damage Model, in: Computational Modelling of Concrete Structures (EURO-C 2018), CRC Press, Bad Hofgastein (Austria), 2018, pp. 921–932.

[16] T. Li Piani, J. Weerheijm, M. Peroni, L. Koene, G. Solomos, L. J. Sluys, Dynamic Characterization of Adobe in compression: The effect of fibres with soil binders, in: FraMCoS-X : Fracture Mechanics of Concrete and Concrete Structures, Bayonne (France), 2019.

[17] P. Ladevèze, A damage computational approach for composites: Basic aspects and micromechanical relations, Computational Mechanics 17 (1995) 4–15. doi:10.1007/BF00356486.

[18] L. Pereira, J. Weerheijm, L. Sluys, A numerical study on crack branching in quasi-brittle materials with a new effective rate-dependent nonlocal damage model, Engineering Fracture Mechanics 182 (2017) 689–707. doi:10.1016/j.engfracmech.2017.06.019.
URL http://linkinghub.elsevier.com/retrieve/pii/S0013794417303028

[19] J. Lemaitre, J. Chaboce, Mechanics of Solid materials, 1990.

[20] J. Mazars, F. Hamon, S. Grange, A model to forecast the response of concrete under severe loadings : the nu damage model, Procedia Materials Science 3 (2014) 979–984. doi:10.1016/j.mspro.2014.06.159.
URL www.sciencedirect.com

[21] Z. liang Wang, Y. chi Li, R. F. Shen, J. G. Wang, Numerical study on craters and penetration of concrete slab by ogive-nose steel projectile, Computers and Geotechnics 34 (1) (2007) 1–9. doi:10.1016/j.compgeo.2006.09.001.

[22] J. Lee, G. L. Fenves, Plastic-Damage Model for Cyclic Loading of Concrete Structures, Journal of Engineering Mechanics 124 (8) (1998) 892–900. doi:10.1061/(ASCE)0733-9399(1998)124:8(892).
URL http://dx.doi.org/10.1061/(ASCE)0733-9399(1998)124:8(892){%}5Cnhttp://ascelibrary.org/doi/pdf/10.1061/(ASCE)0733-9399(1998)124:8(892)

[23] L. Pereira, J. Weerheijm, L. J. Sluys, Simulation of dynamic behaviour of quasi brittle materials with new rate dependent damage model, in: 9th International Conference on Fracture Mechanics of Concrete and Concrete Structures (FraMCos-9), 2015, p. 14. doi:10.21012/FC9.036.

[24] R. Ortiz, E. Deletombe, Y. Chuzel-Marmot, Assessment of damage model and strain rate effects on the fragile stress/strain response of ice material, International Journal of Impact Engineering 76 (2015) 126–138. doi:10.1016/j.ijimpeng.2014.09.011.
URL http://dx.doi.org/10.1016/j.ijimpeng.2014.09.011

[25] https://dianafea.com/manuals/d944/Analys/node435.html.

[26] V. P. Nguyen, Multiscale failure modelling of quasi-brittle materials. Manual to the implemented jem/jive code, Ph.D. thesis, Delft University of Technology (2011).
URL https://repository.tudelft.nl/islandora/object/uuid{%}3A1af168bf-7975-4044-8eb4-dd42216f7aaf

[27] L. J. Sluys, R. De Borst, Rate dependent modelling of concrete fracture, Heron 36(2), 3-16. (1991) (1992).

[28] L. F. Pereira, J. Weerheijm, L. J. Sluys, A new rate-dependent stress-based nonlocal damage model to simulate dynamic tensile failure of quasi-brittle materials, International Journal of Impact Engineering 94 (2016) 83–95. doi:10.1016/j.ijimpeng.2016.04.002.
URL http://dx.doi.org/10.1016/j.ijimpeng.2016.04.002

[29] M. Jirásek, B. Patzák, Models for quasibrittle failure: Theoretical and computational aspects, ECCM-2001, European Conference on Computational Mechanics (2001) 70–71.

[30] K. Ravi-Chandar, An experimental investigation into dynamic fracture: I. Crack initiation and arrest, International Journal of Fracture 3 (4) (1984) 105–262. doi:10.1007/s00018-012-1041-2.

[31] P. D. Washabaugh, W. G. Knauss, A reconciliation of dynamic crack velocity and Rayleigh wave speed in isotropic brittle solids, International Journal of Fracture 65 (2) (1994) 97–114. doi:10.1007/BF00032282.

[32] T. Li Piani, D. Krabbenborg, L. Koene, J. Weerheijm, M. Peroni, G. Solomos, L. Sluys, Submitted paper, chapter 4, 2019.

[33] J. K. Zhou, L. M. Ge, Effect of strain rate and water-to-cement ratio on compressive mechanical behavior of cement mortar, Journal of Central South University 22 (3) (2015) 1087–1095. doi:10.1007/s11771-015-2620-9.

[34] R. Pedersen, Computational Modelling of dynamic failure of cementitious materials, Ph.D. thesis, TU Delft University (2010).

[35] P. H. Bischoff, S. H. Perry, Compressive behaviour of concrete at high strain rates, Materials and Structures 24 (6) (1991) 425–450. doi:10.1007/BF02472016.

[36] E. Cosenza, G. Maddaloni, G. Magliulo, M. Pecce, R. Ramasco, Seismic design of concrete structures (italian), Iuss Press, Pavia, 2007.

[37] R. Park, N. Pristley, W. Gill, Ductility of Square Confined Concrte Columns, in: Concrete Column Ductility, 1982.

[38] D. Silveira, E. al., Mechanical properties of adobe bricks in ancient constructions, Construction and Building Materials 28 (1) (2012) 36–44. doi:10.1016/j.conbuildmat.2011.08.046.
URL http://dx.doi.org/10.1016/j.conbuildmat.2011.08.046

[39] Swiss Standard SN 670 010b, Characteristic Coefficients of soils, Association of Swiss Road and Traffic Engineers.

[40] P. Ladevèze, O. Allix, J. F. Deü, D. Lévêque, A mesomodel for localisation and damage computation in laminates, Computer Methods in Applied Mechanics and Engineering 183 (1-2) (2000) 105–122. doi:10.1016/S0045-7825(99)00214-5.

[41] O. Allix, J.-F. Deu, Delayed-Damage Modelling for Fracture Prediction of Laminated Composites under Dynamic Loading, Engineering Transactions 45 (1) (1997).
URL http://et.ippt.gov.pl/index.php/et/article/view/680

[42] O. Lengliné, R. Toussaint, J. Schmittbuhl, J. E. Elkhoury, J. P. Ampuero, K. T. Tallakstad, S. Santucci, K. J. Måløy, Average crack-front velocity during subcritical fracture propagation in a heterogeneous medium, Physical Review E - Statistical, Nonlinear, and Soft Matter Physics 84 (3) (2011) 1–13. doi:10.1103/PhysRevE.84.036104.

[43] A. Berezovski, G. A. Maugin, On the propagation velocity of a straight brittle crack, International Journal of Fracture 143 (2) (2007) 135–142. doi:10.1007/s10704-007-9053-x.

[44] Q. H. Zuo, F. L. Addessio, J. K. Dienes, M. W. Lewis, A rate-dependent damage model for brittle materials based on the dominant crack, International Journal of Solids and Structures 43 (11-12) (2006) 3350–3380. doi:10.1016/j.ijsolstr.2005.06.083.

[45] O. Allix, J.-F. Deu, Delayed-Damage Modelling for Fracture Prediction of Laminated Composites under Dynamic Loading, Engineering Transactions 45 (1) (2015).
URL http://et.ippt.gov.pl/index.php/et/article/view/680

[46] H. Hao, B. Tarasov, Experimental Study of Dynamic Material Properties of Clay Brick and Mortar at Different Strain Rates 8 (2) (2008) 117.
URL http://search.informit.com.au/documentSummary;dn=137784543477420;res=IELENG

[47] H. Hao, B. Tarasov, Experimental Study of Dynamic Material Properties of Clay Brick and Mortar at Different Strain Rates 8 (2) (2008) 117.
URL http://search.informit.com.au/documentSummary;dn=137784543477420;res=IELENG

[48] G. Magenes and G.M. Calvi, In-plane seismic response of brick masonry walls, Earthquake Engineering and Structural Dynamics,1091-1112,26(11), (1997).

[49] CEB (Comite Euro-International du Beton) : CEB-FIP Model Code 1990.

[50] E. C. Simons, J. Weerheijm, L. J. Sluys, A viscosity regularized plasticity model for ceramics, European Journal of Mechanics 72 (July 2017) (2018) 310–328. doi:10.1016/j.euromechsol.2018.05.009.
URL https://doi.org/10.1016/j.euromechsol.2018.05.009

[51] S. Wang, M. H. Zhang, S. T. Quek, Mechanical behavior of fiber-reinforced high-strength concrete subjected to high strain-rate compressive loading, Construction and Building Materials 31 (2012) 1–11. doi:10.1016/j.conbuildmat.2011.12.083.
URL http://dx.doi.org/10.1016/j.conbuildmat.2011.12.083

6

TESTING AND MODELLING THE BALLISTIC RESPONSE OF ADOBE

"The principles of war are the same as those of a siege.
Fire must be concentrated on one point, and
as soon as the breach is made,
the equilibrium is broken
and the rest is nothing."

Napoleon Bonaparte, 1769-1821

In this paper, a new one-dimensional phenomenological model is developed for the assessment of the ballistic performance of Adobe. Adobe is a masonry largely spread in areas of the world involved in military operations. Addressing fundamental ballistic parameters such as residual velocity or penetration depth for this building technology is necessary. The model follows the hypotheses for the ballistic response of concrete targets to high velocity impacts, provided with a dominant contribution of shear friction typical of soils. The hypotheses at the basis of the model are consistent with all experimental evidence collected by authors on Adobe. Adobe brick and mortar belong to the material class of concrete, whereas the overall mechanical parameters are determined by the internal soil mixture, including the percentage of fibre reinforcement. Despite its relative simplicity, the model is capable of well predicting ballistic test results currently available in literature for Adobe, including the data of an experimental campaign recently performed by the authors on real Adobe walls in the field.

This chapter is based on "Ballistic model for the prediction of penetration depth and residual velocity in Adobe: a new interpretation of the ballistic resistance of soil masonry "in *Defence Technology*, 2018.

6.1. INTRODUCTION

The recent progression of urban warfare in the world is leading governments to invest in research focused on the ballistic response of building materials. Among these, Adobe, a masonry made of sun dried soil bricks and mud mortar, is a construction type largely spread in areas of the world involved in armed conflicts. Among the possible approaches to interpret the ballistic response of structures, so-called ballistic phenomenological models, analytical models which parametrize the inertial, viscous and bearing strength contributions to the resistance of the target during penetration, are well suited to promptly estimate fundamental ballistic parameters during in field operations, such as depth of penetration or residual velocity for given trajectory, bullet type and striking velocity. Two of these models have been recently proposed to assess the ballistic performance of Adobe masonry (eq.6.1). One is based on stationary body motion in medium, consistent with the hypothesis of a pure Stokes' drag force as main resistance to penetration [1, 3] (eq. 6.1a); while the other is based on a shock wave approach, originally developed for simulating hypervelocity impact on graphite targets (eq.6.1b) [2]. Both of them share the same linear dependence between the final depth of penetration of the projectile (P) and its impacting velocity (v_0), which matches the experimental results obtained from laboratory tests on semi-infinite targets of Adobe in [3] and [5].

$$\begin{cases} a: P = \dfrac{D\rho_p}{k\rho_t} v_o \\ \\ b: P = \dfrac{D\rho_p}{\alpha C \rho_t} v_o \end{cases} \tag{6.1}$$

Where D is the impactor diameter, k is a calibration constant, ρ is the density (of the projectile p and target t), v_o is the impact velocity on target, α is a shape coefficient and C is the bulk wave speed. Both formulas show a linear dependence on the impacting velocity and on the ratio of target and projectile densities [4]. The good agreement using the few sources of data currently available for Adobe in literature is evidence that the response mechanisms of the material to penetration result in a linear relationship between impacting velocity and penetration depth [1, 3–5]. However, the hypotheses at the basis of the two models are not consistent with each other and a definite interpretation of the ballistic mechanisms of resistance of Adobe has not been achieved yet [4]. Therefore, a new ballistic campaign aiming at experimentally addressing the ballistic response of real Adobe walls subjected to impacts at striking velocities lower than 1000 m/s using small caliber projectiles was recently performed. Elaboration of results shared in [4] had confirmed some experimental trends given in [5] and [3], such as the linear dependence between P and v_o, as proved by a decent statistical correlation with experimental data using eq.6.1, considering the natural scatter inherent real shooting tests in the field [4] (Figure 6.1). Besides, experiments have also confirmed previous findings by authors on the constitutive nature of Adobe bricks and mortar, which are both inserted in the material class of concrete provided with a major influence of soil granulometry on the values of the overall mechanical properties [6–8]. A new ballistic phenomenological model consistent with experimental evidence is proposed in this paper for Adobe. This is rooted from a model originally developed by Forrestal in 1994 to simulate high veloc-

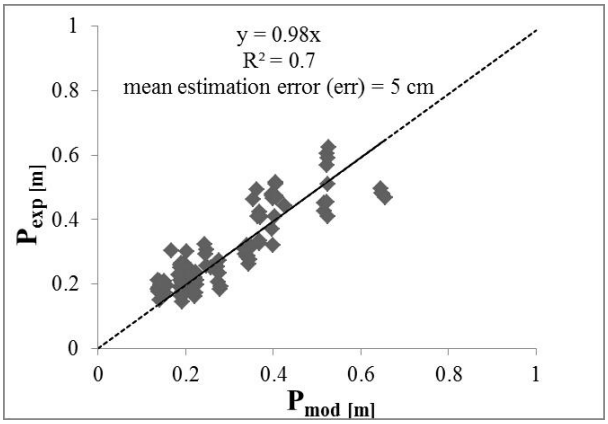

Figure 6.1: *Experimental-predicted terminal penetration depths using eq.6.1(a) on data from [4]*

ity penetrations of projectiles into geo-material targets such as concrete [9], adapted in order to include the shear resistance of soil for deep penetration. In the next sections, the model is presented, including its preliminary experimental hypotheses and some practical examples of application.

6.2. EVIDENCE FROM A BALLISTIC CAMPAIGN ON ADOBE MASONRY IN THE FIELD

The model takes its roots from elaboration of the results of a ballistic campaign performed by authors between 2011 and 2013, consisting of more than 150 impact tests on real Adobe walls in the field. Three test series of six shots each involved ten Adobe walls of different thickness (from 40 to 80cm) built using three typologies of bricks and mortar with different fibre reinforcement (from 3% to 30% by weight) and density (from 800 to 1400 kg/m^3). Impactors included seven small caliber bullets with different geometrical (from 7.82 to 12.7mm in diameter) and weight properties (from 8 to 45 g). Each wall was shot at a velocity range between 600m/s and 900 m/s at different temperature and humidity conditions along two years. The reader is referred to [4] for a detailed explanation of the campaign and its results. In the following, only the major findings emerging from elaboration of test results are resumed:

- Penetration process in Adobe walls is characterized by an initial limited crater region with radial cracks followed by a cylindrical region with diameter equal to the impactor's diameter. Impactors do not experience significant deformation during penetration [4] (Figure 6.2(a));
- Inertia of target has a minor influence on the ballistic resistance of Adobe for impacting velocities below 1000 m/s (Figure 6.2(b)). Also the fact that the diameter of the tunnel region equals the caliber of the impactor confirms that the effect of inertia can be neglected for these impact conditions. This statistical finding confirms data elaboration results from other laboratory tests on Adobe in [3, 5].

(a)

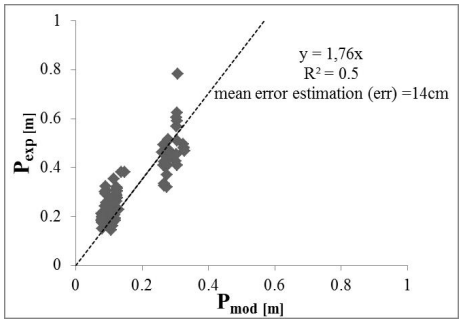

(b)

Figure 6.2: *Example of crater region before tunnelling after test [4] (a), Experimental-predicted terminal penetration depths using the Resal model (which considers the inertial contribution of target resistance) in [4] (b)*

- Compression strength is an aleatory parameter for Adobe, varying over seasons and years. This happens because sundried bricks contain water, which varies according to atmospheric conditions, affecting the mechanical properties of the material. This finding confirms previous results achieved for Adobe by the authors, who proposed a compressive strength law for Adobe being negatively dependent on mixture water content [4, 6, 8]. Therefore, the use of compressive strength to predict the ballistic response of Adobe in the field is discouraged.

- For a given thickness, the ballistic performance of a wall of Adobe decays proportionally to the number of brick-layers emplaced along its thickness. Comparing tests on walls of different thickness using same types of bricks, bullets and velocity ranges, the penetration depth proportionally increases with the increasing number of layers emplaced along thickness [4]. This finding confirms a phenomena already observed in case of penetration tests on multi-layered concrete targets [13].

6.3. THE ADOBE BALLISTIC MODEL

The framework of the well-known ballistic model for concrete targets developed by Forrestal et al. in [9] is adopted as a starting point. The model shapes the main mechanisms of resistance activated by concrete targets in front of the nose of high velocity impactors. According to post-test observations, two different regions are taken into account in the

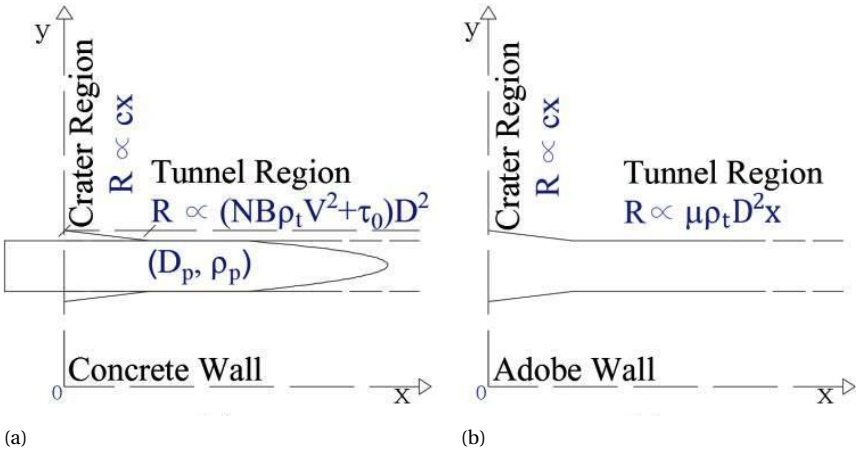

Figure 6.3: *Forrestal model (a) and Adobe ballistic model (b): Proportionality of target reaction forces*

model. A "cavity region" with a length of about two projectile shank diameters is followed by a "conical region" with cross diameter nearly equal to the projectile diameter. The resulting equation of motion in [9] is resumed in eq.6.2 as a function of depth, and the set of forces exerted on the projectile nose in the two regions of the model are graphically presented in Figure 6.3(a):

$$\begin{cases} m\dfrac{dv}{dt} = cx \quad \text{for} \quad 0 < x < 2D \\ m\dfrac{dv}{dt} = (NB\rho_t V^2 + \tau_o)\dfrac{\pi D^2}{4} \quad \text{for} \quad x \geq 2D \end{cases} \tag{6.2}$$

where m is the projectile mass and v is its speed at time t, R is the total reaction force, c is a dimensional constant, x is the horizontal coordinate of the projectile with diameter D and N is a nose shape caliber factor, function of the conical radius head of the impactor.

In the tunnel region, the resisting force results from a combination of compression and shear mechanisms. The compression part was made proportional to the square velocity (v^2) of the projectile through a compressibility function (B), multiplied with the density of the target (ρ_t). According to the experimental finding on the contribution of target inertia given as hypothesis of the model in Sec. 6.2, the quadratic velocity term of eq. 6.2(b) is neglected for the new Adobe ballistic model and only shear is thus considered. Experimental research has recently highlighted the relative contributions of the different mechanisms of energy dissipation in deep penetration of high velocity impactors in geo-materials, showing that the highly dissipative phenomenon of shear deformation is dominant [10]. In soil targets, energy absorption in shear is mainly due to friction between grains, enhanced by the high mean stresses experienced in front of the penetrating projectile. In absence of direct tests, in the original Forrestal model the shear strength parameter (τ_o) was related to the unconfined compressive strength of concrete

through an empirical function (S in [9]). For the Adobe model, a simple Coulomb friction resisting force linearly depending on the depth of penetration is proposed in the tunnel region [10, 11]. It reads $R = \mu\rho_t g A_p x(t)$ where μ is the internal frictional coefficient, $A-pp$ is the cross sectional area of the projectile and g is the gravitational acceleration (Figure 6.3(b)). Eq. 6.2 is updated for the crater and tunnel regions:

$$-m_p \frac{dv}{dt} = \mu\rho_t g A_p x \tag{6.3}$$

Where m_p is the projectile mass. Decomposing it is obtained:

$$-m_p v dv = \mu\rho_t g A_p x dx \tag{6.4}$$

Integration of the updated equation with respect to velocity and final depths of penetration (P) larger than 2D, leads to eq.6.5

$$-m_p \int_{v_o}^{0} v\,\mathrm{d}v = \mu\rho_t g A_p \int_0^P x\,\mathrm{d}x \tag{6.5}$$

For the case of an impacting sphere the final penetration depth is:

$$P \sim \sqrt{\frac{D\rho_p}{\mu\rho_t}}\, v_0 \tag{6.6}$$

The Adobe ballistic model is conceptually different in its interpretation from the models recently developed (eq. 6.1), but it is characterized by a similar mathematical formulation for the depth of penetration. They both are linearly proportional on the impacting velocity and they depend on the impactor diameter and ratio between impactor and target densities, despite in eq.6.6 this dependency is rooted. Moreover, this ratio is scaled by the internal frictional coefficient; however these differences would simply affect the value of the calibration factor k in eq.6.1(a).

6.4. AN APPLICATION OF THE MODEL ON MILITARY TESTS ON ADOBE WALLS IN THE FIELD

Due to its mathematical structure, the ballistic model in eq.6.6 fits the available sources of data on Adobe available in literature, which address a linear response between impacts of steel spheres at velocities below 1.5 km/s on targets with density of 1.8 g/cm3 [1, 3, 5]. In this section, the model is validated against the results of the ballistic campaign performed on real Adobe walls in the field presented in Sec. 6.2 and reported in [4]. For validation purposes, also in the Adobe ballistic model a calibration factor k is introduced as in eq.6.1, which automatically includes g and the constant of friction in eq. 6.3 in absence of related experimental data. As in the original model proposed by Forrestal et al.[9], due to the different shapes of tested impactors, resistance in eq. 6.3 is equipped with a nose caliber factor (N), calculated according to the ACE formula [14]. Due to the different walls layout, this term also includes a linear function depending on

the number of brick layers along thickness of the wall (n_{layers}) [13]. The final formula adopted for calibration with respect to all 130 tests is reported in eq. 6.7:

$$P = \sqrt{\frac{n_l m_p}{kN_{ace}\rho_t A_p}} v_o \tag{6.7}$$

The outcome of the analytical prediction of the experimental terminal depths of penetration is shown in Figure 6.4(a). Considering the intrinsic scatter of results inherent in field tests and the simplicity of the model, the Adobe ballistic model (k=180) is capable of predicting the terminal penetration depth on Adobe with high accuracy (coefficient of determination higher than 0.9 and mean absolute error of predictions lower than 5cm). The Adobe model predicts the penetration depth with a mean error always smaller than 6% of the target thickness. For 40 cm thick walls, the mean error is 2.5 cm and for 80 cm walls the error is 4.8 cm. The model properly captures experimental results for all types of bricks and mortar tested, despite possessing significantly different physical-mechanical properties Figure 6.5. The calibrated model is subjected to a further validation with respect to the performed experimental campaign in terms of residual velocity (v_r). In fact, few shootings tests resulted into perforation (ten cases). Among them, five hit Type B bricks of 40 cm walls using the same type of projectile and therefore they were considered for analysis. Their range of impact velocities was relatively modest (25m/s) and thus experimental results were averaged. The penetration depth was compared with respect to the results of the integration of eq.6.5 over the total thickness of the wall H (40 cm). The resulting formulation starting from eq.6.3 combined with eq.6.7 is given in eq. 6.8. The result of the calculations reveals a value for residual velocity consistent with the one experimentally observed (Figure 6.4(b)). Differences in values might be caused by the effects of projectile exit at boundaries.

$$v_r = \sqrt{\frac{m_p v_o^2 - kN\rho_t A_p H^2}{m_p}} \tag{6.8}$$

6.5. CONCLUSION

In this paper, a new semi-empirical ballistic model is presented for Adobe for small calibers with impact velocities up to 900m/s. It is developed by adapting a model originally defined for concrete in order to include the dominant frictional resistance experienced by soil targets in deep penetration. The proposed model has a similar mathematical formulation as previously defined models applied for the same material but they differ in the physical interpretation of the resisting mechanisms activated upon impact. The schematization and assumptions of the new model are based on the results of research accomplished by the authors during the last years on Adobe. This model, accounting for the physics of penetration on earthen walls, well predicts the experimental data available in literature for Adobe, including the new data recently shared by the authors, both in terms of penetration depth and residual velocity.

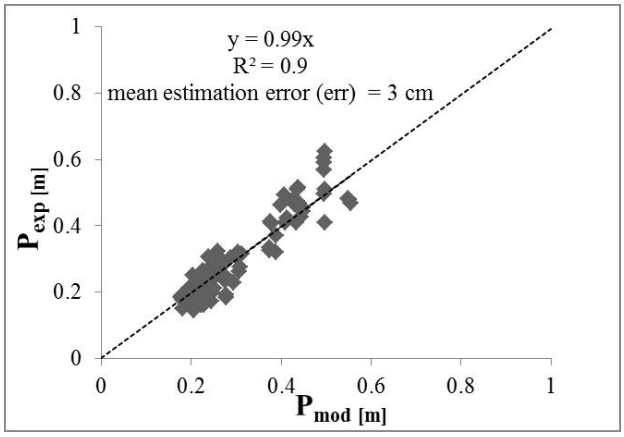

(a)

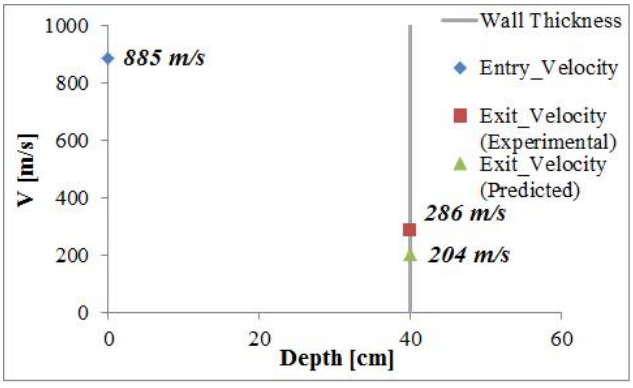

(b)

Figure 6.4: Experimental-predicted (a) terminal penetration depths considering penetration tests and (b) residual velocity for perforation tests impacting Type B bricks of Wall 40cm-thick at velocity of 885m/s.

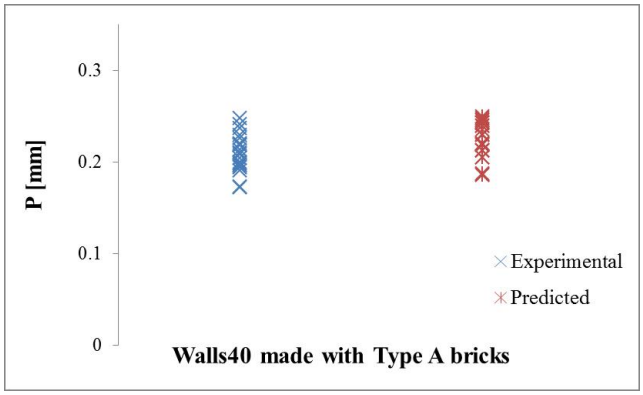

(a)

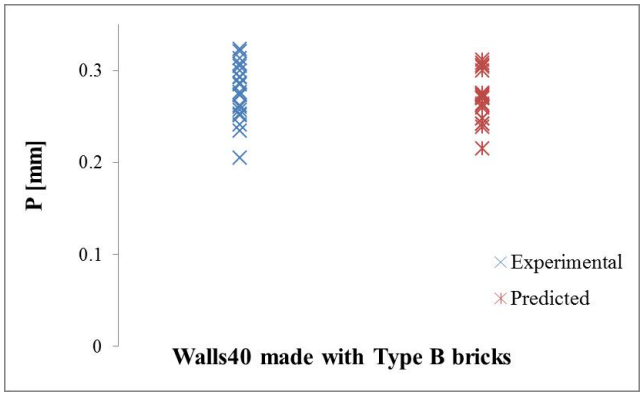

(b)

Figure 6.5: Experimental-predicted terminal penetration depths considering shot on Type A, $\rho = 1250 kg/m^3$ (a) and Type B, $\rho = 810 kg/m^3$ (b) bricks.

REFERENCES

[1] A. Heine, M. Wickert,Scale-independent description of the rigid-body penetration of spherical projectiles into semi-infinite adobe targets, International Journal of Impact Engineering 75 (2015) 27–29.

[2] G. Seisson, D. Hébert, L. Hallo, J. M. Chevalier, F. Guillet, L. Berthe, M. Boustie, Penetration and cratering experiments of graphite by 0.5-mm diameter steel spheres at various impact velocities, International Journal of Impact Engineering 70 (2014) 14–20. doi:10.1016/j.ijimpeng.2014.03.004.

[3] A. Heine, K. E. Weber, M. Wickert, Experimental Investigation of the Penetration and Perforation of building materials by projectiles, in: 26th International Symposium on Ballistics (12-16 Sept.), Miami, Fl, 2011.

[4] T. Li Piani, L. Koene, J. Weerheijm, L. Sluys, The Ballistic Resistance of Adobe Masonry: an analytical model for penetration in soil bricks and mortar. In: International symposium on ballistics impacts on structures (17th ISIEMS), Bad Neuenahr; 2017.

[5] A. Heine, M. Wickert, Ballistic Resistance of Semi-Infinite and finite Thickness Adobe targets, in: 29th International Symposium on Ballistic, Edinburgh, Scotland, UK, May 9-13, Edinburgh, 2016.

[6] T. Li Piani, D. Krabbenborg, J. Weerheijm, L. Koene, L. J. Sluys, The Mechanical Performance of Traditional Adobe Masonry Components: An experimental-analytical characterization of soil bricks and mud mortar, Journal of green building 13 (3) (2018) 17–44.

[7] T. Li Piani, J. Weerheijm, L. Koene, L. J. Sluys, The Adobe Delta Damage Model, in: Computational Modelling of Concrete Structures (EURO-C 2018), CRC Press, Bad Hofgastein (Austria), 2018, pp. 921–932.

[8] T. Li Piani, J. Weerheijm, L. Koene, L. J. Sluys, Modelling the Mechanical Response of Adobe Components under Uniaxial Loading, Key Engineering Materials 774 (2018) 650–657.

[9] M. Forrestal, B. Altman, J. Cargile, S. Hanchak, An Empirical Equation for Penetration depth of Ogive Nose Projectiles into concrete targets, Internation Journal of Impact Engineering 15 (4) (1994) 395–405.

[10] M. Iskander, S. Bless, M. Omidvar, Rapid Penetration into Granular Media: Visualizing the fundamental physics of rapid earth penetration, Elsevier Ltd, Amsterdam, 2015.

[11] H. Katsuragi, D. J. Durian, Drag force scaling for penetration into granular media, Physical Review 87 (5) (2013) 2–6. arXiv:arXiv:1304.4212v1, doi:10.1103/PhysRevE.87.052208.

[12] M. J. Forrestal, V. Luk, Penetration of 7075-T651 Aluminium targets with ogival rods (1992).

[13] G. Ben-Dor, A. Dubinsky, T. Elperin, Ballistic properties of multilayered concrete shields, Nuclear Engineering and Design 239 (10) (2009) 1789–1794. doi:10.1016/j.nucengdes.2009.05.015.

[14] Q. M. Li, X. W. Chen, Dimensionless formulae for penetration depth of concrete target impacted by a non-deformable projectile, International Journal of Impact Engineering 28 (1) (2003) 93–116. doi:10.1016/S0734-743X(02)00037-4.

7

A Normative Revision for the Production, Testing and Design of Adobe

"Men's courses will foreshadow certain ends,
to which, if persevered in, they must lead.
But if the courses be departed from,
the ends will change."

Scrooge in *A Christmas Carol*, by C. Dickens

Adobe is a traditional masonry made of raw earthen bricks and mortar. A critical analysis of the normative bodies currently available for adobe inherent to the material characterization is addressed in this paper. The importance of a normative update for adobe comes from a specific global conjuncture. After centuries of progressive abandon, the eco efficient production methods and product properties of this building technology are gaining renovated attention in Europe. Furthermore, its cheapness and spread availability can tackle housing affordability issues in many developing countries where earthen buildings are traditionally spread in areas prone to earthquakes or involved into military operations. Therefore, a safe assessment of this vernacular and sustainable building technique is of paramount importance in today's building industry. Guidelines and prescriptions related to test methods, materials selection and properties requirements by the available building codes for adobe around the world are assessed in the study. They have been evaluated in light of the most recent scientific findings on the material, physical and mechanical properties of adobe available in literature, with particular attention to the ones recently produced by the authors over the last five years of research. These are derived from several experimental campaigns as well as corresponding numerical simulations inherent to

This chapter is based on "Safe Use of a Sustainable Building Material: A Reappraisal of Adobe" in *under review*, 2019

physical-mechanical characterization tests in the static and dynamic regimes on various earthen bricks and mortar with different soil composition, water content and fiber percentages. On the basis of these findings, some issues have been identified in relation to the knowledge condensed in the prescriptions, requirements and procedures of the available norms for the material characterization of adobe. A series of guidelines in this paper is aimed at orienting future research on adobe as well as fostering the process of updating its current normative body.

7.1. INTRODUCTION

Goal number 11 of the UN urban agenda is concerned with making cities inclusive, safe, resilient and sustainable. The introduction of the concept of sustainability in the building construction industry is urgent because of its current impact on the increasing threats inherent to natural material scarcity and global pollution. Construction industry nowadays influences up to half of the total anthropogenic emissions of dioxin in the atmosphere and is responsible for more than one third of the total energy and water use. A relevant portion of these contributions regards only the material production phase [1]. Thus, sustainable alternatives to current building practices are cogent priorities and researches aimed at reducing the environmental impact of building materials while respecting performance requirements have been recently started around the world. For example, biological fibers have been recently tested as sustainable alternatives to steel in reinforced concrete. Natural binders or aggregates have been partially replacing Portland cement in concrete [2]. Alternatives to baking processes such as air drying procedures are studied for baked clay bricks [3]. Most of the aforementioned practices, despite being applied to new materials, are far from being new. In particular, they belong to the tradition of adobe. In adobe masonry, bricks are made of soil mixed with natural fibers locally available in the field. Mixtures are then cast in moulds and sundried without baking [4]. Fiber inclusion as well as air drying contribute to the eco-sustainability of adobe as a material. Adobe is fully disposable and almost fully recyclable. It causes almost null carbon footprint and ensures also higher acoustical and thermal performance than classical modern materials. Unfortunately, the effects inherent to air drying and fiber inclusion as well as other sustainable practices tied to adobe tradition on its mechanical performance have not been addressed yet. In fact, use of adobe decayed in industrialized societies in favour of artificial building materials with higher performance and standardized production methods [5]. As a result, most of the adobe buildings in the world are currently not designed according to any standard. However, more than two billion people still live in earthen dwellings mainly spread in regions of developing countries involved into military operations or prone to severe earthquakes and many adobe buildings of architectural value can be still encountered in Europe as well [6]. Thus in the specific case of adobe, sustainability is intertwined with other global urgencies inherent to safety and housing affordability tasks [7]. As a result, a comprehensive characterization of earthen material is of paramount importance nowadays. Normative efforts for the material characterization of adobe have started about fifty years ago in different areas of the world. The first attempts to characterize earthen materials for constructions relate to the standards in Germany [8], [9] and in New Zealand [10] and the most widely used reference nowadays according to literature studies is the Australian

earth building handbook [11]. Other guidelines can be found in different areas of the world, including Mexico, Peru, California and Spain [12]–[14]. In codes for adobe, indications about material selection and test requirements are often lacking, scarce or not consistent among the different guidelines. This occurs also because adobe is a site dependent material whose properties depend on the local resources availability and building traditions, that prevented a uniform treatment of the subject. Nevertheless, it is the lack of definite knowledge on the mechanical properties of earthen mixtures that mostly prevent a shared standardization process of adobe similar to modern building materials. Comprehensive studies on the mineralogical, physical and mechanical properties of adobe are still rare in literature: if this is true in statics, literature production on the dynamic performance of adobe is almost null [15]. Thus, over the last five years research by the authors has been devoted to comprehensively studying the properties of adobe. Earthen bricks and mortar with different soil and fiber proportions have been physically as well as mechanically studied at different humidity contents [16]. In particular, the role of fibers and water content have been experimentally studied also in the dynamic regime, in ranges of strain rates which cover earthquakes and ballistic impacts [17]. The studies resulted in theories, analytical models and numerical tools developed to assess the material performance of adobe, including the role of its mineralogical composition at a meso-scale [17]–[19]. In this paper, knowledge gained on the performance of adobe is focused on the critical analysis of the material characterization norms condensed in the heterogeneous normative production currently available for adobe in the world. In the following paragraphs, indications provided in codes on the subjects of soil selection, sample testing and material requirements are analysed and compared to the main results of the research by the authors and also with respect to literature sources. Final recommendations are meant to detect issues in current prescriptions but also to find areas of research which still need further efforts.

7.2. MATERIAL CHARACTERIZATION OF ADOBE IN THREE STEPS

Material standardization derives from a shared definition of soil selection, test methods and product performance. In the following paragraphs, a normative review is based on the analysis of these three main subjects.

7.2.1. MATERIAL SELECTION

Traditional adobe bricks result from mixtures of clay, silt, sand, water and air. In most cases, bricks' soil is mixed with natural fibers while mortar contains limited or no fiber amounts. Despite already back in the 90' s scientific papers in literature recommended a proper characterization of the soil granulometry, plasticity and compaction properties of adobe with building purposes, importance on the selection and identification practices of soil mixtures for earthen building applications is still not reflected in current design codes [20]. All codes for adobe currently available agree in selecting soils with no organic content and avoiding soluble salts above 0.5-2% [10], [11], [13]. Thus, top soil shall not be used. Potable water is recommended for mixing soil. Granulometry ranges are the most common recommendation contained in current building codes for adobe as indications of the cohesion properties of the final product [11], [13]. Guidelines mainly focus

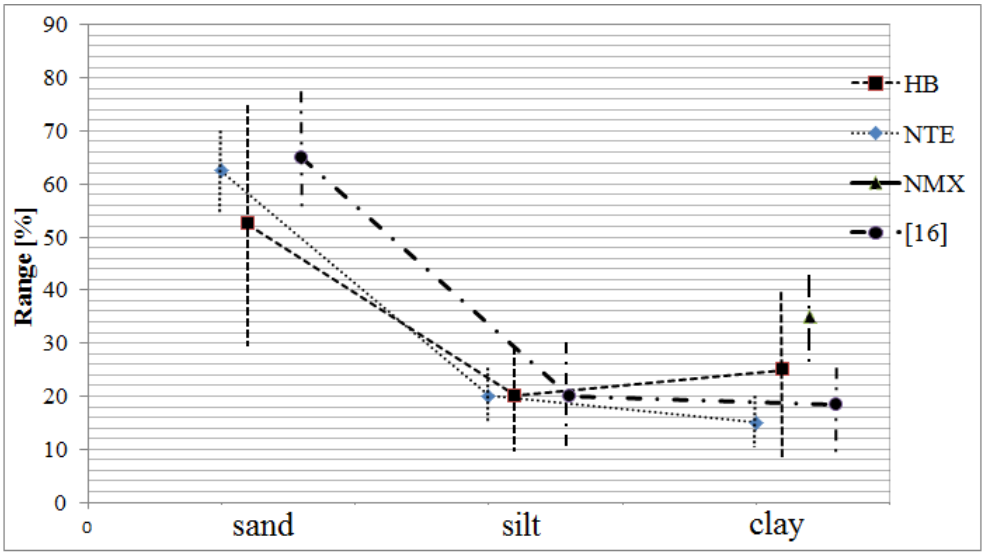

Figure 7.1: *Granulometry ranges for soil mixtures of adobe for building purposes according to Peru (NTE), New Mexico (NMX) and Australian (HB) codes compared with survey by the authors in [16]*

on the quantitative evaluation of clay amount in the mixture. In fact clay is the binder for the cohesionless granular fraction of the soil and is responsible for providing strength to the dried material [16]. All codes agree that a minimum of 10% by weight of clay should be present in the mixture [11]. However, recommended ranges vary also significantly around the different normative bodies, including in experimental characterization campaigns found in literature. As a result, maximum recommended clay percentage and foremost relative proportions with the larger size aggregates are still not defined neither agreed [4], [11]. For instance, maximum aggregate size recommended can range between 5 mm to 25mm [11]–[13]. This uncertainty happens because the adopted mixture is dependent on local availability of raw resources and an optimal clay amount is also determined by its mineralogical family and mutual proportions with the larger particles of the soil mixture. Expansive clay such as smecticte or montmorillonite are highly cohesive but also cause shrinkage cracks in the resulting adobe bricks. In this regards the use of expansive soil (i.e. “black earth”) is sometimes discouraged in codes [10], but studies in literature reveal that an optimum balance between expandable and non expandable soil is possible and desired to ensure adequate strength to the brick [21]. As a result of the possible combinations available in literature, consistency in the normative assessment of the optimal ranges of soil particles for earthen building purposes is lacking. The (loose) ranges contained in the Australian standard include the best quantitative soil mixture compositions for building purposes identified by the authors for adobe in [16] (Figure 7.1).

Besides availability of raw materials, quantity of clay as well as other soil elements and including mixing water depend on a vernacular building practice typical for adobe. It consists of mixing soil with natural fibers. This practice is tied to earthen architec-

ture and dates back to ancient Egypt [5]. It takes roots in the need for limiting shrinkage cracks naturally forming in the brick during curing process under sun. In fact, fibers ensure better drainage systems. Recommended materials are rice, barley, maize, wheat and including animal hair. Obviously, inclusion of fibers necessarily influences the initial mineralogical composition and the mixing water content and has an impact also on the physical-mechanical behaviour of the final product. However, despite a consolidated practice, the assessment of the mixture properties after fiber inclusion is currently not regulated by characterization standards for adobe. Instead, judgment of its opportunity in soil mixtures in codes is deputized again to the user and regulated only by not defined limits of not "excessive use" [11]. Actually, fiber inclusion in adobe guidelines is often considered as a stabilization technique of otherwise unsuitable soil compositions and suggested as an alternative to the introduction of cementitious bituminous binders recommended for highly clayey soils [10]–[12]. In this regard, fibers are suggested to improve the mechanical properties in hardness and strength, especially in tension [10]. The current interpretation on the role of fibers in many building codes for adobe is instead in contradiction with the main experimental trends observed for fibrous adobe in the field [16], [17]. The most common effect observed when adding fibers to soil mixtures tested in statics and dynamic regimes at different loading rates and directions is a decay of the mechanical properties of the resulting brick, namely strength and elastic modulus (Figure 7.2). Therefore, higher amounts of clay might be needed to partially recover the initial product strength if reinforced with fibers. The effects of fibers on the mechanical performance of adobe have been interpreted by the authors as the consequence of a loss of cohesion in the meso-structure of the soil mixture after fiber insertion. Particles can be separated by fibers and interaction between clay floccules to bind the cohesion less fraction of the mixture is less effective. This particularly happens for fiber amounts above 10% b.w. Also a few cases in which fibers strengthen the soil mixture can be encountered in literature [22], [23]. This happens because cohesion of the brick's macro-structure results from the mineralogical properties and relative proportions of the soil and by the material, quality and quantity of the added fibers, including their mutual interactions with clay binders at the meso-scale. This interpretation suggests that an optimum mixture of fiber and soil elements capable of reducing shrinkage and enhancing the mechanical performance exists. However, only a few codes currently prescribe cohesion tests for characterization purposes and they all require them to be performed only on the soil before fiber mixing [11]. Laboratory tests are recommended only in very few standard [8], [11]. In most of the cases, they imply the evaluation of Attemberg limits but only few quantitative indications are found, despite in broad ranges (16-30 for the plastic index and 30-50 for the liquid index) [11]. Quantitative evaluations inherent to soil plasticity as indication of soil consistency (without fibers) in standard are instead more commonly related to simple in field tests such as the Ribbon test, with an acceptance rate of 60-120mm for the broken pieces [11].

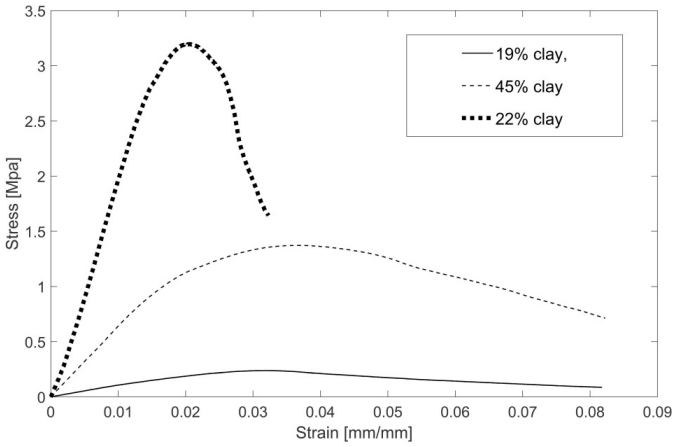

Figure 7.2: *Experimental stress-strain curves after static compression tests on two bricks containing about the same fiber content (30%b.w.) and different percentages in clay (about 20% and 45%) and on one brick containing only clay (22%)*

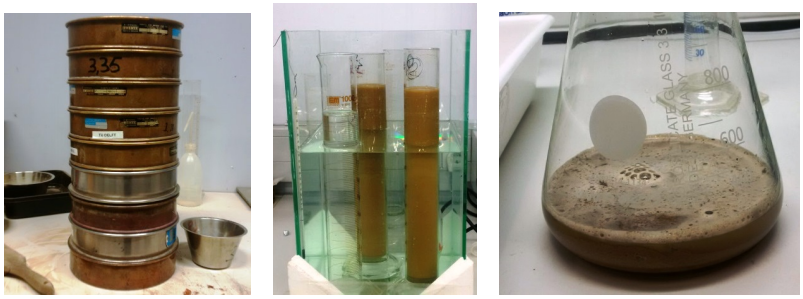

(a) (b) (c)

Figure 7.3: Sieving (a) and hydrometer (b) test, with preliminary chemical treatment of fibers (c)

7.2.2. MATERIAL TESTING

As emerged in the material selection phase, test methods and requirements inherent to the characterization of adobe components are not comprehensively neither consistently registered among the available codes [8]-[14]. A representative list of characterization tests required according to three different normative bodies on adobe is provided in Table 7.1. In adobe building codes, in-field tests are still considered as acceptable alternatives to more rigorous laboratory test methods. In-field tests are recommended provided the presence of the person responsible for final construction, despite most of earthen dwellings in the world are still designed and fabricated by owners themselves, often without the necessary specialist technical competences. Also the level of sophistication of the testing procedures and requirements rely on the user judgement on the importance of the building project [10]. Some characterization tests in codes are even fully sensorial, such as the smell test to verify the presence of organic matter in soil mixtures [11]. The most widely used test to determine the grading of a soil mixture is the sedimentation bottle test, in which the shaking of a jar containing loose soil is aimed at ascertaining approximate fine and sand particles [11]. Instead, sieving and hydrometer tests are strictly recommended only in few norms [8]. Granulometry tests were performed by the authors using the BS 1377-2 norm for classification methods on soils for civil engineering purposes (Figure 7.3a-b) [24]. In fact, this code also includes the preliminary treatment of soil mixtures with natural fibers. Tests were performed starting from cured bricks of several mineralogical compositions. This implied the preliminary desegregation of the product into its original soil mixture. Organic content was excluded using mechanical and chemical treatment (Figure 7.3c). Dissolution was accomplished using hydrogen peroxide. In case of highly fiber reinforced mixtures this process can require more cycles of chemical treatment.

Also the mechanical characterization of adobe is not solely prescribed according to laboratory standards but in-field compressive and flexural tests are often possible and still preferred [10]–[13]. However, mechanical properties can be rigorously derived from the standard commonly used for modern materials such as concrete. Compression tests on adobe samples were performed in [16] using UNI EN 772-1 for modern masonry materials [25]. Required levels of plane parallelisms for testing purposes were achieved using

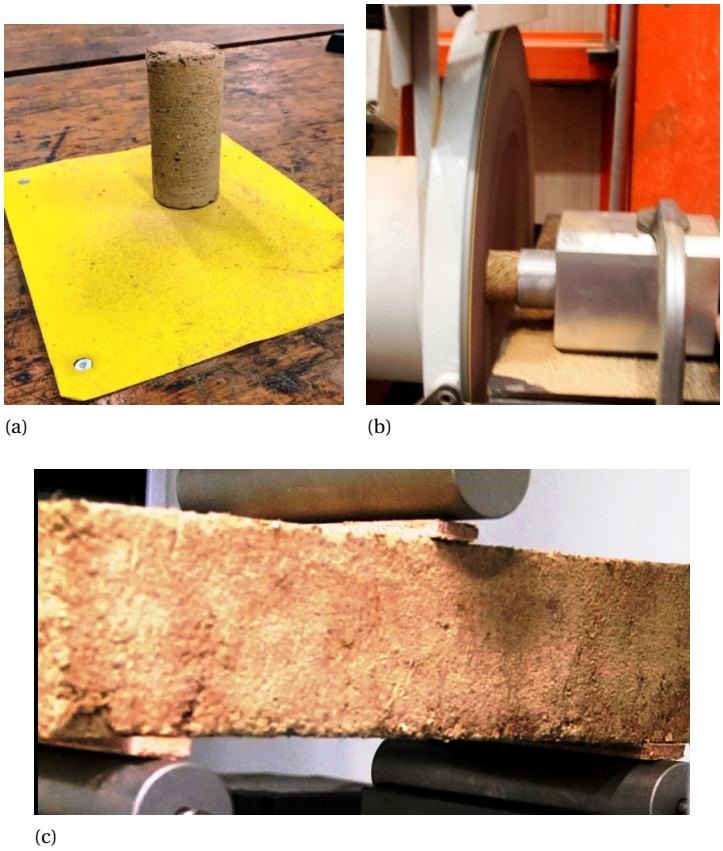

(a) (b)

(c)

Figure 7.4: Sanding paper (a) and sanding machine (b) for rectification purposes and layer interposition in a three point bending test (c)

mechanical rectification procedures which did not cause visible damage and achieved precisions included in standard tolerance (Figure 7.4 a-b). However, the interposition of layers of materials of significantly different properties for plane parallelism purposes is not recommended in the case of adobe.

Three point bending tests were performed according to UNI EN 12390-5 [26]. In this case, no indentation occurs when wooden stripes between adobe surfaces and steel rolls are interposed (Figure 7.4 c). Literature studies and norms for adobe indicate that applied deformation rates above 5 mm/min may be not adequate for testing soft earthen materials. This limit is generally respected in literature studies and suggested by the authors. Displacement controlled tests at velocities of 1-2 mm/min are suggested especially for soft adobe tested in compression and tension [16]. Higher values are discouraged also because the mechanical properties of adobe have been recently found to be sensitive to the applied loading rate [17].

If methods of investigation are uncertain, material performance requirements in codes

Table 7.1: List of main tests required for the characterization of adobe described by the Australian (HB), New Zealand (NZS) and Mexico (NMX) codes, distinguishing laboratory from in-field test (in italic) and denoting with * tests without quantitative requirement limits

Property	HB	NZS	NMX
grading	*Bottle test*; Sieving/sedimentation	*	*
organic content	*Smell**	*	*
plasticity	Casagrande;*Ribbon;Touch*	*	*
durability	Water absorption*;*Spray**	*Wet/dry*; Spray**	*Water retention**
shrinkage	*Box*	*Box**	*
density	Oven drying*	*	*
compression	Uniaxial; *Drop*	Uniaxial; *Drop*	Uniaxial
tension	Bending/*Flexure*	*Flexure**	Flexure

are controversial as well. Prescribed values for important physical and mechanical properties are often lacking or incomplete (Table 7.1). Not strictly quantitative recommendations relying on the arbitrary judgment of the user according to the specific need and destination of the product are often encountered in codes for the assessment of many parameters [10], [11]. This is the case for instance for the smell or the wet/dry in-field tests. When not lacking, test limits are often not uniform among different sources. Most of the quantitative requirements normed in codes for adobe nowadays focus on the assessment of minimum strength values in compression and tension. However, there is often no agreement about the minimum required performance and the assessment of important mechanical parameters for masonry design is also missing.

7.2.3. MATERIAL PERFORMANCE

PHYSICAL PROPERTIES

Mixtures of adobe are casted in moulds and dried under the sun for a minimum of 28 days in an exterior environment before testing [10], [11]. Both literature references and current standard for adobe recommend to protect bricks from wind and rain during drying [10]. During this phase, natural fibers explicate their role. They fasten this process facilitating draining from mixture through cavities and prevent the formation of severe shrinkage cracks. Shrinkage is abundant during drying of earthen materials and is allowed also according to codes, provided that shrinkage cracks do not jeopardize the material properties of the product [10], [12]. Caution is recommended in [10] if short fine cracks spread randomly at the surface of the brick are observed. In [11], it is preferred to exclude products with crack lengths above 7 cm. Only [9] recommends quantitative limits of 2% for the property of linear shrinkage. Shrinkage cracks represent a significant issue especially in case of high amounts of expandable clays in soil mixtures or in absence of fibers. Therefore, it can represent a threat for mud mortar. Characterization of mud mortar receives very little attention in codes and it is treated only in [8], [10]. Despite its importance on the overall performance of adobe walls is recognized, physical tests on mortar are usually prescribed only if different soil materials than for the

(a) (b)

Figure 7.5: Shrinkage of mortar after five days of curing (a): volumetric shrinkage of 18% (b)

bricks is used. This implies neglecting the influence of fibers during production of material and life cycle of the structure. Different shrinkage rates between bricks and mortar can be responsible for initial loss of adherence and de-cohesion issues which may soon affect structural integrity. Unfortunately, also scientific studies on the material characterization of adobe mortar are lacking and only two references concerning the physical mechanical assessment of mud mortar have been found in literature [16], [27]. Physical tests by the authors on mud mortar have confirmed faster drainage processes than bricks for the same curing conditions (Figure 7.5).

Even if the same soil is used for bricks and mortar, also the corresponding values for the property of density are different after 28 days of curing. Density in adobe is significantly influenced by fiber addition and its inclusion in the mixture significantly reduces the density of the resulting brick. This is a common trend observed in literature and quantified during a recent experimental campaign [17]. Comparing the density of two bricks with the same soil composition but only one mixed with 18%b.w. of fibers shows that density of the fibrous sample has decreased with 40%. As a result of different compositions, density values among different bricks also greatly vary in literature. They usually range between 800 kg/m^3 for fibrous mixtures to 1800 kg/m^3 for clayey bricks [16], [17]. This range is close to the one recommended in standards for adobe (1200 kg/m^3 – 2000 kg/m^3) [11]. Tested mortar in [16] showed a density of 1400 kg/m^3 whereas the one in [27] was almost 2000 kg/m^3. Durability performance of cured adobe is addressed in codes using in-field tests. The most common property evaluated (without specific restrictions) is erosion against water simulating raining conditions or dry/wet cycles to which adobe walls may be exposed to during its life cycle [10]-[11]. Instead, the assessment of the moisture content at 28 days of drying before wall fabrication is not required by codes. It is generally assumed that water content after curing is lower than 4% [10]. This is not always the case and actually depends on the internal composition of the product. This was inferred in [16] during an experimental campaign aimed at testing the mechanical performance of bricks and mortar made with different clay and fiber percentages. Bricks mixed with 30%b.w. of fiber and containing 45% of clay contained more than 6% of water after 28 days of curing, whereas the same fiber amount in a mixture with half of the clay almost halved its initial moisture level (Figure 7.6). This suggests that 28 days are not always sufficient to ensure a fully dried product. Furthermore, presence of fibers in the mixture has been found to have a minor influence on the final level of water content at cured conditions of bricks. In particular, for a certain amount of fibers, water

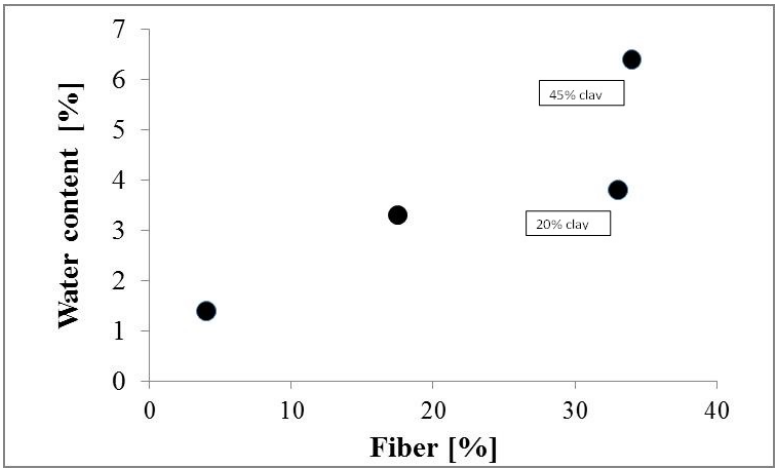

Figure 7.6: *Water content at 28 days of curing for four different adobe bricks as a function of the mixing fibers: focus on the moisture content for two bricks with similar amount of fiber but different clay percentages.*

content increases significantly with the increment of the clay proportion. This is interpreted as a consequence of the fact that the areas of the mixtures surrounding fibers are fully dried after 28 days. Thus, the final water content depend on the spatial distribution of the fibers in the mixture, with particular concern to concentrations of clay. In fact, water can still be retained by floccules of clay due to its affinity toward water: it swells in its presence and it shrinks in its absence [28]. Finally, eco-efficient physical properties such as thermal resistance are not contemplated by codes, with the exception of [11] where a typical range of the expected performance is included between 0.25-0.6 m^2K/W.

MECHANICAL PROPERTIES IN COMPRESSION

Assessing the interstitial water content in adobe components prior to construction is of paramount importance. Not only water affects the durability performance of the structure due to erosion phenomena [4] but it also directly influences the nominal strength of the masonry components and walls. Guidelines consider adobe bricks as fully dried after 28 days of curing, when the water content is expected to be lower than 4% [10]. However, also water levels below 2% are sufficient to determine a significant decrement in the parameters in strength, whereas a minor influence is exerted in deformation (Figure 7.7). This has been experimentally proved testing adobe bricks at different moisture levels (including oven drying) in static and dynamic compression tests in [16], [17]. As previously described, fiber inclusion does not limit this phenomena (Figure 7.7a-b).

The rate of decay of the strength of adobe due to interstitial water has been quantified in [16] as a function of the mineralogical composition of the mixture. By testing samples with different clay and fibers at certain drying conditions, it was revealed that the mineralogical composition of adobe can accelerate or decrease the loss of the mechanical property. In particular, statistical regression of experimental data on adobe resulted in the law of eq.7.1 for the prediction of strength at a given humidity as a function of its internal composition, namely fiber, clay and water contents (Figure 7.8)[16]:

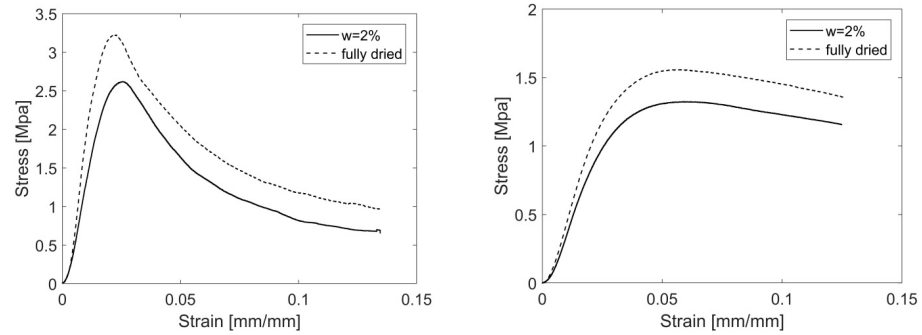

Figure 7.7: Stress-Strain curves for fiber free adobe bricks (a) and fibrous bricks (b) air dried at laboratory conditions (w≈ 2%) and dried in the oven (reduction of about 20% in strength)

$$f_b \propto \frac{clay}{fiber} w^{\propto -\frac{clay}{fiber}} \tag{7.1}$$

Where w stands for water and all variables are expressed in volumetric percentages. The shape of the law is similar to the trend empirically derived for baked clay bricks in [3], where the rate of decay increases for higher clay contents. As expected from the formulation in eq.7.1, the slope of strength decay experimentally derived for adobe mortar (with low or no fiber content) is in general higher than for adobe bricks and it is found to be similar to one of the slopes determined in [3] for only clay bricks.

The properties and testing procedures of cured adobe bricks in compression are covered the best by current standards. However, indications and recommendations among different sources are often not consistent, both in the prescribed test setup as well as in the required performance levels (Table 7.2). The minimum values for strength prescribed by codes after aspect ratio correction are however generally consistent with the values usually found for adobe bricks and mortar in literature. Most common values for adobe range between 0.8MPa and 2MPa. Figure 7.10 shows the nominal strength distribution for adobe after elaboration of a database collecting more than 150 static characterization tests in literature supplemented with authors data [16]. The resulting average value of strength is found to be about 1.3 MPa, with 0.95 fractile of about 0.3 MPa. The unconfined values of strength are usually determined in literature using the aspect correlation factors commonly prescribed for concrete [29] (Figure 7.9). Instead codes in [11] and [10] prescribe a more conservative law for adobe and recommend slenderness's of 3-5 as representative of the unconfined strength. Applying this law to the available tests in the database, the average strength is equal to 1.2 MPa, with 0.95 fractile of about 0.2 MPa.

Despite the specific shape of the curves in Figure 7.9, there are almost no systematic studies publicly available in literature on the size and shape dependencies of adobe [30]. Preliminary size dependence studies by the authors reveal a significant sensitivity

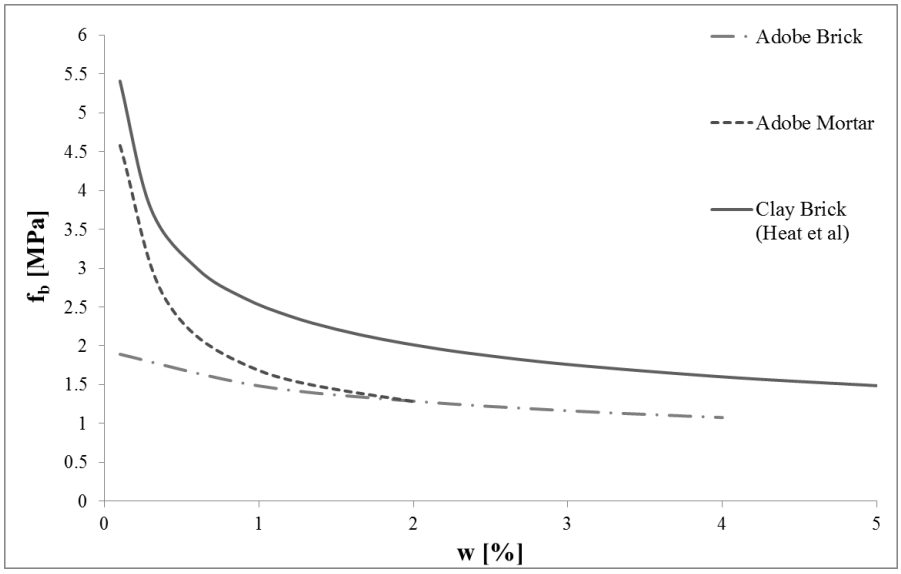

Figure 7.8: *Compressive strength law for adobe dependent on water content. Examples of predicted trends for one type of adobe brick and one type of adobe mortar using eq.7.1, compared with law derived in [3] for clay bricks*

Table 7.2: Prescribed strengths (and additional indications) for four building codes on adobe

Standard	*Requirement*	*Indications*
NZS	Minimum>1.3MPa	after aspect ratio correction (Fig.7.9)
NTE	80% fractile > 1.18 Mpa	after aspect ratio correction
NMX	Average>2 MPa	on flat direction/no geometry info
HB	Average>2 MPa	after aspect ratio correction (Fig. 7.9)

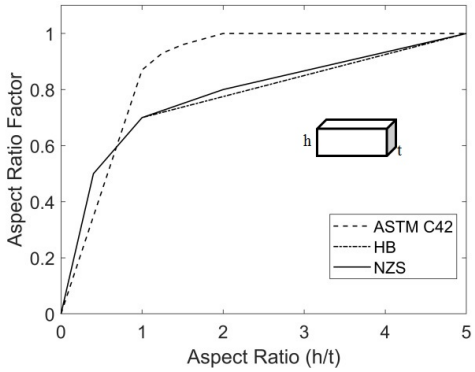

Figure 7.9: *Aspect ratio correction law in strength for concrete compared with the laws proposed in the Australian and New Zealand code for adobe*

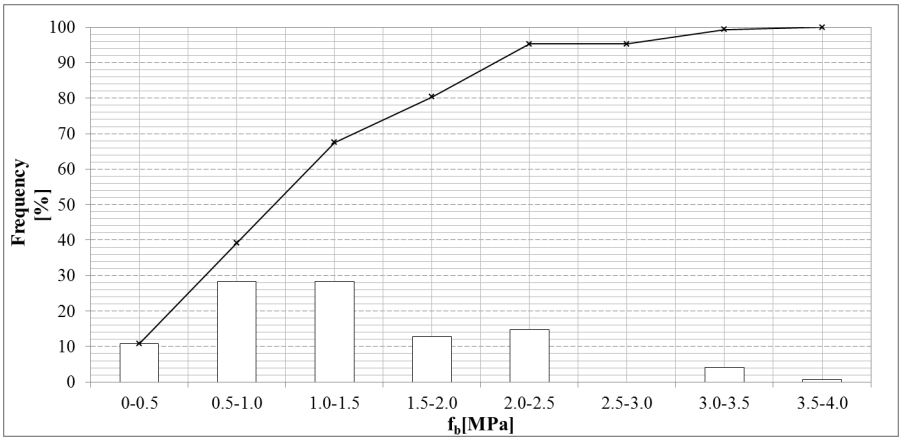

(a)

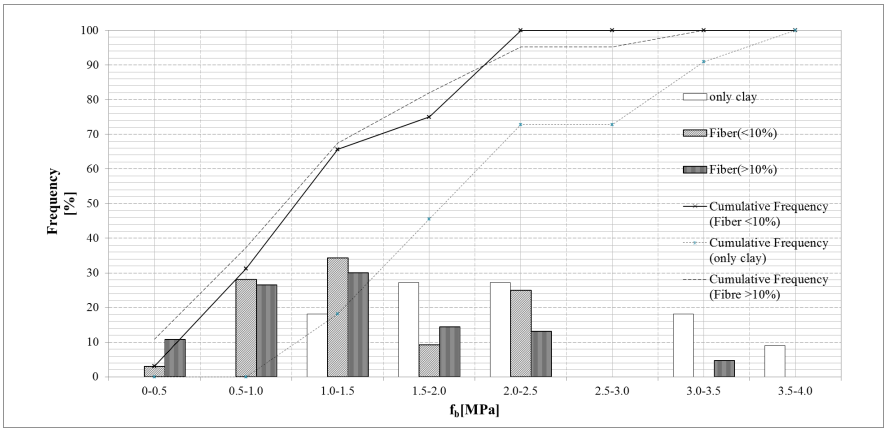

(b)

Figure 7.10: Relative frequency (histogram) and cumulative frequency (line) for the unconfined strength of adobe in literature (including data from authors) considering all data (a) or disaggregating data according to fiber ratios in the mixtures (b)

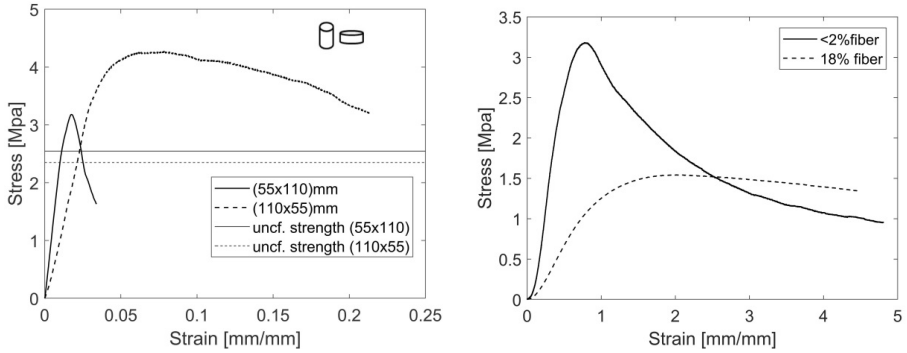

(a) (b)

Figure 7.11: Stress- Strain behaviour and unconfined strength values for two adobe samples with same soil and fiber composition and different slenderness(a) and with same geometry but different fiber percentages (b) tested in uniaxial compression

to sample dimensions in the response in strength and deformation (Figure 7.11a). However, derived values for nominal strength are consistent with the conservative aspect ratio laws depicted for adobe in Figure 7.9. As for shape dependence, in [30] a correlation between tests on cylinders and cubes was found with a slope of 0.94.

Furthermore, aside the role of water content, the mechanical characterization of adobe in standards does not address the influence of fiber content on strength either, despite that most common trends in literature relate fiber in soil mixtures to a decay of the mechanical parameters of the material (Par. 7.2.1). However, recognizing this role is not always easy in literature. Analysing Figure 7.10b, fiber free samples do not possess strength values lower than 1 MPa, whereas fibrous bricks have a significant statistical incidence in the 0.5-1MPa and 1.0-1.5 MPa ranges. However, fibers can confer to the brick also values of strength above 3MPa. As explained in Par. 7.2.1. the outcome of fiber inclusion depends also on the specific characteristics of the applied soil. However, there are only few systematic studies aimed at quantitatively addressing the role of fibers in adobe bricks [31]. Tests by the authors show that parameters in strength and stiffness are significantly affected by fibers whereas their inclusion is always accompanied by an enhanced ductility and retarded failure (Figure 7. 11b). The major contribution associated to the presence of fibres in the mixture on the mechanical performance of adobe is related to the material ductility. Fibers allow the bridging of the stress through cracks, limiting their entity and holding together the vital cores of the matrix until large deformation stages. Indications on the elastic stiffness of adobe bricks are not provided in standards. Data in literature reveal a significant scatter in values, with ranges between 10 MPa and 2500 MPa. However, most common values lie between 50 MPa and 200 MPa (Figure 7.12). The only reference to this parameter in standards relates to the stiffness of the adobe wall, which should be designed as 300 times the corresponding strength in [10]. Calculating E as a ratio of the strength reduces the scatter in value associated to stiffness, since strength and stiffness are found to react is a similar manner to clay, fiber

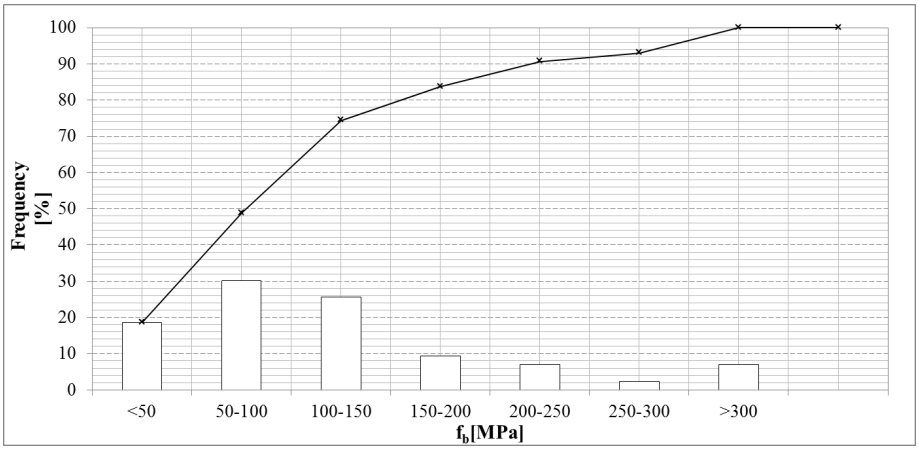

Figure 7.12: *Relative frequency (histogram) and cumulative frequency (line) of the elastic stiffness of adobe*

and water contents in the mixture [17]. However the recommended value in standards is lower than the ratios commonly encountered for adobe bricks. Considering only data set in [16], E=60-80fb, whereas considering data in literature E=120-180fb [32].

Besides the assessment of the mechanical parameters in compression, the definition of the entire curve in compression is of paramount importance for masonry materials. In fact, deformation curves can be used to develop constitutive models for non linear analyses [33]. Research by the authors has revealed that constitutive models originally developed for concrete can be used to address the curve of response of bricks and mortar of adobe. In [17] a constitutive model has been developed to assess the stress-strain plots of adobe bricks made of different mineralogical composition and water content and subjected to various loading rates, from statics to dynamic impact (Figure 7.13a). The law recalled in eq. 7.2 takes roots from the Popovics' model developed for cement geo-pastes in statics [34]. It properly addresses the typical non linearity observed in the curves of response of adobe in compression, characterized by micro-cracking processes starting in the pre-peak phase of the curve and in the final quasi-brittle softening behaviour. Ductility in response of adobe is enhanced when soil mixtures are provided with natural fibers (Figure 7.11b). Varying parameter n in eq. 7.2 as a function of fiber content, the different slopes of response experimentally derived for adobe bricks with different fiber percentages were reproduced (n ranged between about 1.5 and 3.5 in [17]). The model in eq. 7.2 modifies the original formulation in [34] implementing rate dependent functions of logarithmic shape (DIF) designed for the dynamic assessment of adobe in [17] (Figure 7.14).

$$\sigma = (f(DIF)E)\left(\frac{n}{n-1+\left(\frac{f(DIF)\epsilon E}{DIF f_b}\right)^n}\right)\epsilon \tag{7.2}$$

In fact, the response of adobe at high strain rate loadings has been recently experimentally assessed [17]. Strain rates in the order of 120 s^{-1} were achieved using Hopkinson bar tests. Tests revealed that adobe is a material sensitive to the deformation rate.

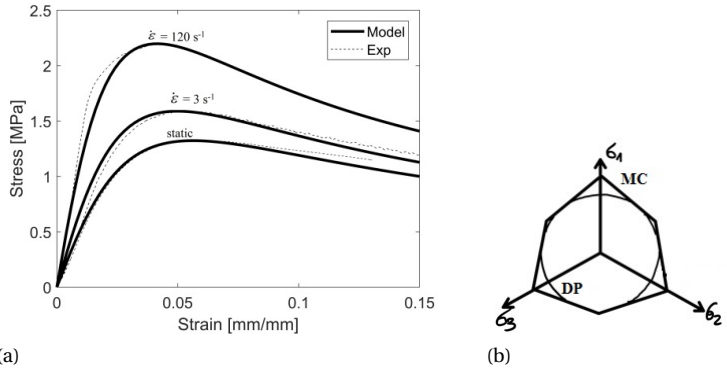

Figure 7.13: Experimental-numerical stress strain curves in compression for a fibrous adobe compressed at three different loading rates from statics to high velocity impacts, addressed using eq. 7.2 (a) and damage surface proposed for numerical simulations of adobe bricks in compression (b)

The dynamic increase factor of the mechanical property of strength for adobe lies in the lower boundary of the cloud of data usually associated to concrete [35]. Moreover, if soil mixtures are provided with fibers, rate sensitivity of the resulting brick decays. This is consistent with interpreting a reduction of cohesion after fiber inclusion. Instead water content in the mixture enhances sensitivity to the deformation rate for a physical principle of viscosity called Stefan effect (Figure 7.14) [17].

The scarcity of constitutive models describing the non linear response in compression up to failure for adobe is reflected in the lack of numerical models for the material simulation of bricks and mortar [36]. Constitutive models as in eq. 7.2 can be implemented in numerical frameworks, together with the definition of damage or plasticity surfaces. In [18], a smoothed Mohr Coloumb damage surface as in Figure 7.13b, implemented in a finite element isotropic damage model recently developed by the authors to simulate the response of adobe bricks and mortar, was suitable for interpreting the damage process of soil based masonry materials loaded in compression. This constitutive law has been validated against a wide range of loading conditions, including impact penetration tests on adobe walls [19].

MECHANICAL PROPERTIES IN TENSION

As for many quasi brittle materials used in masonry, correctly addressing the response of adobe in tension is very important. The mechanical characterization of adobe in tension in current codes mainly concerns the evaluation of its strength parameter. Quantitative values are evaluated mainly from flexural tests, despite literature studies suggest that splitting tests better reproduce the uniaxial tensile state [30]. Experimental data available for adobe in tension in literature and including tests in [16] is shown in Figure 7.15. Averages and 0.95 fractile values respectively are 0.4 MPa and 0.15 MPa. According to codes, minimum values for strength of 0.34 MPa is prescribed in [12], while 0.25 MPa is requested in [8]-[10]. This requirement is met by 65% of the experimental data for adobe in tension available in literature.

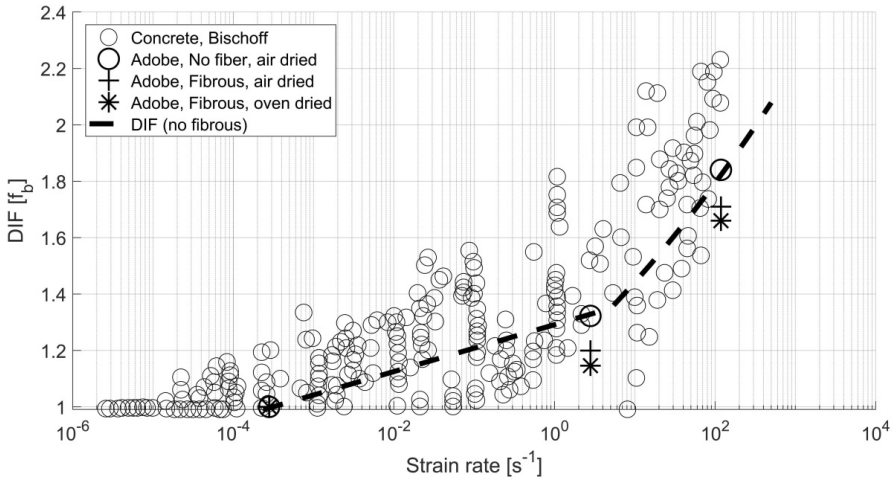

Figure 7.14: *Average experimental dynamic increase factors in compression for two types of adobe bricks with different fiber proportions and water contents compared with literature data on concrete and addressed using logarithmic DIF functions in [17]*

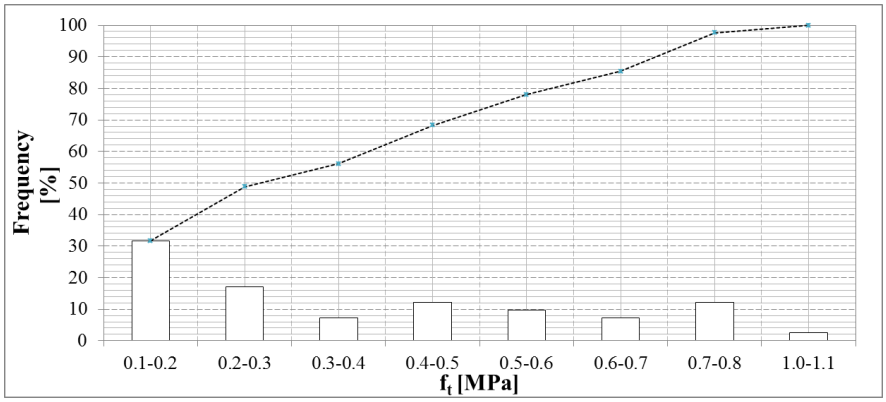

Figure 7.15: *Relative frequency (histogram) and cumulative frequency (line) for the tensile strength for adobe using data in literature (including authors')*

Also in tension, mixing soil with fibers results in average to a lower strength performance and to an enhanced ductility (Figure 7.16). With a value of 0.7 MPa, adobe mortar tested in [16] possesses one of the highest values of tensile strength encountered in literature for adobe.

Tensile strength relates to the parameter in compression in ranges between 0.18fb [5] and 0.4fb [22]. In [16], this ratio ranges between 0.3fb and 0.7fb, with a median equal to 0.57fb. These values are in general higher than the minimum levels suggested in [10], included between 10% and 20% of the compressive strength [10].

The failure process of adobe in tension is typically more brittle than in compression. A localized failure has characterized bricks and mortar subjected to bending tests in [16], independently from water content and fiber inclusion in the mixture. Typical curves of response are characterized by an elastic phase followed by softening with exponential shape (Figure 7.16b). Numerical simulations of bending tests on adobe using the model in [18] show that a constitutive law in RILEM TC 162 [37] originally prescribed for steel fiber reinforced concrete is suitable to numerically assess the localized damage failure experimentally observed in adobe (Figure 7.17). The adopted constitutive model in tension is linear elastic with an elastic modulus being the same as in compression until the attainment of the stress level associated to the first crack in bending, which anticipates softening.

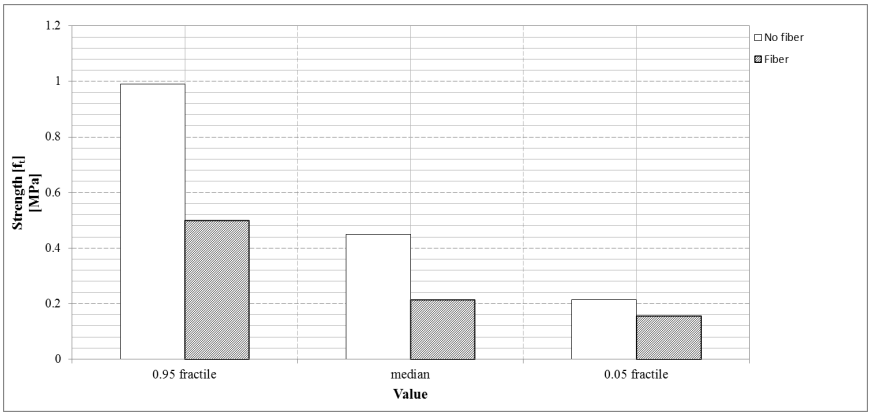

(a)

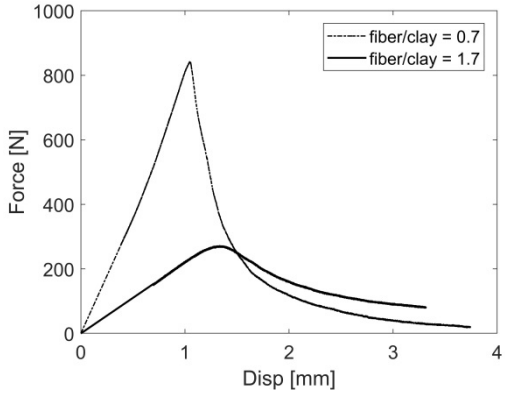

(b)

Figure 7.16: Relative frequency for the tensile strength of adobe bricks disaggregated for fiber free and fibrous adobe samples (a) and Force – displacement plots in bending tests in [16] on two adobe bricks with different fiber proportion ratios (b)

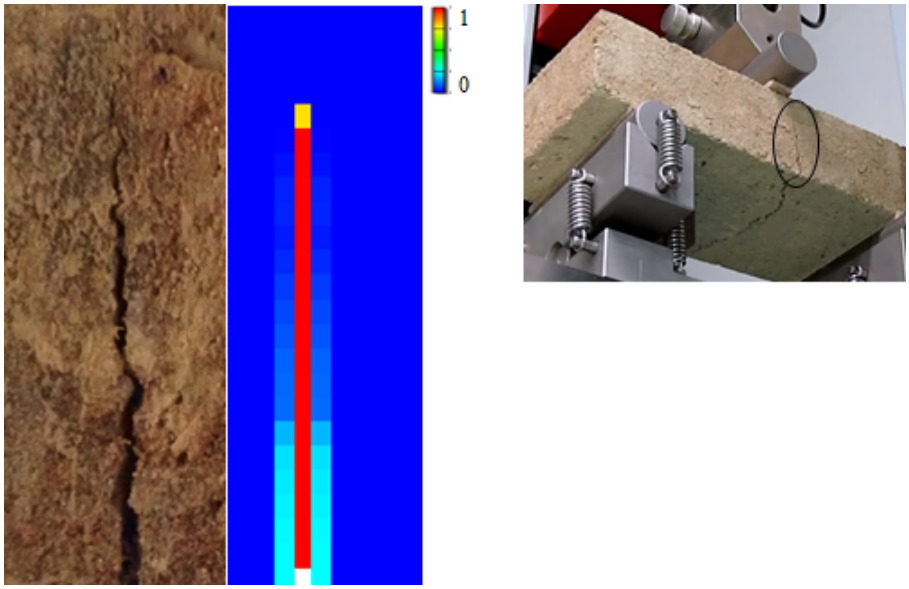

Figure 7.17: *Experimental crack and numerical damage (using Rilem) localized in the middle of a brick subjected to bending test [18]*

7.3. CONCLUSIONS

A normative review of the codes currently available for the material characterization of adobe bricks and mortar is reported in this study. The prescriptions provided by the normative bodies for adobe around the world related to test methods, soil selection and material properties have been critically addressed. They have been compared with the most recent scientific findings produced for adobe regarding the assessment and interpretation of its physical-mechanical properties. To this end, the experimental data, theoretical interpretations and numerical elaborations produced by the authors over the last years on adobe have been used as main reference. From the analysis, lack of knowledge, consistency and completeness in the current normative body stand out and a normative update is needed. It is acknowledged that in contexts of scarcity, compliance with codes is subordinated to the need to provide a shelter economically and quickly. However, the recent application of principles of circular economy in building industry makes sustainable vernacular materials and practices as possible options also in countries characterized by intense diossine emissions like the European ones. Therefore, a safe use of a sustainable building material in current society goes through a comprehensive assessment of the building technology and the consequent characterization. Among others, two areas of improvement are deemed as priority:

- Definition of a shared set of identifying properties for the physical-mechanical performance of adobe components, both bricks and mortar. The assessment of the drying conditions preliminary to tests on samples is a priority. Thus, the influence of moisture on the mechanical performance must be integrated both at an experimental characterization and at a material design level. Required properties should not solely relate to the characterization of the mechanical parameters of the resulting brick but rather to the evaluation of its originary soil. Soil particle distributions are not sufficient to certify suitability of adobe as a building material, but a comprehensive study is needed, with particular reference to the plasticity and cohesive property of the mixture. These must not only be determined on the raw soil, but also directly on the final mixture used to produce the brick, namely including the assessment of fiber-soil mixtures properties.

- Homogenization of test procedures, methods and requirements for each targeted property. Simplistic identification tests in the field must be preferably substituted by laboratory tests because they are often not sufficient to determine exhaustive information of fundamental properties for adobe. Standard methods can be adapted from codes for modern building materials for masonry. Furthermore, for each property, acceptable ranges of values or minimum requirements should be carefully defined to ensure prescribed levels of safety. These values should concern the properties in strength and deformation of the brick as well as the physical properties of the mixture. Given the site dependency inherent to soil selection, prescriptions are expected in terms of ranges for the soil distribution properties and in terms of strict minimum requirements for cohesion, durability and plasticity properties.

REFERENCES

[1] Transitieteam Bouw, Circulaire Bouweconomie, p.38., 2018.

[2] J. Reis, Fracture and flexural characterization of natural fiber-reinforced polymer concrete, Construction and Building Materials, Vol 20, n.9, 2006

[3] A. Heath, P. Walker, C. Fourie, and M. Lawrence,"Compressive strength of extruded unfired clay masonry units", Proc. Inst. Civ. Eng. Constr. Mater. 162, n. 3, 105-112, 2009.

[4] R. Coffman, N. Agnew, G. Austin, and E. Doehne, "Adobe mineralogy: characterization of adobes from around the world", Int. Conf. Conserv. Earthen Archit. Las Cruces, New Mex. U.S.A., vol. 1, no. May, 1990.

[5] D. Silveira,Mechanical properties of adobe bricks in ancient constructions, Construction and Building Materials, vol. 28, n. 1, 36-44, 2012.

[6] Centre de recherche et application en terre CRATERRE

[7] G. Wekerle and P Jackson, Urbanizing the security agenda, City, Vol 9, n.1, 33-49, 2005

[8] DIN 18952: Methods of test for earth (1956), 2008.

[9] Lehmbau Regeln. Begriffe Baustoffe Bauteile. Braunschweig Wiesbaden, Germany: Friedr. Vieweg and Sohn Verlagsgesellscahaft mbH, 1999.

[10] NZS 4298: Materials and workmanship for earth buildings, New Zeal. Tech. Committe, vol. 4298, p. 91, 1998

[11] HB 195, The Australian earth building handbook-Standards Australia International, NSW 2001. 2001.

[12] New Mexico Earthen Building Materials Code, Title 14, Chapter 7 (Part 4),2004. New Mexico

[13] Sencico Norma Tecnica Edificacion, NTE E 0.8 Adobe, 2000.

[14] California Code of Regulations for Adobe in New Constructions, Title 24, Part 10., 2011

[15] M. Larcher et al., Dynamic Increase Factor of Masonry Materials: Experimental Investigations, ISIEMS, International Symposium for the Interaction of Munitions with Structures, 2013, p. 10.

[16] T. Li Piani, D. Krabbenborg, J. Weerheijm, L. Koene, L. J. Sluys, "The Mechanical Performance of Traditional Adobe Masonry Components: An experimental-analytical characterization of soil bricks and mud mortar", Journal of green building 13 (3) (2018) 17–44.

[17] T. Li Piani, J. Weerheijm, M. Peroni, L. Koene, G. Solomos L. J. Sluys, "Dynamic Characterization of Adobe in compression: The effect of fibres with soil binders", FraMCoS-X: Fracture Mechanics of Concrete and Concrete Structures, 2019.

[18] T. Li Piani, J. Weerheijm, L. Koene, L. J. Sluys, "The Adobe delta damage model: A locally regularized rate-dependent model for the static assessment of soil masonry bricks and mortar", Engineering Fracture Mechanics, Vol 206, 114-130,2019. Press, Bad Hofgastein (Austria), 2018, pp. 921–932.

[19] T. Li Piani, J. Weerheijm, L. J. Sluys, "Ballistic model for the prediction of penetration depth and residual velocity in Adobe: A new interpretation of the ballistic resistance of earthen masonry", Defence Technology, 14, n.5,4–8, 2018

[20] H. Houben and H. Guillaud, Earth construction: a comprehensive guide, Engineering Fracture Mechanics, ITDG Publishing, 1994

[21] G. Austin, Adobe as a building material, Engineering Fracture Mechanics, New Mex. Bur. Mines Miner. Resour. Socorro, 1984

[22] A. Caporale, F. Parisi, D. Asprone, R. Luciano, and A. Prota, "Comparative micromechanical assessment of adobe and clay brick masonry assemblages based on experimental data sets", Composite Structures, Vol 120, 208-220,2015.

[23] E. Quagliarini and S. Lenci, "The influence of natural stabilizers and natural fibres on the mechanical properties of ancient Roman adobe bricks", Cultural heritage, vol. 11, no. 3, 2010.

[24] BS 1377-2: 1990, Methods of test for soils for civil engineering purposes, Classification tests.

[25] UNI EN 772-1:2015 Test Methods for masonry elements. Title 1: Determination of compressive strength.

[26] UNI EN 12390-5: Tests on hardened concrete. Title 5: Bending tests on concrete specimens, 2009.

[27] R. Aguilar, M. Montesinos, and S. Uceda, "Mechanical characterization of the structural components of Pre-Columbian earthen monuments: Analysis of bricks and mortar from Huaca de la Luna in Peru", Case Studies in Construction Materials, vol. 6, 2017.

[28] E. Smith, "Adobe bricks in New Mexico", Circular 188, New Mexico Bureau of Mines and Mineral Resources., p. 89, 1982.

[29] ASTM C42: Standard Test Method for Obtaining and Testing Drilled Cores and Sawed Beams of Concrete

[30] D. Silveira, H. Varum, and A. Costa, "Influence of the testing procedures in the mechanical characterization of adobe bricks", Construction and Building Materials, 2013

[31] S. Yetgin, A. Cavadar, "The effects of the fiber contents on the mechanic properties of the adobes", Construction and Building Materials, 2008

[32] A. Caporale, F. Parisi, D. Asprone, R. Luciano, and A. Prota, "Critical surfaces for adobe masonry: Micromechanical approach", Composites Part B, 2014.

[33] J. Ingham, D. Biggs, "Uniaxial Compressive Strength and Stiffness of Field-Extracted and Laboratory-Constructed Masonry Prisms", J. Materials in Civil Engineering, 2014.

[34] S. Popovics, "A numerical approach to the complete stress strain curve of concrete", Cement and Concrete, 1973

[35] P. Bischoff and S. Perry, "Compressive behaviour of concrete at high strain rates", Material Structures, 1991.

[36] R. Illampas, D. Charmpis, and I. Ioannou, "Finite Element Simulation of the Structural Response of Adobe Masonry Buildings Subjected To Lateral Load", 2014.

[37] RILEM TC 162-TDF: Test and design methods for steel fibre reinforced concrete. Sigma-epsilon design method. Final Recommendation, 2004.

8

CONCLUSIONS AND FUTURE PERSPECTIVES

In this study, experimental guidelines, physical theories and numerical models have been developed to characterize the material performance of adobe masonry. These achievements were made possible by the combined experimental-numerical approach adopted for this research. Adobe still denotes a non engineered building technology. However, methods and models are now available to test, simulate and interpret adobe with the rigour and certainty usually applied for modern building materials. This chapter provides an overview of the characterization process, merging the experimental and numerical conclusions reported at the end of each chapter into three groups. The first concerns the main findings experimentally derived in this study on the role that the mineralogical components in the mixture exert on the resulting physical-mechanical properties of adobe. The second describes the constitutive framework developed to address the main experimental patterns depicted in the mechanical response of adobe regardless of its specific composition. The third focuses on the capability of the numerical model developed for adobe to produce objective simulations of quasi-brittle masonry materials.

- The mechanical properties of adobe strongly depend on its mineralogical composition. Interstitial water affects durability and weakens the nominal strength of adobe. Compressive strength is inversely proportional to the water amount in the mixture at a given humidity condition and its rate of increment in dynamic regimes increases with its content. Interstitial water weakens the chemical forces between binder particles in the mixture and causes a chemical reaction which is proportional to the velocity of the applied load. Fibers included in the soil mixture strongly influence the mechanical performance of the material both in strength and ductility. In most of the cases, fibers in adobe decrease the strength and its dynamic increase factor in dynamics, whereas they enhance ductility of the brick. Their inclusion in soil mixtures mostly cause de-adherence with the binding frac-

tion of the matrix, which enhances porosity and increases the number of flaws in the mixture.

- Regardless of its internal composition, failure behaviour of adobe tested in compression and tension at different loading conditions is always characterized by the formation of macro-cracks visible at the surface of the specimen and corresponding softening response. Bricks and mortar of adobe are indeed quasi-brittle materials. Like a quasi brittle material, the mechanical response of adobe is characterized by softening, that results from the material degradation after micro-flaws stemming and coalesce into macro-cracks. Softening functions originally developed for concrete can thus be adapted to design the uniaxial behavior of adobe. If equipped with rate dependent functions, their validity can be extended also in the dynamic regime. Pressure-dependent constitutive models such as the Drucker-Prager surface inscribing the Mohr Coulomb domain correctly interpret most of the features of the observed failure patterns. The parameters of the constitutive laws vary according to the internal compositions, namely the higher ductility in the material reponse provided by fibers and lower strength determined by water in the mixture. Softening functions and constitutive models can be incorporated in finite element models that simulate the mechanical response of adobe at generic loading conditions. Interpreting failure as a progressive degradation of the elastic stiffness of the material, continuum damage mechanics constitutes a suitable numerical approach for the phenomenological interpretation of the response of adobe.

- Local regularization algorithms can solve mesh dependence in damage models both for static and dynamic analyses. Rate dependent functions can be used to regularize a local damage model recently defined for concrete and that could be previously regularized only using a non-local approach. The concept of a bounded damage rate originally developed for delamination problems in composites can be effectively integrated in material models aimed at simulating the mechanical response of geomaterials such as concrete and adobe. A formulation of damage delay based on the Dirichlet boundary condition history solves the numerical pathology of the local model while enhancing physical consistency with the quasi-brittle nature of response and inherent rate dependence experimentally observed in dynamics for adobe. Displacement based analyses solved using an implicit scheme provides mesh independent simulations in statics and dynamics within a robust algorithm.

The doctoral research has produced achievements which allowed the characterization of the main physical-mechanical properties of adobe. However, as in every scientific work, limitations, neglected issues or exceptions have also characterized this doctoral research. These can provide important sources of information and might serve as an identification of weak spots in the current stage of knowledge and open new trajectories and approaches of investigation. In the following, issues in each of the previous chapters are reported:

- As a masonry material, the mechanical response of adobe bricks and the inher-

ent material parameters are size dependent. The values for strength and ductility derived from tests can be significantly influenced by the adopted size and shape of the sample, including the different set up and testing devices used in the laboratory. A proper assessment of these contributions require the production of large experimental data sets on various geometries and also numerical simulations. Both are lacking in literature for adobe and are expected in the future. A preliminary experimental investigation of size dependence on adobe was performed by the authors in 2018 and further studies will follow. Statistical and deterministic size effects can also be evaluated using the numerical model developed in this study for adobe.

- The hypothesis of homogeneity at a macro scale as a basis of the continuum damage framework developed for adobe is not always met in the actual production of bricks and mortar of adobe in the field. Especially in contexts of scarcity around the world, production of earthen building materials in the field can still be characterized by the absence of material selection requirements, production chains and quality controls that, instead, are well established in case of modern building materials. For specific choices in the raw materials selection or in case of some vernacular building practices, adobe bricks after drying can sometimes be characterized by a large number and extensions of micro-flaws and defects which would not make them suitable neither for numerical simulations using the model nor for construction purposes.

- The assessment of the contributions that radial inertia and steel platens-specimen friction exert on the dynamic increase factors of the material at high strain rates are important to be numerically evaluated to comprehensively quantify the true dynamic performance of adobe. In a simulation of the split hopkinson bar test, this would require the numerical implementation of the geometrical and mechanical properties of the entire setup and of the selection of the contact algorithm at the boundaries of the bar with the specimens.

- A direct dependence between the damage delay function and the actual strain rate of each integration point rather than on the derivative of the external velocity rate causes a degradation of the mesh independence performance of the numerical model. This results from the re-activation of intense strain localization in areas of the spatial domain characterized by higher rates of deformation at initiation of failure. Averaging techniques of the induced displacement rates caused by external loadings on the model can be studied for complex multi-directional loading scenarios, which are not trivial.

- The ballistic phenomenological model neglects the source of energy dissipations related to the transition between different media during penetration. This is the case of the mortar joints in masonry. This issue is expected to have a minor influence in the case of adobe, but should be properly addressed. Furthermore, also the influence of the boundary exits in the energy dissipation equations is neglected because of the semi-infinite medium hypothesis of the model. Cases of projectile fragmentation due to penetration are excluded by the hypotheses of the ballistic

phenomenological models. These phenomena can be studied using the numerical model developed in this study if erosion algorithms are implemented.

Despite the achievements of this thesis, many challenges still remain towards a more complete understanding of adobe. In particular, two areas of research are deemed as priority in light of the demanding normative tasks raised in Chapter 7. They are:

- At a material level, the optimization of the best mineralogical composition which ensures optimal durability, ductility and strength properties of the resulting adobe brick and mortar. For a given soil, experimental studies should be aimed at determining the best materials, quantity and orientation of mixing fibers which enhance the physical properties of adobe and increase its mechanical performance. The assessment of the optimal mixture may take profit from the development of multiphysics and multiscale numerical modelling techniques. They should be capable to model the meso-scale structure of the adobe component, namely the soil particles, voids, water and fibers. In addition, new building production and construction processes capable of removing randomness in the manual production of adobe bricks can help to ensure quality control requirements.

- At a structural level, the assessment of the properties of homogeneity of adobe as a masonry. Contrary to modern masonry, adobe bricks and mud mortar belong to the same material class and share the same material properties and inherent physical-mechanical trends. However, techniques of homogenization in design codes and numerical applications should be carefully evaluated because of the different shrinkage rates of adobe with different fiber content. Substantial differences can cause the loss of monolithic behaviour after localized interfacial cracks. The study of the interaction between bricks and mortar in adobe walls is recommended both at an experimental and numerical level, by means of simulations of interface problems with water percolation. The model developed in this study can be applied for this scope implementing discrete interfaces with proper constitutive relationships.

CURRICULUM VITÆ

Tiziano LI PIANI

05-06-1989 Born in Oristano, Italy.

TERTIARY EDUCATION

2015–2019 Ph.D. in Applied Mechanics (Computational Mechanics Group)
Civil Engineering Faculty
Delft University of Technology
Promotor : Prof. dr. ir. L. J. Sluys
Daily supervisor/copromotor : Dr. ir. J. Weerheijm

2012–2014 MSc in Structural Engineering
Civil Engineering Faculty
University of Pavia
Final Grade: 110/110 *cum Laude*

2009–2012 BSc in Civil Engineering
Civil and Environmental Engineering Faculty
University of Pavia
Final Grade: 110/110 *cum Laude*

ACADEMIC EXPERIENCE

2018-2019 Reviewer for "*International Journal of Impact Engineering*"
"*Journal of Green Building*"and International conferences

2018-2019 Daily Supervisor of Master student
Delft University of Technology

2017 Daily Supervisor of Bachelor student
Delft University of Technology

2017-2019 Teaching Assistant for the course CIE5123 on *f.e.m*
Delft University of Technology

HONOURS AND AWARDS (2016-2019)

2018-2019	Interviewed (twice) by the European Commission on the granted project "*D.I.F. Adobe*"
2018	Appeared on TU Delft website (news) and Youtube channel (https://www.tudelft.nl/citg/over-faculteit/afdelingen/materials-mechanics-management-design-3md/news/; https://www.youtube.com/watch?v=2mxwoS9vFlw)
2018	Winner of the "*Best Contribution Award*" at the 2018 International Conference on Defence Technology, Beijing (China)
2018	Leader of the consortium between TU Delft, TNO, Dutch Ministry of Defence winner of the public announcement "*2017-1-RD-ELSA-HopLab*" called by European Commission -Department of Space, Security and Migration with the proposal: "*The Dynamic Performance of Adobe (D.I.F. Adobe)*"
2017	Winner (first classified) of the National Grant "*Admeto Pettinari and Paolo Andreini*" by CSR-Cassa Sovvenzione e Risparmio (Saving Bank of Italy) for Italian MSc and PhD students abroad
2017	Awarded of "Independent PhD" by the Italian *Institute for Advanced Strategic and Political Studies (IASSP)*, Italy (devoid of academic purposes)
2017	Invited to the Italian Parliament in Rome to present the counter-terrorism project "*Operative Guidelines for the protection of places of worship: A new approach for the security design of sensitive buildings*"
2017	Mentioned in "*Preventing terrorists attacks using an engineering model (in italian)"* online article published in the national magazine "Formiche"
2016	Invited speaker to the Italian Parliament in Rome

LIST OF PUBLICATIONS (2015-2019)

JOURNAL PAPERS (SCIENTIFIC STUDIES)

7. **T. Li Piani**, J. Weerheijm, L. Koene, L.J. Sluys, *Safe use of sustainable building materials: a reappraisal of Adobe*, (2019), (under review).

6. **T. Li Piani**, J. Weerheijm, L.J. Sluys, *Dynamic simulations of traditional masonry materials at different loading rates using an enriched damage delay : Theory and practical applications*, Engineering Fracture Mechanics, **218**, (2019).

5. **T. Li Piani**, J. Weerheijm, M. Peroni, D. Krabbenborg, L. Koene, G. Solomos, L.J. Sluys, *Dynamic behaviour of Adobe in compression: the role of fibers and water content at various loading rates*, (2019), (under review).

4. **T. Li Piani**, J. Weerheijm, L. Koene, L.J. Sluys, *The Adobe delta damage model: A locally regularized rate-dependent model for the static assessment of soil masonry bricks and mortar*, Engineering Fracture Mechanics, **206**, 114-130 (2019).

3. **T. Li Piani**, J. Weerheijm, L.J. Sluys, *Ballistic model for the prediction of penetration depth and residual velocity in Adobe: A new interpretation of the ballistic resistance of earthen masonry*, Defence Techology, **14(5)**, 4-8 (2018).

2. P. Morandi, L. Albanesi, F. Graziotti, **T. Li Piani**, A. Penna, G. Magenes, *Development of a dataset on the in-plane experimental response of URM piers with bricks and blocks*, Construction and Building Materials, **190**, 593-611 (2018).

1. **T. Li Piani**, D. Krabbenborg, J. Weerheijm, L. Koene, L.J. Sluys, *The mechanical performance of traditional Adobe masonry components: An experimental-analytical characterization of soil bricks and mud mortar*, Journal of Green Building, **13(3)**, 17-44 (2018).

THESES AND JOURNAL PAPERS (STRATEGIC STUDIES AND SOCIAL SCIENCES)

4. **T. Li Piani**, *Local trends and global dynamics of religious terrorism in the African continent*, NATO Defence College Foundation paper, 10 (2019).

3. **T. Li Piani**,*Structural design and the social function of space as vulnerability factor and solution to urban terrorism (italian)*, Security Terrorism Society (STS), (2)8, 7-17 (2018).

2. A.R.C. Cavalcanti, **T. Li Piani**, *Housing by people and work: Design principles for residents of favelas in economies of commerce and service*, The Plan Journal, 4(1), (2019).

1. **T. Li Piani**, *Operative guidelines for the protection of places of worship: A new approach toward security design of sensitive buildings*, Institute for Advanced Strategic and Political Studies, ISBN: 97888940373-2-6, 70pp (2017).

CONFERENCE PROCEEDINGS

9. **T. Li Piani**, J. Weerheijm, L. Koene, L.J. Sluys, *Safe use of sustainable building materials: The case of Adobe*, 2nd International Conference on Sustainable Building Materials, ICSBM 2019, Eindhoven (the Netherlands), (2019).

8. **T. Li Piani**, J. Weerheijm, M. Peroni, L. Koene, G. Solomos, L.J. Sluys, *Dynamic Increase Factors for Adobe: Addressing the dynamic strength in compression for earthen materials*, 18th International Symposium on the Interaction of the Effects of Munitions with Structures, ISIEMS - 2019, Panama City Beach (Florida, US) (2019).

7. **T. Li Piani**, J. Weerheijm, M. Peroni, L. Koene, G. Solomos, L.J. Sluys, *Dynamic characterization of Adobe in compression: The influence of fiber fraction in soil mixtures*, 10th International Conference on Fracture Mechanics of Concrete and Concrete Structures, FraMCoS-X, Bayonne (France), (2019).

6. **T. Li Piani**, J. Weerheijm, L.J. Sluys, *Ballistic model for the prediction of penetration depth and residual velocity in Adobe*, 2018 International Conference on Defence Technology, Beijing (China), (2018).

5. P. Morandi, L. Albanesi, F. Graziotti, **T. Li Piani**, A. Penna, G. Magenes, *Lateral strength of URM piers: comparison between codified criteria and in plane test results*, 10th International Masonry Conference, Milan (Italy), (2018).

4. P. Morandi, L. Albanesi, F. Graziotti, **T. Li Piani**, A. Penna, G. Magenes, *Database collecting in plane test results of urm piers with bricks and blocks*, 16th International Conference on Earthquake Engineering, Thessaloniki (Greece), (2018).

3. **T. Li Piani**, J. Weerheijm, L.J. Sluys, *Modelling the Mechanical Response of Adobe Components under Uniaxial Loading*, 17th International Conference on Fracture and Damage Mechanics **14(5)**, Advances in Fracture and Damage Mechanics XVII, Key Engineering Materials, 650-657, Seville (Spain), (2018).

2. **T. Li Piani**, J. Weerheijm, L. Koene, L.J. Sluys, *The Adobe delta damage model*, Computational Modelling of Concrete and Concrete Structures, EURO-C 2018, CRC Press, Bad Hofgastein (Austria), 921-933, (2018).

1. **T. Li Piani**, J. Weerheijm, L. Koene, L.J. Sluys, *The ballistic resistance of Adobe masonry: An analytical model for impacts on mud bricks and mortar*, 17th International Symposium on the Interaction of the Effects of Munitions with Structures, ISIEMS - 2017, Bad Neunham (Germany), 10-18, (2017).

LONG ABSTRACTS

3. **T. Li Piani**, J. Weerheijm, L.J. Sluys, *Dynamic simulation of masonry materials at different loading velocities using an updated damage delay algorithm of regularization: theory and practical applications*, VI International Conference on Computational Modeling of Fracture and Failure of Materials and Structures, CFRAC, Braunschweig (Germany), (2019).

2. **T. Li Piani**, *After Sri Lanka: Anatomy of terrorist attacks in Churches (italian)*, Italian Institute for International Political Studies ISPI, analysis, p. 10, (2019).

1. **T. Li Piani**, J. Weerheijm, L. Koene, L.J. Sluys, *Modelling the mechanical response of adobe components under uniaxial loadings*, 6th European Conference on Computational Mechanics (Solids, Structures and Coupled Problems ECCM - ECFD 2018), Glasgow (UK), (2018).

Propositions

accompanying the dissertation

EXPERIMENTAL-NUMERICAL MATERIAL CHARACTERIZATION OF ADOBE MASONRY

by

Tiziano LI PIANI

1. Not always what ties, unites. Not always what surrounds, protects. Not always what adds is beneficial. This holds for human relationships and also counts for fibers and water in the mixture of adobe.
2. Post-Renaissance's specialization of scientific competences benefits from the recovery of an integrated neo-Hellenic metaphysics perspective.
3. Despite the technological capacities of current food industry, pasta still remains the most eaten food in Italy. No matter how ancient a mixture is, it can still satisfy contemporary needs if the recipe is good enough. The recipe for the safest and most sustainable adobe can be found and its ingredients already exist.
4. It is easier programming with hands dusted with mud.
5. A thick dictionary is meaningless if filled up with many words devoid of their definitions. A reliable numerical model not only describes reality with calibrated parameters but allows the physical-mechanical interpretation of the fitted parameters.
6. The best way to prevent bullet penetration in adobe is to avoid war. The most probable way is designing adobe against the weapon that has not been fabricated yet.
7. Structural design against natural and man-made hazards must account for the social function every building is characterized by. In built environments connoted by high social value, the design of the building as an individual entity is not sufficient to ensure safety to its residents and to the inhabitants of the city against terrorism.
8. If the same perfection required by a doctorate regarding professional competences is applied to the moral conduct, academia is the oven of enlightened thinkers for the sake of society. Otherwise it may generate anomalies and even monsters.
9. If 8. is correctly applied, it is the responsibility of the academic to actively participate in society.
10. Visualizing constantly the future happiness quickly approaches it to the present.

These propositions are regarded as opposable and defendable, and have been approved as such by the promotor Prof. dr. ir. L.J. Sluys and the copromotor Dr. ir. J. Weerheijm.

Stellingen

behorende bij het proefschrift

EXPERIMENTAL-NUMERICAL MATERIAL CHARACTERIZATION OF ADOBE MASONRY

door

Tiziano LI PIANI

1. Niet alles wat verenigt, verbindt. Niet alles wat omringt, beschermt. Niet alles wat toegevoegd wordt is heilzaam. Dit geldt voor menselijke relaties maar ook voor vezels en water in het mengsel van adobe materiaal.

2. Postrenaissancistische specialisatie van wetenschappelijke competenties moet profiteren van het herstel van een geïntegreerd Nieuwgrieks metafysica-perspectief.

3. Ondanks de huidige technologische mogelijkheden van de voedselindustrie, blijft pasta nog steeds het meest gegeten voedsel in Italië. Onafhankelijk van hoe oud een mengsel is, kan het nog steeds voldoen aan de hedendaagse behoeften als het recept maar goed is. Het is mogelijk om een recept voor het veiligste en meest duurzame adobe te vinden en zijn de ingrediënten al aanwezig.

4. Het is makkelijker om te programmeren met handen besmeurd met modder.

5. Een dik woordenboek is waardeloos als het vol staat met woorden die hun definities missen. Een betrouwbaar numeriek model beschrijft niet alleen de werkelijkheid met gekalibreerde parameters, maar maakt ook de fysisch-mechanische interpretatie van de aangebrachte parameters mogelijk.

6. De beste manier om kogelpenetratie in adobe te voorkomen, is oorlog te vermijden. De meest aannemelijke manier is om adobe metselwerk te ontwerpen dat bestand is tegen wapens die nog niet zijn gefabriceerd.

7. Bij structureel ontwerp moet rekening worden gehouden met dynamische gevaren waartegen een gebouw bestand moet zijn en met de sociaal maatschappelijke waarde die elk gebouw kenmerkt. In een dichtbebouwde omgeving van hooge maatschappelijke waarde, is het ontwerp van een gebouw als een individuele entiteit niet volvoende om anti-terrorism veiligheid van de omgeving te waarborgen.

8. Wanneer dezelfde perfectie die vereist wordt van een doctoraat voor wat betreft professionele competenties wordt toegepast op de morele perfectie, is de academische wereld een broedkamer van verlichte denkers in dienst van de samenleving. Als dat niet zo is, genereert het anomalieën en zelfs monsters.

9. Als 8 correct wordt toegepast, is het de verantwoordelijkheid van de academicus om actief deel te nemen aan de samenleving.

10. Door constant het toekomstige geluk te visualiseren, komt het snel binnen handgereik.

Deze stellingen worden opponeerbaar en verdedigbaar geacht en zijn als zodanig goedgekeurd door de promotor prof. dr. L.J. Sluys en de copromotor dr. J. Weerheijm.